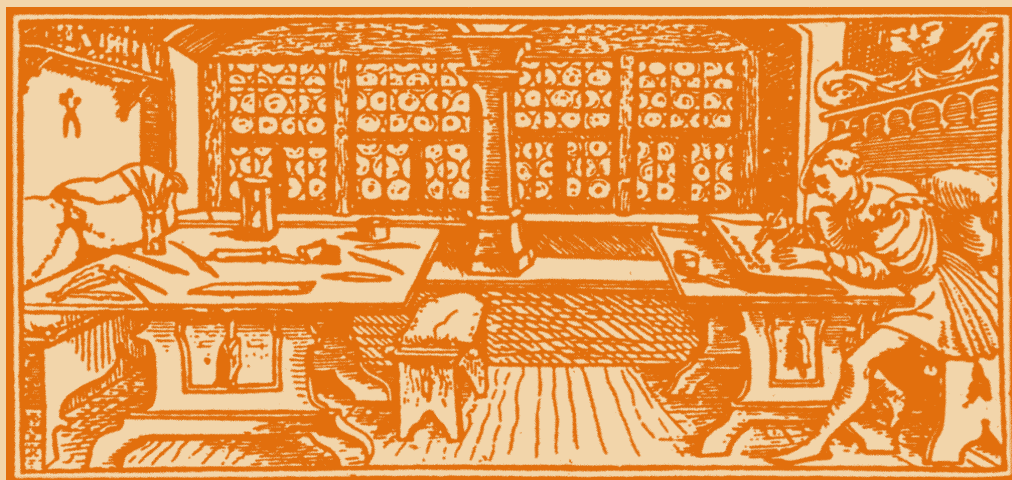


STUDIA

UNIVERSITATIS
BABEȘ-BOLYAI

C h e m i a

C L U J - N A P O C A 2 0 0 3



STUDIA

UNIVERSITATIS BABEȘ-BOLYAI

CHEMIA

2

EDITORIAL OFFICE: Republicii no. 24, 3400 Cluj-Napoca ♦ Phone 0264-40.53.52

SUMAR - CONTENTS - SOMMAIRE - INHALT

M.V. DIUDEA, Capra a Leapfrog Related Map Operation.....	3
M.V. DIUDEA. Nanotube Covering Modification.....	17
MIHAELA CĂPRIOARĂ, CS.L. NAGY, M. DIUDEA, Modeling Physico-Chemical Properties of Polychlorinated Biphenyls on the Grounds of Hypermolecule Concept.....	27
CS. NAGY, M.V. DIUDEA, Carbon Allotropes with Negative Curvature	37
CRINA VEREȘ, MIHAELA CĂPRIOARĂ, CS.L. NAGY, M.V. DIUDEA, Modeling Biological Activity of (3-(pyridylmethyl)-benzoquinone Derivatives	47
I. PANEA, ADINA GHIRIȘAN, F. IURA, R. GROPEANU, I.A. SILBERG, Azocoupling Products. Part III. Spectroscopic Investigation and Synthesis of some Azocoupling Products Between 1-(4-hydroxy-6-methylpyrimidin-2-yl)-3-methylpyrazolin-5-one with Aromatic Diazonium Salts.....	55
I. PANEA, ADINA GHIRIȘAN, I. BÂLDEA, I. SILAGHI-DUMITRESCU, LILIANA CRĂCIUN, I.A. SILBERG, Azocoupling products. Part IV. The Structure of Dyes Obtained by Azo-Coupling Reaction of 1-(4-hydroxy-6-methylpyrimidin-2-yl)-3-methylpyrazolin-5-one with Aromatic Diazonium Salts	67
L. COPOLOVICI, I. BÂLDEA, Logarithmic Extrapolation Method for Kinetic Determination of Amine Mixtures.....	85
CARMEN MĂIEREANU, E. CONDAMINE, I. SILAGHI-DUMITRESCU, M. DĂRĂBANȚU, 1-Aza-5-hydroxymethyl-3,7-dioxabicyclo[3.3.0]octanes: Chelating Properties Related to their Conformational Chirality	91
CARMEN MĂIEREANU, I. SILAGHI-DUMITRESCU, CAMELIA BERGHIAN, MONICA PINTEA, MARIJANA FAZEKAS, M. DĂRĂBANȚU, Stereocontrolled Synthesis by Anomeric Effects of Substituted 1-aza-3,7-dioxabicyclo[3.3.0]octanes	103

CAMELIA BERGHIAN, NELLY PLÉ, G. PLÉ, M. DĂRĂBANȚU, First Example of Selective Nucleophilicity of 1-aza-5-hydroxymethyl-3,7-dioxabicyclo-[3.3.0]octanes in Alkoxide Form	113
CAMELIA BERGHIAN, CARMEN MĂIEREANU, NELLY PLÉ, ALAIN TURCK, E. CONDAMINE, M. DĂRĂBANȚU, First Example of 1-aza-5-hydroxymethyl-3,7-dioxabicyclo[3.3.0]octane-5-yl-methoxy System as Directed Ortho-Metallation Group	127
I. OPREAN, BIANCA MOLDOVAN, R. OPREAN, EI-MS Unidirectional Triple Hydrogen Rearrangement. I. The Case of Long Chain Phenylazobenzoates....	139
BIANCA MOLDOVAN, I. OPREAN, R. OPREAN, EI-MS Unidirectional Triple Hydrogen Rearrangement. II. The Case of Long Chain Benzoates.....	145
R. TÖTÖS, I. SILAGHI-DUMITRESCU, Synthesis and Reactivity of Difluoromethylene Bridged Diphospha-Derivatives	149
R. SILAGHI-DUMITRESCU, S. AMTHOR, CS. PAIZS, C. MAJDIK, M.TOȘA, P. MOLDOVAN, A. SAS, L. TAMAS, F.D. IRIMIE, Horseradish Peroxidase – Catalysed Oxidation of Water – Insoluble Phenotiazines.....	165
T. FRENTIU, MICHAELA PONTA, NADIA ALEXA, GEORGIANA MECULESCU, M. SELINA, BELA ABRAHAM, E. CORDOȘ, Study of Arsenic Determination in Soil by Spectrometric Methods With and Without Hydride Generation	171
GABRIELA SZABÓ, CS. BOLLA, L. JANOS, CS. RACZ, The Influence of Lipoic Acid on Briggs-Rauscher Oscillating Reaction	181
VIRGINIA DANCIU, L.C. COTEȚ, VERONICA COȘOVEANU, P. MARGINEAN, Preparation and Porous Structure Determination of Resorcinol-Formaldehyde and Carbon Aerogels	185

CAPRA – A LEAPFROG RELATED MAP OPERATION

MIRCEA V. DIUDEA

*Faculty of Chemistry and Chemical Engineering
Babes-Bolyai University, 400028 Cluj, Romania
diudea@chem.ubbcluj.ro*

ABSTRACT. A map M is a combinatorial representation of a closed surface. Its corresponding graph can be either a periodic covering or an irregular one. Several operations on the map allow its transformation in tilings eventually of chemical interest. A new operation called "capra" is defined and exemplified. It is compared with the well known leapfrog and quadrupling transformations and its implications in the adjacency matrix eigenvalue spectra discussed.

INTRODUCTION

The discovery of fullerenes and related nanostructures has generated an explosion of research in theoretical and applied sciences. These new carbon allotropes show unusual properties (electronic, optical, mechanical, catalytic or capillarity), with no known analogy in nature. They are promising candidates for the development of nanodevices and super strong composites. Several books in this field have already been published.¹⁻⁵

A fullerene is, according to a classical definition, an all-carbon molecule consisting entirely of pentagons (exactly 12) and hexagons ($N/2-10$). Non-classical fullerene extensions to include rings of other sizes have been considered.^{6,7} Heterocyclic large cages have also been studied.⁸

A map M is a combinatorial representation of a closed surface.^{9,10} The graph associated to the map is called regular if all its vertices have the same degree. Let us denote in a map: v - number of vertices, e - number of edges, f - number of faces and d - vertex degree. A subscript index will mark the corresponding parameters in the parent (zero) and (iteratively) transformed maps (1,2,...).

Recall the basic relations in a map:

$$\sum dv_d = 2e \quad (1)$$

$$\sum sf_s = 2e \quad (2)$$

where v_d and f_s are the number of vertices of degree d and number of s -gonal faces, respectively. The two relations are joined in the celebrated Euler¹¹ formula:

$$v - e + f = \chi(M) = 2(1 - g) \quad (3)$$

with χ being the Euler *characteristic* and g the genus¹² of a graph (e.g., $g = 0$ for a planar graph and 1 for a toroidal graph). Positive/negative χ values indicate positive/negative curvature of a lattice. This formula is useful for checking the consistency of an assumed structure.

OPERATIONS ON MAPS

Several operations on maps are known and used for various purposes.

Stellation St of a face is achieved by adding a new vertex in its center and connecting it with each boundary vertex. It is also called a *capping* operation or (centered) *triangulation*.⁹ When all the faces of a map are thus operated, it is referred to as an *omnicapping* operation. The resulting map shows the relations:

$$St(M): \quad v = v_0 + f_0; \quad e = 3e_0; \quad f = 2e_0 \quad (4)$$

so that the Euler's relation holds.

Dualization Du of a map is built as follows: locate a point in the center of each face. Join two such points if their corresponding faces share a common edge. The transformed map is called the (Poincaré) *dual* $Du(M)$. The vertices of $Du(M)$ represent the faces of M and *vice-versa*.⁹ Thus the following relations exist:

$$Du(M): \quad v = f_0; \quad e = e_0; \quad f = v_0 \quad (5)$$

Dual of the dual recovers the original map: $Du(Du(M)) = M$.

Medial Me is an important operation of a map.^{9,10,13} It is constructed as follows: put the new vertices as the midpoints of the original edges. Join two vertices if and only if the original edges span an angle. More exactly, the two edges must be incident and consecutive within a rotation path around their common vertex in the original map.

The medial graph is a subgraph of the line-graph.¹² In the line-graph each original vertex gives rise to a complete graph while in the medial graph only a cycle C_d (i.e., a d -fold cycle, d being the vertex degree) is formed. The medial of a map is a 4-valent graph and $Me(M) = Me(Du(M))$. The transformed parameters are:

$$Me(M): \quad v = e_0; \quad e = 2e_0; \quad f = f_0 + v_0 \quad (6)$$

The medial operation rotates parent s -gonal faces by π/s .

Truncation Tr is achieved by cutting of the neighborhood of each vertex by a plane close to the vertex, such that it intersects each edge incident to the vertex. Truncation is similar to the medial, with the main difference that each old edge will generate three new edges in the truncated map. The transformed parameters are:

$$Tr(M): \quad v = d_0 v_0; \quad e = 3e_0; \quad f = f_0 + v_0 \quad (7)$$

Leapfrog Le is a composite operation^{10,13-19} that can be written as:

$$Le(M) = Du(St(M)) = Tr(Du(M)) \quad (8)$$

A sequence stellation-dualization rotates parent s -gonal faces by π/s . Note that the vertex degree in $Le(M)$ is *always* 3, as a consequence of the involved triangulation. The transformed parameters are identical to those of $Tr(M)$, eq. 7. Leapfrog operation is illustrated, for a square face, in Figure 1.

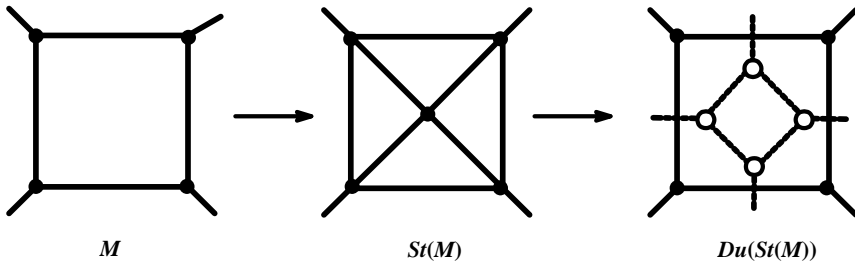


Figure 1. Leapfrog of a square face of a trivalent map

Note that a bounding polygon is formed around each original vertex. In the more frequent cases of tetra- and three-valent vertices, the bounding polygon is an octagon and a hexagon, respectively (Figure 2).

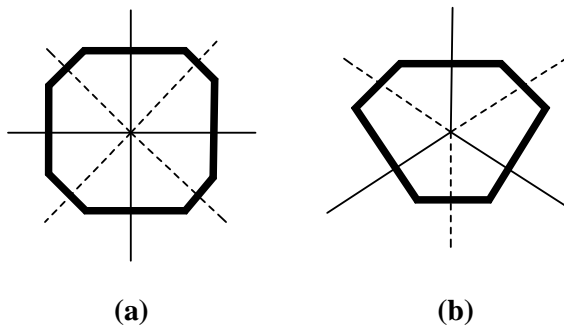


Figure 2. Dualization of the omnicapped faces around a four-degree (a) and three-degree (b) vertex

Leapfrog operation is exemplified in case of $M =$ Dodecahedron (Figure 3).

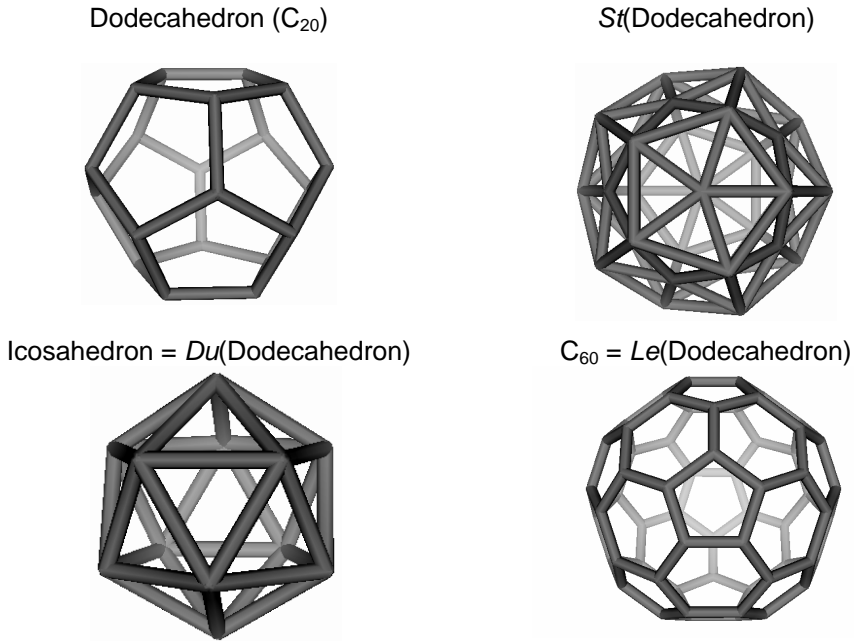


Figure 3. Leapfrog operation of a trivalent cage

Quadrupling Q is a transformation that preserves the initial orientation of all parent faces in the map.^{13,18,20} It is also called the *chamfering* transformation.²¹⁻²³

Q operation involves two π/s rotations, so that the initial orientation of the polygonal faces is conserved. Note that the quadrupling operation keeps the map vertices with their original valency. Clearly, the quadrupling transform of a four-valent map will not be anymore a regular graph.

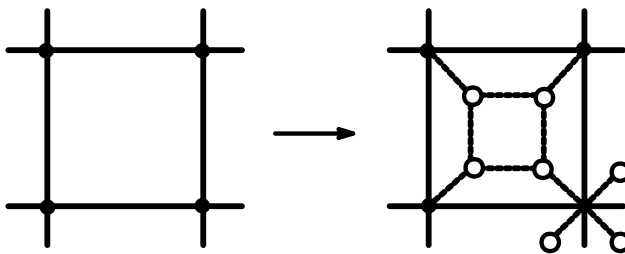


Figure 4. Quadrupling a square face of a four-valent map.

The transformed parameters are:^{13,18}

$$Q(M): \quad v = (d_0 + 1)v_0; \quad e = 4e_0; \quad f = f_0 + e_0 \quad (9)$$

Q may be written as a composite operation:

$$Q(M) = Du(Str(Me(M))) \quad (10)$$

where Str is a “reduced” St , with the meaning the triangles (e.g., those resulting by the medial operation) will not further be triangulated. This sequence of simple operations works well in trivalent maps M with no triangles.

The leapfrog and quadrupling operations can be used to get *isolate pentagons* in spherical fullerenes.²⁰

Dual of the stellation of a medial Dsm is related to the Q operation, differing by the inclusion of the classical stellation in its sequence:

$$Dsm(M) = Du(St(Me(M))) = Le(Me(M)) \quad (11)$$

It is just the leapfrog of the medial and works well in four-valent square maps (Figure 5), thus completing each other with Q . The operation was useful in the decomposition of the chamfering operation.

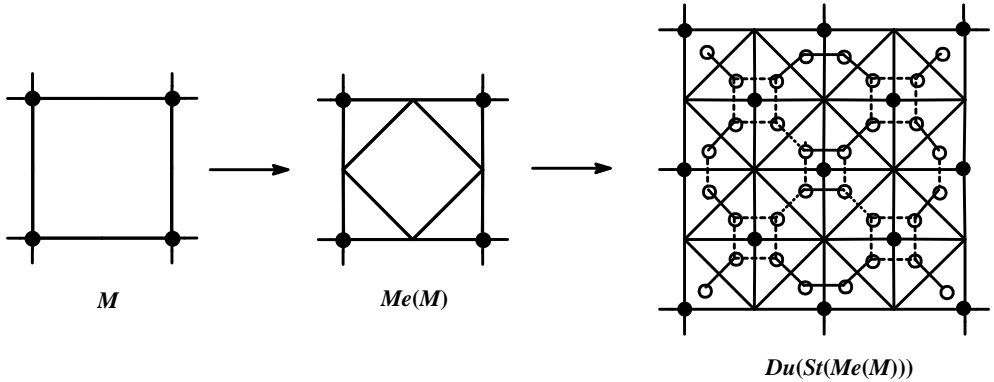


Figure 5. Dual of the stellation of a medial Dsm transformation of a square four-valent map.

It rotates the parent s -gonal faces by an even number of π/s , so that the original mutual orientation of edges-faces by Dsm is preserved. The transformed parameters are:^{12,17}

$$Dsm(M): v = 2d_0v_0 = 4e_0; e = 6e_0; f = f_0 + e_0 + v_0 \quad (12)$$

This operation, applied to square tiled tori, provided a $[4, 8]$ covering with a multiplication ratio of 8.^{13,18}

CAPRA OPERATION

Capra (the goat) is the Romanian corresponding of the *leapfrog* English children game. This name originates in a suggestion of A. T. Balaban about the *Le* operation. Thus, we call the herein proposed operation *Capra Ca*, which is defined as follows: put two points of degree two on each edge of the map (operation called *E2* in ref.¹⁵). Put a vertex in the center of each face of *M* and make (1, 4) connections, starting with a two-valent vertex. This operation we call *pentangulation Pe*, by analogy to the triangulation (see above). The last simple operation is a (reduced) truncation and thus:

$$Ca(M) = Trr(Pe(E2(M))) \quad (13)$$

It rotates the parent *s*-gonal faces by $\pi/2s$. The sequence above discussed is illustrated in Figure 6.

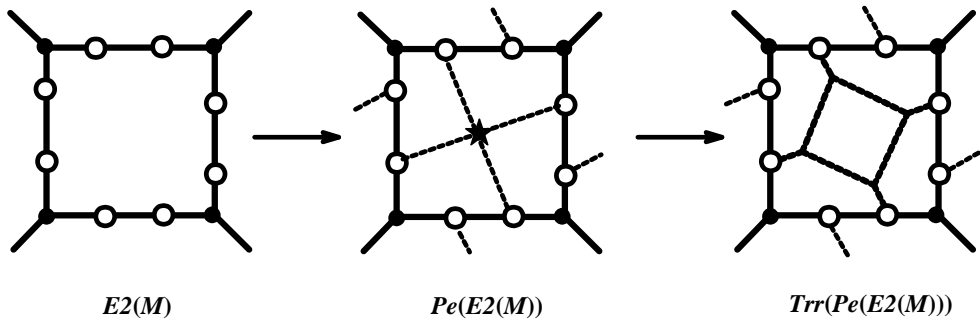


Figure 6. *Capra* as a sequence of elementary operations.

Ca-operation insulates each parent face by its own hexagons, in the opposite to *Le* and *Q*, in which two parent faces share one hexagon. It is illustrated Figure 7, for the cube.

Figure 8 illustrates the *capra* transformed of two other Platonic objects. Observe the clear difference between the regular trivalent lattice of C_{140} (*Ca*(Dodecahedron)) and that of C_{132} (*Ca*(Icosahedron)) which is an irregular net. It is due to the original five-valent vertices, preserved by *Ca*-operation (just as in case of *Q*) and dispersed among the newly introduced trivalent ones. In this last case, the triangles induce a strong positive curvature of the cage surface.

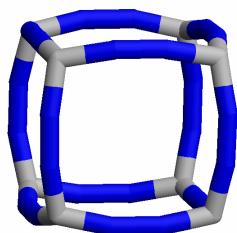
The transformed parameters are:

$$Ca(M): \quad v = (2d_0 + 1)v_0 = v_0 + 2e_0 + s_0f_0; \quad e = 3e_0 + 2s_0f_0; \quad f = (s_0 + 1)f_0 \quad (14)$$

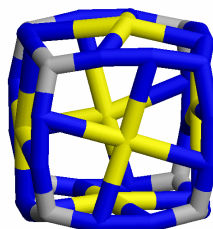
In case of a trivalent regular *M* the vertex multiplication ratio is 7. Clearly, maps/graphs of degree other than 3 will not be regular anymore (see Figure 8).

CAPRA – A LEAPFROG RELATED MAP OPERATION

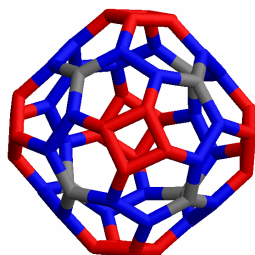
$E2(\text{Cube})$



$Pe(E2(\text{Cube}))$



$Trr(Pe(E2(\text{Cube})))$



$\text{Ca}(\text{Cube})$ – Schlegel projection

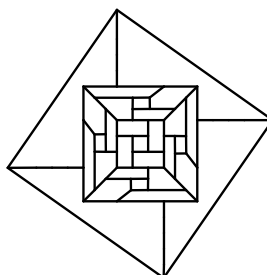
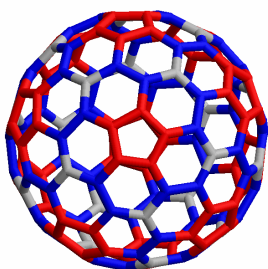


Figure 7. *Ca-operation in Cube and its Schlegel version*

$\text{Ca}(\text{Dodecahedron}) = C_{140}$



$\text{Ca}(\text{Icosahedron}) = C_{132}$

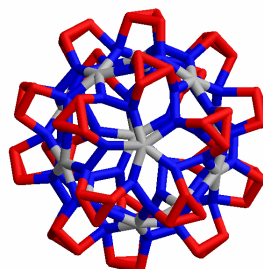


Figure 8. *Ca-operation in a trivalent- and a pentavalent-cage, respectively.*

A case apart is the open nanotubes (g changes from 0 (cylinder) to 1 (tube), by opening): $Tuz[c,n]$ (a "zig-zag" ($c/2,0$) tube)²⁴ and $Tua[c,n]$ (an "armchair" ($c/2,c/2$) tube), where c is the number of atoms in a cross-section while n is the number of cross-sections along the tube. The constitutive parameters for the tubes and Ca-transformed objects are given below:

$$\begin{array}{ll}
 \text{Tuz}[c,n] \quad v_0 = cn & v = v_0 + 2e_0 + 6f_0 = 7v_0 - 4c \quad (15) \\
 e_0 = cn + (c/2)(n-1) = v_0 + (v_0 - c)/2 & e = (21v_0 - 15c)/2 \\
 f_0 = (c/2)(n-1) = (v_0 - c)/2 & f = 7(v_0 - c)/2
 \end{array}$$

$$\begin{array}{ll}
 \text{Tua}[c,n] \quad v_0 = cn & v = 7v_0 - 8c \quad (16) \\
 e_0 = v_0 + v_0/2 - c & e = 21v_0/2 - 15c \\
 f_0 = v_0/2 - c & f = 7v_0/2 - 7c
 \end{array}$$

When the pentangulation starts with the second point of degree 2, the result of Ca operation is the enantiomeric pair of the object built up by the first point procedure. Thus, $(CaS(M) : CaR(M))$ represent a "racemic" pair, in the *sinister-rectus* chemical terms. All the non-specified Ca -transforms are $CaS(M)$. Figure 9 illustrates such a pair derived from the TUZ[8,3].

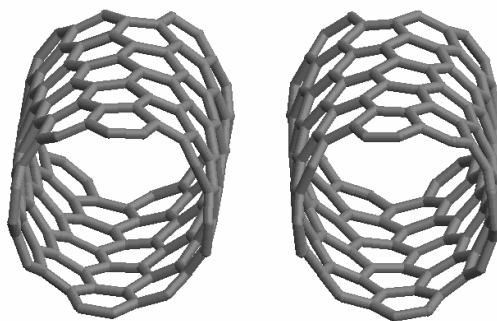


Figure 9. A "racemic" pair of Ca -transformed TUZ[8,3]

STRUCTURES WITH NEGATIVE CURVATURE

There exist natural materials, like zeolites, that show low density^{25,26} coming from their constitutive micro pores. These pores can be simulated, *e.g.*, by structures tessellated entirely by heptagons (*e.g.*, the Klein tessellation) embedded into infinite periodic surfaces of negative curvature of genus >1 .^{23,27-29}

Capra transformed cages are easily transformed into all-heptagonal nets by the $E1$ operation (*i.e.*, insertion of one two-valent vertex) applied to every edge resulted in the truncation step. Figure 9 illustrates this transformation in cube.

A new Ca -operation on the object in Figure 10, $Ca(Ca(\text{Cube})_{[7]}) = Ca_2(\text{Cube})_{[7]}$, will result in a more relaxed structure, illustrated as embeddings in the periodic surfaces of negative curvature, in 2D and 3D, in Figure 11.

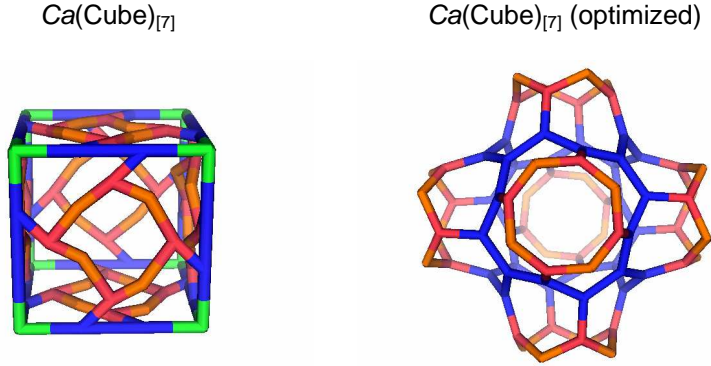


Figure 10. *E1 operation in Cube*

The iterative application of Ca needs some modifications of eq. (14). In this respect, $Ca_n(M)$ will denote the n^{th} iteration while $Ca_n(M)_{[7]}$ the iteration made on the $Ca(M)_{[7]}$ (i.e., the all heptagonal cage of negative curvature). Relations (1) and (2) are re-written as: $2e_0 = d_0v_0 = s_0f_0$. The transformed parameters for the iterative Ca are given in Table 1.

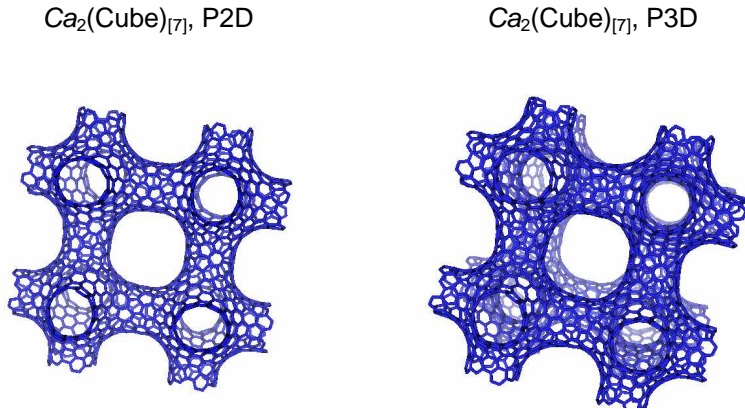


Figure 11. *Periodic surfaces of negative curvature, in 2D and 3D, respectively*

Note that, in case of the cube, the relation (20') is equivalent to (15), meaning $Ca_2(Cube)_{[7]}$ is equivalent with three interlacing *Tuz* nanotubes, following the rectangular 3D coordinates.

The $[7]$ tiling embedded in the dodecahedron leads, after appropriate capping, to the celebrate “phantasmagoric” ^[260]Fullerene of Fowler³⁰ (Figure 12).

Twice Ca -operation applied on both the primary Ca -transformed cage and $[7]$ tiling is illustrated in Figure 13, for the tetrahedron. Observe the two extremes: positive and negative curvatures, respectively, of the lattices originating in the same parent cage.

A sequence of CaS, CaR will provide non-twisted objects. More about this subject will be presented in a future paper.

Table 1.

The transformed parameters for the iterative Ca operation		
Operation	Parameter	eq
1 $Ca(M)$	$v_1 = (2d_0 + 1)v_0 = v_0 + 2e_0 + s_0f_0 = v_0 + 4e_0$ $e_1 = 7e_0$ $f_1 = (s_0 + 1)f_0 = f_0 + 2e_0$	(17)
2 $Ca(M)_{[7]}$	$v_{1[7]} = v_1 + s_0f_0 = v_0 + 6e_0$ $e_{1[7]} = 9e_0$ $f_{1[7]} = f_1 - f_0 = 2e_0$	(18)
3 $Ca_2(M)$	$v_2 = v_1 + 2e_1 + s_1f_1 = v_1 + 2e_1 + [6(s_0f_0) + s_0f_0]$ $= v_0 + 32e_0$ $e_2 = 7^2 \cdot e_0$ $f_2 = (s_1 + 1)f_1 = f_0 + 16e_0$ $v_2 = 7^2 \cdot v_0 ; d_0 = 3$	(19) (19')
4 $Ca_2(M)_{[7]}$	$v_{2[7]} = v_{1[7]} + 2e_{1[7]} + 7f_{1[7]} = v_0 + 38e_0$ $e_{2[7]} = 3v_0 + 108e_0$ $f_{2[7]} = (7 + 1)f_{1[7]} = 16e_0$ $v_{2[7]} = 7v_{1[7]} - 3(4e) ; M = \text{Cube}$	(20) (20')
5 $Ca_n(M)$	$v_n = 8v_{n-1} - 7v_{n-2} ; n \geq 2 ; d_0 > 3$ $v_n = 7^n \cdot v_0 ; d_0 = 3$ $e_n = 7^n \cdot e_0 = 7^n \cdot 3v_0 / 2$ $f_n = f_0 + (7^n - 1) \cdot v_0 / 2$	(21) (21') (21'') (21''')

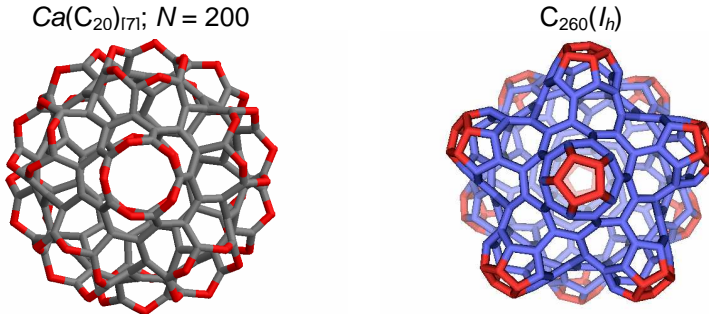


Figure 12. Capping the $[7]$ tiling of Dodecahedron results in the all $[5, 7] C_{260}$ cage of icosahedral symmetry

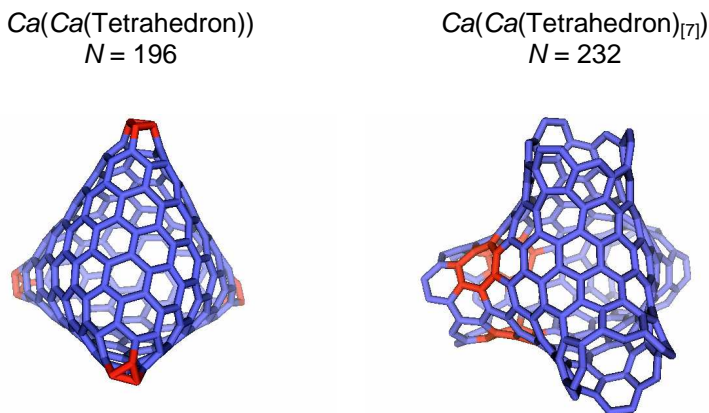


Figure 13. Two extremes: positive and negative curvatures, respectively, of the lattices coming, by Ca, from Tetrahedron

The genus of the $\text{Ca}(M)_{[7]}$ objects is calculable as follows:

$$\chi(M)_{[7]} = v_{1[7]} - e_{1[7]} + f_{1[7]} = 2 - 2g = v_0 - e_0 \quad (22)$$

$$g = (e_0 - v_0 + 2) / 2 = f_0 / 2 \quad (23)$$

Relation (23) comes from the spherical character of the parent polyhedron, for which $v_0 - e_0 + f_0 = 2$. Clearly, lattices with $g > 1$ will have negative $\chi(M)_{[7]}$ and consequently negative curvature. For the five Platonic solids, the genus of the corresponding $\text{Ca}(M)_{[7]}$ is: 2 (Tetrahedron); 3 (Cube); 4 (Octahedron); 6 (Dodecahedron) and 10 (Icosahedron).

SPECTRAL PROPERTIES INVOLVING Ca OPERATION

In simple Hückel theory,³² the energy of the i^{th} π -molecular orbital $E_i = \alpha + \lambda_i \beta$ is calculated on the grounds of the adjacency matrix associated to the molecular hydrogen depleted graph.

The π -electronic shells of neutral fullerenes are classified, function of their eigenvalue spectra, as:³¹ (i) *properly closed*, PC, when $\lambda_{N/2} > 0 \geq \lambda_{N/2+1}$; (ii) *pseudo-closed*, PSC, in case $\lambda_{N/2} > \lambda_{N/2+1} > 0$; (iii) *meta-closed*, MC, with $0 \geq \lambda_{N/2} > \lambda_{N/2+1}$ and (iv) *open*, OP, when the $N/2^{\text{th}}$ (HOMO) and $N/2+1^{\text{th}}$ (LUMO) molecular orbitals are degenerate, $\lambda_{N/2} = \lambda_{N/2+1}$. The gap is taken as the absolute value of the difference $E_{(\text{HOMO})} - E_{(\text{LUMO})}$. In nanotubes and tori, an open shell involving degenerate frontier orbitals: HOMO₋₁, HOMO, LUMO and LUMO₊₁ is called metallic M.

Ca-operation, applied on a finite structure, leaves unchanged its π -electronic shells. There exist exceptions, the most notably being the transformed $Ca(Tuz/a[c,n])$ of nanotubes (for symbols see ref. 33) which all have PC shell disregarding the character of their parent shell. Table 2 lists some examples in nanotubes and tori.

In the opposite, *Le* provides PC shell in fullerenes^{15,34} and M shell in tori.³⁴ The other classical operation *Q* is, however, closer to *Ca*, both as construction and spectral aspects.

Interesting results are obtained in the Platonic polyhedra and their *Ca*-transforms (Table 3). The twice $Ca(M)_{[7]}$ would be low energy forms of carbon,^{28,29} with exceeding electrons (see the last column in Table 3) in some degenerate antibonding orbitals. It is predicted to be electron-donating structures which stabilize as cations. No major modifications appear, in the spectrum of such objects, when $CaS(CaS(M)_{[7]})$ is changed by $CaR(CaS(M)_{[7]})$, see Table 3. Details will be given in a future paper.

Calculations of eigenvalues and map operations were made by TopoCluj 2.0 and CageVersatile 1.1 original softwares.^{35,36}

Table 2.
Spectral data of nanotubes $Tuz/a[c,n]$ and tori $Z/A[c,n]$
and their *Ca*-transforms

	Structure	<i>N</i>	HOMO ₋₁	HOMO	LUMO	LUMO ₊₁	Gap	Shell
1	Tuz[8,4]	32	0.705	0	0	-0.705	0	OP
2	Ca(Tuz[8,4])	192	0.273	0.017	-0.017	-0.273	0.034	PC
3	Tuz[10,4]	40	0.095	0.095	-0.095	-0.095	0.190	PC
4	Ca(Tuz[10,4])	240	0.064	0.064	-0.064	-0.064	0.129	PC
5	Tua[4,8]	32	0.532	0	0	-0.532	0	OP
6	Ca(Tua[4,8])	192	0.265	0.024	-0.024	-0.265	0.048	PC
7	Tua[4,10]	40	0.310	0.169	-0.169	-0.310	0.338	PC
8	Ca(Tua[4,10])	248	0.132	0.095	-0.095	-0.132	0.189	PC
9	Z[8,10]	80	0.414	0.414	-0.414	-0.414	0.828	PC
10	Ca(Z[8,10])	560	0.169	0.169	-0.169	-0.169	0.337	PC
11	A[8,12]	96	0	0	0	0	0	M
12	Ca(A[8,12])	672	0	0	0	0	0	M

Table 3.
Spectral data of the Platonic polyhedra and their *Ca*-transforms

	Structure	HOMO ₋₁	HOMO	LUMO	LUMO ₊₁	Gap	Shell	Ex. e
1	<i>M</i> = Tetrahedron	3	-1	-1	-1	0	OP	
	$Ca(M)_{[7]}$	0.154	0.154	0.154	-0.614	0	OP	
	$CaS(CaS(M)_{[7]})$	-0.005	-0.005	-0.005	-0.306	0	OP	4
	$CaR(CaS(M)_{[7]})$	-0.010	-0.010	-0.010	-0.325	0	OP	4
2	<i>M</i> = Cube	1	1	-1	-1	2	PC	
	$Ca(M)_{[7]}$	0	0	0	-0.188	0	OP	
	$CaS(CaS(M)_{[7]})$	-0.010	-0.010	-0.127	-0.127	0.117	MC	6
	$CaR(CaS(M)_{[7]})$	-0.004	-0.004	-0.141	-0.141	0.137	MC	6

	Structure	HOMO ₋₁	HOMO	LUMO	LUMO ₊₁	Gap	Shell	Ex. e
3	<i>M</i> = Dodecahedron	1	0	0	0	0 OP		
	<i>Ca</i> (<i>M</i>) _[7]	0	0	0	-0.165	0 OP		
	<i>CaS</i> (<i>CaS</i> (<i>M</i>) _[7])	-0.069	-0.069	-0.069	-0.131	0 OP		6
	<i>CaR</i> (<i>CaS</i> (<i>M</i>) _[7])	-0.070	-0.070	-0.070	-0.138	0 OP		6
4	<i>M</i> = Octahedron	0	0	0	-2	0 OP		
	<i>Ca</i> (<i>M</i>) _[7]	0.222	0	0	0	0 OP		
	<i>CaS</i> (<i>CaS</i> (<i>M</i>) _[7])	0.008	-0.044	-0.044	-0.044	0 OP		2
	<i>CaR</i> (<i>CaS</i> (<i>M</i>) _[7])	0.021	-0.058	-0.058	-0.058	0 OP		2
5	<i>M</i> = Icosahedron	-1	-1	-1	-1	0 OP		
	<i>Ca</i> (<i>M</i>) _[7]	0.101	0.101	0.101	0.101	0 OP		
	<i>CaS</i> (<i>CaS</i> (<i>M</i>) _[7])	-0.022	-0.022	-0.022	-0.022	0 OP		6
	<i>CaR</i> (<i>CaS</i> (<i>M</i>) _[7])	-0.029	-0.029	-0.029	-0.029	0 OP		6

CONCLUSIONS

A new operation on maps, called *Capra Ca*, was proposed and discussed in comparison with the well-known leapfrog *Le* and quadrupling *Q* operations. Note that the Goldberg^{37,38} relation: $m = (a^2 + ab + b^2)$; $a \geq b$; $a + b > 0$ predicts our operation in the series: *Le*: (1, 1), $m = 3$; *Q*: (2, 0), $m = 4$ and *Ca*: (2, 1), $m = 7$.

Ca-operation insulates each parent face by its own hexagons (*i.e.*, coronene-like substructures), in contrast to *Le* and *Q*. The transformed constitutive parameters were given.

The utility of this operation is in building of large cages that preserve the symmetry and spectral properties of the parent structures and in extremely facile access to several constructions with negative curvature.

Clearly, many other authors have used such a transformation but no paper, in our best knowledge, has been devoted so far.

Acknowledgements. This paper was supported by the Romanian CNCSIS GRANT 2003.

REFERENCES

1. K. Tanaka, T. Yamabe, and K. Fukui, *The science and technology of carbon nanotubes*, Elsevier, 1999.
2. M. Endo, S. Iijima and M. S. Dresselhaus, *Carbon Nanotubes*, Pergamon, 1996.
3. M. S. Dresselhaus, G. Dresselhaus, and P. C. Eklund, *Science of fullerenes and carbon nanotubes*, Acad. Press, San Diego, 1996.
4. Taylor, R., Ed., *The chemistry of fullerenes*, World Scientific: Singapore, 1995.
5. P. W. Fowler and D. E. Manolopolous, *An atlas of fullerenes*, Oxford University Press, Oxford, U.K., 1995.
6. Y. D. Gao and W. C. Herndon, *J. Amer. Chem. Soc.*, **1993**, *115*, 8459.
7. P. W. Fowler, T. Heine, D. E. Manolopoulos, D. Mitchell, G. Orlandini, R. Schmidt, G. Seiferth and F. Zerbetto, *J. Phys. Chem.*, **1996**, *100*, 6984.

8. A. Müller, P. Kögerler, and Ch. Kuhlmann, *J. Chem. Soc., Chem. Commun.*, **1999**, 1347-1358.
9. T. Pisanski, and M. Randić, in *Geometry at Work*, M. A. A. Notes, **2000**, 53, 174-194.
10. P. W. Fowler and T. Pisanski, *J. Chem. Soc. Faraday Trans.* **1994**, 90, 2865-2871.
11. L. Euler, *Comment. Acad. Sci. I. Petropolitanae*, **1736**, 8, 128-140
12. F. Harary, *Graph Theory*. Addison-Wesley, Reading, MA, **1969**.
13. M. V. Diudea, and P. E. John, *Commun. Math. Comput. Chem. (MATCH)*, **2001**, 44 103-116.
14. P. W. Fowler, *Phys. Lett.*, **1986**, 131, 444.
15. P. W. Fowler and J. I. Steer, *J. Chem. Soc., Chem. Commun.*, **1987**, 1403-1405.
16. P. W. Fowler and K.M.Rogers, *J. Chem. Soc., Faraday Trans.*, **1998**, 94, 1019-1027.
17. P. W. Fowler and K.M.Rogers, *J. Chem. Soc., Faraday Trans.*, **1998**, 94, 2509-2514.
18. M. V. Diudea, P. E. John, A. Graovac, M. Primorac, and T. Pisanski, *Croat. Chem. Acta*, **2003**, 76, 153-159.
19. G. Brinkmann, P. W. Fowler, and M. Yoshida, *MATCH Commun. Math. Comput. Chem.*, **1998**, 38, 7-17.
20. P. W. Fowler, J. E. Cremona, and J. I. Steer, *Theor. Chim. Acta*, **1988**, 73, 1.
21. A. Deza, M. Deza and V. P. Grishukhin, *Discrete Math.*, **1998**, 192, 41-80.
22. M. Goldberg, *Tôhoku Math. J.*, **1934**, 40, 226-236.
23. A. Ceulemans, R.B. King, S. A. Bovin, K. M. Rogers, A Troisi, and P. W. Fowler, *J. Math. Chem.*, **1999**, 26, 101-123.
24. A. L. Ivanovskii, *Russ. Chem. Rev.*, **1999**, 68, 103-118.
25. R. B. King, *J. Phys. Chem.*, **1996**, 100, 15096-15104.
26. R. B. King, *J. Chem. Inf. Comput. Sci.*, **1998**, 38, 180-188.
27. R. B. King, *Croat. Chem. Acta*, **2002**, 75, 447-473.
28. M. O'Keeffe, G. B. Adams and O. F. Sankey, *Phys. Rev. Lett.*, **1992**, 68, 2325-2328.
29. T. Lenosky, X. Gonze, M. Teter and V. Elser, *Nature*, **1992**, 355, 333-335.
30. A. Dress and G. Brinkmann, *MATCH- Commun. Math. Comput. Chem.*, **1996**, 33, 87-100.
31. P. W. Fowler and T. Pisanski, *J. Chem. Soc., Faraday Trans.*, **1994**, 90, 2865-2871.
32. E. Hückel, *Z. Phys.*, **1931**, 70, 204.
33. M. V. Diudea, T. S. Balaban, E. C. Kirby, and A. Graovac, *Phys. Chem. Chem. Phys.*, **2003**, in press.
34. M. Yoshida, M. Fujita, P. W. Fowler and E. C. Kirby, *J. Chem. Soc., Faraday Trans.*, **1997**, 93, 1037-1043.
35. M. V. Diudea, O. Ursu, and C. L. Nagy, "Babes-Bolyai" University, **2002**.
36. M. V. Diudea and M. Stefu, "Babes-Bolyai" University, **2002**.
37. M. Goldberg, *Tôhoku Math. J.*, **1937**, 43, 104-108.
38. M. Dutour and M. Deza, LIGA, ENS/CNRS, Paris, **2003** (preprint).

NANOTUBE COVERING MODIFICATION

MIRCEA V. DIUDEA

*Faculty of Chemistry and Chemical Engineering
"Babes-Bolyai" University, 400028 Cluj, ROMANIA
E-mail: diudea@chem.ubbcluj.ro*

ABSTRACT. Nanotube tiling can be modified, from the polyhex [6] to [4, 8] and [5, 7] coverings, by following various routes for the well-known Stone-Wales SW edge rotation. The interchanging of Z[6] to A[6] and vice-versa is, for the first time, shown to proceed via an R[4, 8] intermediate, by SW isomerization. A new "azulenic" [5, 6, 7] covering is proposed. Isomerization routes are given in terms of edge-rotating operators, *i.e.*, lattice row-column numbers associated to the edge endpoints of the repeat units in the parent net.

INTRODUCTION

Nanotubes are uni-dimensional carbon allotropes, tessellated entirely by hexagons and thus being closest to the graphite among all the graphitoids. They are obtained from graphite by several techniques,¹⁻³ and show unusual properties (electronic, optical, mechanical, catalytic or capillarity), with no known analogy in nature. An intensive experimental and theoretical research on nanotubes is nowadays developing. Carbon nanostructures became part of real chemistry: they have been functionalized or inserted in supramolecular assemblies.

A Stone-Wales⁴ edge rotation is illustrated in Figure 1. The SW-edge (in bold) shares two cycles of size (s_m, s_n) to be reduced, after rotation, to (s_{m-1}, s_{n-1}) . Correspondingly, the two cycles joined by the SW-edge will increase their size from (s_p, s_r) to (s_{p+1}, s_{r+1}) .

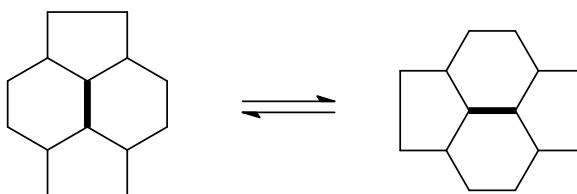


Figure 1. *Pyracylenic (Stone-Wales) isomerization*

This paper presents some isomerization ways of [6] lattice, embedded in the cylinder, leading to some more energy rich nets, seen as possible intermediates in recovering the parent [6] structure, eventually in its pairing embedding isomer. Isomerization routes, leading to known or new coverings are also presented.

ISOMERIZING [6] NANOTUBES

Covering⁵ transformation is one of the ways in understanding chemical reactions occurring in fullerenes.⁶⁻⁸

Let $Z[6]$ be embedded in the cylinder, as $ZC_6[c, n]$, or the "zig-zag" ($c/2, 0$) nanotube,⁹⁻¹¹ Figure 2. Similarly, the embedding of $A[6]$ is $AC_6[c, n]$, and the nanotube is called "armchair", Figure 3.

Let denote by $H_{(i,j),(p,r)}$ the edges lying parallel to the horizontally oriented tube generator, in the schematic lattice representation; the first subscript bracket encodes the relative location of the start-point of rotating edges along the tube while the second one the location of edges around the tube. Mark $V_{(i,j),(p,r)}$ the edges lying perpendicular to the tube generator. The marked edges will be rotated in the following isomerization and the above symbols play the role of a true rotational operator, as shown in the following.

The polyhex [6] covering is transformed into the "rhomboidal-bathroom-floor" tiling¹² $R[4, 8]$, by operations:

$$H_{(1,3),(1,3)}(Z[6]) = R[4, 8] = V_{(1,3),(1,3)}(A[6]) \quad (1)$$

and the corresponding products are illustrated in Figures 2 and 3. The starting objects in these figures represent pair isomers of different embeddings, in the cylinder, of the same net having $16 \times 8 = 128$ atoms.

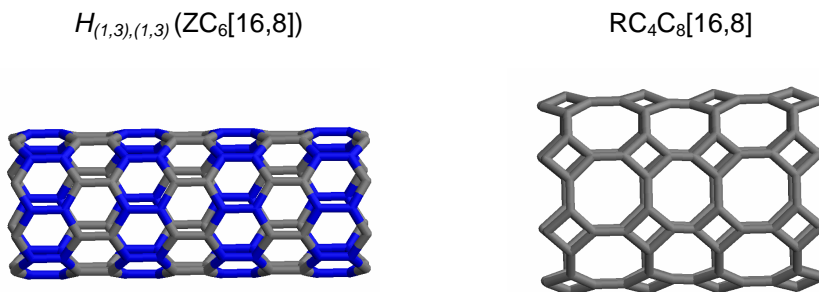


Figure 2. A ZC_6 nanotube of 128 atoms and its SW isomer.

When the SW isomerization follows a spiral path, like that illustrated in Figure 4, the product is, after optimization by an MM procedure, a "squared-bathroom-floor" $SC_4C_8[c, n]$ lattice.¹³ The operation can be written as:

$$V_{(1,5),(1,5)}(Z[6]) = S[4, 8] \quad (2)$$

Similarly, the operation:

$$V_{(1,5),(1,5),1a}(Z[6]) = SP[5, 7] \quad (3)$$

leads to a spiral $SPC_5C_7[c, n]$ net,¹⁴ Figure 5. Note the combination $V\&Z$, for describing a spiral path and the subscript $1a$ for a "leave one row/column out" way in getting an "alternating" spiral net.

NANOTUBE COVERING MODIFICATION

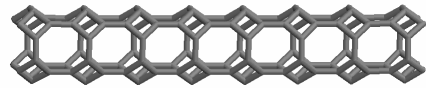
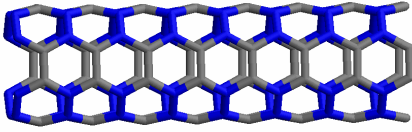
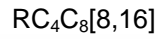
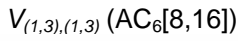


Figure 3. An AC_6 nanotube of 128 atoms and its SW isomer.

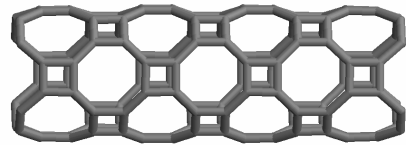
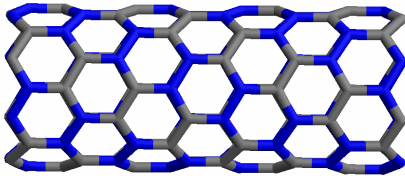
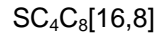
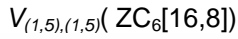


Figure 4. A spiral path of SW edge rotation

The same operations can be done by the $A[6]$ net thus resulting the corresponding pair embedding isomers.

Different azulenic [5, 7] lattices can be obtained by the following operations:

$$H_{(1,5),(1,5)}(Z[6]) = V[5, 7] \quad (4)$$

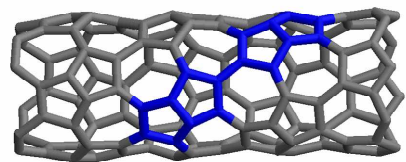
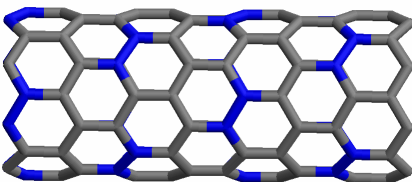
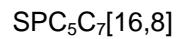
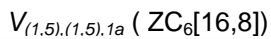


Figure 5. A spiral path of SW edge rotation and its spiral net product

$$V_{(1,5),(1,5)}(A[6]) = H[5, 7] \quad (5)$$

These coverings will be illustrated in the next section.

ISOMERISING [4, 8] NANOTUBES

The [4, 8] covering, particularly $R[4, 8]$, transforms to either AC_6 or ZC_6 net by operations:

$$H_{(1,4),(1,4)}(R[4, 8]) = A[6] \quad (1')$$

$$V_{(1,4),(1,4)}(R[4, 8]) = Z[6] \quad (1'')$$

as a unique intermediate of the [6] net isomerization (the different embeddings disregarded).

Other isomerizations of this covering are:

$$H_{(1,7),(1,7)}(R[4, 8]) = H[5, 7] \quad (6)$$

$$V_{(1,7),(1,7)}(R[4, 8]) = V[5, 7] \quad (7)$$

the corresponding objects being illustrated in Figure 6. Note that the pentaheptite $H/V[5, 7]$ lattice is encountered in the chemical net of $ThMoB_4$.¹⁵ It is a *2-isohedral* tiling,¹⁶ (*i.e.*, it has only two face orbits), with the local signature $(t_5, t_7) = (1, 3)$, meaning every pentagon has t_5 pentagonal neighbors and every heptagon has t_7 heptagonal neighbors. Crespi *et al.*¹⁷ have stated that such nanotubes would be metallic.

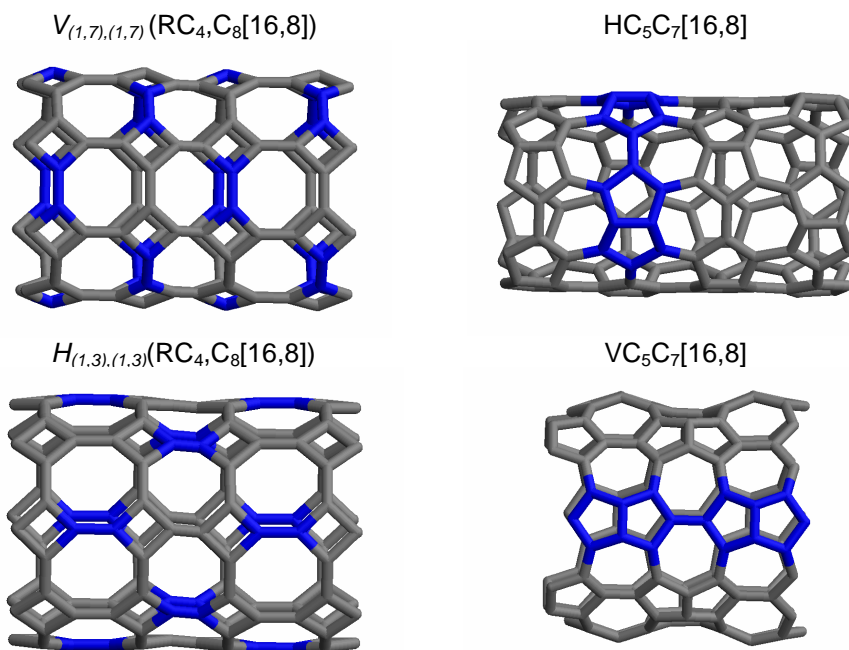


Figure 6. SW isomerization of $RC_4,C_8[16,8]$ resulting two embedding isomers of the $H/V[5, 7]$ lattice.

Other combinations of SW rotation, on R[4, 8], are as follows:

$$V_{(1,3),(1,6)}(H_{(1,4),(1,7)}(R[4, 8])) = HA[5, 7] \quad (8)$$

$$H_{(1,6),(1,3)}(V_{(1,7),(1,4)}(R[4, 8])) = VA[5, 7] \quad (9)$$

the objects being presented in Figures 7 and 8, respectively. The net is a 2-*isohedral* tiling and has the signature [2, 4]. It is a periodic (*i.e.*, face-regular) covering, described as capped tubulenes elsewhere.¹⁸

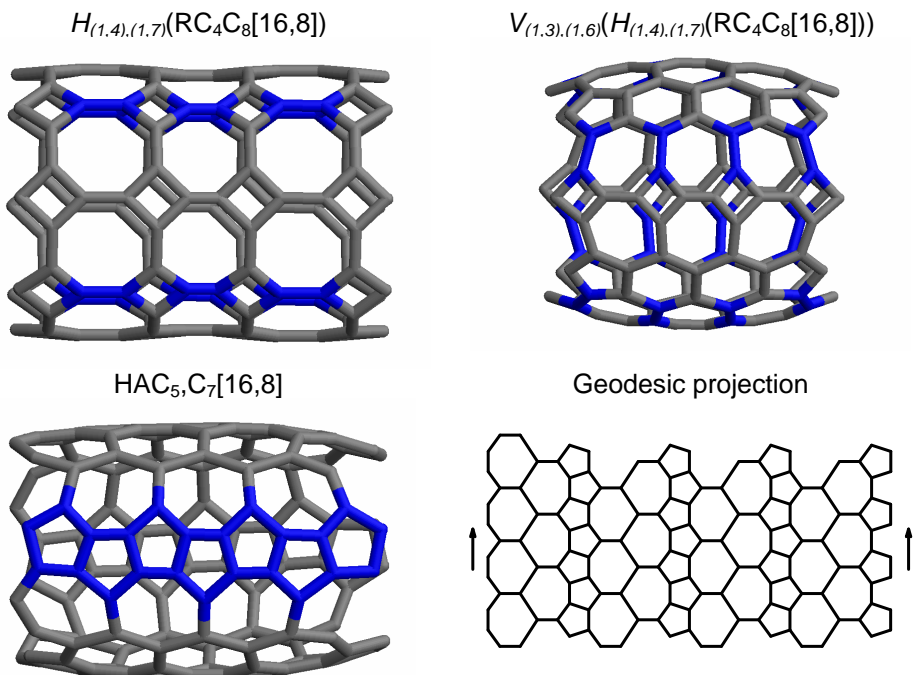


Figure 7. The pathway to HA[5, 7] lattice.

Geodesic projections are useful in understanding the connectivity in a lattice embedded in a given surface.

Other isomerizations are derivable from the above ones:

$$V_{(1,5),(1,6)}(H_{(1,4),(1,7)}(R[4, 8])) = HA[5, 6, 7] \quad (10)$$

$$H_{(1,6),(1,5)}(V_{(1,7),(1,4)}(R[4, 8])) = VA[5, 6, 7] \quad (11)$$

and the objects are presented in Figures 9 and 10. This novel lattice has the local signature: $t_{5j}(0, 4, 1)$; $t_{6j}(2, 2, 2)$; and $t_{7j}(1, 4, 2)$, $j = 5, 6, 7$. It is a “fully azulenoid” covering, in the terminology of Kirby.¹⁹

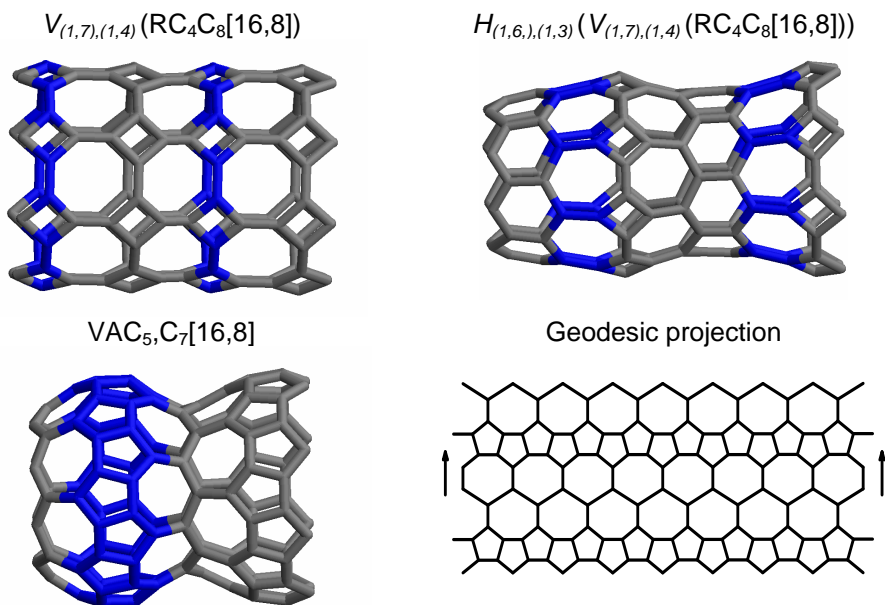


Figure 8. The pathway to $\text{VA}[5, 7]$ lattice.

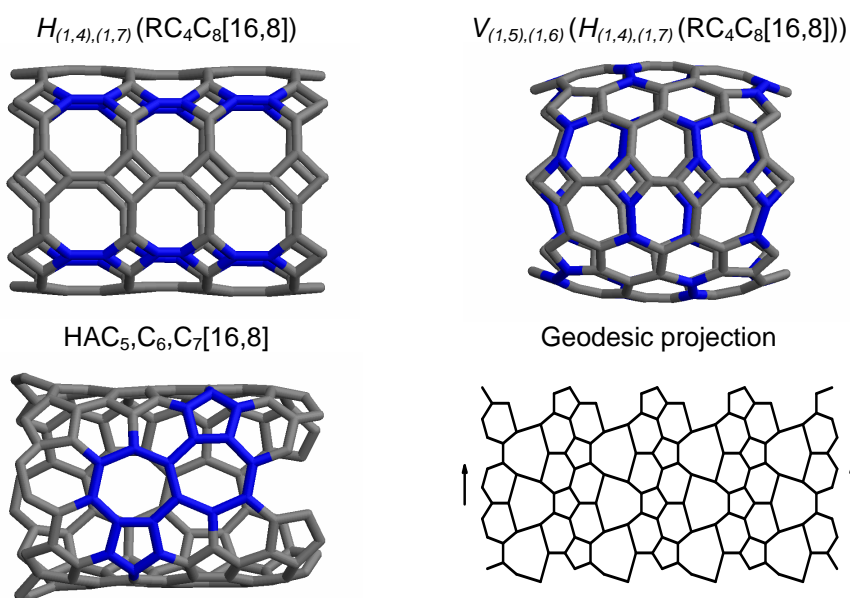


Figure 9. The pathway to $\text{HA}[5, 6, 7]$ lattice.

Note that the $[4, 8]$ lattices are deductible from the primary square covering, embedded in the cylinder, by some basic operations on maps.^{20, 21} Such non-chemical transformations will be discussed in a future paper.

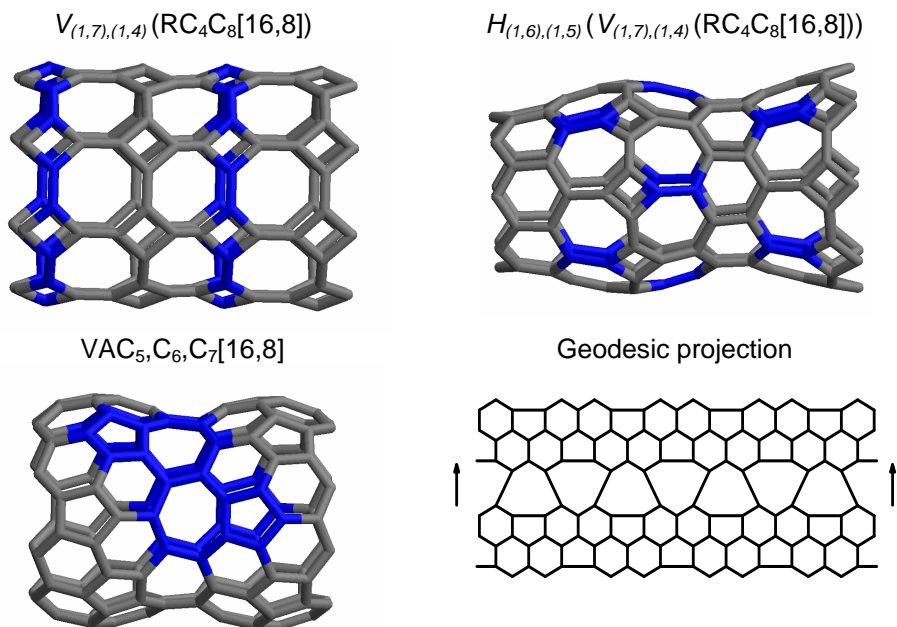


Figure 10. The pathway to VA[5, 6, 7] lattice.

ENERGETICS AND SPECTRAL PROPERTIES

In the simple Hückel molecular orbital HMO theory,²² the energy of the i^{th} molecular orbital $E_i = \alpha + \lambda_i \beta$ is calculated from the eigenvalues λ_i of the adjacency matrix associated with the molecular hydrogen-depleted graph. The π -electronic shells of neutral molecules are classified, according to their eigenvalue spectra, as:²³ (i) *properly closed*, PC, when $\lambda_{N/2} > 0 \geq \lambda_{N/2+1}$; (ii) *pseudo-closed*, PSC, when $\lambda_{N/2} > \lambda_{N/2+1} > 0$ and (iii) *open*, OP, when HOMO-LUMO molecular orbitals are degenerate, $\lambda_{N/2} = \lambda_{N/2+1}$ and the HOMO-LUMO gap (taken as the absolute value of the difference $E_{\text{HOMO}} - E_{\text{LUMO}}$, in $|\beta|$ units) vanishes.

The metallic M character (a property taken from the Solid State Physics) is associated with an open shell π -electronic structure having four non-bonding orbitals (NBOs = zero eigenvalues), a condition reached by the graphite sheet and some tori and nanotubes.²⁴

The spectral data of the herein discussed nanotubes are listed in Table.

As shown in Table, various coverings provide different π -electronic shells. Their π -energy E_π is calculated as:²⁵

$$E_\pi = \alpha \cdot n_e + \beta \cdot \sum_{i=1}^N g_i \cdot \lambda_i \quad (6)$$

where α and β are the standard HMO parameters, n_e is the number of π -electrons, while g_i is the occupation number of the i^{th} molecular orbital.

TableSpectral properties and energy per atom: E_π ($|\beta|$) and E-MM (kcal/mol).

	Structure	HOMO ₋₁	HOMO	LUMO	LUMO ₊₁	Gap	Shell	E_π	E-MM
1	AC ₆ [8,24]	0.148	0.072	-0.072	-0.148	0.143	PC	1.550	3.567
2	ZC ₆ [16,12]	0.017	0	0	-0.017	0.000	OP	1.542	2.444
3	VC ₅ C ₇ [8,24]	0.184	0.139	0.107	0.048	0.032	PSC	1.510	6.939
4	HC ₅ C ₇ [16,12]	0.212	0.198	0.141	0.141	0.057	PSC	1.501	4.059
5	HC ₅ C ₇ [8,24]	0.187	0.121	0.121	0.099	0	OP	1.514	8.903
6	SPC ₅ C ₇ [16,12]	0.202	0.093	0.093	0.018	0.000	OP	1.507	5.045
7	SC ₄ C ₈ [16,12]	0.042	0.042	-0.042	-0.042	0.084	PC	1.455	11.185
8	RC ₄ C ₈ [16,12]	0	0	0	0	0	M	1.441	10.641
9	RC ₄ C ₈ [8,24]	0	0	0	0	0	M	1.454	14.325
10	HAC ₅ C ₇ [16,12]	0.184	0.018	0.018	0	0	OP	1.499	6.705
11	HAC ₅ C ₆ C ₇ [16,12]	0	-0.004	-0.004	-0.029	0	OP	1.508	3.373
12	C ₆₀	0.618	0.618	-0.139	-0.139	0.757	PC	1.553	4.460

The total π -electron energy, has a topological essence by the spectral parameter λ_i . Taking $\alpha = 0$ (the reference energy) and $\beta = 1$ (the unity energy), it is immediate $E_\pi = \lambda_i$. It has been shown²⁶ that E_π is proportional not only to the π -, but also the σ -electron energy of the C-C bonds. In the absence of large steric strain in the carbon skeleton, E_π can be used for calculating several thermodynamic functions of chemical compounds. In the case of conjugated benzenoid hydrocarbons, the enthalpies calculated by using the total π -electron energy have been found closer to the experimental values than the values computed by some highly parametrized molecular-mechanics MM and semiempirical procedures.²⁵

The "topological resonance energy" TRE of Aihara²⁷⁻²⁹ and Gutman *et al.*^{30,31} is defined as the difference $E_\pi - E_{ref}$ between the total π -energy of a conjugated (aromatic) system and the energy of some reference structures (also calculated by a topological background). The systems having TRE > 0 are classified as "aromatic", those having TRE < 0 as "antiaromatic" while those for which TRE \approx 0 as "non-aromatic". Figure 10 illustrates the plot of the π -energy vs the MM+ energy of the herein discussed nanotubes.

Keeping in mind the (-) sign of β parameter, the plot in Figure 10 clearly indicates a proportionality between E_π and the total MM+ energy, which accounts for the energy of σ -frame rather than for that of π -electrons.

The A[6] covering (Table, entry 1), appears to be the most aromatic structure (compare with C₆₀, Table, entry 12), even though the MM energy of its open nanotube embedding is somewhat higher than that corresponding to Z[6] (Table, entry 2). This is due to a higher strain energy of its σ -frame.

The next are the pentaheptite [5, 7] lattices (Table, entries 3-6), for which "azulenic" polarization is expected. The same comments as for A[6] are true for V[5, 7] in the sub-set of azulenic nets. As above mentioned, the tubes H/VC₅C₇ are expected to be metallic; our results indicate this character is conditioned by the tube dimensions (particularly the c-dimension – see the PSC/OP variation of their shell - Table).

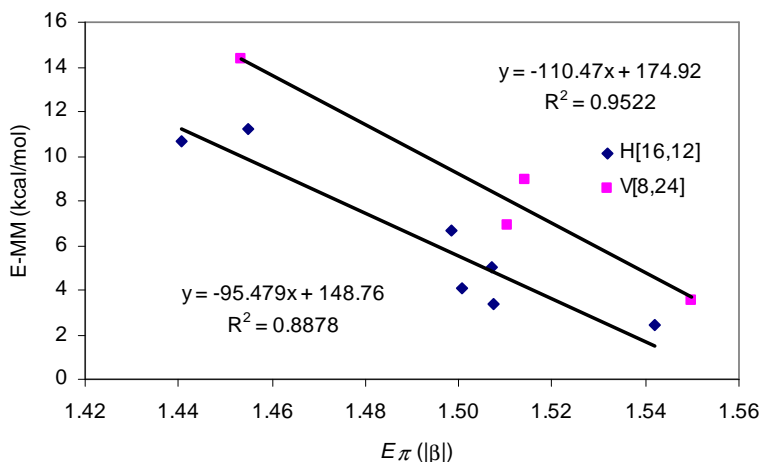


Figure 10. The plot of the π -energy vs the MM+ energy in nanotubes of various covering

The [4, 8] coverings (Table, entries 8 and 9) show the lowest stability among the lattices herein discussed. The most interesting seems the R[4, 8] net, capable to isomerize in all but spiral discussed lattices. It has a metallic π -shell and the lowest E_{π} suggesting no conjugation, a normal fact for an anti-aromatic structure.

An intriguing electronic structure shows $HAC_5C_6C_7[16,12]$ (Table, entry 11), which frontier orbitals are antibonding (near non-bonding) and degenerate. Its low E_{π} could be explained by the "azulenic" conjugation of the isolated C_5C_7 pair as well as by the low strain energy of its skeleton, relaxed by means of the negatively curved heptagons (see the low value of MM energy). Note that the $HAC_5C_6C_7[12,4]$ repeat unit can be capped by two hexagons to give the fullerene C_{60} ; thus, the tube $HAC_5C_6C_7[12,n]$ is a true C_{60} -like periodic nanostructure. Their electronic properties depend, however, of the tube dimensions.

Molecular modeling was performed on a 2x1GHz Pentium III PC using the MM+ force field, with the parametrization supplied by HyperChem software (version 4.5, Hypercube, Inc.).³² Structures were optimized by using the Polak-Ribier conjugate-gradient method, the energy minimization was terminated at an RMS gradient <0.01 kcal/(Å·mol) for all structures. Spectral data were calculated by the TOPOCLUJ software package.³³ The Stone-Wales edge rotations have been performed by the CageVersatile 1.1 original program.³⁴

CONCLUSIONS

The coverings herein discussed all are face-regular or periodic structures. Nanotube tiling can be modified from the polyhex [6] to [4, 8] which seems to be a crucial intermediate between pure [6] and mixed [5, 7], [5, 6, 7] etc. The Stone-Wales SW edge rotation is the tool that makes possible the tiling modification. As shown elsewhere,⁷ cascade SW rotations are true chemical reactions and their products have to be looked for in the soot of vaporized graphite.

Acknowledgement. This paper was supported by a Romanian CNCSIS 2003 GRANT.

REFERENCES

1. M. Endo, S. Iijima and M. S. Dresselhaus, *Carbon Nanotubes*, Pergamon, **1996**.
2. M. S. Dresselhaus, G. Dresselhaus, and P. C. Eklund, *Science of fullerenes and carbon nanotubes*, Acad. Press, San Diego, **1996**.
3. K. Tanaka, T. Yamabe, and K. Fukui, *The science and technology of carbon nanotubes*, Elsevier, **1999**.
4. A. J. Stone and D. J. Wales, *Chem. Phys. Lett.* **1986**, *128*, 501-503.
5. B. Grünbaum and G. C. Shephard, *Tilings and Patterns*, Freeman, New York, **1985**.
6. D. J. Klein and H. Zhu, in: A. T. Balaban, (Ed.), *From Chemical Topology to Three - Dimensional Geometry*, Plenum Press, New York, **1997**, pp. 297-341.
7. Y. Zhao, B. I. Yakobson, and R.E. Smalley, *Phys. Rev. Lett.*, **2002**, *88*, 185501.
8. M. Deza, P. W. Fowler, M. Shtorgin, and K. Vietze, *J. Chem. Inf. Comput. Sci.*, **2000**, *40*, 1325-1332.
9. A. L. Ivanovskii, *Russ. Chem. Rev.*, **1999**, *68*, 103-118.
10. M. V. Diudea, O. Ursu, and B. Parv, *Studia Univ. "Babes-Bolyai"*, **2003**, *48*, 11-20.
11. M. V. Diudea, T. S. Balaban, E. C. Kirby, and A. Graovac, *Phys. Chem., Chem. Phys.*, **2003** (in press).
12. M. Stefu and M. V. Diudea, *MATCH Commun. Math. Comput. Chem.*, **2003** (in press).
13. M. V. Diudea, B. Parv, P. E. John, O. Ursu, and A. Graovac, *MATCH Commun. Math. Comput. Chem.*, **2003**, *49*, 23-36.
14. M. V. Diudea, B. Parv, and E. Kirby, E. C. *MATCH Commun. Math. Comput. Chem.*, **2003**, *47*, 53-70.
15. M. O'Keeffe and B. G. Hyde, *Crystal Structures*, Mineralogical Society of America, Washington DC, **1996**.
16. B. Grünbaum, H. D. Löckenhoff, G. C. Shephard, and A. Temesvari, *Geom. Dedicata*, **1985**, *19*, 109-174.
17. V. H. Crespi, L. X. Benedict, M. L. Cohen, and S. G. Louie, *Phys. Rev. B*, **1996**, *53*, 13303-13305.
18. M. V. Diudea, I. Silaghi-Dumitrescu, and A. Graovac, *Croat. Chem. Acta*, **2003** (submitted).
19. E.C. Kirby, *MATCH Commun. Math. Comput. Chem.* **1996**, *33*, 147-156.
20. M. V. Diudea, P. E. John, A. Graovac, M. Primorac, and T. Pisanski, *Croat. Chem. Acta*, **2003**, *76*, 153-159.
21. M. V. Diudea, *PCCP*, **2002**, *4*, 4740-4746.
22. E. Hückel, *Z. Phys.*, **1931**, *70*, 204-286.
23. P. W. Fowler and T. Pisanski, *J. Chem. Soc., Faraday Trans.*, **1994**, *90*, 2865-2871.
24. M. Yoshida, M. Fujita, P. W. Fowler, and E. C. Kirby, *J. Chem. Soc., Faraday Trans.*, **1997**, *93*, 1037-1043.
25. I. Gutman and Y. Hou, *MATCH Commun. Math. Comput. Chem.*, **2001**, *43*, 17-28.
26. L. J. Schaad and B. A. Hess, *J. Am. Chem. Soc.*, **1972**, *94*, 3068.
27. J. Aihara, *J. Am. Chem. Soc.*, **1976**, *98*, 2750-2758.
28. J. Aihara, *J. Mol. Struct. (Theochem)*, **1994**, *311*, 1-8.
29. J. Aihara, D. Babic and I. Gutman, *MATCH Commun. Math. Comput. Chem.*, **1996**, *33*, 7-16.
30. I. Gutman, M. Milun, and N. Trinajstić, *MATCH Commun. Math. Comput. Chem.*, **1975**, *1*, 171-175.
31. I. Gutman, M. Milun, and N. Trinajstić, *J. Am. Chem. Soc.*, **1977**, *99*, 1692-1704.
32. HyperChem [TM], release 4.5 for SGI, © **1991-1995**, Hypercube, Inc.
33. M. V. Diudea, O. Ursu, and Cs. L. Nagy, TOPOCLUJ, "Babes-Bolyai" University, Cluj, **2002**.
34. M. V. Diudea and M. Stefu, CageVersatile CV 1.1, "Babes-Bolyai" University, Cluj, **2003**.

MODELING PHYSICO-CHEMICAL PROPERTIES OF POLYCHLORINATED BIPHENYLS ON THE GROUNDS OF HYPERMOLECULE CONCEPT

MIHAELA CAPRIOARA, CSABA L. NAGY AND MIRCEA V. DIUDEA

*Faculty of Chemistry and Chemical Engineering,
Babeș-Bolyai University, 400028 Cluj, Romania*

ABSTRACT. Biphenyls (PCBs) represent a class of pollutants with great environmental impact. For such chemicals, QSPR studies were performed in order to emphasize the relation between some topochemical and electronic parameters and their molecular properties. The models are described on the ground of hypermolecule concept. Local group mass, autocorrelated by a multivariate regression, are used for molecular description. A map of relevant positions in the hypermolecule, most probably involved in the global (*i.e.*, molecular) property could be drawn. The hypermolecule, in this case, has the meaning of a "mean molecule" in the set. A general procedure for developing and validating models using the above concept is given. Within this frame, a method of data reduction (*i.e.*, selection of relevant descriptors) is exemplified.

INTRODUCTION

An important aspect of modern toxicology research is estimation of properties of environmental pollutants from their molecular structure.¹ The potential toxicity of a compound is normally assessed on the basis of a wide variety of relevant physico-chemical properties. The application of QSPR techniques to the elucidation of the ways in which structure determines chemical and physical properties has already become an essential tool in the area of chemistry.

An enormous attraction of QSPR is that it potentially combines the ability to predict chemical and physical properties of as yet unmeasured or unknown compounds with the ability to understand just how the structure influences a particular chemical and physical property.

Polychlorinated biphenyls (PCBs) are ubiquitous environmental pollutants with different physical and chemical properties, but with quite different biochemical effects.² Only few of them exhibit high direct toxicity. Exposure by most of them and by some of their metabolites may result in immunodeficiency, neurotoxic effects including impaired learning, teratogenic effects and endocrine disruptions.^{3,4} These compounds originate from various human activities (and also from natural sources) are of special interest because of their global distribution, persistence, high tendency to bioaccumulate and known or suspected toxicity.

The physicochemical properties (*e.g.*, the partition coefficient in octanol-water system, $\log P$) and molecular structures of PCBs are strongly related to their toxic effects on biological systems. We tried to identify those structural features that could be relevant in the relationship $\log P$ - PCBs. In modeling this molecular property, we used some simple molecular descriptors, based on atom group substituent or on the whole molecule.

This paper is focused on development of novel QSPR models using molecular descriptors and available experimental physico-chemical data. General structures of biphenyl herein investigated are presented in Table 1.

MATERIALS AND METHODS

The correlating study was performed on a set of PCBs,⁶ being the property $\log P$. Table 1 lists the general formula of biphenyls, property and name of compounds.

Among the physico-chemical properties of PCBs, partitioning behavior of these compounds in various media is important in spreading the pollutants in the environment. In general, lipophilicity increases with increasing degree of chlorination. Lipophilicity is known to be involved in their toxicity.

2.1 Chemical Data

The physico-chemical properties were previously modeled by using molecular linear free energy relationship descriptors (LFER). Modeling $\log P$ for the set of the 16 PCBs led to an r value of 0.9868 and predictive correlation of 0.9614.⁶⁻⁸

2.2 Calculation of Molecular Descriptors

In order to model the correlation of physico-chemical property with the molecular structure, (QSPR models) the structure must be described in a numerical form. The arrangement of chlorine atoms on the biphenyl structure can be accounted for, by the *hypermolecule HM* concept,⁹ viewed as a "mean molecule" of the whole set.¹⁰

In the construction of the hypermolecule, a *row-vector* P_i of dimension N_{HM} is attached to each molecule M_i :

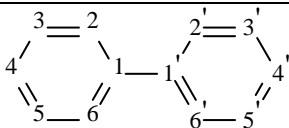
$$P_i = \{ P_{ij}; j = 1, 2, \dots, N_{HM} \} \quad (1)$$

where N_{HM} is the number of vertices in the hypermolecule. The molecules of the set are superimposed according to their maximal common substructures.

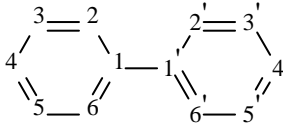
In the associated vector, the matching positions take $P_{ij} = 1$ while for the non-matching ones $P_{ij} = 0$. The description of the j^{th} position in *HM* (e.g., the chemical and/or topological nature of the j^{th} atoms) is given by X_{ij} .

The hypermolecule and the molecules under study can be numerically described by using some molecular *topological descriptors* TD_i .^{11,12}

Table 1

General structure of biphenyl. Chemicals and their $\log P^a$		
Compound	Structure	
Biphenyl		
Code	Compound	$\log P$
PCB1	Biphenyl	3.98
PCB2	4-chloro-biphenyl	4.61
PCB3	2,2'-dichloro-biphenyl	4.73
PCB4	4,4'-dichloro-biphenyl	5.58
PCB5	2,4,5-trichloro-biphenyl	5.81

MODELING PHYSICO-CHEMICAL PROPERTIES OF PCB'S

Compound	Structure	
Biphenyl		
Code	Compound	logP
PCB6	2,2',5-trichloro-biphenyl	5.6
PCB7	2,2',5,5'-tetrachloro-biphenyl	6.09
PCB8	2,3,4,5-tetrachloro-biphenyl	6.41
PCB9	2,2',4,5,5'-pentachloro-biphenyl	6.44
PCB10	2,3,4,5,6-pentachloro-biphenyl	6.52
PCB11	2,2',4,4',5,5'-hexachloro-biphenyl	6.8
PCB12	3,3',4,4',5,5'-hexachloro-biphenyl	7.55
PCB13	2,2',3,3',4,4',6-heptachloro-biphenyl	6.99
PCB14	2,2',3,3',5,5',6,6'-octachloro-biphenyl	7.15
PCB15	2,2',3,3',4,5,5',6,6'-nonachloro-biphenyl	8.16
PCB16	2,2',3,3',4,4',5,5',6,6'-decachloro-biphenyl	8.26

^avalues by Bodor's logP dataset

$$TD_i = \sum_j TD_{ij} = \sum_j a_j P_{ij} X_{ij} \quad (2)$$

where P_{ij} and X_{ij} have the meaning above mentioned while a_j is the regression coefficient as given by the multivariate regression $\log P = f(X_j)$. The above TD s are "ad-hoc" descriptors^{13,14} depending on the set of molecules considered and the selected molecular property. Therefore, all the polychlorinated biphenyls can be described using particular local properties that characterize both the substituted/unsubstituted aromatic positions.

As local property for calculating TD s, we used X_{ij} = the group mass related to each position in PCBs.

2.3 Statistics

For developing the QSPR models, the two sets of PCBs were submitted to REGLINEWIN (a home made statistical software package). The correlating equation is of the form:

$$Y_i = b_0 + \sum_{j=1}^m b_j \cdot TD_{ij} \quad (3)$$

where Y_i is the dependent variable, TD_{ij} are the predictor variables, $m < n$, n being the number of structures in the set.

A general algorithm for generating a correlating model was carried out:

- 1) select a training data set of compounds with great structural diversity and generate the *hyper molecule*.
- 2) perform a Leave-one-out analysis on the input set of local descriptors.
- 3) calculate the global descriptors by using appropriate weights in the training set.

- 4) find a regression function by using statistical tools.
- 5) test the predictive capacity of the model.

RESULTS AND DISCUSSION

The results of correlating analysis will be presented separately for each of the two sets.

3.1 Set of 16 PCBs, Property: $\log P$.

This subset of PCBs consists of 16 polychlorinated compounds and the property is $\log P$ (Table 1). Within this set, we delimited a training set ($n = 12$) and a test set ($n = 4$).

Lipophilicity controls the free energies of PCBs binding to AhR.¹⁵ Comparing to other chemicals, PCBs have very high P values:¹⁶ $\log P$ s are in the range [4.5 – 8.5]. Consequently, PCBs tend to adsorb to unpolar surfaces and accumulate in lipophilic matrices. For these compounds, the lipophilicity is related directly to bioconcentration and inversely to aerobic degradation.

Keeping in mind the physical nature of the PCB property we used a mass descriptor MD as independent variable. This descriptor accounts for vertices as groups of atoms, e.g., CH, C-Cl, etc.

3.1.a Hypermolecule model

A *hypermolecule* already generated, we calculated MD s for all molecules in the training set. The group mass M_i for each vertex fragment in PCBs is multiplied by the regression coefficients in a multivariate regression including all positions in the hypermolecule (see Table 2).

Table 2

Training set ($n = 12$). Group mass descriptors M_i and regression coefficients c_i corresponding to aromatic positions.

Molecule	M_2	M_3	M_4	M_5	M_6	$M_{2'}$	$M_{3'}$	$M_{4'}$	$M_{5'}$	$M_{6'}$
c_i	0.01	0.02	0.01	0.03	0.00	0.01	0.02	0.01	0.01	-0.01
PCB1	13.01	13.01	13.01	13.01	13.01	13.01	13.01	13.01	13.01	13.01
PCB2	13.01	13.01	47.46	13.01	13.01	13.01	13.01	13.01	13.01	13.01
PCB5	47.46	13.01	47.46	47.46	13.01	13.01	13.01	13.01	13.01	13.01
PCB6	47.46	13.01	13.01	47.46	13.01	47.46	13.01	13.01	13.01	13.01
PCB7	47.46	13.01	13.01	47.46	13.01	47.46	13.01	13.01	47.46	13.01
PCB8	47.46	47.46	47.46	47.46	13.01	13.01	13.01	13.01	13.01	13.01
PCB9	47.46	13.01	47.46	47.46	13.01	47.46	13.01	13.01	47.46	13.01
PCB10	47.46	47.46	47.46	47.46	47.46	13.01	13.01	13.01	13.01	13.01
PCB11	47.46	13.01	47.46	47.46	13.01	47.46	13.01	47.46	47.46	13.01
PCB12	13.01	47.46	47.46	47.46	13.01	13.01	47.46	47.46	47.46	13.01
PCB13	47.46	47.46	47.46	13.01	47.46	47.46	47.46	47.46	13.01	13.01
PCB14	47.46	47.46	13.01	47.46	47.46	47.46	47.46	13.01	47.46	47.46

The leave-one-out LOO procedure is required to select among the 10 positions ($k = 10$) the corresponding relevant descriptors. It resulted in a map of relevant positions in the hypermolecule, most probably involved in the global (*i.e.*, molecular) property (see Table 3). The hypermolecule, in this case, has the meaning of a "mean molecule" in the set.

Table 3

Training set ($n = 12$). Statistical parameters of the LOO procedure tested on partial descriptors set.

Number of descriptors (k)	Model (multivariate regression)	Irrelevant positions	Correlation coeff. (r) (after descriptor elimination)
k-1	$\log P = f(M_i), i = 1, 2, \dots k-1$	M_6	0.9992
k-2	$\log P = f(M_i), i = 1, 2, \dots k-2$	M_6, M_6'	0.9979
k-3	$\log P = f(M_i), i = 1, 2, \dots k-3$	M_2, M_6, M_6'	0.9966
k-4	$\log P = f(M_i), i = 1, 2, \dots k-4$	M_2, M_5, M_6, M_6'	0.9945

From Table 3, it appears that a satisfactory statistics is ensured by a map comprising $k-4$ relevant positions: $M_3, M_4, M_5, M_2', M_3', M_4'$, for which the local parameters global mass descriptor MD are given in Table 4.

Table 4

Regression coefficients (c_i) and molecular mass descriptor in the training set.

Number of descriptors (k-4)	M_3	M_4	M_5	M_2'	M_3'
c_i	0.019	0.019	0.035	0.019	0.02
Molecules	MD	P_{obs}	P_{calc}	Residual	
PCB1	1.586	3.98	3.98	0	
PCB2	2.226	4.61	4.62	-0.01	
PCB5	3.426	5.81	5.82	-0.01	
PCB6	3.436	5.6	5.83	-0.23	
PCB7	3.436	6.09	5.83	0.26	
PCB8	4.071	6.41	6.465	-0.055	
PCB9	4.076	6.49	6.47	0.02	
PCB10	4.071	6.52	6.465	0.055	
PCB11	4.436	6.8	6.83	-0.03	
PCB12	5.136	7.55	7.53	0.02	
PCB13	4.586	6.99	6.98	0.01	
PCB14	4.786	7.15	7.18	-0.03	

Model generation. The structure- $\log P$ model for PCBs fits a linear function, its quality being estimated by the correlation coefficient (r), the standard error of estimate (s), the Fischer ratio (F) and the coefficient of variance ($CV\%$), the last one being a ratio of s to the property mean value in the set. The regression analysis was performed using the REGLINWIN package. The following QSPR model was generated:

$$\log P = 2.394 + MD \quad (4)$$

$$n = 12; k = 6; r = 0.9946; s = 0.114; F = 902.23; CV\% = 1.852$$

$$\text{Random correlation: } r_1 = 0.650; r_2 = 0.674; r_3 = 0.535$$

We tried several partitions of the whole set of 16 molecules into a training set and a test set and we concluded that the final results do not depend significantly on the specific manner of choosing the members of each subset. A random test showed a marked drop in the correlation coefficient, with the meaning that no chance correlation occurred.

Figure 1 shows the plot of $\log P$ vs. MD values in the PCBs training set.

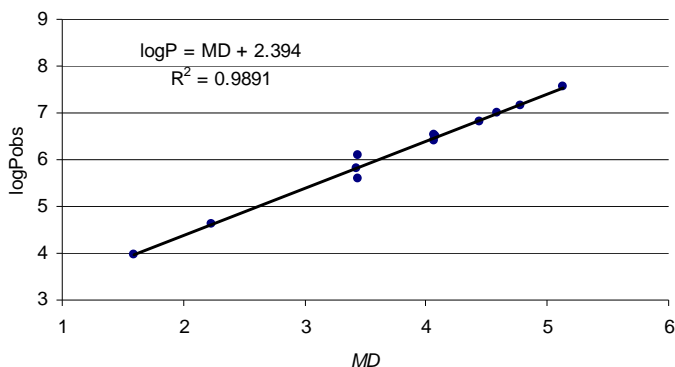


Figure 1. Plot of $\log P$ vs. calculated MD values.

Model validation. In order to verify the predicting ability of this QSPR model, we first calculated MD s for the test molecules ($n = 4$) using their corresponding vertex-group mass and the regression coefficients prior generated for the training set (see Table 5 – we suppose the partition coefficient in the predicting set is unknown).

Table 5

Molecular mass descriptors MD in test set ($n = 4$). Estimated $\log P$ from the linear regression model eq (4)

Molecules	MD	$\log P_{\text{calc}}$ (eq. 4)	$\log P$	Residual
PCB3	2.236	4.63	4.73	0.1
PCB4	2.586	4.98	5.58	0.6
PCB15	5.426	7.82	8.16	0.34
PCB16	5.786	8.18	8.26	0.08
$\log P = 0.5318 + 0.96071 \cdot \log P_{\text{calc}}$			$r = 0.9916$	

The model (4) is excellent both in estimation and prediction, as shown in Table 5 and the correlation equation of the calculated (by eq 4) values vs the observed ones.

3.1.b Average Descriptors and the Eigenvalue of S Matrix

The symmetry of the biphenyl skeleton suggests the superimposing of different positions, above considered as separate positions. Thus, we calculated the following descriptors: $AM_2 = \text{av}(M_2, M_2', M_6, M_6')$; $AM_3 = \text{av}(M_3, M_3', M_5, M_5')$ and $AM_4 = \text{av}(M_4, M_4')$. Each average value was further divided by 2, thus accounting for 8 possible equivalent structures. Data are given in Table 6.

The second path matrix [17] $\mathbf{S} = \mathbf{S}(G)$ is defined as the difference between the squared adjacency matrix and the diagonal matrix **DEG** of vertex degrees in G :

$$\mathbf{S} = \mathbf{S}(G) = \mathbf{A}^2 - \mathbf{DEG} \quad (5)$$

The characteristic polynomial of \mathbf{S} is:

$$ChS(x, G) = \det(x \cdot \mathbf{I} - \mathbf{S}) = \sum_{k=0}^n b_k(G) \cdot x^{n-k} \quad (6)$$

The matrix \mathbf{S} counts the all distinct path of length two in G . The first eigenvalue of \mathbf{S} (*i.e.*, the first root of $ChS(x, G)$) is used in the following for modeling $\log P$ in the PCBs in Table 1.

In trivariate regression, with the three averaged mass descriptors, one obtains:

$$\log P = 2.918 + 0.022 \cdot AM_2 + 0.062 \cdot AM_3 + 0.038 \cdot AM_4 \quad (7)$$

$$n = 16; r = 0.9661; s = 0.353; CV\% = 5.63; F = 56.023$$

A global descriptor AMD is again calculable (*cf.* eq 2) as a linear combination of the the above three averaged mass descriptors. Data are given in Table 6.

Table 6

Averaged mass descriptors AM_i and the global descriptor AMD

Molecules	$\log P$	AM_2	AM_3	AM_4	AMD	EV_S
c_i		0.022	0.062	0.038		
PCB1	3.98	10.125	13.011	13.011	1.525	2.842
PCB2	4.61	10.253	21.624	13.011	2.064	3
PCB3	4.73	30.238	13.011	13.011	2.718	3.107
PCB4	5.58	13.011	13.011	47.464	2.372	3
PCB5	5.81	10.568	21.624	30.238	3.022	3.282
PCB6	5.6	19.128	13.011	30.238	2.914	3.265
PCB7	6.09	19.236	13.011	47.464	3.561	3.265
PCB8	6.41	19.331	21.624	30.238	3.451	3.338
PCB9	6.49	19.365	21.624	47.464	4.099	3.385
PCB10	6.52	19.358	30.238	30.238	4.295	3.535
PCB11	6.8	19.428	30.238	47.464	3.727	3.385
PCB12	7.55	28.229	30.238	47.464	4.485	3.382
PCB13	6.99	36.702	38.851	13.011	1.973	3.601
PCB14	7.15	36.742	30.238	47.464	2.883	3.591
PCB15	8.16	47.464	47.464	30.238	5.15	3.692
PCB16	8.26	47.464	47.464	47.464	5.797	3.692

The monovariate regression is now:

$$\log P = 2.918 + AMD \quad (8)$$

$$n = 16; r = 0.9661; s = 0.3265; CV\% = 5.186; F = 196.15$$

In view of improving the correlation, we added a new descriptor, namely the first eigenvalue of the S matrix EV_S . The bivariate regression obtained is:

$$\log P = -1.331 + 0.703 \cdot AMD + 1.575 \cdot EV_S \quad (9)$$

$$n = 16; r = 0.979; s = 0.268; CV\% = 4.251; F = 149.94$$

The analysis of the residuals, by eq 9, revealed two outliers, as shown in Table 7. The best model is obtained on 14 PCBs:

$$\log P = -1.790 + 0.654 \cdot AMD + 1.741 \cdot E_S \quad (10)$$

$$n = 14; r = 0.9908; s = 0.185; CV\% = 2.99; F = 296.62$$

$$LOO: q = 0.984; \text{Random: } r = 0.583$$

A random mixing of the modeled property showed a significant drop in the correlation coefficient value. Prediction ability of the model (eq 10) is very good ($q = 0.984$). The explicit variance is higher than 0.98 (see the plot, Figure 2). The data of the model (10) are given in Table 8.

Table 7

Outlier analysis			
Number of molecules (n)	Model (multivariate regression)	Outliers	Correlation coefficient (r) (after descriptor elimination)
n	$\log P = f(M_i), i = 1, 2, \dots, n$	-	0.979
$n - 1$	$\log P = f(M_i), i = 1, 2, \dots, n-1$	PCB12	0.9858
$n - 2$	$\log P = f(M_i), i = 1, 2, \dots, n-2$	PCB12, PCB8	0.9908

Table 8

Data of the model (10)						
	Molecules	AMD	EV_S	P_{obs}	P_{calc}	Residual
1	PCB1	1.525	2.842	3.98	4.155	0.175
2	PCB2	2.064	3	4.61	4.783	0.173
3	PCB3	1.973	3.107	4.73	4.909	0.179
4	PCB4	2.883	3	5.58	5.319	-0.261
5	PCB5	2.718	3.282	5.81	5.702	-0.108
6	PCB6	2.372	3.265	5.6	5.446	-0.154
7	PCB7	3.022	3.265	6.09	5.871	-0.219
8	PCB9	3.561	3.385	6.49	6.432	-0.058
9	PCB10	3.451	3.535	6.52	6.621	0.101
10	PCB11	4.099	3.385	6.8	6.784	-0.016
11	PCB13	3.727	3.601	6.99	6.917	-0.073
12	PCB14	4.485	3.591	7.15	7.395	0.245
13	PCB15	5.15	3.692	8.16	8.006	-0.154
14	PCB16	5.797	3.692	8.26	8.43	0.17

The molecular descriptors used in the second part of our study are intercorrelated as shown in Table 9. Their collinearity is pretty good for a multilinear regression.

MODELING PHYSICO-CHEMICAL PROPERTIES OF PCB'S

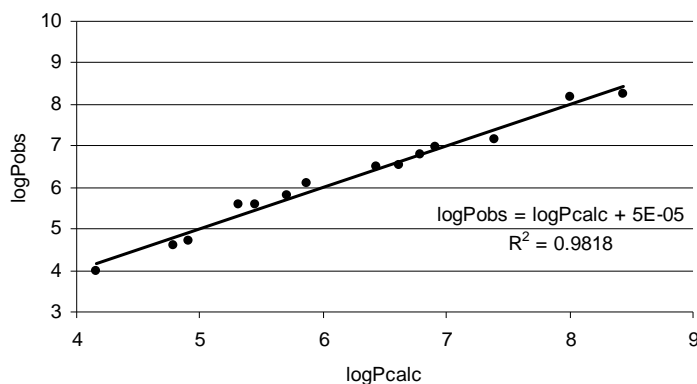


Figure 2. Plot of $\log P$ vs. $\log P$ calculated by eq. 10

Table 9

Intercorrelation of the averaged mass and EV_S descriptors

	AM_2	AM_3	AM_4	EV_S
AM_2	1	0.794	0.153	0.790
AM_3		1	0.157	0.849
AM_4			1	0.360
EV_S				1

CONCLUSIONS

In the present paper, we have used (local) molecular descriptors for encoding a *hypermolecule*, as a "mean molecule" in the set, in case of a physico-chemical property.

The local descriptors are fitted by means of multivariate regression and represent "ad-hoc" (or "autocorrelated") descriptors, which change with the set and selected property.

A general procedure for developing and validating models using the concept of the hypermolecule was given. Within this frame, two ways of data reduction (*i.e.*, selection of relevant descriptors) were exemplified.

REFERENCES

1. H. Kubinyi, *Quant. Struct.-Act. Relat.* **1994**, *13*, 285-294.
2. M. V. Diudea, *J. Chem. Inf. Comput. Sci.* **1997**, *37*, 300-305.
3. J. G. Topliss and R. P. Edwards, *J. Med. Chem.* **1979**, *22*, 1238-1244.
4. S. C. Basak, G. D. Grunwald, B. D. Gute, K. Balasubramanian, and D. Opitz, *J. Chem. Inf. Comput. Sci.* **2000**, *40*, 885-890.

5. G. G. Oakley, U. Devanaboyina, L. W. Robertson, and R. C. Gupta, *Chem. Res. Toxicol.* **1996**, *9*, 1285-1292.
6. M. D. Erickson, *Analytical Chemistry of PCBs*, Butterworth Publishers, Boston, **1986**.
7. E. M. Silberhorn, H. P. Glauert, and L. W. Robertson, *CRC Crit. Rev. Toxicol.* **1990**, *20*, 439-496.
8. D. Mackay, W. Y. Shiu, and K. C. Ma, *Illustrated Handbook of Physical-Chemical Properties and Environmental Fate for Organic Chemicals*. Volume I+II. Lewis Publishers Inc., Boca Raton, FL, USA, **1992**.
9. J. A. Platts, M. H. Abraham, D. Butina, and A. Hersey, *J. Chem. Inf. Comput. Sci.* **2000**, *40*, 71-80.
10. P. Buchwald, and N. Bodor, *Curr. Med. Chem.* **1998**, *5*, 353-380.
11. R. P. Schvarzenbach, P. M. Gschwend, and D. M. Imboden, *Environmental Organic Chemistry*, John Wiley&Sons, New York, **1992**.
12. O. M. Minailiuc, and M. V. Diudea, TI-MTD Model. Applications in Molecular Design, in: *QSPR/QSAR Studies by Molecular Descriptors*, Nova Science Publishers, Inc., **2001**, pp. 363-388.
13. R. P. Sheridan, *J. Chem. Inf. Comput. Sci.* **2000**, *40*, 1456-1469.
14. I. Motoc, S. Holban, R. Vancea, and Z. Simon, *Studia Biophys. (Berlin)* **1977**, *66*, 75-78.
15. A. T. Balaban, A. Chiriac, I. Motoc, and Z. Simon, *Steric Fit in QSAR (Lectures Notes in Chemistry, Vol. 15)*, Springer, Berlin, **1980**, Chap. 6.
16. A. A. Toropov, and A. P. Toropova, *Internet Electronic Journal of Molecular Design*, **2002**, *1*, 108-114.
17. D. J. G. Marino, P. J. Peruzzo, E. A. Castro and A. A. Toropov, *Internet Electronic Journal of Molecular Design*, **2002**, *1*, 115-133.
18. S. A. Kafafi, H. Y. Afeefy, A. H. Ali, H. K. Said, and A. G. Kafafi, *Environ. Health Perspect.* **1993**, *101*, 422-428.
19. H. Fiedler, H. Hoff, J. Tolls, C. Mertens, A. Gruber, and O. Hutzinger, *Environmental Fate of Organochlorines in the Aquatic Environment. Organohalogen Compd.* **15**, ECO-INFORMA Press, Bayreuth, 199 Pages, ISBN 3928379119, **1994**.
20. P. E. John and M. V. Diudea, *MATCH Commun. Math. Comput. Chem.*, **2003** (accepted).

CARBON ALLOTROPES WITH NEGATIVE CURVATURE

CSABA L. NAGY and MIRCEA V. DIUDEA

*Faculty of Chemistry and Chemical Engineering,
Babeș-Bolyai University, 400028 Cluj, Romania*

ABSTRACT. New allotropes of carbon, with various curvatures, have been theorized (and experimentally obtained) by replacing, in the graphite planar sheet, hexagons with other n -gons. When $n < 6$, the objects are finite, positively curved cages, as the classical spherical fullerenes. In case $n > 6$, the process results in either finite or infinite objects with negative curvature. Several well-known and new tilings with negative curvature are constructed and their topology discussed. Strain energy of an infinite lattice, with the repeat unit derived by iterating capra operation on the cube, is evaluated by the POAV1 approach.

INTRODUCTION

The traditionally recognized allotropes of carbon are the diamond and graphite. The structure of diamond is an infinite three-dimensional lattice, of sp^3 hybridized carbon atoms; all atoms and bonds are equivalent. The structure of graphite represents the tiling of the plane with hexagons. It again contains only one kind of sp^2 hybridized carbon atom, with 120° bond angles.

Fullerenes, new allotropes of carbon, represent finite cage molecular structure, with positive Gaussian curvature. Such curvature can be acquired by replacing, in the graphite planar sheet, hexagons with rings of size smaller than six. In classical fullerenes, the pentagons produce positive curvature necessary for the cage closure. They have no dangling bonds, and are topologically homeomorphic to the sphere, thus having genus $g = 0$. Compared with graphite, fullerenes show strain energy, since the angles in the regular pentagon are 108° .

A question of interest is what structures may result if, in graphite, hexagons are replaced by sevenfold, or larger sized rings. Such nets cannot form closed polyhedra, since rings larger than six induce negative curvature. Such structures are infinite periodic surfaces, with zero mean curvature. They are known as infinite periodic minimal surfaces IPMS's, also called Schwarzites. Of particular interest are those IPMS's of the highest symmetry, such as the P and D surfaces (see below).

THEOREMS OF THE SURFACE CURVATURE

A sp^2 carbon net can be embedded in an allowed surface S , such that no edge-crossing occurs. Among many embeddings, two embeddings ε_1 and ε_2 are combinatorially equivalent if there is a one-to-one correspondence between their vertices edges and faces, such that the incidences between their constitutive substructures are preserved.

In the differential-geometric view, the curvature is the rate of direction changing at the point p on a curve. The curvature k at p is defined as the inverse of the radius of the tangent circle to the curve. If a surface is considered, then two

circles are needed and two principal curvatures k_1 and k_2 (either maximal or minimal) are derived. The Gaussian curvature κ , at the point p of S , is the product of the two local orientations of the curved surface: $\kappa = \pm k_1 \cdot k_2$ and the mean

curvature is $H = \frac{1}{2}(k_1 + k_2)$.

A *curvature mismatch* is derivable by comparing differential-geometric curvature with some graphical combinatorial curvature. It comes out from the angles of various polygons of a covering, as a measure of non-planarity (or curvature). The *angle defect* at p means the deviation from 2π of the sum of the face angles ϕ_f :

$$\phi_p = 2\pi - \sum_f^{\sim P} \phi_f = 2\pi - \sum_f^{\sim P} (\pi - 2\pi / n_f) \quad (1)$$

A *combinatorial curvature* is calculated as the sum over all local angular defects (see below).

A surface is *orientable* when it has two sides and *non-orientable* when it is one sided, like the Mobius strip. The *Gauss-Bonet¹ theorem* relates the geometric curvature to the topology:

$$\int_S \kappa dA = 2\pi\chi(S) \quad (2)$$

where $\chi(S)$ is the Euler characteristic and it is differently expressed for the two kinds of surfaces:

$$\chi(S) = 2 - 2g(S) \quad \text{orientable surface} \quad (3)$$

$$\chi(S) = 2 - n(S) \quad \text{non-orientable surface} \quad (4)$$

In the above relations, g denotes the *genus*, being the number of handles required to be attached to the sphere to make it homeomorphic to S . The parameter n is the number of *cross-caps* needed in the same view, in case of a non-orientable surface.²

Descartes' theorem states that, if S is a topohedral surface in 3D, then the overall angular defects are proportional to the Euler's characteristic $\chi(S)$:

$$\sum_p^S \phi_p = 2\pi\chi(S) \quad (5)$$

In a topohedron, the count of vertices v , edges e and faces f , is given by the Euler's relation.^{3,4}

$$\chi(S) = v - e + f \quad (6)$$

If $g = 0$ the equation reduces to the familiar version of *Euler's theorem*,³ for polyhedra, i.e., topohedra embedded in the sphere. If a polyhedron has all degree 3 vertices, and each edge is shared by two faces, then:

$$2e = 3v = \sum_n n \cdot f_n \quad (7)$$

where f_n denotes the number of n -gonal faces. Substituting this into (6) results in:

$$\sum_n (6-n)f_n = 12(1-g) = 6\chi \quad (8)$$

If we consider polygons with $n = 3, 4 \dots 9$ sides, equation (8) becomes:

$$3f_3 + 2f_4 + f_5 - f_7 - 2f_8 - 3f_9 = 12(1-g) \quad (9)$$

In (9), $f_3, f_4 \dots f_9$ are defects in the graphitic structure, which contribute to the curvature of the polyhedra; f_6 is not present since hexagon produces zero Gaussian curvature. Tiling a surface, of genus g , with only one kind of polyhedron f_n , is found by setting, in (9), $f_{\neq n} = 0$. Table 1 lists the solutions of (9) for tiling surfaces of genus 0, 2 and 3 (the repeat units).

Table 1

	$g = 0$ (sphere)		$g = 2$ (D surface)	$g = 3$ (P surface)
f_3	4 (tetrahedron)	f_7	12	24
f_4	6 (cube)	f_8	6	12
f_5	12 (dodecahedron)	f_9	4	8

Equation 9 does not give information on the number of hexagonal rings, thus any number of hexagons may be used (except one).

CARBON STRUCTURES EMBEDDED ON P AND D IPMS'S

Since H. A. Schwarz has discovered (in 1890) the first negative Gaussian curvature infinite surface (with zero mean curvature at each point and periodic in all three directions), other IPMS's have been described: P, D, T, CLP, and H surfaces, having octahedral, tetrahedral, cubic, trigonal prismatic and triangular unit cells, respectively.

Such surfaces are defined by their repeat units, as unit cells. The mean curvature H vanished at each point in minimal surfaces, so that $k_1 = -k_2$, and $\kappa \leq 0$. They are saddle-shaped everywhere except at certain *flat points*. Figure 1 illustrates some tiling of the P surface, where the flat points are represented by: a hexagon (1a); a triangle of hexagons (1b) or coronene, connected in different ways (1c and 1d).

Of particular interest are those IPMS's of highest symmetry, the P and D surfaces, which have genus 3 and 2, respectively. The unit cell of the P surface can be viewed as an octahedral junction of six tubes. The diamond D surface has the topology of a surface wrapping around the diamond lattice.

The first contemporary scientists who recognized the negative curvature allotropes of carbon were Mackay and Terrones.⁵ Their P surface is covered with octagons and hexagons, using 12 octagons and 80 hexagons on the unit cell. The diamond D surface is tiled with six octagons and 40 hexagons per unit cell. Figure 2a illustrates the unit cell of P surface; the octagons appear when connecting the units, as shown in Figure 2b.

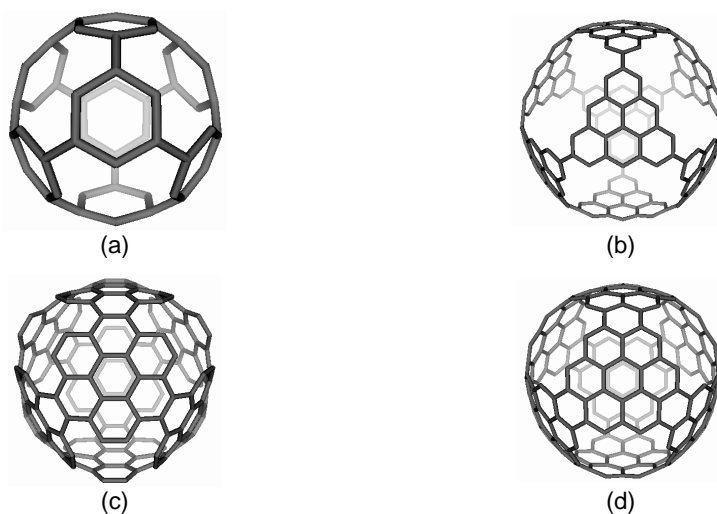


Figure 1. Examples of the flat points in some *P* minimal surfaces

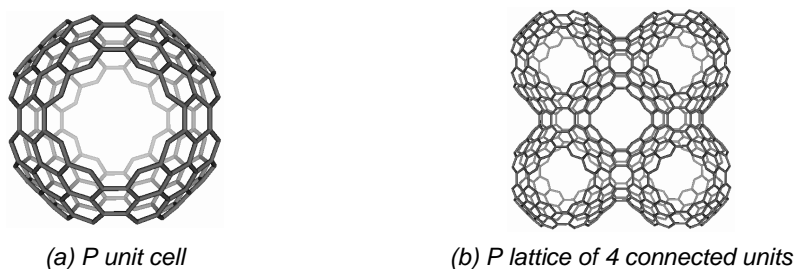


Figure 2.

The tiling of *P* and *D* surfaces with heptagons and hexagons was performed by Lenosky *et al.*⁶ The *P* tiling contains 216 atoms, while the *D* tiling 192 atoms, per unit cell. Figure 3 presents these minimal surfaces and the lattice resulted by connecting four and six units, respectively.

The simplest possible tiling of the *P* and *D* surface was given by O'Keeffe *et al.*⁷ These structures are covered with hexagons and octagons and have only one kind of carbon atom. The *P* surface repeat unit is derivable from C_{60} by removing six "double" bonds, such as the remaining structure has cubic symmetry tiled with 8 hexagons and 12 octagons (appearing when connecting the unit cells - Figure 4a).

The *D* surface consists of four hexagonal rings disposed on the points of the tetrahedron, being connected, by octagons, in a lattice (Figure 4b).

All the above structures represent infinite surfaces. There were also proposed finite cage fullerenes with negative gaussian curvature, of high genus (above 5) and tiled only with hexagons and heptagons. Such structures, consisting of a huge number of atoms, were called holey-balls and holey-tubes. Their high genus indicates the presence of channels, in which small molecules can be guests.⁸

CARBON ALLOTROPES WITH NEGATIVE CURVATURE

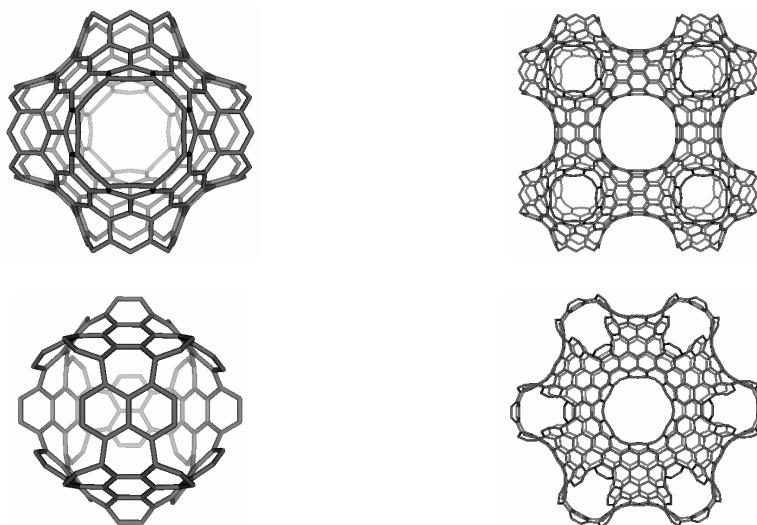
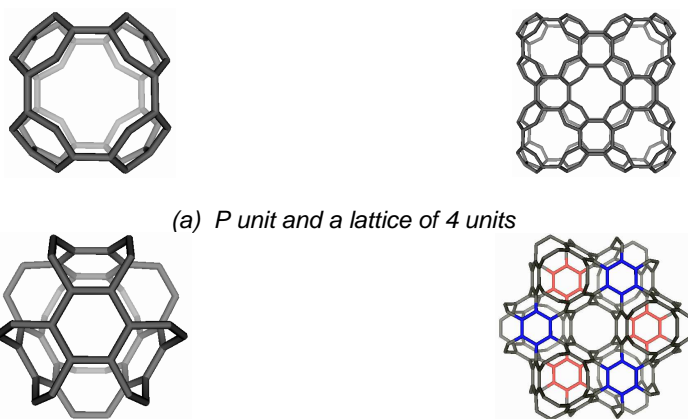


Figure 3. *P* and *D* unit cells, by Lenosky et al., and derived lattices



(a) *P* unit and a lattice of 4 units

(b) *D* unit and a lattice of 6 units

Figure 4. *IPMS's* by O'Keeffe et al.

Besides the highly symmetrical *P* and *D* surfaces, other periodic surfaces, called *G*, *H* and *I-WP*, were constructed and their energy per atom compared with that of C_{60} .⁹ They all are more stable than C_{60} , the main reason being the bond angles and lengths of graphite better preserved in heptagonal and octagonal rings than in the pentagons of C_{60} . The planarity of the bonds can be improved by adding hexagons, e.g., by leapfrog operation.¹⁰

The simplest minimal surfaces tiled with only one kind of polygon are those having the Klein graph (heptagons - Figure 5a) and Dyck graph (octagons - Figure 5b) as repeat units.



Figure 5. Klein (a) and Dyck (b) graphs

The symmetry of these graphs was described by King, he suggested that structures decorating the genus 3 P surface share the automorphism group of the Klein graph.¹¹⁻¹⁷

Table 2 gives their constitutive substructure count.

Table 2

G (graph)	v (vertices)	e (edges)	f (faces)
Klein	56	84	$f_7 = 24$
Dyck	32	48	$f_8 = 12$

Both structures are representations of the automorphism of (heptakis and octakis, respectively) octahedral group.¹¹ The next section will show how these two units can result by an elegant transformation of the cube. This operation can be used to generate negatively curved units (of minimal surfaces) originating in the three Platonic trivalent polyhedra: tetrahedron, cube and dodecahedron.

CAPRA – A NOVEL MAP OPERATION

A map M is a combinatorial representation of a surface. Map operations transform the parent map into map derivatives.^{18,19} The number of vertices in the transformed map may be m times (m , integer) that in the parent map, as given by the Goldberg^{20,21} relation:

$$m = (a^2 + ab + b^2); a \geq b; a + b > 0 \quad (10)$$

which predicts m as follows:

identity operation	$I: (1, 0)$	$m = 1$
leapfrog operation	$Le: (1, 1)$	$m = 3$
quadrupling (chamfering) operation	$Q: (2, 0)$	$m = 4$
capra operation	$Ca: (2, 1)$	$m = 7$

Capra is a complex operation on maps. The first step is a homeomorphic $E2$ transformation of each edge in the parent graph (by inserting 2 vertices of degree two on each edge - Figure 6a). It is followed by pentangulation of the above expanded face (connecting every fourth vertex of the face boundary with a new vertex on the face center - Figure 6b). Truncation of this new vertex (and its incident edges) results in a closed map preserving the original vertices (and their valency) and faces (surrounded now by hexagons - Figure 6c). The parent faces are twisted by $\pi/2n$.

CARBON ALLOTROPES WITH NEGATIVE CURVATURE

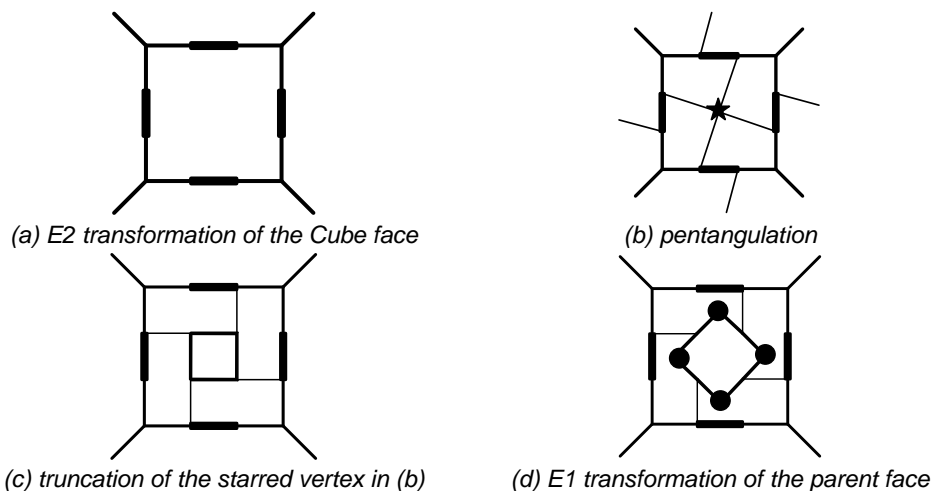


Figure 6. Capra transformation of a cube's face.

The operation can continue by an En homeomorphic transformation of the parent faces, thus resulting open maps with all polygons of the same $(6+n)$ size. The capra operation can be formulated as:

$$Ca(M) = Trr(Pe(E2(M))) \quad \text{for closed maps} \quad (11)$$

$$Ca(M)_{[6+n]} = En(Trr(Pe(E2(M)))) \quad \text{for open maps } (n = 1, 2 \dots) \quad (12)$$

Figure 7 presents the closed and open capra transforms of the tetrahedron.



Figure 7. Capra-transforms of the Tetrahedron

The pentangulation of a face can be done either clockwise or counter-clockwise. The result is an enantiomeric pair of objects: $CaS(M)$ and $CaR(M)$, in terms of the sinister/rectus stereochemical isomers. Figure 8 illustrates Schlegel projections of such a pair derived from the cube.

The sequence $CaS(CaS(M))$ results in a twisted transform, while $CaR(CaS(M))$ will straighten the (central part of) structure. Figure 9a shows such a transform from the cube. By removing the terminal twisted part of the structure, it results in a unit cell (of 176 atoms - Figure 1b) which gives a relaxed minimal P surface (Figure 9b).

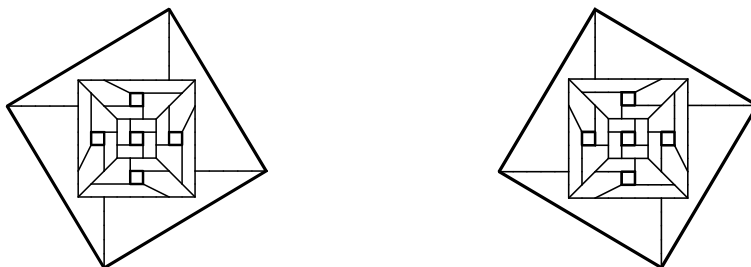


Figure 8. Enantiomer pair of the capra transforms of the cube (Schlegel projection)



Figure 9.

A similar unit can be derived from the tetrahedron, giving the corresponding D surface, exemplified in Figure 10 (six units).

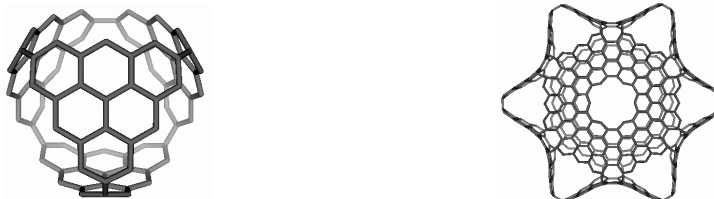


Figure 10.

Different structures will result when constructing surfaces only by $\text{CaS}(\text{Cube})_{[7]}$, or by pairs of $\text{CaS}(\text{Cube})_{[7]}$ and $\text{CaR}(\text{Cube})_{[7]}$. In the first case, construction is made by *identification* of edges in two units; it results in a quite strained structure, but tiled with only one kind of face (*i.e.*, heptagons - Figure 11a). By connecting the dangling bonds from pairs of CaS and CaR , results a straight structure, containing additional hexagons (Figure 11b).



Figure 11. Two connections of the units originating in capra transforms of the Cube

STRAIN ENERGY CALCULATION

In the POAV1 theory²²⁻²⁵ the π -orbital axis vector is defined as the vector which makes equal angles $\theta_{\sigma\pi}$ to the three σ -bonds of the sp^2 carbon atom and the *pyramidalization* angle is obtained as:

$$\theta_p = \theta_{\sigma\pi} - 90^\circ \quad (13)$$

This angle is used for estimating the strain energy, induced by a pyramidalized carbon atom, by:

$$SE = 200 \cdot (\theta_p)^2 \quad (14)$$

with θ_p being measured in radians. The difference $120 - \frac{1}{3} \sum \theta_p$ gives the deviation to planarity. Data of POAV1 analysis for the structure in Figure 9b (one repeat unit and 6 x 8 additional points, for the connecting octagons: 176 + 48 = 224 atoms) are given in Table 3.

Compare the strain energy per atom in Table 3 (in kcal/mol) with the values for C_{60} (8.257) and its tubulenic dimer (5.198) and find a more relaxed sp^2 carbon lattice, very close to the graphite sheet.

Table 3

Atom		Angle (deg)			Deviation	θ_π	SE	
Level	No.	1	2	3	(deg)	(deg)	(kcal/mol)	
1	1	120.544	119.606	119.560	0.290	1.789	1.560	
2	3	118.751	121.849	118.642	0.758	2.893	12.238	
3	6	118.829	119.290	121.097	0.784	2.943	25.328	
4	3	118.102	118.176	122.113	1.609	4.219	26.029	
5	6	119.150	119.360	117.925	3.565	6.301	116.089	
6	3	127.523	118.136	110.738	3.603	6.288	57.809	
7	3	117.924	119.353	119.126	3.597	6.329	58.571	
8	3	122.435	117.317	113.442	6.806	8.727	111.349	
Total								
224								408.972
SE/Atom = 1.826 (kcal/mol)								

CONCLUSIONS

Several carbon lattices, embedded in some infinite surfaces of negative curvature, have been discussed in the light of some celebrate theorems of surface curvature.

Single face negatively curved units was shown to be easily constructible by the capra operation on the Platonic trivalent polyhedra.

Strain energy of an infinite lattice, with the repeat unit derived by iterating capra-operation on the cube, is evaluated by the POAV1 approach. It was found that its strain is lower than that in C_{60} and its tubulenic dimer, in agreement with the data in literature. Clearly, IPMS's consist of relaxed sp^2 carbon lattices, very close to the graphite sheet. They mimic the microporous, low density, natural materials, like zeolites.

REFERENCES

1. O. Bonnet, *C. R. Acad. Sci. Paris*, **1853**, 37, 529-532.
2. D. J. Klein, *J. Chem. Inf. Comput. Sci.*, **1994**, 34, 453-459.
3. L. Euler, *Comment. Acad. Sci. I. Petropolitanae*, **1736**, 8, 128-140.
4. D. J. Klein and H. Zhu, in: A. T. Balaban (Ed.), *From chemical topology to three-dimensional geometry*, Plenum Press, **1997**, 297-341.
5. A. L. Mackay and H. Terrones, *Nature*, **1991**, 352, 762.
6. T. Lenosky, X. Gonze, M. Teter and V. Elser, *Nature*, **1992**, 355, 333-335.
7. M. O'Keeffe, G. B. Adams and O. F. Sankey, *Phys. Rev. Lett.*, **1992**, 68, 2325-2328.
8. H. Terrones and M. Terrones, *Carbon*, **1998**, 36, 725-730.
9. H. Terrones and A. L. Mackay, *Prog. Crystal Growth and Charact.*, **1997**, 34, 25-36.
10. D. Vanderbilt and J. Tersoff, *Phys. Rev. Lett.*, **1992**, 68, 511-513.
11. A. Ceulemans, R. B. King, S. A. Bovin, K. M. Rogers, A. Troisi and P. W. Fowler, *J. Math. Chem.*, **1999**, 26, 101-123.
12. R. B. King, *Discrete Mathematics*, **2002**, 244, 203-210.
13. R. B. King, *Croat. Chem. Acta*, **2000**, 73, 993-1015.
14. R. B. King, *J. Phys. Chem.*, **1996**, 100, 15096-15104.
15. R. B. King, *Croat. Chem. Acta*, **2002**, 75, 447-473.
16. R. B. King, *Discrete Mathematics*, **2000**, 51, 235-248.
17. R. B. King, *J. Chem. Inf. Comput. Sci.*, **1998**, 38, 180-188.
18. Diudea, M. V.; John, P. E.; Graovac, A.; Primorac, M.; Pisanski, T., *Croat. Chem. Acta*, **2003**, 76, 153-159.
19. M. V. Diudea, *Studia Univ. "Babes-Bolyai"*, **2003**, 48, 2, 3-22.
20. M. Goldberg, *Tôhoku Math. J.*, **1937**, 43, 104-108.
21. M. Dutour and M. Deza, LIGA, ENS/CNRS, Paris, **2003** (preprint).
22. R.C. Haddon, *J. Am. Chem. Soc.*, **1990**, 112, 3385.
23. R.C. Haddon and K. Raghavachari, in: W.E. Billups and M.A. Ciufolini, *Buckminsterfullerenes*, VCH, **1993**, pp. 185-215.
24. R. C. Haddon and S.-Y. Chow, *J. Am. Chem. Soc.*, **1998**, 120, 10494.
25. R. C. Haddon, *J. Phys. Chem. A*, **2001**, 105, 4164.

MODELING BIOLOGICAL ACTIVITY OF (3-PYRIDYLMETHYL)BENZOQUINONE DERIVATIVES

CRINA V. VERES, MIHAELA CAPRIOARA, CSABA L. NAGY
and MIRCEA V. DIUDEA

*Faculty of Chemistry and Chemical Engineering,
Babes-Bolyai University, 400028 Cluj, Romania*

ABSTRACT. (3-Pyridylmethyl)benzoquinone derivatives inhibit thromboxane A_2 synthase and leukotriene biosynthesis enzymes. For such chemicals, a QSAR study has been performed in order to stress the relation between the molecular structures and their biological activity. The models are built up on the ground of hypermolecule concept. Partial charges, autocorrelated by a multivariate regression, are used for molecular description. The hypermolecule has the meaning of a complement of the investigated biological receptor space. A general procedure for developing and validating QSAR models is given.

INTRODUCTION

Lipoxygenases (LOX) are a family of cytosolic enzymes. They are monomeric proteins that contain a "non-heme" iron per molecule in the active site as high-spin Fe(II) in the native state, and high-spin Fe(III) in the activated state.¹⁻³ Lipoxygenases as dioxygenases recognize the 1,4-pentadiene structure of polyunsaturated fatty acids and catalyze their oxygenation to corresponding lipid hydroperoxides. LOX have a high degree of homology in the proposed iron binding region and the primary reactions they catalyze are essentially the same. Lipoxygenases are responsible for the biosynthesis of leukotrienes, eicosanoids, monohydroperoxy- and dihydroperoxy-polyenoic fatty acids, lipoxins. An overproduction of these products can cause disturbances in the metabolic reactions, and are involved in some metabolic diseases and pathologies. These effects have been linked to immunological and radiation disorders, tumors, toxicoses, hypodinyamy, coronary and angiological pathologies (vasospasm, thrombosis and arteriosclerosis).

The major products of 5-LOX, leukotrienes (LT), are a family of important biologically active molecules. LTB_4 is a potent chemotactic agent and inflammatory mediator⁴ and the peptidoleukotrienes LTC_4 and LTD_4 are powerful spasmogens in vascular and bronchial tissues⁵. Elevated levels of LT are associated with a number of inflammatory conditions including asthma, psoriasis, ulcerative colitis, and rheumatoid arthritis, and indeed LT have been recovered from various pathological tissues. Therefore, potent inhibitors of this enzyme are candidate drugs for the treatment of these diseases.^{6,7} These inhibitors can be broadly classified into two main categories: first, competitive lipid substrate inhibitors and, second, redox-type inhibitors, which act by intermediate produced during the catalytic step.⁸

(3-Pyridylmethyl)benzoquinone derivatives⁹ inhibit thromboxane A_2 synthase and leukotriene biosynthesis enzymes. For the inhibition of 5-LOX the experiments were made in human blood (human whole blood assay).

Many thousands of compounds have been screened as LOX inhibitors in industrial laboratories and a large number of active compounds with novel structures are undergoing clinical trials. This evaluation provides data sets suitable for quantitative structure-activity relationships (QSAR). The laboratory tests utilized in identifying lipoxygenase inhibitors are: human granulocytes, rat basophilic cells (RBL-1) and human whole blood assay (HWBL).

For drugs acting as LOX inhibitors, the hydrophobicity¹⁰⁻¹⁴ is an important property, also significant in their susceptibility to the attack of the P450 enzymes.¹⁵

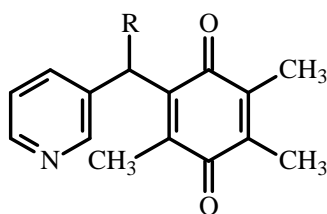
METHODS

A QSAR study was made for the (3-pyridylmethyl)benzoquinone derivatives.⁹ The negative logarithm of IC_{50} was used in the correlation analyses. Thus a higher $\log 1/IC_{50}$ value represents a more potent compound. The following QSAR model is obtained with the data reported in Structure 1 and Table 1:

$$\log 1/IC_{50} = 0.49(\pm 0.234)MR - 1.914(\pm 0.421)I_{COOH} - 1.641(\pm 0.535)I_{Ph} + 2.174(\pm 2.077) \quad (1)$$

$$n = 19, r = 0.957, r^2 = 0.916, q^2 = 0.858, s = 0.359, F_{3,15} = 6.949$$

In the following QSAR model, MR is the overall calculated molecular refractivity. Since MR is a primarily measure of the bulk of the substituent, the positive coefficient for this term indicates that molecules are contacting polar space in the enzyme¹⁶, not hydrophobic space. A positive coefficient might suggest an interaction depending on the polarizability of the substituents although there is a little evidence for the importance of such an effect. On the other hand I_{COOH} and I_{Ph} (indicator variables having a value of 1 when R has a carboxylic or phenyl group) have negative signs, which mean that the presence of these groups decreases the inhibition of LOX.



Structure 1

However, if the experimental measured lipophilicity $\log P_E$ is used in place of MR , equation (2) is obtained:

$$\log 1/IC_{50} = 0.498(\pm 0.149)\log P_E - 1.439(\pm 0.562)I_{Ph} + 4.461(\pm 0.533) \quad (2)$$

$$n = 19, r = 0.921, r^2 = 0.849, q^2 = 0.810, s = 0.467, F_{2,16} = 33.118$$

Equation 2 shows that there is a linear relationship between the biological activity (BA) $\log 1/IC_{50}$ and $\log P_E$ (experimental lipophilicity).

Table 1

R	CD ₁	CD ₂	CD ₄	CD ₅	CD ₆	CD ₈	CD ₁₃	CD ₁₅	CD ₁₆	CD ₁₉	Y
ci	2758.2	2313.8	224.5	8758.1	1395	-15326	-101.05	9339.8	10725	-20586	
Me	0.034	0.031	-0.232	0.063	0.118	0.062	0.060	0.118	0.018	0.018	5.022
CH ₂ Me	0.033	0.031	-0.235	0.064	0.117	0.062	0.060	0.117	0.017	0.017	6.018
(CH ₂) ₃ Me	0.033	0.031	-0.239	0.064	0.117	0.062	0.060	0.116	0.016	0.016	6.081
(CH ₂) ₅ Me	0.033	0.031	-0.241	0.064	0.116	0.062	0.060	0.115	0.016	0.015	7.137
=CH(CH ₂) ₄ Me(Z)	0.037	0.033	-0.240	0.065	0.118	0.063	-0.004	0.119	0.018	0.019	6.585
=CH(CH ₂) ₄ Me(E)	0.037	0.033	-0.240	0.065	0.118	0.063	-0.004	0.119	0.018	0.019	6.658
(CH ₂) ₄ OH	0.035	0.032	-0.233	0.065	0.117	0.063	0.063	0.117	0.017	0.017	7.000
(CH ₂) ₅ OH	0.034	0.032	-0.241	0.065	0.117	0.063	0.062	0.116	0.017	0.016	7.000
(CH ₂) ₄ OAc	0.038	0.035	-0.239	0.068	0.120	0.065	0.069	0.120	0.019	0.020	6.602
(CH ₂) ₅ OAc	0.037	0.034	-0.240	0.067	0.119	0.065	0.066	0.119	0.019	0.018	7.060
(CH ₂) ₃ COOH	0.038	0.034	-0.238	0.067	0.120	0.065	0.069	0.120	0.020	0.020	5.000
(CH ₂) ₄ COOH	0.034	0.037	-0.240	0.067	0.119	0.064	0.066	0.119	0.019	0.019	4.222
(CH ₂) ₅ COOH	0.036	0.033	-0.241	0.066	0.118	0.064	0.064	0.118	0.018	0.018	5.032
(CH ₂) ₆ COOH	0.035	0.033	-0.242	0.066	0.118	0.064	0.063	0.117	0.017	0.017	5.155
=CH(CH ₂) ₄ COOH	0.039	0.035	-0.239	0.068	0.119	0.065	0.000	0.121	0.020	0.021	5.143
Ph	0.036	0.032	-0.243	0.066	0.117	0.063	0.079	0.117	0.017	0.017	5.119
PhCH=C(Me)COOH	0.038	0.035	-0.246	0.068	0.119	0.065	0.083	0.119	0.018	0.019	4.000
PhCH=CHCOOH	0.038	0.034	-0.245	0.068	0.119	0.065	0.083	0.119	0.018	0.019	4.060
Ph(CH ₂) ₂ COOH	0.038	0.034	-0.245	0.068	0.118	0.065	0.082	0.119	0.018	0.018	4.000

CALCULATION OF MOLECULAR DESCRIPTORS

In order to achieve the QSAR, the structure is encoded in a numerical form. The arrangement of substituent groups on the (3-Pyridylmethyl)benzoquinones can be accounted for by the *hypermolecule HM* concept,¹⁷ viewed as a complement of the investigated biological receptor space. In the construction of the hypermolecule, a *row-vector* P_i of dimension N_{HM} is attached to each molecule M_i :

$$P_i = \{P_{ij}; j = 1, 2, \dots, N_{HM}\} \quad (3)$$

where N_{HM} is the number of vertices in the hypermolecule. The molecules of the set are superimposed according to their maximal common substructures. In the associated vector, the matching positions take $P_{ij} = 1$ while for the non-matching ones $P_{ij} = 0$. The description of the j^{th} position in *HM* (e.g., the chemical and/or topological nature of the j^{th} atoms) is given by X_{ij} .

The hypermolecule and the molecules under study can be numerically described by using some molecular *topological descriptors* TD_i :^{18,19}

$$TD_i = \sum_j TD_{ij} = \sum_j a_j P_{ij} X_{ij} \quad (4)$$

where P_{ij} and X_{ij} have the meaning above mentioned while a_j represent the regression coefficients as given by the multivariate regression $\log BA = f(X_i)$. The above *TDs* are "ad-hoc" descriptors^{20,21} depending on the set of molecules considered and the selected molecular property. Therefore, all the (3-pyridylmethyl)benzoquinones can be described using particular local properties that characterize both the substituted/ unsubstituted positions.

As local property for calculating *TDs*, we used X_{ij} = partial charges related to each position in (3-pyridylmethyl)benzoquinones.

STATISTICS

For developing the QSAR models, the set of (3-Pyridylmethyl) benzoquinones was submitted to REGLINEWIN (a home made statistical software package). The correlating equation is of the form:

$$Y_i = b_0 + \sum_{j=1}^m b_j \cdot TD_{ij} \quad (5)$$

where Y_i is the dependent variable, TD_{ij} are the predictor variables, $m < n$, n being the number of structures in the set.

The correlating algorithm follows the steps:

1. generate the *hypermolecule*
2. perform Leave-one-out LOO analysis on the set of local descriptors
3. calculate the global descriptors by using partial charges
4. find the best regression equation
5. test the predictive capability of the model

DESCRIPTOR REDUCTION

The LOO procedure was applied on the set of descriptors in view of finding the relevant descriptors (i.e., the relevant positions in the hypermolecule). The results are listed in Table 2.

Table 2

No of descriptors	Model (MLR)	Irrelevant positions	r^*
$k-1$	$BA = f(C_i), i = 1, 2, \dots k-1$	C_{11}	0.999
$k-2$	$BA = f(C_i), i = 1, 2, \dots k-2$	C_{11}, C_{12}	0.998
$k-3$	$BA = f(C_i), i = 1, 2, \dots k-3$	C_{11}, C_{12}, C_{13}	0.996
$k-4$	$BA = f(C_i), i = 1, 2, \dots k-4$	$C_{11}, C_{12}, C_{13}, C_{14}$	0.995
$k-5$	$BA = f(C_i), i = 1, 2, \dots k-5$	$C_{11}, C_{12}, C_{13}, C_{14}, C_{15}$	0.992
$k-6$	$BA = f(C_i), i = 1, 2, \dots k-6$	$C_{11}, C_{12}, C_{13}, C_{14}, C_{15}, C_{16}$	0.989
$k-7$	$BA = f(C_i), i = 1, 2, \dots k-7$	$C_{11}, C_{12}, C_{13}, C_{14}, C_{15}, C_{16}, C_{17}$	0.988

*after descriptor elimination

From Table 2, it appears that a satisfactory statistics is ensured by a map comprising $k-7$ ($C_{11}, C_{12}, C_{13}, C_{14}, C_{15}, C_{16}, C_{17}$) relevant positions, for which the partial charge descriptors CD_i are given in Table 1.

The numbering of the hypermolecule is given in Structures 2 (initial map) and 3 (final map).

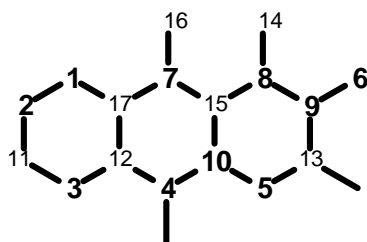
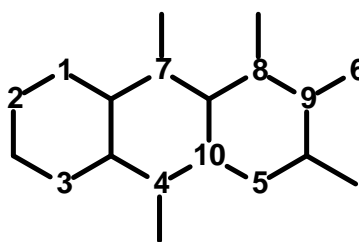

Structure 2

Structure 3

Table 3 lists the global CD descriptor (i.e., the sum of CD_i descriptors over all vertices), experimental and calculated biological activity values and the residuals (i.e., the difference between the experimental and calculated BAs) as well.

Table 3

	Molecule	CD	$BA_{obs.}$	$BA_{calc.}$	Residual
1	Me	806.94	5.022	4.928	0.094
2	CH_2Me	807.835	6.018	5.809	0.209
3	$(CH_2)_3Me$	807.993	6.081	5.965	0.116
4	$(CH_2)_5Me$	809.211	7.137	7.165	-0.028
5	$=CH(CH_2)_4Me(Z)$	808.680	6.585	6.641	-0.056
6	$=CH(CH_2)_4Me(E)$	808.680	6.658	6.641	0.017
7	$(CH_2)_4OH$	809.041	7	6.997	0.003
8	$(CH_2)_5OH$	809.073	7	7.029	-0.028

	Molecule	CD	BA _{obs.}	BA _{calc.}	Residual
9	(CH ₂) ₄ OAc	808.372	6.602	6.338	0.264
10	(CH ₂) ₅ OAc	808.790	7.06	6.749	0.311
11	(CH ₂) ₃ COOH	807.230	5	5.213	-0.213
12	(CH ₂) ₄ COOH	806.223	4.222	4.221	0.001
13	(CH ₂) ₅ COOH	807.285	5.032	5.267	-0.235
14	(CH ₂) ₆ COOH	807.498	5.155	5.477	-0.322
15	=CH(CH ₂) ₄ COOH(E+Z)	807.117	5.143	5.102	0.042
16	Ph	807.354	5.119	5.335	-0.216
17	PhCH=C(Me)COOH	805.762	4	3.766	0.234
18	PhCH=CHCOOH	806.099	4.06	4.098	-0.038
19	Ph(CH ₂) ₂ COOH	806.159	4	4.157	-0.157

The best QSAR model found is:

$$\log 1/IC_{50} = -810.46 + 1.01 \cdot CD \quad (6)$$

$n = 19$; $r = 0.988$; $s = 0.181$; $cv\% = 3.22$; $F = 683.71$

Random correlation: $r_1 = 0.662$; $r_2 = 0.691$;

A random test showed a marked drop in the correlation coefficient, with the meaning that no chance correlation occurred.

The model was cross-validated by LOO procedure applied on the set of molecules. Figure 1 presents the plot cross-validated BA vs. experimental BA, (i.e., $\log 1/IC_{50}$). The excellent result in prediction ($q = 0.985$; $q^2 = 0.970$) proves the quality of the model.

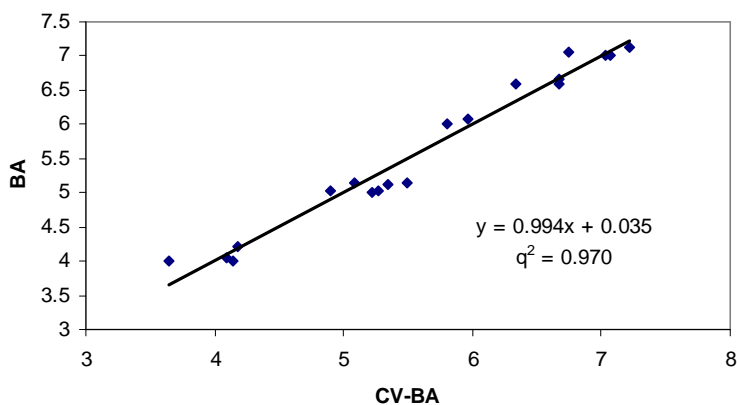


Figure 1. The plot of LOO calculated vs. experimental biological activity.

CONCLUSIONS

Partial charges were used as local descriptors for encoding the *hypermolecule*, that mimics the biological receptor space.

The descriptors have been fitted by means of multivariate regression and represent "ad-hoc" (or "autocorrelated") descriptors, which change with the set of molecules and selected property.

Within the hypermolecule model, data reduction (*i.e.*, selection of relevant descriptors) was achieved. The statistics of the model derived on the final map (the relevant substituted positions) are excellent both in estimation and prediction, surpassing the literature reported results.

REFERENCES

1. P. M. Hilbers, A. Rossi, A. Finazzi-Agro, G. A. Veldink and F. G. J. Vliegthart, *Biochim. Biophys. Acta*, **1994**, *1211*, 239-242.
2. C. W. Stallings, B. A. Kroa, R. T. Carroll, A. L. Mertzner and M. O. Funk, *J. Mol. Biol.*, **1990**, *211*, 685-687.
3. J. C. Boyington and L. M. Amzel, *J. Mol. Biol.* **1990**, *165*, 12771-12773.
4. A. G. Gilman, T.W. Rall, A. S. Nies, P. Taylor (Ed.) *The Pharmacological Basis of Therapeutics*, McGraw-Hill International Editions, Medical Series, **1992**, pp. 600-617.
5. M. O'Donnell and A. Welton, *Therapeutic Approaches in Inflammatory Disease*, Eds. A. J. Lewis and N. S. Doherty, Elsevier, New York, **1989**, p. 169.
6. P. J. Piper, L. G. Letts, M. N. Samhoun, J. R. Tippins and M. A. Palmer, *Advances in Prostaglandin, Thromboxane and Leukotriene Research*, Vol 9, Raven Press, New York, **1982**, p. 169.
7. K. Muller, *Arch. Pharm.*, **1994**, *327*, 3-19.
8. R. D. Abeysinghe, P. J. Roberts, Ch. E. Cooper, K. H. MacLean, R. C. Hider, J. B. Porter, *J. Biol. Chem.*, **1996**, *271*, 7965-7972.
9. S. Ohkawa, S. Terao, Z. Terashita, Y. Shibouta, and K. Nishikawa, *J. Med. Chem.*, **1991**, *34*, 267-276.
10. K. H. Kim, Y. C. Martin, D. W. Brooks, D. Dyer and G. W. Carter, *J. Pharm. Sci.*, **1994**, *83*, 433-438.
11. K. H. Kim, Y. C. Martin and D. W. Brooks, *Quant. Struct. Act. Relat.*, **1996**, *15*, 491-497.
12. Y. Naito, M. Sugiura, Y. Yamaura, C. Fukaya, K. Yokoyama, Y. Nakagawa, T. Ikeda, M. Senda and T. Fujita, *Chem. Pharm. Bull.*, **1991**, *39*, 1736-1745.
13. J. B. Summers, B. P. Gunn, J. G. Martin, M. B. Martin, H. Mazdiyasi, A. O. Stewart, P. R. Young, J. B. Bouska, A. M. Goetze, R. D. Dyer, D. W. Brooks and G. W. Carter, *J. Med. Chem.*, **1988**, *31*, 1960-1964.
14. J. B. Summers, K. H. Kim, H. Mazdiyasi, J. H. Holms, J. D. Ratajczyk, A. O. Stewart, R. D. Dyer and G. W. Carter, *J. Med. Chem.*, **1990**, *33*, 992-998.
15. C. Hansch and L. Zhang, *Drug Metab. Rev.*, **1993**, *25*, 1-48.
16. C. Hansch and J. Caldwell, *J. Comput.-Aided Mol. Des.*, **1991**, *5*, 441-453.
17. J. A. Platts, M. H. Abraham, D. Butina, and A. Hersey, *J. Chem. Inf. Comput. Sci.*, **2000**, *40*, 71-80.

18. R. P. Schvarzenbach, P. M. Gschwend and D. M. Imboden, *Environmental Organic Chemistry*, John Wiley&Sons, New York, **1992**.
19. O. M. Minailiuc and M. V. Diudea, TI-MTD Model. Applications in molecular Design, in: *QSPR/QSAR Studies by Molecular Descriptors*, Nova Science Publishers, Inc., **2001**, pp. 363- 388.
20. R. P. Sheridan, *J. Chem. Inf. Comput. Sci.*, **2000**, *40*, 1456-1469.
21. I. Motoc, S. Holban, R. Vancea and Z. Simon, *Studia Biophys. (Berlin)* **1977**, *66*, 75-78.

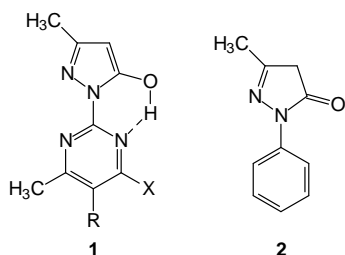
AZOCOUPLING PRODUCTS. III.¹ SPECTROSCOPIC INVESTIGATION AND SYNTHESIS OF SOME AZOCOUPLING PRODUCTS BETWEEN 1-(4-HYDROXY-6-METHYL-PYRIMIDIN-2-YL)-3-METHYL-PYRAZOLIN-5-ONE AND AROMATIC DIAZONIUM SALTS

**IOAN PANEA, ADINA GHIRISAN, FLORIN IURA, RADU GROPEANU
and IOAN A. SILBERG**

*Department of Organic Chemistry, Faculty of Chemistry and
Chemical Engineering, Babes-Bolyai University
11th Arany János St., 400028 Cluj-Napoca, Romania*

ABSTRACT. By azocoupling of 1-(4-hydroxy-6-methyl-pyrimidin-2-yl)-3-methyl-pyrazolin-5-one (11) with disubstituted benzene diazonium salts (3) three new dyes (12-14) were synthesized. The comparative electronic absorption and ¹H-NMR studies of these compounds (12-14) and of other azocoupling products (4-10, 15) of 11 with *ortho*-, respectively *para*- monosubstituted benzenediazonium salts support the manifestation of the azo-hydrazone tautomerism for the examined dyes. However, in aprotic solvents and in acidic medium only one species has been detected for the studied dyes. The ¹H-NMR spectra of these dyes recorded in deuterio-chloroform prove the hydrazone structure (4a-10a, 12a-15a) of the detected species. In methanolic solution the hydrazone tautomer is favored with respect to the azohydroxy tautomer by the *ortho*-substituent in benzenic ring of the examined azocoupling products (8, e.g.), as a manifestation of the *ortho* effect of the substituent. It is described also the *ortho* effect of the substituent situated in the *ortho*-position of the benzenic ring of azocoupling products 8-10, 15 concerning the acidity and the chemical shift of their mobile hydrogen having the ¹H-NMR signal at about 14 ppm. The *ortho* effect of nitro group is unusually strong ($\Delta\delta_{o-p} = 1.5$ ppm).

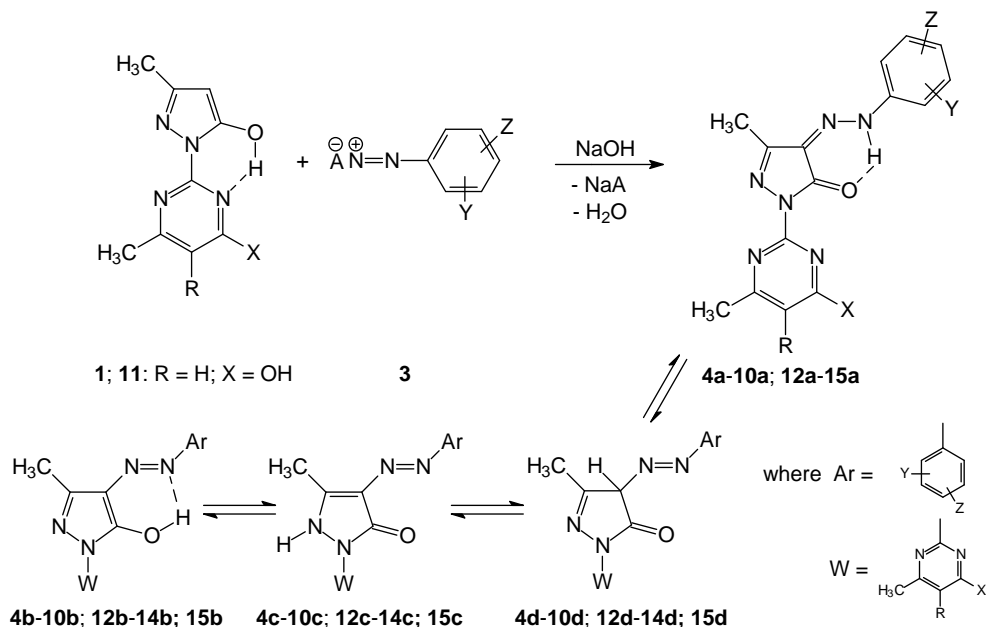
1. INTRODUCTION



Taking into account the proved structural [1] and reactivity [1-3] analogy between 1-(6-methyl-5-R-4-X-pyrimidin-2-yl)-3-methyl-pyrazolin-5-ones (**1**) and 1-phenyl-3-methyl-pyrazolin-5-one (**2**) as well as the known utilisation of the latter to the manufacturing by azocoupling [4-6] of a series of commercial dyes, we have carried out [2,3,7,8] the azocoupling of **1** with aromatic diazonium salts (**3**).

The electronic absorption spectra of the obtained azocoupling products (**4**) exhibit in the range of 350-600 nm one, two or three bands as a function of (i) the substituent in the benzenic, respectively pyrimidinic ring; (ii) the solvent and (iii) the acidity or basicity of the methanolic solution used for the recording of the spectra [8,9]. This behavior has been attributed [8,9] to the possible tautomerism of the azocoupling products (**4a-4d**).

¹ Part II: reference [8]



1: R = H, C₁-C₄ Alkyl; X = OH, OCH₃, Cl;

3: Y = H, CH₃, COOH, NO₂, Cl; Z = R, X, Y, NHC(=O)CH₃, N(CH₃)₂, OC₂H₅, Br, COOCH₃, SO₂NH₂;

4: R, X as in 1; Y, Z as in 3;

5: R = H; X = OH; Y = H; Z = 4-NO₂;

10: R = H; X = OH; Y = 2-NO₂; Z = H;

6: R = H; X = OH; Y = H; Z = 4-CH₃;

12: R = H; X = OH; Y = 3-CH₃; Z = 4-NO₂;

7: R = H; X = OH; Y = H; Z = 4-Cl;

13: R = H; X = OH; Y = 2-CH₃; Z = 4-CH₃;

8: R = H; X = OH; Y = 2-CH₃; Z = H;

14: R = H; X = OH; Y = 3-NO₂; Z = 4-C₂H₅;

9: R = H; X = OH; Y = 2-Cl; Z = H;

15: R = H; X = OH; Y = 2-NO₂; Z = 4-CH₃.

SCHEME 1

In the above mentioned studies [8,9] we brought arguments especially for the hydrazone (**4a**) and the hydroxyazo (**4b**) tautomers. The hydrazone forms **4a** were sustained among other things by NOESY spectra [9]. These spectra recorded in CDCl₃ have showed an interaction and therefore a spatial close proximity of the mobile hydrogen atom (responsible for the ¹H-NMR signal at 13-14 ppm) with the hydrogen atoms situated on the benzenic ring in *ortho*-position with respect to the two nitrogen atoms bridge between the rings of the azocoupling products **4**. Such a spatial arrangement is compatible only with the hydrazone tautomer **4a** when one takes also into account the expected electronic absorption spectra of all tautomers **4a-4d** and that observed in fact for **4** in CHCl₃ [9]. The lowest field ¹H-NMR signal (13-14 ppm) of the azocoupling products **4** corresponds to strongly chelated hydrazone N-H of **4a** (compare [10]). As a consequence of these observations it was of interest to examine the effect of the substituent in the mentioned *ortho*-position of the benzenic

ring on the lowest field $^1\text{H-NMR}$ signal of the azocoupling products **4**. This effect may give useful information on the structure of tautomeric azocoupling products **4** (see [11]). On the other hand, the azohydroxy tautomers **4b** were supported especially by the effects of the alkali or acid addition on the electronic absorption spectra of the azocoupling products **4** in methanolic solutions. These effects have been totally different [9] for the azocoupling product substituted with a nitro group in *para* position of the benzenic ring (**5**) comparative to other azocoupling products of this series (e.g. **6**, **7**). Therefore, it was interesting to examine whether these effects manifest themselves for the azocoupling products substituted in *ortho*- position of the benzenic ring (e.g. **8-10**) in a similar manner as for the *para*- isomers (e.g. **5-7**). Consequently, a purpose of this work is the comparative study of the electronic and $^1\text{H-NMR}$ spectra of three pairs consisting of isomeric products (**5-10**) obtained by azocoupling of 1-(4-hydroxy-6-methyl-pyrimidin-2-yl)-3-methyl-pyrazolin-5-one (**11**) with *ortho*-, and with *para*-substituted benzenediazonium salts (**3**), respectively. This study should contribute to the elucidation of the tautomerism of the azocoupling products **4** and of the *ortho* effect of some substituents. Another aim is the synthesis of three new in benzenic ring disubstituted azocoupling products (**12-14**)² and their spectroscopic (electronic and $^1\text{H-NMR}$) study, comparative to other already studied [8,9] similar dyes (**4**).

RESULTS AND DISCUSSIONS

A. Electronic absorption study

Table 1

Some chemical and physical data of the newly synthesized dyes (**12-14**).

Substituents Y, Z; compound no.	Yield (%)	Melting point (°C)	Elemental analysis data Calcd./found (%)			UV-VIS data in methanol λ [nm], (ϵ , mol ⁻¹ ·cm ⁻¹)
			C	H	N	
Y=3-CH ₃ , Z=4-NO ₂ 12	92	289-290	52.03/ 52.10	4.06/ 4.20	26.56/ 26.30	425 (38.000)
Y=2-CH ₃ , Z=4-CH ₃ 13	95	254-255	60.35/ 59.90	5.32/ 5.50	24.85/ 24.70	392 (15.800) 428 (17.200)
Y=3-NO ₂ , Z=4-C ₂ H ₅ 14	95	246-247	53.26/ 53.30	4.43/ 4.60	25.58/ 25.50	388 (16.200)

The Table 1 and Figure 1 report some data for the newly synthesized azocoupling products **12-14**. The electronic absorption spectra of these, similarly to other studied [8,9] 1-(pyrimidin-2-yl)-3-methyl-pyrazolin-5-one azocoupling products (e.g. **5-7**; see Figure 2, curves 1-3), exhibit in the range 350-600 nm (Figure 1) one (**12-14**), two (**13**) or three (**14**) absorption bands (even if some of them appear only as shoulders) as a function of the substituents on the benzenic ring, of the solvent and of the acidity or the basicity of the methanolic solutions used for recording the

² The compounds for which several tautomers are possible are indicated in the corresponding figure **1**, **2**, **4-15** not accompanied by letters, except when a definite tautomer is under discussion. The examined azocoupling products **5-10**, **12-15** differentiate only by the substituents in the benzenic ring. The substituent positions are related to the hydrazono (or azo) bridge.

spectra. Also, the effect of acid or alkali addition to the methanolic solution of each new dye (**12-14**) is similar to that observed [8,9] for the azocoupling products **4** unsubstituted or mono-substituted in the benzenic ring (e.g. **5-7**; compare Figure 1 with Figure 2). On this basis one can assume that the newly synthesized azocoupling products (**12-14**) manifest very probably the azo-hydrazone tautomerism that was already assigned for similar reasons [8,9], in the case of some analogues dyes. However, since the visible spectra of these dyes recorded in chloroform, acetic acid and acidified methanol show practically the same unique absorption maximum (e.g. Figure 1a) the examined azocoupling products have been detected in mentioned solvents as a unique species, namely the hydrazone tautomer (**12a-14a**).

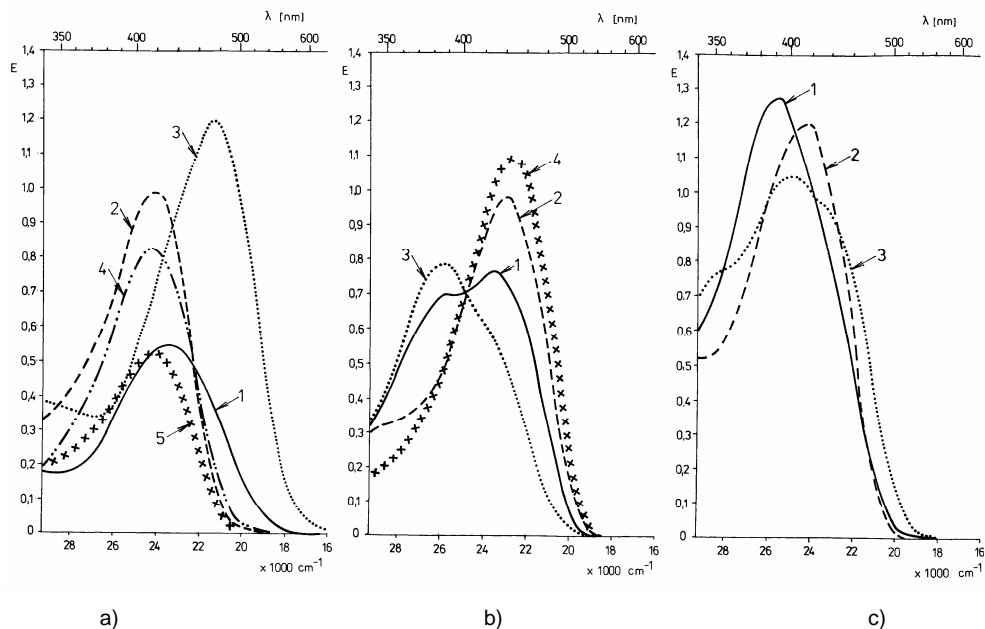


Figure 1. The electronic absorption spectra of the newly synthesized compounds: a) **12**; b) **13**; c) **14**. Curves 1: methanolic solution; curves 2: methanolic 0.1 mol/dm^3 HCl solution; curves 3: methanolic 0.1 mol/dm^3 KOH solution; curves 4: chloroformic solution; curves 5: acetic acid solution.

The Figure 2 presents the absorption spectra of three pairs of isomeric azocoupling products (**5, 10**; **6, 8**; **7, 9**) in the range 350-600 nm. One isomer of each pair has the substituent of the benzenic ring in *para* position (**5-7**) while the other bears the same substituent in the *ortho* position (**8-10**). These spectra in absolute methanol present for every pair practically the same absorption maxima. However, for the azocoupling products having the substituent in *ortho*-position the absorption band, corresponding to the longest absorption maximum, is a little narrower and lacks the shoulder that can appear for *para* substituted isomers (e.g. **6**) at lower wavelength (Figure 2b, curves 1 and 4). This shoulder was assigned [9] to the hydroxyazo tautomer (e.g. **6b**). Consequently, the absence of the shoulder for the *ortho*-isomers (e.g. **8**, Figure 2b) can signify the increase of the content of hydrazone tautomer (e.g. **8a**) in these cases (compare [11]).

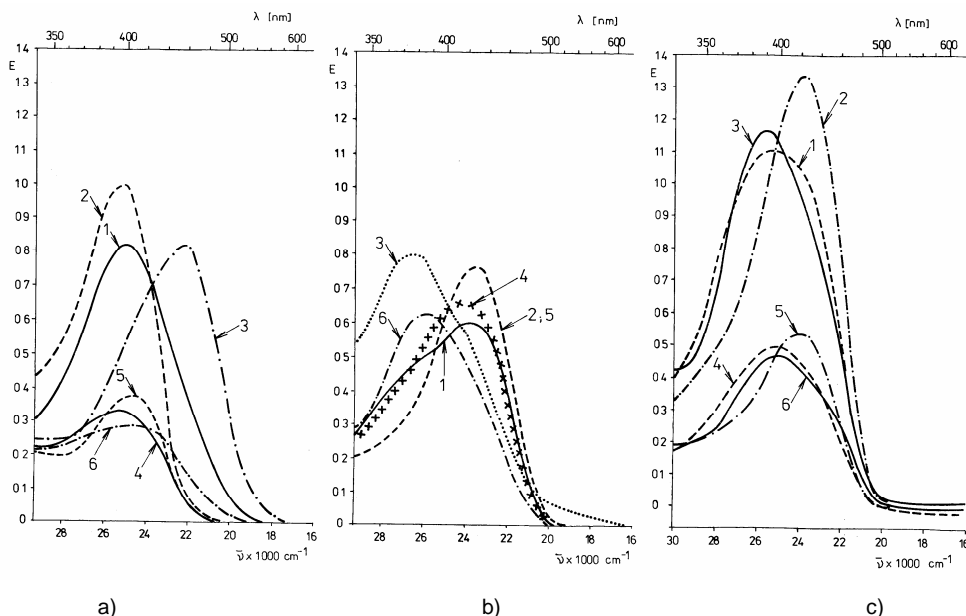


Figure 2. The electronic absorption spectra of three pairs of isomeric *para*- and *ortho*-substituted azocoupling products: a) nitro-substituted (**5**, **10**); b) methyl-substituted (**6**, **8**); c) chloro-substituted (**7**, **9**). Curves 1, 2, 3: for *para*-substituted products (**5-7**); curves 4, 5, 6: for *ortho*-substituted products (**8-10**). Curves 1, 4: methanolic solution; curves 2, 5: methanolic 0.1 mol/dm³ HCl solution; curves 3, 6: methanolic 0.1 mol/dm³ KOH solution.

The effects of the addition of acid respectively of alkali, up to a concentration of 0.1 mol/dm³ on the electronic absorption spectrum of the azocoupling product **8** (methyl substituted in *ortho*-position) recorded in methanol are practically identical to those observed for the corresponding *para* substituted isomer **6** (Figure 2b). Also, these effects are very similar for the *para* (**7**) and *ortho* (**9**) chloro-substituted azocoupling products (Figure 2c). On the contrary, these effects on the methanolic solution of the *ortho*-nitro-substituted azocoupling product (**10**) are different from those observed for the *para*-substituted isomer (**5**). Thus, while the HCl addition up to 0.1 mol/dm³ over the methanolic solution of the *para* isomer **5** causes a very weak (~ 5nm) hypsochromic shift of the longest wavelength band, the same addition to the absolute methanolic solution of the *ortho* isomer **10** determines a bathochromic shift (~ 10 nm) of the longest wavelength band of **10**. The different behaviour of *ortho*-nitro substituted azocoupling product comparative to the *para* isomer **5** may be caused by the *ortho*-effect of the nitro group. This effect may be exerted in **10** by the formation of intramolecular hydrogen bonding (compare [12]) between *ortho*-nitro group and hydrazoneic N-H of the hydrazone tautomer **10a**.

On the other hand, KOH addition up to 0.1 mol/dm³ in methanolic solution of **5** and **10**, respectively, has induced in both cases a bathochromic shift which is much stronger for **5** (~60 nm) than for **10** (~10 nm). The strong bathochromic shift in the case of **5** may be explained [9] by the dissociation *via* deprotonation of the more acidic pyrazolic -OH (compare [13]) of the azohydroxy tautomer **5b**. Only the

very extensively delocalized anion resulted by the described dissociation of the pyrazolic –OH in the azohydroxy tautomer **5b** (the delocalization being extended between *para* nitro group of the benzenic ring and the pyrazolic oxygen) is compatible with such an absorption at much greater wavelength as compared to the undissociated species. The acidifying is due to the conjugation of the donor pyrazolic –OH with the strong withdrawing –NO₂ group in *para* position of the benzenic ring of the azohydroxy tautomer **5b**. Thus, the much lower bathochromic shift determined by addition of KOH to the methanolic solution of **10** can signify a much lower acidity of **10**. This low acidity of **10** may determine its decreased dissociation to form an extensive delocalized anion of the type resulted by deprotonation of **5** and implies a lower bathochromic shift. This low acidity of **10** may be explained by a possible stabilization of the low acidity (compare [13]) hydrazonic tautomer **10a** by the already presumed intramolecular hydrogen bonding between hydrazonic N-H and the *ortho*-nitro group of the benzenic ring, as a manifestation of the *ortho*-effect of the nitro group. The implication of the tautomeric azohydroxy-hydrazono equilibrium in the explanation of acidity difference (and on this basis of longest wavelength band position in alkaline medium) between *para*- (**5**) and *ortho*- (**10**) nitro-substituted azocoupling products (*para*>*ortho*) is supported also by the fact that the acidity of the corresponding nitro-anilines is reversed (*para*<*ortho* [12]). Indeed, if the acidity of the *para*- and *ortho*-nitro-substituted azocoupling products **5** and **10**, respectively, would be determined only by the hydrazonic tautomers **5a** and **10a**, respectively, which have the hydrazonic N-H group bond to the nitro-substituted benzenic ring as in the corresponding anilines, the acidity of **5** and **10** (*para*>*ortho*) should vary as the one for the nitroanilines (*para*<*ortho* [12]), which is not the case.

A strong bathochromic shift (~60 nm) has been observed also in the case of the addition of alkali to the methanolic solution of the azocoupling product substituted in the benzenic ring in *para* with nitro and in *meta* with methyl (**12**, Figure 1a). In exchange, the addition of alkali to the methanolic solution of the *ortho*-nitro-*para*-methyl-substituted azocoupling product (**15**) caused no bathochromic shift. Consequently, the differentiation of the effect of alkali addition as a function of the nitro group position in the benzenic ring of azocoupling products **4** manifests itself similarly both in mono- and di-substituted derivatives. Therefore, the discussed effect of alkali addition may be used to establish the position of the nitro-group in benzenic ring of the azocoupling products **4** in the case when this group may be situated either in *ortho* or in *para*-position.

B. ¹H-NMR Study

The ¹H-NMR data of the new azocoupling products (**12-14**) together with those of the examined pairs of *ortho*- and *para*- substituted isomers (**5**, **10**; **6**, **8**; **7**, **9**) and of the azocoupling product (**15**) between **11** and the diazonium salt obtained from 4-methyl-2-nitro-aniline are presented in Table 2.

The ¹H-NMR spectra of the azocoupling products **5-10**, **12-15** recorded in CDCl₃ solution show the formal existence of a single species and the presence of a mobile hydrogen atom by a very low field signal (δ between 13 and 15 ppm). Such a deshielded proton signal in the ¹H-NMR spectra of other azocoupling products of

1-(pyrimidin-2-yl)-3-methyl-pyrazolin-5-ones (**1**, **11**) or of 1-phenyl-3-methyl-pyrazolin-5-one (**2**) has been assigned [8-10] to the strongly chelated hydrazonic N-H (e.g. **4a**). Therefore, it is very probable that in CDCl_3 the examined azocoupling products (**5-10**, **12-15**) are detectable by $^1\text{H-NMR}$ practically only as hydrazonic tautomers **5a-10a**, **12a-15a**. The greater chemical shift of the lowest field $^1\text{H-NMR}$ signal in the case of each azocoupling product monosubstituted in benzenic ring in *ortho*-position (**8-10**), comparative to the corresponding *para*-monosubstituted product (**5-7**) proves a close steric proximity effect (compare [14]) of *ortho* substituent on the mobile hydrogen that determines such a signal. This is a manifestation of the *ortho*-effect and it is compatible with the hydrazonic structure (**5a-10a**) of examined pairs of isomeric azocoupling products in chloroformic solutions. As is known [15] the difference between the behaviour of *ortho*- and *para*-substituted isomeric derivatives has been defined as the simplest quantitative measure of the *ortho*-effect. In NMR study the examined difference is that of the chemical shifts (see [16]). The chemical shift difference of the lowest field $^1\text{H-NMR}$ signal between the *ortho*- and *para*- isomer ($\Delta\delta_{o-p}$) of the azocoupling products bearing in the benzenic ring a methyl- (**8**, **6**) or chloro- (**9**, **7**) substituent ($\Delta\delta_{o-p}\sim 0.26$ ppm) is due, very probably, to the intramolecular van der Waals shift (see [14]) or, in other words, to the steric effect contribution (see [17]) to the *ortho* effect. This steric effect is expected to be a function of the bulk or size of the substituent.

As is known, the apparent sizes [18] and the van der Waals radii³ [19a], respectively, of the methyl group and of the chlorine atom are relatively similar [19b]. However, although the apparent size of the nitro group is smaller than the one of the methyl group and of the chlorine atom [18], the chemical shift difference of the lowest field $^1\text{H-NMR}$ signal between *ortho*- (**10**) and *para*- (**5**) isomers of the azocoupling products mono-nitro-substituted in benzenic ring is unusually great ($\Delta\delta_{o-p}\sim 1.5$ ppm).

This is due to the fact that the *ortho*-effect of nitro group includes, beside the steric effect, the contribution of the intramolecular hydrogen bonding formation (compare [17, 20]) between nitro and the hydrazonic NH group of the hydrazonic tautomer **10a**. This interpretation is supported by the similar explanation of the effect on electronic absorption spectra of acid or alkali addition to the methanolic solution of **10**.

The above discussed *ortho*-effects of methyl and nitro groups, respectively, on the lowest field $^1\text{H-NMR}$ signal of the *ortho*-mono-methyl-, and mono-nitro-substituted azocoupling products, respectively, (**8**, **10**) manifest themselves also in practical identical way with the disubstituted azocoupling products, provided that only one of the *ortho* positions is substituted with a methyl (**13**) or nitro (**15**) group, respectively (Table 2).

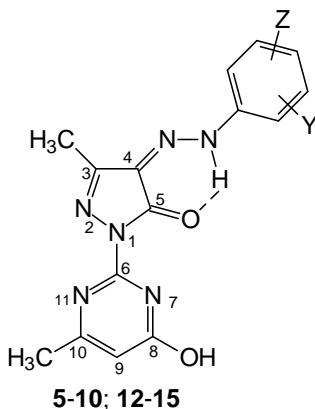
It is worth noting that: (i) the *ortho*-effect of the nitro group on the chemical shift of mobile hydrogen generating the lowest field signal in the azocoupling products **10**, **15** ($\Delta\delta_{o-p}\sim 1.5$ ppm) is much stronger than in *ortho*-nitro-aniline ($\Delta\delta_{o-p}\sim 0.7$ ppm [21]) although in the hydrazonic structure assigned for these (**10a**, **15a**) the mentioned mobile hydrogen belongs to a NH group directly linked to the nitro-substituted benzenic ring as in *ortho*-nitro-aniline; (ii) the chemical shift of hydrazonic NH hydrogen in all studied azocoupling products **4-10**, **12-15** is much greater (about 7-9 ppm) than

³ The van der Waals radius is considered the best steric parameter [17]

that of the aminic hydrogen in corresponding anilines (compare Table 2 with [21]); (iii) the variation of the chemical shift of the mobile hydrogen, that gives the herewith discussed lowest field signal in the azocoupling products **4**, as a function of the substituent nature in *para* position of benzenic ring of these (**4**), is inverted [9] comparative to that of the aminic hydrogen in corresponding anilines [21]. All these observations relating to the lowest field $^1\text{H-NMR}$ signal in the azocoupling products **4-10**, **12-15** may be understood on the basis of chelated intramolecular hydrogen bonding formation between the hydrazonic NH group and the pyrazolin-5-onic C=O group, respectively the nitro group - when this group is present in the *ortho*-position of the benzenic ring - of the hydrazono tautomer **4a-10a**, **12a-15a**.

Table 2

The $^1\text{H-NMR}$ data (chemical shift δ [ppm], multiplicity,* number of hydrogen atoms and coupling constant J [Hz]) of azocoupling products **5-10**, **12-15** recorded in CDCl_3



Substituents Y, Z; Compound no.	Hydrogens of the groups						
	$\text{C}_3\text{-CH}_3$	$\text{C}_{10}\text{-CH}_3$	$\text{C}_9\text{-H}$	Benzenic ring	Pyrimidinic NH or OH	Hydrazonic NH	Other
Y=H, Z=4- NO_2 5	s, 3H 2.48	s, 3H 2.39	s, 1H 6.15	7.62, d, 2H, 7.50 8.32, d, 2H, 7.50	s, 1H 10.93	s, 1H 13.17	-
Y=H, Z=4- H_3C 6	s, 3H 2.41	s, 3H 2.34	s, 1H 6.07	7.24 d, 2H, 8.00 7.37 d, 2H, 8.00	s, 1H 11.21	s, 1H 13.20	benzylic 4- CH_3 2.37 s, 3H
Y=H, Z=4- Cl 7	s, 3H 2.44	s, 3H 2.37	s, 1H 6.11	7.44 m, 4H	s, 1H 11.15	s, 1H 13.17	-
Y=H, Z=2- H_3C 8	s, 3H 2.44	s, 3H 2.36	s, 1H 6.10	7.15-7.40 m, 3H 7.78 d, 1H, 8.10	s, 1H 11.23	s, 1H 13.45	benzylic 2- CH_3 2.42 s, 3H

Substituents Y, Z; Compound no.	Hydrogens of the groups						
	C ₃ -CH ₃ s, 3H	C ₁₀ -CH ₃ s, 3H	C ₉ -H s, 1H	Benzenic ring	Pyrimidinic NH or OH s, 1H	Hydrazoneic NH s, 1H	Other
Y=H, Z=2-Cl 9	2.43	2.35	6.09	7.21 t, 1H, 7.50 7.38 t, 1H, 7.45 d, 1H, 7.84 d, 1H, 8.00	11.18	13.44	-
Y=H, Z=2- NO ₂ 10	2.49	2.38	6.14	7.40 t, 1H, 7.60 7.80 t, 1H, 8.20 d, 1H, 8.50 8.35 d, 1H, 8.30	11.15	14.63	-
Y=3-CH ₃ , Z=4-NO ₂ 12	2.48	2.39	6.15	7.40 s, 1H 7.44 d, 1H, 8.19 d, 1H, 9.00	10.95	13.10	benzylic 3- CH ₃ 2.73 s, 3H
Y=2-H ₃ C, Z=4-H ₃ C 13	2.44	2.34	6.09	7.06 s, 1H 7.12 d, 1H, 8.20 7.66 d, 1H, 8.20	11.29	13.48	benzylic 2-CH ₃ 2.39 s, 3H benzylic 4-CH ₃ 2.36 s, 3H
Y=3-O ₂ N, Z=4-H ₃ C ₂ 14	2.44	2.36	6.10	7.46 d, 1H, 7.50 7.66 d, 1H, 7.50 8.13 s, 1H	11.23	13.12	CH ₃ -CH ₂ - 1.32 t, 3H, 7.3; CH ₃ -CH ₂ - 2.93 q, 2H, 7.3;
Y=2-NO ₂ , Z=4-H ₃ C 15	2.47	2.36	6.15	7.58 s, 1H, 8.30 8.06 d, 1H, 8.30 8.13 s, 1H	11.13	14.57	benzylic CH ₃ 2.47 s, 3H

* s: singlet; d: doublet; t: triplet; q: quartet; m: complex multiplet.

CONCLUSIONS

The different number of absorption bands in the range 350-600 nm of the electronic spectrum of each azocoupling products (**12-14**) as a function of (i) the substituent located in benzenic ring, (ii) the solvent and (iii) the acid or alkali addition to the methanolic solutions, supports the tautomerism of these dyes. However, in aprotic solvents and in acidic conditions has been detected only one species. The ¹H-NMR spectra prove the hydrazoneic structure **12a-14a** of this species.

The comparative spectroscopic study of the pairs of isomeric azocoupling products, *ortho*- (**8-10**) and *para*- (**5-7**) substituted, respectively, shows the manifestation of the *ortho*-effect of the substituent on the acidity and the chemical shift of the mobile hydrogen, that causes the lowest field ¹H-NMR signal of the examined dyes. This proves the steric proximity of the *ortho*-substituent and the mobile hydrogen in the azocoupling products **8-10**, a situation compatible with chelated hydrazoneic structure **8a-10a** of these. However, the different visible spectrum of the *ortho*-isomer (**8; 10**) with respect to *para*-isomer (**6, 5**) in methanol, respectively by addition of alkali, in

the case of several examined azocoupling products, may be explained only by the assumption of the involvement of both hydrazone- and azohydroxy-tautomer in these circumstances.

The very strong *ortho*-effect of the nitro-group in azocoupling products **10**, **15** may be determined by the formation of intramolecular hydrogen bonding between this group and the discussed mobile hydrogen of the dyes **10**, **15**.

EXPERIMENTAL

The procedure for the preparation of 1-(4-hydroxy-6-methylpyrimidin-2-yl)-3-methyl-pyrazolin-5-one (**11**) was previously described [22]. Aromatic amines used for the preparation of diazonium salts **3** were commercial products; their diazotization was achieved by standard methods [6, 23a]. The coupling reaction between diazonium salts **3** and 1-(4-hydroxy-6-methylpyrimidin-2-yl)-3-methyl-pyrazolin-5-one (**11**) was performed [7] in similar conditions to those used [6,23b] for the azoic coupling of 1-phenyl-3-methyl-pyrazolin-5-one (**2**).

Elemental analysis were carried out at the Chemistry and Pharmaceutical Research Institute Cluj-Napoca.

Melting points were taken with an Electrothermal IA 6304 apparatus and are uncorrected. UV-VIS spectra were recorded on a Zeiss-Jena Specord UV-VIS spectrophotometer; the analytical grade reagents and solvents were provided by Reactivul (Bucharest), Merck (Darmstadt) and Fluka (Buchs); they were used without further purification. Each solution was prepared in corresponding solvent and diluted to the requested concentration or directly to the needed concentration ($\sim 10^{-5}$ mol/dm³) for electronic absorption spectroscopy measurement. The ¹H-NMR spectra were recorded in CDCl₃ at room temperature with a Varian Gemini 300 (300MHz) spectrophotometer.

General procedure for the azoic coupling: 0.01 mol 1-(4-hydroxy-6-methyl-pyrimidin-2-yl)-3-methyl-pyrazolin-5-one (**11**) was treated with a warm solution prepared from 0.01-0.02 mol sodium hydroxide, 0.05 mol sodium carbonate and 20 cm³ water (pH~10). This mixture was cooled to 0-5°C and into it was poured, under stirring and keeping the temperature below 10°C, one of the diazonium salts **3**, freshly prepared from 0.01 mol of the corresponding aromatic amine. Usually the coupling reaction was rapid, the reaction mixture became coloured immediately; however, the mixture was stirred for 0.5-12 hours at 15°C. After that the pH of the mixture was corrected to 6-7 with acetic acid. The suspension was filtered off, washed with water on the filter, dried and crystallized from methanol. The newly synthesized dyes **12-14**, the yields and some characteristics of these are presented in Table 1.

ACKNOWLEDGEMENT

The financial support of the study by the Romanian National University Research Council (CNCSIS Grant A) is gratefully acknowledged.

REFERENCES

1. Baldea I., Ghirisan A., Silberg I.A., Cristea I. *Rev. Roum. Chim.*, 1997; **42**, 767.
2. Baldea I., Ghirisan A., Panea I. *J. Chem. Soc., Perkin Trans. 2*, 1992, 1715.
3. Panea I., Cristea I. *Chimia*, 1991, **45(10)**, 92.
4. Krohs W., Hensel O. *Pyrazolone and Dioxypyrazolidine*, editor Cantor, Aulendorf in Württemberg, 1961.
5. Lenoir J. In: Venkataraman K, editor. *The Chemistry of Synthetic Dyes*, Vol. V. Academic Press, London, 1971, p. 354-356.
6. Zollinger H. *Color Chemistry*, VSH Basel, 1991. p. 110-137.
7. Panea I., Ghirisan A., Cristea I., Gropeanu R. *Rom. Pat. 114797C₁*, 1999.
8. Panea I., Ghirisan A., Cristea I., Gropeanu R., Silberg I.A. *Heterocycl. Commun.*, 2001, **7**, 563.
9. Panea I., Ghirisan A., Baldea I., Silaghi-Dumitrescu I., Craciun L., Silberg I.A. To be published
10. a) Elguero J., Marzin C., Katrytzky A.R., Linda P. *The Tautomerism of Heterocycles*. New York: Academic Press, 1976. p.336-339 and references therein. b) Hinsche G., Uhlemann E., Zeigan D., Engelhardt G. *Z. Chem.* 1981, **21**, 414. c) Mustroph H. *Z. Chem.*, 1987, **27**, 281. d) El-Haty M.T. *Asian J. Chem.* 1991, **3**, 189.
11. Haessner R., Mustroph H., Borsdorph R. *J. Prakt. Chem.*, 1985, **327**, 555.
12. Kamlet M.J., Minesinger R.R. *J. Org. Chem.*, 1971, **36**, 610.
13. a) Arriau J., Campillo J.P., Elguero J., Pereillo J.M. *Tetrahedron*, 1974, **30**, 1345. b) Wojciekowski K., Szadowski J. *Dyes and Pigments*, 2000, **44**, 137
14. Jackman L.M., Sternhell S. *Application of Nuclear Magnetic Resonance Spectroscopy in Organic Chemistry*, 2nd edition. London, Pergamon Press, 1969. p. 71,72, 204-207.
15. a) Hajo M., Utaka M., Yoshida Z. *Tetrahedron*, 1971, **27**, 2713. b) Bauerova I., Ludwig M. *Collect. Czech. Chem. Commun.*, 2001, **66**, 770.
16. Kulhanek J., Pytela O., Lyčka A. *Collect. Czech. Chem. Commun.*, 2000, **65**, 106.
17. a) Charton M. *Progr. Phys. Org. Chem.*, 1971, **8**, 235. b) Pytela O., Lyčka A. *Collect. Czech. Chem. Commun.*, 1994, **59**, 2005.
18. Eliel E.L., Wilen S.H., Mander L.N. *Stereochemistry of Organic Compounds*. New York: John Wiley and Sons, 1994. p. 1144.
19. a) Carey F.A., Sundberg R.J. *Advanced Organic Chemistry*, 2nd edition. Part A, Structure and Mechanisms. New York: Plenum Press, 1984. p.103. b) Whitaker A. *J. Soc. Dyers Colour.*, 1995, **111**, 66.
20. Pytela O., Prusek O. *Collect. Czech. Chem. Commun.*, 1999, **64**, 1617.
21. Lynch B.M., Macdonald BC, JGK Webb. *Tetrahedron*, 1968, **24**, 3595.
22. Cristea I., Farcasan V., Panea I. *Rom. Pat. 84355*, 1984.
23. Sanielevici H., Urseanu F. *Sinteze de coloranti azoici*. Bucharest: Editura Tehnica, 1987. a) Vol. I, p. 36-41, 219; b) Vol I, p224; c) Vol. II, p. 56, 131, 145, 166, 176, 188-190, 198-200, 396.

AZOCOUPLING PRODUCTS. PART IV[†]. THE STRUCTURE OF DYES OBTAINED BY AZO-COUPLING REACTION OF 1-(4-HYDROXY-6-METHYLPYRIMIDIN-2-YL)-3-METHYLPYRAZOLIN-5-ONE WITH AROMATIC DIAZONIUM SALTS

IOAN PANEA^a, ADINA GHIRISAN^a, IOAN BALDEA^a, IOAN SILAGHI-DUMITRESCU^a, LILIANA CRACIUN^b and IOAN A. SILBERG^a

^a"Babes-Bolyai" University of Cluj-Napoca, Faculty of Chemistry and Chemical Engineering, 11 Arany Janos Str., 400028 Cluj-Napoca, Romania,

^bCiba Specialty Chemicals 50 White Plains Road, PO BOX 2005 Tarrytown, NY 10591-9005, USA

ABSTRACT. The number and positions of the absorption bands have been studied for the title dyes, in the range of 350-600 nm, as a function of solvent nature, acidity or basicity of the solutions as well as of the nature of the substituent X in para position on the benzene ring. The obtained results, including Hammett correlations, quantum calculation by using AM₁-SM₂ method and the mechanism of formation of the dyes **5** prove the existence of some tautomeric azo-hydrazono- and pyrazolin-5-one-5-hydroxypyrazole (**5a** ⇌ **5b** ⇌ **5c** ⇌ **5d**) equilibria, coupled with acid-base equilibria. The visible and (¹H-, ¹³C-) NMR spectra support the hydrazone structure **5d** of the only species detectable in the used aprotic solvents.

INTRODUCTION

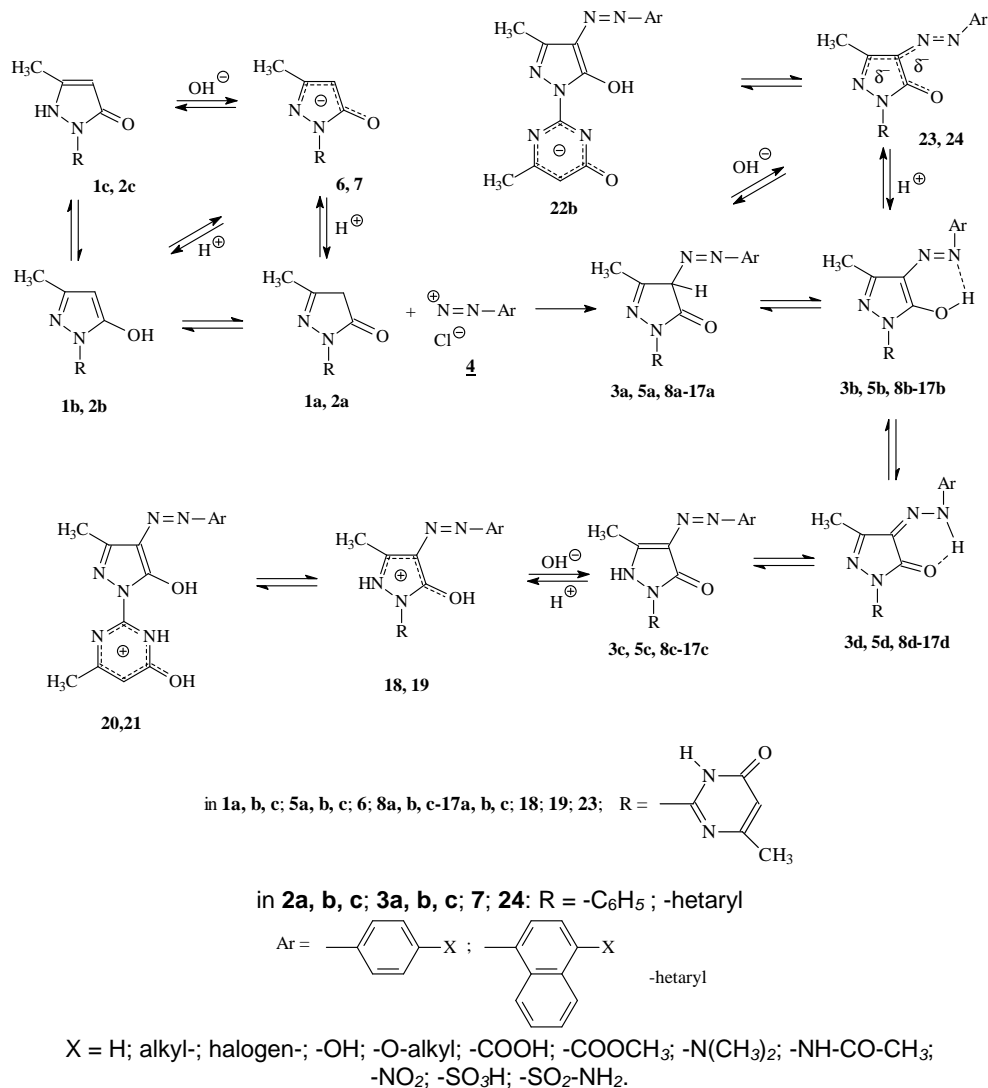
Taking into account the formal analogy between 1-(3,4-dihydro-6-methylpyrimidin-4-one-2-yl)-3-methylpyrazolin-5-one **1** and 1-phenyl-3-methyl-pyrazolin-5-one **2** and the fact that the last is commonly employed in obtaining¹⁻⁴ of commercial dyes **3** we performed⁵⁻⁷ the azo coupling of **1** with aromatic diazonium salts **4**. The results were a series of coloured azocoupling products **5** of 1-pyrimidinyl 5-pyrazolone **1**, exhibiting strong absorption bands in visible range. Beside this first argument for the real analogy between the two substituted pyrazolones **1** and **2**, there exists⁵⁻¹² a similar tautomerism (**1a-c**, **2a-c**), although ¹H-NMR spectra in CDCl₃ indicated different structures: ketomethylene **2a** in the case of 1-phenyl derivative^{9,10} and hydroxypyrazolic **1b** or iminopyrazolonic **1c** in the case of 1-pyrimidinyl derivative¹², respectively.

Another proof for their analogy came from the kinetics of the azocoupling reaction^{6, 8, 11}. Both compounds participate in the azocoupling process as mesomeric anions **6**, **7** and follow the same mechanism. All these arguments justify the supposition that the dyes **3**, **5** are also structural analogues.

The structural study of dyes **3** obtained by azocoupling of 1-phenyl-3-methyl-pyrazolin-5-one **2** and of the analogue hetaryl-pyrazolin-5-ones has lead to many contradictory assessments^{3, 4, 7b, 9, 13-28}. For such dyes, four tautomeric forms **3a- 3d** were formulated^{3, 9, 15, 20, 21, 25}, each of them can exist²⁰ as two E/Z diastereoisomers, and a series of conformers. It is worth mentioning that the majority of papers published within the last 30 years support the existence of hydrazone

[†] Part III. Reference [7b]

tautomer **3d** in a Z configuration, as a prevalent form^{3, 7b, 9, 15, 17, 18, 21b} or as the only form^{13, 14, 19, 20, 22, 23, 25} of the dyes **3**. It must be underlined however, that the detection of a single tautomeric form does not rule out the tautomeric equilibria^{14, 21b, 29}.



Scheme 1

The purpose of this work is to determine the structure of azocoupling dyes **5** and, on the basis of the analogy between **5** and **3**, to contribute to the elucidation of the controversial structure of commercial dyes **3**. For the sake of simplicity we will use in general the denomination of the azoic pyrazolin-5-one tautomers **5a**, **5c** and for the substituent in position 1-(pyrimidinic), that corresponding to the lactimic form. To indicate the compounds, in general, we will use figures without letters, e.g. **5**.

RESULTS AND DISCUSSION

Electronic spectra; general presentation

The electronic absorption spectra at wavelength over 350 nm for azocoupling products **5** of 1-(4-hydroxy-6-methyl-pyrimidin-2-yl)-3-methyl- Δ^3 -pyrazolin-5-one **1** exhibit one, two or three intense and relatively narrow bands, as a function of (i) the nature of the substituent on the benzene ring in the azocoupling products **5**, (ii) the nature of the solvent (protic or aprotic), and (iii) the acidity or basicity of the medium. These spectra are presented in Figure 1-4 and Table 1. It should be mentioned that within this wavelength range and under similar conditions there are also two absorption bands, one of them observed at least as a shoulder near the main one, for various aryl-**3** or hetaryl-pyrazolin-5-one azodyes. This behaviour has been attributed to the tautomerism^{7b, 21} or to the simultaneous presence of the corresponding anion^{20, 30, 31}. Such a second band may be distinguished too on the published spectra^{17, 23, 25} of some 1-phenyl-3-methyl-pyrazolin-5-one azodyes **3**.

Electronic spectra recorded in absolute ethanol and methanol

Among the recorded electronic spectra of the studied compounds **5**, the most illustrative concerning the tautomerism are those obtained in absolute ethanol or methanol (Fig. 1A, B; 2, 3). For example, the absorption spectrum of 1-(4-hydroxy-6-methyl-pyrimidin-2-yl)-3-methyl-4-(4-N-dimethylaminophenylazo)-pyrazolin-5-one [**5**: Ar = 4(CH₃)₂N-C₆H₄] **8** exhibits three bands above 350 nm, quite well outlined (Fig. 1A, B) with molar absorptivities of the order of magnitude of 10⁴. On the other hand, 4-(phenylazo)-[**5**: Ar = C₆H₅] **9**, 4-(4-methylphenylazo)-[**5**: Ar = 4-CH₃-C₆H₄] **10**, 4-(4-hydroxyphenylazo)-[**5**: Ar = 4-HO-C₆H₄] **11**, 4-(4-methoxyphenylazo)-[**5**: Ar = 4-CH₃O-C₆H₄] **12**, 4-(4-ethoxyphenyl-azo)-[**5**: Ar = 4-C₂H₅O-C₆H₄] **13** and 4-(4-chlorophenylazo)-[**5**: Ar = 4-Cl-C₆H₄] **14**, -1-(4-hydroxy-6-methyl-pyrimidin-2-yl)-3-methyl-pyrazolin-5-one respectively, exhibit in absolute methanol two bands over 350 nm. There are also compounds **5** such as 4-(4-acetylaminophenylazo)-[**5**: Ar = 4-H₃CCONH-C₆H₄] **15**, 4-(4-sulphonamido-phenylazo)-[**5**: Ar = 4H₂N-SO₂-C₆H₄] **16** and 4-(4-nitrophenylazo)-[**5**: Ar = 4-O₂N-C₆H₄] **17**, -1-(4-hydroxy-6-methylpyrimidin-2-yl)-3-methylpyrazolin-5-one, respectively, presenting only one band. These data could indicate the detection of three species in the first case **8**, two species in the second case (**9** – **11**) and apparently only one species in the third case (**15**–**17**). Within all these molecular species should exist the most extended delocalisation of π electrons because their absorption bands are in the visible range with molar absorptivities of 10⁴ mol⁻¹cm⁻¹.

Spectra recorded in aprotic solvents

On the contrary, by using aprotic solvents (benzene, CCl₄, CHCl₃, dioxane, dimethyl-sulfoxide, anhydrous pyridine), the absorption spectra of all the dyes **8** – **17** exhibit only one band over 350 nm, corresponding to the longest wavelength of those in absolute ethanol or methanol for each dye (Fig. 1, 2, 4; Table 1). This behaviour can be explained by the presence of some tautomeric equilibria **5a** \leftrightarrow **5b** \leftrightarrow **5c** \leftrightarrow **5d**, the position of which depends on the nature of the substituent X as well as on the nature of the solvent. When only a band was recorded in absolute methanol (**15** – **17**), or when aprotic solvents were used (**8** – **17**), the equilibrium seems to be completely shifted towards one of the tautomers, namely that exhibiting the absorption band at the longest wavelength in absolute alcohol.

Table 1

UV-Vis-spectral data of some dyes **5** obtained by azocoupling of 1-(4-hydroxy-6-methyl-pyrimidin-2-yl)-3-methyl-pyrazolin-5-one **1** with 4-substituted benzenediazonium salts (4-X-C₆H₄-N=N⁺Cl⁻)

X-; (dye)	λ_{\max} [nm] (ϵ), in CHCl ₃	λ_{\max} [nm] (ϵ), in CH ₃ OH	$\lambda_{1\max}$ [nm] $\bar{\nu}_1$ [cm ⁻¹] in CH ₃ OH; HCl 0.1 M	$\lambda_{2\max}$ [nm] $\bar{\nu}_2$ [cm ⁻¹] in CH ₃ OH; KOH 0.1 M	$\Delta\nu =$ $\bar{\nu}_1 - \bar{\nu}_2$ [cm ⁻¹]	σ_p (ref. 32) for X
(CH ₃) ₂ N- (8)	530 (30000)	530 (24800) 450 (18630) sh 400 (10350) sh	527 (19000) *[HCl] = 2.6 × 10 ⁻⁴ mol	435 <u>397</u> (25150)sh	-6150	-0.83
OH- (11)		440 (16300) 390 (13850)	450 (22200)	437 <u>383</u> (26150)sh	-3950	-0.36
H ₃ CO- (12)	455 (22000)	435 (23150) 380 (20250)	448 (22300)	410 sh <u>382</u> (26200)	-3900	-0.27
H ₅ C ₂ O- (13)		450 (22830) 385 (20000)	452 (22150)	410 sh <u>385</u> (26000)	-3850	-0.24
H ₃ C- (10)		423 (28600) 383 sh (23175)	430 (23200)	410 sh <u>384</u> (26100)	-2900	-0.16
H ₃ C-CO-NH (15)		445 (25000)	444 (22500)	420 sh <u>395</u> (25300)	-2800	-0.09
H- (9)	420 (23000)	410 (19930) 380 (23900)	417 (24000)	410 sh <u>379</u> (26400)	-2400	0
Cl- (14)		415 sh 394 (23250)	420 (23800)	415 sh <u>390</u> (25650)	-1850	+0.23
H ₂ N-SO ₂ ⁻ (16)		397 (20600)	408 (24640)	<u>418</u> sh (23900) 408	+740	+0.62
O ₂ N- (17)	414 (22000)	420 (41765)	416 (24000)	<u>474</u> (21050)	+2950	+1.24 ^{***}

sh = shoulder

*The values λ_2 and ν_2 used to calculate the $\Delta\nu$ are those underlined; they correspond to the azohydroxy tautomeric form, as such and/or as anions (see discussion). The λ_1 values correspond to hydrazoneic tautomers **5d**.

For this dye was used a lower HCl concentration because at 0.1 mol the protonation of **8 occurred and the presence of hydrazoneic tautomer became negligible.

***Here was used the σ_p^- value³² since the NO₂ group is through-conjugated with the chromophore system containing the deprotonated pyrazolic HO group of azohydroxy tautomer **17b**.

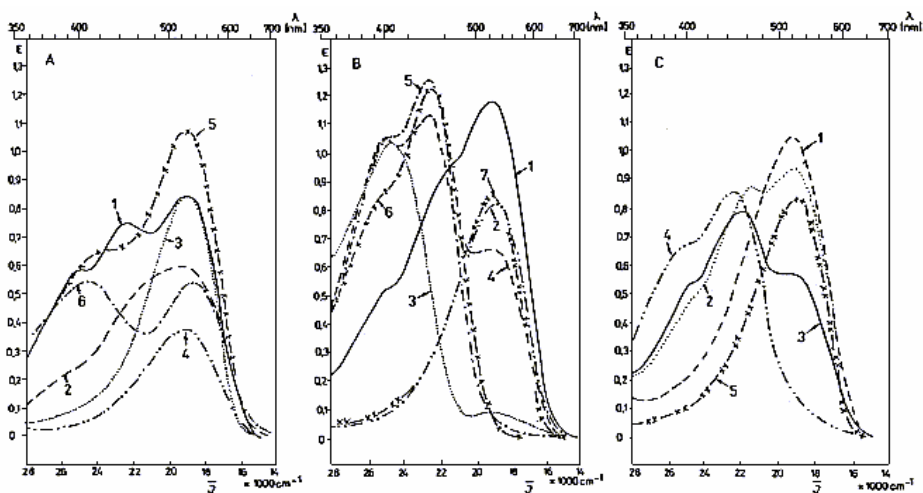


Figure 1. The UV-VIS absorption spectra of 4-[4-(*N*-dimethyl-aminophenylazo)]-1-(4-hydroxy-6-methyl-pyrimidin-2-yl)-3-methyl-pyrazolin-5-one (**8**) in the range 350-600 nm:

- A. in various solvents or solvent mixtures, 1). Absolute ethanol; 2). Ethanol:water (1:1); 3). Chloroform; 4).dimethylsulfoxide; 5). Acetic acid 100%; 6). Acetic acid 96% (4% water);
- B. in absolute methanol, methanol with hydrochloric acid or potassium hydroxide addition, and in chloroform: 1). Absolute methanol ($[8] = 4.36 \times 10^{-5}$ mol); 2). Methanol + HCl ($[8] = 2.14 \times 10^{-5}$ mol; $[HCl] = 2.58 \times 10^{-4}$ mol); 3). Methanol + HCl ($[8] = 4.59 \times 10^{-5}$ mol; $[HCl] = 10^{-1}$ mol); 4). Methanol + KOH ($[8] = 4.29 \times 10^{-5}$ mol; $[KOH] = 6.62 \times 10^{-5}$ mol); 5). Methanol + KOH ($[8] = 4.59 \times 10^{-5}$ mol; $[KOH] = 10^{-1}$ mol); 6). Methanol + KOH ($[8] = 4.3 \times 10^{-5}$ mol); $[KOH] = 1.8$ mol); 7). Chloroform ($[8] = 2.82 \times 10^{-5}$ mol);
- C. in anhydrous pyridine; pyridine with water addition and chloroform: 1). Anhydrous pyridine; 2). Pyridine: water (99.5:0.5); 3). Pyridine: water (98.5:1.5) 4). Pyridine: water (1:99); 5). Chloroform.

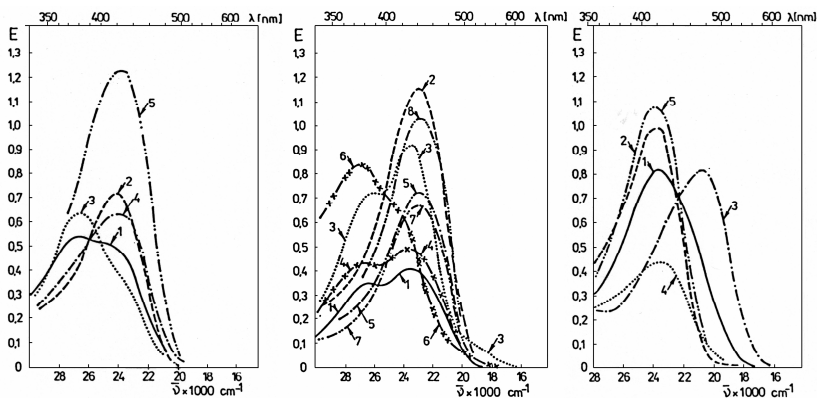


Figure 2. Visible spectra of dye **9** in: 1). Absolute methanol; 2). Methanol + HCl ($[HCl] = 0.1$ mol); 3). Methanol + KOH ($[KOH] = 0.1$ mol); 4). Dimethylsulfoxide; 5). Chloroform.

Figure 3. Visible spectra of dyes **11**, **12**: 1). **11** in absolute methanol; 2). **11** in methanol + HCl ($[HCl] = 0.1$ mol); 3). **11** in methanol + KOH ($[KOH] = 0.1$ mol); 4). **12** in methanol; 5). **12** in methanol + HCl ($[HCl] = 0.1$ mol); 6). **12** in methanol + KOH ($[KOH] = 0.1$ mol); 7). **11** in glacial acetic acid; 8). **12** in glacial acetic acid.

Figure 4. Visible spectra of dye **17** in: 1). Absolute methanol; 2). Methanol + HCl ($[HCl] = 0.1$ mol); 3). Methanol + KOH ($[KOH] = 0.1$ molM); 4). Dimethylsulfoxide; 5). Chloroform.

Effect of the acidification on the electronic spectra and the assignment of the longest wavelength band

The additional proofs for the existence of such equilibria comes from the effect of the addition of HCl or KOH on the spectrum of each dye **8–17** in absolute methanol. Thus, the solution of **8** (2.1×10^{-5} mol), exhibiting three bands in absolute methanol, changes the shape of the spectrum (Fig. 1.B) after acidification with HCl up to 2.6×10^{-4} mol. It presents now only one more intense band in the visible range with the maximum located at 530 nm, corresponding to the one at the longest wavelength in absolute methanol; it is similar to the absorption spectrum recorded in aprotic solvents. This behaviour is compatible with the presence of three tautomeric forms in comparable concentration in absolute methanol; by adding a small amount of HCl, the equilibria are shifted towards the form favoured in weak acidic medium.

A similar change occurs in the case of those dyes **9–14** exhibiting two absorption bands over 350 nm in absolute methanol. Upon acidification with HCl (~ 0.1 mol) only one band appears located at the longest wavelength as compared to the neutral solution. This band corresponds also to the visible band in aprotic solvents or in glacial acetic acid. (Fig. 2, 3). Therefore, the dyes **9–14** behave similarly to **8**, although only two tautomeric forms are present in significant concentration in absolute methanol. In the acidic solution the tautomeric equilibrium is shifted again towards the form favoured in acidic media.

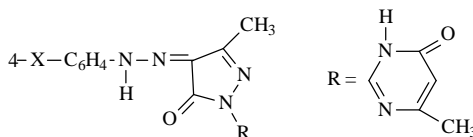
In the case of other hydroxyazoic dyes, including 4-arylozo-1-phenyl-3-methyl-pyrazolin-5-ones **3** it is known^{7b, 21b, 31, 33-40} that the favoured form in acidic media is the hydrazonic one **3d**. Thus, we appreciate that the band located at the longest wavelength in the spectra of dyes **8–17** recorded in absolute ethanol or methanol, is caused by the hydrazonic tautomeric form **5d**. It was detected in the solutions with aprotic solvents as the only form, all equilibria being shifted towards it. This assesment is also in accord with the detection^{9, 13, 14, 20, 22, 25, 27, 31} of only the hydrazonic form **3d** in aprotic solvents, especially in CHCl_3 , for the analogue dyes **3**.

NMR-proofs for hydrazonic structure 5d of the only form detected in aprotic solvents

The hydrazonic structure **5d** in aprotic solvents is also supported by ^1H - and ^{13}C -NMR spectra recorded in CDCl_3 and $(\text{CD}_3)_2\text{SO}$. The ^1H -NMR spectra of **5** exhibit a singlet corresponding to a mobile hydrogen atom at 13-14 ppm (Table 2). In the case of the analogues **3** this signal is considered^{9, 13, 14, 23} as being characteristic for the hydrazonic (N-H) proton.

Table 2

^1H -Chemical shift of N-H group in hydrazono tautomer **5d** of the dyes **5** in CDCl_3 .



X	$(\text{CH}_3)_2\text{N}$	OC_2H_5	OCH_3	CH_3 or H	Br	NO_2 or Cl	COOCH_3
δ (ppm)	13.50	13.35	13.31	13.21	13.18	13.17	13.15

A NOESY experiment with the dyes **10** and **12** (Fig.5) is showing a spatial close proximity of the hydrogen atom causing the signal at 13-14 ppm with the hydrogen atoms of benzene ring in *ortho* position with respect to the two nitrogen atoms bridge between the rings. Such a disposition takes place only with tautomeric forms **5b** and **5d** where the mobile hydrogen atom may be involved in an intramolecular hydrogen bonding.

Since for the hydroxyazoic tautomers **3b** of the dyes **3**, there have not been provided^{39, 41, 42} any intense absorption bands above 400 nm, the same is to be expected for the analogues **5**. Therefore, for the dyes **5** in aprotic solvents, presenting an intense absorption band over 400 nm, the only compatible structure should be the hydrazoneic one **5d**. This structure can form the above mentioned intramolecular hydrogen bonding. It is worth mentioning that for the dyes having hydroxyazo-ketohydrazoneic tautomeric equilibrium, the ketohydrazoneic form exhibits intense absorption bands at the longest wavelength^{7b, 21b, 28, 33-39, 41, 43}. The hydrazoneic structure **5d** for the only form detected in aprotic solvents is also compatible with ¹³C-NMR spectra. The ¹³C- chemical shifts of similar carbon atoms from the corresponding hydrazoneic tautomers **5d**, studied here, and **3d** of the analogue^{13, 14, 22} dyes **3** are practically the same, as presented in Table 3.

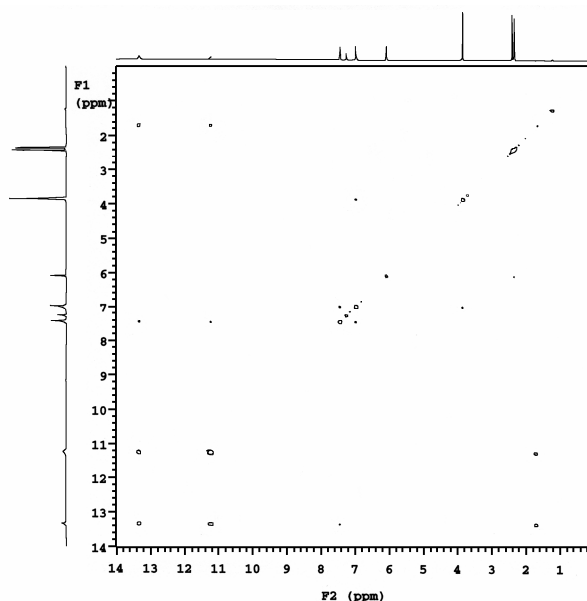


Figure 5. NOESY Spectrum of dye **12**.

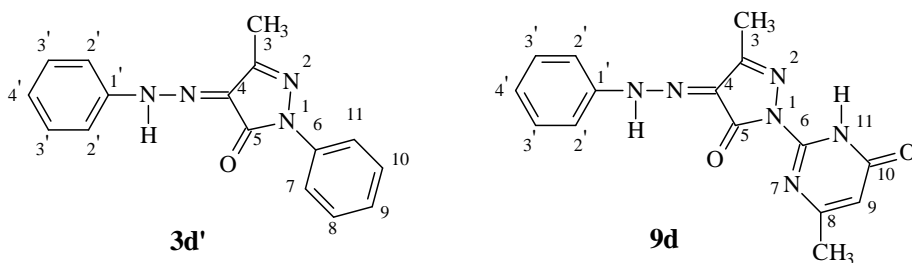
Tautomeric equilibria coupled with protonation equilibria

An additional support for the hydrazoneic structure **8d**, which displays an absorption band at the longest wavelength (530 nm) and for the hydroxyazo structure **8b**, exhibiting an absorption band at the shortest wavelength above 350 nm, comes from the spectra recorded in methanolic solution containing more concentrated acid (up to 0.1 mol HCl).

Upon acidification (up to 0.1 mol HCl) of methanolic solution of **8** carrying a dimethylamino group on benzene ring (5.0×10^{-5} mol) another change of the spectrum occurs. The initial spectrum in absolute methanol exhibiting three bands in the visible, changes into one with a single intense band (see Fig. 1B, curves 1, 3) located at about 400 nm. It corresponds to the shortest wavelength visible band in neutral methanolic solution. Under the acidic conditions, the protonation of the dye molecule is likely to occur^{4, 25}. The protonation causes a large hypsochromic shift of the longest wavelength band (around 130 nm). This is in agreement with a major change of chromophore system of **8**, from the hydrazono **8d** to the hydroxyazo **8b** structure. Because the protonation of nitrogen atoms in azo group causes a bathochromic shift of the absorption maximum⁴, the protonation should take place either at the pyridinic nitrogen atoms of the heterocycles²⁵ [**18**; Ar = (CH₃)₂N-C₆H₄] **19**, [**20**; Ar = (CH₃)₂N-C₆H₄] **21** or at the (CH₃)₂N- group.

Table 3

¹³C-Chemical shifts- δ_c (ppm) of 3-methyl-1-phenyl-4-phenylhydrazono-pyrazolin-5-one **3d'**, its 1-(4-hydroxy-6-methyl-pyrimidin-2-yl)-ic **9d** analogue, and the 4-CH₃ derivative of latter **10d** in CDCl₃. The underlined values are for similar positions and therefore compared.



Position of ¹³ C	Compound			
	3d (ref. 13, 22)	9d	10d	10d ⁺
3	<u>148.4</u>	146.6	<u>146.8</u>	
4	<u>128.4</u>	<u>125.8</u>	<u>125.5</u>	
5	<u>157.7</u>	<u>159.0</u>	<u>159.4</u>	
6	138.0	<u>161.3</u>	<u>161.4</u>	
7	118.4	-	-	
8	128.8	<u>152.5</u>	<u>152.5</u>	
9	125.0	<u>109.5</u>	<u>109.7</u>	
10	128.8	<u>165.8</u>	<u>165.9</u>	
11	118.4	-	-	
1'	<u>141.1</u>	<u>140.4</u>	<u>138.1</u>	<u>137.5</u>
2'	<u>115.7</u>	<u>116.7</u>	<u>116.8</u>	<u>116.6</u>
3'	<u>129.6</u>	<u>129.9</u>	<u>130.7</u>	<u>130.6</u>
4'	<u>125.7</u>	<u>127.5</u>	<u>138.2</u>	<u>136.8</u>
CH ₃ of 3-position	11.7	12.1	12.2	
CH ₃ of 8-position	-	24.6	24.7	
CH ₃ of 4'-position	-	-	21.4	

⁺ Calculated from values of **9d** with increments of the CH₃-substituent in the 4'-position⁴⁹.

These protonated groups of azo form **8b** cannot be involved in the conjugation with the azoic chromophore. Therefore, the longest wavelength absorption band of **8b** and its protonated form, recorded around 400 nm respectively, should be close together. Consequently, the absorption band located at 400 nm should be attributed to the hydroxyazoic form **8b**.

On the other hand, the protonated form of **8** should be in equilibrium with the most stable not protonated species of **8** present in neutral or weak acidic media. As we have shown above, the stable unprotonated species of **8** is the hydrazone tautomer **8d**, with the absorption maximum at 530 nm. A weak band at 530 nm still exists, in the spectra of **8** in acidic (0.1 mol HCl) methanol (Fig. 1B curve 3) along with the main band located at 400 nm and attributed to protonated form. It proves the involvement of the assumed equilibrium and, therefore, supports the assignment of the maximum at 530 nm to the hydrazone tautomer **8d**. The same equilibrium between protonated azoform (**19**, **21**) and hydrazone tautomer **8d** is also evident in the spectra in acetic acid (Fig. 1A, curves 5, 6).

Effect of KOH or water addition on the electronic spectra of the dyes 8-10, 12-14

For the dyes **8-10**, **12-14**, having a substituent X without mobile hydrogen, either electron-donating or weak electron-withdrawing, the hydrazone structure, **8d-10d**, **12d-14d** of the tautomer corresponding to the longest wavelength band in the visible spectra, is supported by the effect caused by addition of potassium hydroxide to their methanolic solutions. A small addition of potassium hydroxide diminishes and a consistent addition suppresses completely the absorption band at the longest wavelength, accompanied by an increasing of the intensity of the other two (Fig. 1B) or the other one (Fig. 2, 3) at shorter wavelength. Such an effect could be expected in the case of azo-hydrazone tautomeric equilibrium **5b** ⇌ **5d** because the alkaline medium favours the azo tautomer and diminishes the concentration of hydrazone tautomer^{21b, 30, 36a, 37, 38, 40}. The above presented effect of alkalis addition proves at the same time the azoic structure **8b-14b** of the tautomer exhibiting the shortest wavelength absorption band on the spectra above 350 nm of the dyes **8-14** in absolute methanol. This effect is very illustrative with the dye **8**. The addition of KOH up to a concentration of 6.6×10^{-5} mol to the solution in absolute methanol of **8** (4.3×10^{-5} mol) brings about an increase of the intensity of the two absorption bands under 500 nm and diminishes the intensity of the absorption band, located at the longest wavelength. The addition of KOH up to 0.1 mol had the result of suppressing the band located at 530 nm in absolute methanol. A similar effect on the shape of the spectra is caused by the addition of twice distilled water to the solution of **8** in anhydrous pyridine. The visible spectrum in anhydrous pyridine exhibits only one absorption band at 530 nm, given by the hydrazone tautomer **8d**. When the water concentration of the pyridine solution reaches 1.5% a spectrum containing three absorption bands was recorded. Higher concentration of water brought about the suppression of the 530 nm band (Fig. 1C). Similar changes of the spectra were observed by water addition to absolute ethanol, glacial acetic acid (Fig. 1A), dimethylsulfoxide or dioxane solution of **8**, but the modifications were not so significant as compared to those observed in pyridine solution. This behaviour evidences however the involvement of hydrogen bonding in determining the stability

of various tautomeric forms (see^{20, 34, 38}). The effects caused by KOH or water addition to solutions of **8** are in agreement with the assumed equilibria $8b \leftrightarrow 8c \leftrightarrow 8d$. The addition shifted the equilibrium towards the azohydroxy form **8b** and/or azoiminic form **8c**. Such equilibria have been ascertained in the case of other azohydroxy dyes^{7b, 21b, 15, 38, 40, 44}, including the ones of 4-arylazo-5-hydroxypyrazole dyes **3b**.

Assignment of the shortest wavelength band at the dyes 8-14

On the basis of previously described phenomena when either HCl, KOH or water was added to the dye solutions, as well as taking in account that hydroxyazoic tautomers absorb light at shorter wavelength^{33, 34, 36-38, 43} as compared to hydrazonic **3d** or azoketoiminic **3c** tautomers⁺, we consider that the absorption band at the shortest wavelength in the range 350-600 nm of alcoholic or pyridine-aqueous solutions of 1-(pyrimidinyl)-5-pyrazolone dyes **8-16** (Fig. 1-3) is due to the hydroxyazoic tautomer **8b-16b**. An additional support for this assignment is the fact that when the basicity of the solution is quite high (2 mol KOH), the intensity of the absorption band of **8** located around 400 nm is decreased and the one located at 450 nm is increased in intensity. Because among the tautomeric forms of 4-arylazo-5-pyrazolone dyes **3**, the form **3b** is the strongest acid⁴⁴, we expect the same to be true with 4-arylazo-1-pyrimidinyl-5-pyrazolone dyes **5**. Therefore the moreover addition of KOH will neutralize more azohydroxy form **5b**. The effect can be interpreted more comprehensibly on the basis of tautomeric and coupled acid-base equilibria (Scheme 1). Indeed, Scheme 1, clearly points out to the connection between the tautomeric and acid-base equilibria.

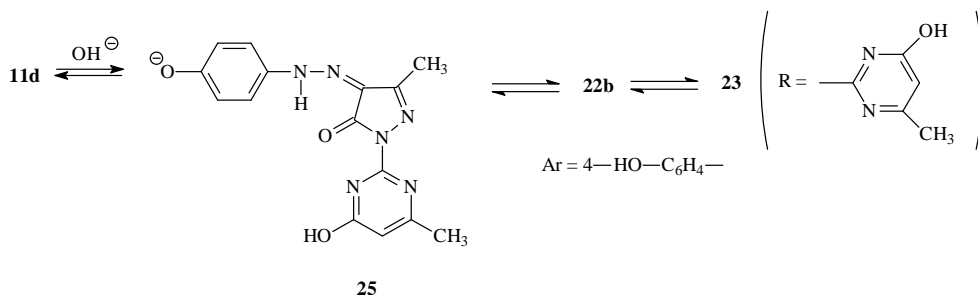
Tautomeric equilibria coupled with deprotonation equilibria

Since the measurements of pKa in the case of 1-(4-hydroxy-6-methylpyrimidin-2-yl)-3-methyl-pyrazolin-5-one **1** have shown that the first step acid dissociation corresponds to 4-hydroxy-6-methylpyrimidinic moiety¹¹, it seems likely that in alkaline media deprotonation of the dyes **8-14** should involve also the pyrimidine moiety of azohydroxylic forms **8b-14b** with the formation of **22b** species. Because the substituent in position 1 of pyrazolonic moiety does not exert any influence within the chromophore system^{17, 28}, the absorption band of hydroxyazoic tautomer **8b-14b** should not be modified by the first deprotonation of pyrimidine moiety **22b**. Therefore the absorption band located at the shortest wavelength in the range 350-600 nm in alcoholic, alkaline-alcoholic or pyridine-aqueous solutions, can be attributed to the azohydroxy tautomer **8b-14b** and for the anion **22b**. A large excess of KOH can bring about a two-fold deprotonation, both in the pyrazole and in the pyrimidine moieties. The absorption band of **8** located at 450 nm, which is rising in intensity upon addition of more KOH (up to 2 mol) (Fig. 1B) could correspond to a doubly deprotonated species of **8**. The less evident modification of the absorption band of **8** around 450 nm upon addition of large amount of KOH solution could be explain by the fact that this maximum may also correspond to the absorption of the azoketoiminic isomer **8c**. This last assignment is compatible with the intermediary position of the absorption band of the azoiminic tautomer between those of the corresponding hydroxyazo- and hydrazono- form⁴³.

+ ⁺only as a supposition^{21, 39, 41} in the case of 4-arylazo-1-phenyl-5-pyrazolones **3**.

On the other hand in the case of dyes **5** having strong electron-withdrawing substituent X, especially for X = -NO₂ (**17**) or with substituent possessing mobile hydrogen (X = -OH) (**11**), the addition of KOH causes other effects than those discussed with dyes **8-10**, **12-14**, having electron-donating or weak electron-withdrawing substituents. Thus, a concentration of 0.1 mol KOH in a methanol solution of **17** brings about a bathochromic shift of about 60 nm (Fig. 4). This quite large shift can be explained by the strong acidifying effect of the nitro group^{30, 31}. Because of this effect the first dissociated proton comes from the pyrazolic hydroxyl group (**23**; Ar = 4-O₂N-C₆H₄-, R = 4-hydroxy-6-methyl-pyrimid-2-yl) of the hydroxy-azo tautomer **17b**, and not from pyrimidine moiety (**22b**; Ar = 4-O₂N-C₆H₄-). Consequently in this particular case (**17**) in alkaline media the azochromophore system has a strong donor (-O⁻) and acceptor (O₂N-) of electrons at the ends (**23**, Ar = 4-O₂N-C₆H₄-). Within this system the conjugation is much more intense as compared with the starting one (**17b**). As it is known⁴⁵, the intensification of conjugation within azodyes leads to a bathochromic shift. A similar effect, by increasing the KOH concentration, up to 0.1 mol has been observed¹⁷ with the analogous 3-methyl-1-phenylpyrazolin-5-one dye (**3b**; Ar = 4-O₂N-C₆H₄-) when the acid dissociation may involve only the proton of pyrazolic -OH (**24**; Ar = 4-O₂N-C₆H₄-).

In exchange, when KOH is brought up to 0.1 mol in the methanolic solution of **11**, it causes the appearance of a supplementary absorption band, not well defined, but as a shoulder, located at 520 nm, and a spectrum with three bands is apparent (Fig. 3). It is very similar to the spectrum of **8** in neutral or weak alkaline alcoholic solutions (Fig. 1B, curve 4), as well as to the one in pyridine-aqueous (1.5% water) solution (Fig. 1C, curve 3). The resemblance of these spectra indicates the similitude of the most extended π-delocalized electron systems. The weak absorption at 520 nm of the dye **11** in alkaline alcoholic solution corresponds to that at 530 nm attributed to the hydrazoneic tautomer **8d**. A delocalized π electron system chromophore very similar to that of **8d** appears in the anion **25**, formed from phenolic hydroxyl group of hydrazoneic tautomer **11d**. That is why we suppose that the weak absorption at 520 nm in 0.1 mol KOH alcoholic solution of **11** is due to its anion **25**. The involvement of tautomeric and acid-base equilibria shown in Scheme 1 and 2 requires the presence of the anion **25** in a small concentration along with other more favoured anions formed by ionisation of pyrimidinic moiety **22b** or pyrazolic moiety **23**.



Scheme 2

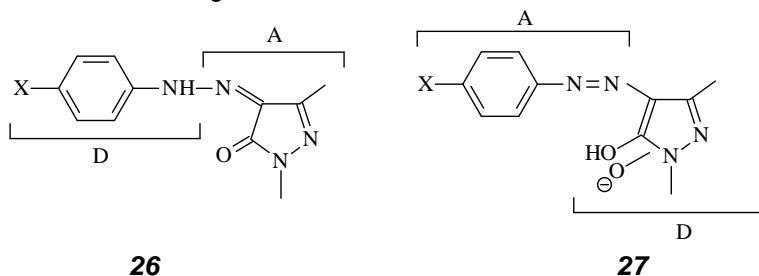
On the other hand the analogy between the chromophore system of **11** and that of **12** should determine similar electronic spectra. This was confirmed with methanol, acidic methanol and glacial acetic acid solution (Fig. 3). However when alkaline methanol solutions were used (0.1 mol KOH) the absorption spectra were

quite different. This difference can be explained only by the acid dissociation of **11** at phenolic hydroxyl, a phenomenon which is not possible with **12**, and demonstrates the involvement of the anion **25**.

Hammett correlations

An attempt has been made to test some Hammett correlations by using the position of the bands over 350 nm (in cm^{-1}) for hydrazonic or the hydroxyazoic tautomers. Each category gave linear relationships⁶ with different slopes, depending on the electron-donating or electron-withdrawing nature of the X substituent on the aryl moiety. Moreover, the position of the absorption bands remained independent on the substituent constant σ_p for the electron-withdrawing substituents in the case of the hydrazonic tautomers **8d-17d**, or for the electron-donating substituents in the case of hydroxyazoic tautomers **8d-17d** or their anions, respectively (Table 1).

Such a behaviour has been described previously⁴⁶ as being characteristic for the absorption bands due to charge-transfer or donor-acceptor chromophores. This behaviour has been recommended²⁰ as a criterion to differentiate between hydrazonic and hydroxyazoic nature of the chromophore. According to this criterion in the hydrazono derivatives **8d-17d**, which have charge-transfer chromophore **26**, the electron-withdrawing substituents X should determine a relatively constant position of the absorption band in the visible range. The electron-donating substituents should determine a shift of the absorption band towards the longer wavelength as the negative value of Hammett substituent constant σ_p is increased. On the contrary, for azoderivatives **8d-17b** (as such or as anions **22b**) the charge-transfer chromophore **27** should involve an invariant position of absorption bands in visible for the electron-donating substituents, and a bathochromic shift directly proportional to the σ_p value for the electron-withdrawing substituents.



The experimental data (Table 1) confirm also, on the basis of this criterion, the hydrazonic nature of the tautomer, which corresponds to the longest wavelength band in absolute alcohol or weak acid alcoholic solution, as well as in aprotic solvents. Alike was confirmed the hydroxyazostructure (as it is **8d-17b** or as the anion **22b**, **23**) for the species presenting the absorption band at the shortest wavelength over 350 nm, for the dyes **8-15**, or of the longest wavelength for the dyes **16**, **17**, in basic solutions (Table 1).

For species involved in equilibria, as attributed to dyes **5**, better Hammett correlation were obtained^{17, 37, 46} by using the difference $\Delta\bar{\nu}$ between the wavenumber of the absorption maxima as compared to the correlations given by the maxima position

themselves. Such a correlation was also found with the difference $\Delta\bar{\nu}$ for hydrazoneic tautomers **8d-17d** and hydroxyazoic (as **8d-17b** and/or their anions **22b**, **23**) ones (Fig. 6).

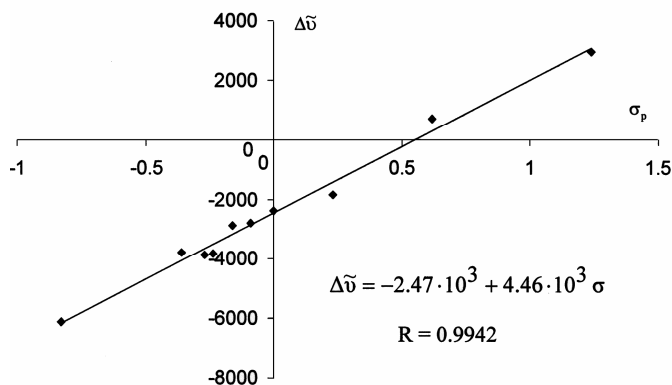


Figure 6 Hammett plot of $\Delta\bar{\nu}$ versus substituent constant σ_p .

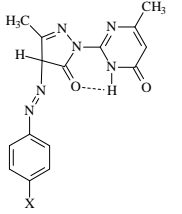
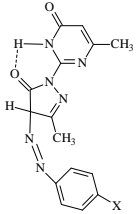
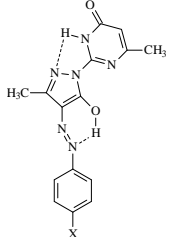
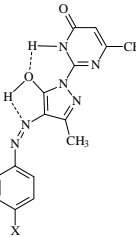
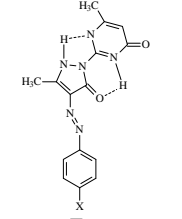
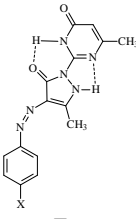
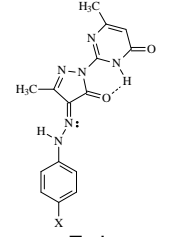
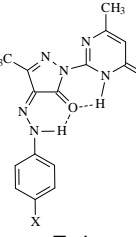
The good correlation coefficient ($r = 0.995$) sustained the involvement of the equilibrium between the mentioned species.

Quanto-mechanical calculation of the relative stability of the possible tautomers

Our measurements did not detect the azoketomethylene form **5a**. However, this form should be involved, at least as an intermediate (" σ " complex at electrophilic aromatic substitution⁴) according to the mechanism of dyes **5** formation, by azocoupling of diazonium salts **4** with mesomeric anion **6** of 1-pyrimidinyl-pyrazolin-5-ones^{6, 8, 17}. The intermediate can undergo changes to other tautomeric forms **5b**, **5c**, **5d** by deprotonation yielding the mesomeric anion **23**, which can be reprotonated (see⁴⁷). These changes involve otherwise 1,3-shifts forbidden by symmetry as suprafacial concerted processes (see Part II of this series) and they depend upon the stability of the involved species. The latter can be estimated by the enthalpy of formation. As shown by calculations carried out by means of AM₁-SM₂ method⁴⁸ the azoketomethylene intermediates **8a**, **10a**, **12a** rank in the third place as far as the stability is concerned (see Table 4). However, their involvement cannot be detected by electronic spectroscopy as it has been done with the other three (**8b**, **8c**, **8d**), or two (**9b**, **9d-13b**, **13d**) type of tautomers in absolute alcohol, because the azoketomethylene tautomers **8a-13a** should have weak absorptions in visible range⁴¹ and they are expected to be masked by the overlapping with stronger absorptions of other tautomers. On the other hand, the stability estimated by the formation enthalpy for the tautomers of **8**, detected in absolute alcohol, correlates itself qualitatively with the intensity of the absorption bands attributed to each of the tautomers (**8b**<**8c**<**8d**) (Fig. 1A, curve 1). Thus the quanto-mechanical calculations agree with the tautomeric forms considered here.

Table 4

The lowest formation enthalpies (kcal/mol) for conformations of E- and Z- configurations of possible tautomers in the case of dyes **8**, **10** and **12** calculated by AM₁-SM₂ method.

Tautomers of the E-isomers	X; compound: (CH ₃) ₂ N; CH ₃ ; CH ₃ -O 8 10 12	Tautomers of the Z-isomers	X; compound: (CH ₃) ₂ N; CH ₃ ; CH ₃ -O 8 10 12
 <p>E-a</p>	92.67 81.16 48.54	 <p>Z-a</p>	<u>92.30*</u> 78.79 46.79
 <p>E-b</p>	98.76 85.38 53.22	 <p>Z-b</p>	<u>96.72</u> 83.39 51.27
 <p>E-c</p>	94.47 81.1 48.93	 <p>Z-c</p>	<u>91.09</u> 77.65 45.77
 <p>E-d</p>	95.79 81.39 50.20	 <p>Z-d</p>	<u>90.87</u> 76.96 45.26

- It is interesting that always the lowest values of formation enthalpies correspond to Z-configurations. Consequently the tautomers should exist in these configurations. Therefore, the values to be compared for the estimation of tautomer stabilities of dye **8** are those underlined.

CONCLUSION

The spectrophotometrical measurements in visible range, (^1H , ^{13}C)-NMR spectroscopy, Hammett correlation of $\bar{\nu}$ or $\Delta\bar{\nu}$ as a function of σ_p , the quantic calculations as well as the mechanistic considerations for the formation of the dyes **5** proved the involvement of various tautomers. The tautomeric equilibria are coupled with acid-base equilibria. Such assumptions provide coherent explanations of all experimental data. Our data clearly show the similitude between commercial dyes **3** and those investigated by us **5**. Thus, some dyes **3** also exhibit two absorption bands in visible that are influenced by the addition of acid or base in the same manner as the one observed for **5**.

For the two types of dyes **3** and **5** there are also other similarities concerning:

- ^1H , ^{13}C -NMR data for common moieties
- Hammett correlations
- The stability order of tautomers ascertained by quantic calculations.

All these analogies of dyes **3** and **5** support the existence of tautomeric equilibria also in the case of **3**. Therefore, to define the appropriate structure of dyes **3** or **5**, one should take into consideration all the tautomeric forms. Their concentrations depend upon the actual conditions (solid state or solution, protic or aprotic solvents, pH, metal complexes, the substrate for the dyes). Sometimes the dyes can exist (solid state) or are detected (solution in CHCl_3) in only one form.

EXPERIMENTAL

The synthesis and purification of the dyes **5** were accomplished as previously described^{5-7, 21b}. Analytical grade reagents and solvents, provided by Reactivul (Bucharest, Romania), Merck (Darmstadt, Germany), UCB (Bruxelles, Belgium) and Fluka (Buchs, Switzerland), were used without further purification. Each solution was prepared in the corresponding solvent and diluted to the requested concentration, or directly to the concentration needed for spectral measurements (10^{-5} M). An UV-VIS Spectrophotometer (Zeiss-Jena) was employed.

NMR (^1H - and ^{13}C -) spectra were obtained in CDCl_3 and $\text{CD}_3\text{-SOCD}_3$ at room temperature by means of a Varian Gemini 300 (300 MHz) and INOVA 500 (500 MHz) spectrometer. The assignments of chemical shifts for ^{13}C -NMR- spectrum of **9** were verified by means of the substituent increments⁴⁹ calculations for **8**, **10** and **12**. The calculated ^{13}C - chemical shifts for dyes **9** substituted in 4-position with CH_3 -, CH_3O - or $(\text{CH}_3)_2\text{N}$ - were practically identical to the experimental values (Table 3).

Full geometry optimisation for all conformations of E- and Z- configurations of tautomers **5a-5d** of dyes **8**, **10**, **12** have been carried out by means of the semiempirical AM1-SM2 method⁴⁸ as implemented in PC-Spartan 1.0 package of program⁵⁰.

ACKNOWLEDGEMENT

The financial support of the study by the Romanian National University Research Council (CNCSIS grant A) is gratefully acknowledged.

REFERENCES

1. W. Krohs and O. Hensel, "Pyrazolone und Dioxypyrazolidine", Editor Cantor, Aulendorf in Wuerttemberg, 1961
2. J. Lenoir, "The Chemistry of Synthetic Dyes", Editor K. Venkataraman, Academic Press, London, 1971, Vol. V, Chap. VI, 328, 353-356
3. H. R. Schwander, *Dyes Pigm.*, 1982, **3**, 134
4. H. Zollinger, *Color Chemistry*, VSH, Basel, 1991, 117-137
5. I. Panea, I. Cristea, *Chimia (Schweiz)*, 1991, **45(10)**, 92
6. A. Ghirisan, *PhD. Thesis, University "Babes-Bolyai"*, Cluj-Napoca, Romania, 1998
7. a) I. Panea, A. Ghirisan, I. Cristea and R. Gropeanu, *Rom. P 114797 C₁/1999*,
b) I. Panea, A. Ghirisan, F. Iura, R. Gropeanu and I. A. Silber, *Studia Univ. "Babes-Bolyai", Chem.*, this issue.
8. I. Baldea, A. Ghirisan and I. Panea, *J. Chem. Soc., Perkin Trans.2*, 1992, 1715.
9. J. Elguero, C. Marzin, A. R. Katritzky and P. Linda, *The Tautomerism of Heterocycles*, Academic Press, New-York, 1976, 313-339.
10. G. E. Hawkes, E. W. Randall, J. Elguero and C. J. Marzin, *J. Chem. Soc., Perkin Trans. 2*, 1977, 1024
11. I. Baldea, A. Ghirisan, I. A. Silber and I. Cristea, *Rev. Roum. Chim.*, 1997, **42(9)**, 767
12. I. Cristea, V. Farcasan, *Rev. Chim.*, Bucharest, 1987, **38**, 674; I. Cristea, I. Panea, *Studia Univ. "Babes-Bolyai", Chem.*, 1995, **40**, 171; I. Panea and I. Cristea, *Studia Univ. "Babes-Bolyai", Chem.*, 1996, **41**, 9
13. G. Hinsche, E. Uhleman, D. Zeigan and G. Engelhardt, *Z. Chem.*, 1981, **21**, 414
14. D. Zeigen, E. Kleinpeter, H. Wilde and G. Mann, *J. Prakt. Chem.*, 1981, **323**, 188
15. J. E. Rockly and L. A. Summers, *Austr. J. Chem.*, 1981, **34**, 1117; and references therein
16. C. P. Singh, R. Jain and A. C. Ojha, *Rev. Roum. Chim.*, 1981, **26**, 1011
17. P. Nikolov, F. Fratev, S. Stoyanov and O. E. Polansky, *Z. Naturforsch.*, 1981, **36a**, 191
18. H. Balli and H. Ritter, *Dyes Pigm.*, 1981, **2**, 93
19. L. G. Kuzmina, L. P. Grigoreva and Iu. T. Strudika, *Khim. Geterosikl. Soedin.*, 1985, 815
20. a) H. Mustroph, *Z. Chem.*, 1987, **27**, 281; b) N. Ertan, *Dyes Pigm.*, 2000, **44**, 41.
21. a) M. F. Abdel-Megeed, *Spectroscopy Letters*, 1987, **20**, 291; b) I. Panea, A. Ghirisan, I. Cristea, R. Gropeanu and I. A. Silber, *Heterocycl. Commun.*, 2001, **7**, 563.
22. A. Lyca and H. Mustroph, *J. Prakt. Chem.*, 1989, **331**, 11
23. M. T. El-Haty, *Assian J. Chem.*, 1991, **3**, 189
24. B. E. Zaitsev, E. V. Nikiforov, M. A. Ryabov and G. V. Sheban, *Khim. Geterosikl. Soedin.*, 1991, 1331; *Chem. Abstr.* 1992, **117**, 47814t
25. E. V. Nikiforov, B. E. Zaitsev, G. V. Sheban, M. A. Riabov and P. I. Abramenko, *Zh. Obsh. Khim.*, 1992, **62**, 1135

26. A. Whitaker, *J. Soc. Dyers Colour.*, 1995, **111**, 66
27. A. Lyca, *Dyes Pigm.*, 1999, **43**, 27; *Chem. Abstr.* 1999, 131, 215635v
28. M. Kamel, M. A. Allam, R. M. Issa, A. T. El-Aref and S. T. El-Aref, *J. Prakt. Chem.*, 1971, **313**, 1131
29. A. R. Katritzky and F. W. Maine, *Tetrahedron*, 1964, **20**, 299
30. I. S. Ioffe, L. M. Kriukova and L. Iu. Kim, *Zh. Org. Khim.*, 1971, **7**, 2193
31. H. Mustroph, J. Potocnak and N. Grossman, *J. Prakt. Chem.*, 1984, **326**, 979
32. O. Exner, "Advances in Linear Free Energy Relationships", Plenum Press, London, 1972, 27-34
33. R. Kuhn and F. Bar, *Liebigs Ann. Chem.*, 1935, **516**, 143
34. A. Burawoy, A. G. Salem and A. R. Thompson, *J. Chem. Soc.*, 1952, 4793; 1953, 1443
35. H. Zollinger, "Azo and Diazochemistry", Interscience Publish, New-York, 1961, 324
36. a). Y. Yagi, *Bull. Chem. Soc. Jpn.*, 1964, **37**, 1875, b). Y. Yagi, *Bull. Chem. Soc. Jpn.*, 1964, **37**, 1878, 1881; *Chem Abstr.* 1965, **63**, a). 1910c, d, b). 1911b, 1911g
37. J. Griffiths, *J. Soc. Dyers Color.*, 1972, **88**, 106
38. R. A. Cox and E. Buncel, "The Chemistry of the Hydrazo, Azo and Azoxy Groups", Editor S. Patai, Part. 2, Wiley, London, 1975, 838-859; and references therein
39. B. E. Zaitsev, V. A. Zaiteva, A. K. Molodkin, E. S. Obraztova, *Zhur. Neorg. Himii*, 1979, **24**, 127
40. S. J. Bell, E. P. Mazzola and B. Coxon, *Dyes Pigm.*, 1989, **11**, 93
41. J. Elguero, R. Jaquier and G. Tarrago, *Bull. Soc. Chim.Fr.*, 1966, 2990
42. R. Gunther, E. Jahne, H. Hartmann and M. Schulze, *J. Prakt. Chem.*, 1987, **329**, 945
43. L. A. Summers, P. F. H. Freeman and D. J. Shields, *J. Chem. Soc.*, 1965, 3312
44. J. Arriau, J. P. Campillo, J. Elguero and J. M. Pereillo, *Tetrahedron*, 1974, **30**, 1345
45. H. Zollinger, "Azo and Diazochemistry", Interscience Publish, New-York, 1961, 312
46. H. Mustroph, *J. Prakt. Chem.*, 1985, **327**, 121; H. Mustroph, *Z. Chem.*, 1985, **25**, 270, 385
47. A. R. Katritzky and J. M. Lagowski, "Advances in Heterocyclic Chemistry", Editor A. R. Kartitzky, Academic Press, London, 1963, **1**, 317
48. M. J. S. Dewar, E. G. Zoebisch, E. F. Healy and J. J. P. Stewart, *J. Amer. Chem. Soc.*, 1985, **107**, 3902; C. J. Cramer and D. G. Truhlar, *J. Amer. Chem. Soc.*, 1991, **113**, 8305
49. R. M. Silverstein, G. C. Bassler and T. C. Morrill, "Spectrometric Identification of Organic Compounds", 5th Edition, John Wiley and Sons, New-York, 1991, Table 5.9
50. Wavefunction, Inc., 18301, von Karman Avenues Suite 370, Irvine, CA 92612 USA

LOGARITHMIC EXTRAPOLATION METHOD FOR KINETIC DETERMINATION OF AMINE MIXTURES

LUCIAN COPOLOVICI and IOAN BALDEA

Department of Physical Chemistry, "Babeş-Bolyai" University, 400028 Cluj-Napoca, 11 Arany Janos St., Romania, E-mail: clucian@chem.ubbcluj.ro

ABSTRACT. A kinetic method for the simultaneous determination of binary mixtures of aromatic amines and of β -naphthol and 1-phenyl-3-methylpyrazolin-5-one by logarithmic extrapolation is reported. The method involves the formation of an azo dye between coupling agent and a diazonium salt formed from the amine in the presence of nitrite in weak acidic media. The reaction is monitored spectrophotometrically by the formation of an azodye absorbing at 420 nm.

Keywords: kinetic methods, para-toluidine, azodye

INTRODUCTION

The method is based on the equation describing the modification of absorbance under pseudo-first order conditions.

Total concentration of analyte is determined from total concentration of products or via initial rate. The relative errors were in the range of 0.5 to 6% for the most cases.

The logarithmic extrapolation method is the most commonly used graphical linear method for the simultaneous kinetic determination of two species in a mixture. The method has been used in analytical chemistry for the determination of mixture of organic species¹⁻³ or heavy metal ions⁴⁻⁶.

This method features several advantages, namely⁷:

- no prior knowledge of the rate constant of the analytes is necessary;
- it is less prone to error as the linear plot is constructed from several points;
- rate constant ratios as low as five are acceptable under certain condition.

The purpose of the present study is to use the logarithmic extrapolation method for the determination of *para*-toluidine and aniline in mixture and of β -naphthol and 1-phenyl-3-methylpyrazolin-5-one, respectively. Indicator reaction is of a Bratton-Marshall type, the formation of an azodye.

Despite of the great variety of methods reported, the Bratton-Marshall procedure is still the most widely used for the determination of sulphonamides in clinical work^{8,9}. Bratton-Marshall method is based on transformation of the free primary aromatic amine into a diazonium salt by means of nitrous acid; the diazonium salt is rapidly coupled with a chromogenic reagent such as *N*-(1-naphthyl)ethylenediamine¹⁰. It is also known that the semiquinone radicals derived by partial oxidation of aromatic *p*-diamines have intense color and react with various aromatic amines and phenols to give intensely colored indamine and indoaniline dyes. The increase of absorbance can be used to indicate the reaction advancement and consequently the reaction rate^{11, 12}.

In this work, indicator reaction is a coupling one between benzenediazonium salts (**1**) formed *in situ* (proceeding from aniline and/or *para*-toluidine) and 1-phenyl-3-methylpyrazolin-5-one (**2**) or β -naphthol (**3**) with HNO_2 .

The kinetics of the reaction has been previously investigated. The reaction obeyed a rate law of first-order in each, diazonium salt and coupling agent, and the effect of the acidity is known¹².

EXPERIMENTAL

All reagents but coupling agent were of analytical-reagent grade and solutions were prepared in de-ionized and four-distilled water or reagent grade ethanol. 1-phenyl-3-methylpyrazolin-5-one (**2**) was prepared in our laboratory as previously described¹³ and purified by re-crystallization from ethanol. Stock solution (1×10^{-3} M) was prepared in ethanol. Sodium nitrite (1 M) and (**2**) (5×10^{-3} M) solution were prepared in de-ionized water and ethanol respectively. A 4.6×10^{-3} M perchloric acid solution was also used to generate the hydrogen ion as requiring.

Kinetic measurements have been performed spectrophotometrically by means of a JASCO V-530 spectrophotometer. It has an automatic data linked acquisition to a computer. Temperature was controlled at $20 \pm 0.1^\circ\text{C}$ by means of a LAUDA M 12 temperature - controlled bath connected to the cell holder.

The reaction was followed at an appropriate wavelength (420 nm) of the dye formed by coupling reaction. 1.0 mL of standard aromatic amine solution, 0.5 mL of (**2**) 5×10^{-3} M and 0.5 mL of perchloric acid 4.6×10^{-3} M were placed in a 5 cm path length cuvette and accurately diluted to 11.5 mL. The reaction was initiated by rapid addition and thoroughly mixing of 0.25 mL solution of sodium nitrite 1 M over 11.5 mL of other reactants mixture. It was previously kept in the temperature bath for at least 15 min. The progress of the reaction was monitored and kinetic data (absorbance vs. time) were collected and processed by computer. The initial rate was measured after the induction period, within the domain of linear dependence (about 300 s). Each sample was repeated for at least three times for the same set of experimental conditions. Replicate run data yielded the same results within the error limits of 0.5 %.

RESULTS AND DISCUSSION

Para-toluidine or aniline in weakly acidic solutions react with nitrous acid to yield a diazonium salt. In the presence of 1-phenyl-3-methylpyrazolin-5-one (**2**) or β -naphthol (**3**), diazonium salt forms azo dyes (**4**) and (**5**) by a quite rapid coupling reaction respectively. The reactions are present in figure 1.

An attempt has been made to determine either a mixture of two aromatic amines or a mixture of 1-phenyl-3-methylpyrazolin-5-one and β -naphthol using *para*-toluidinediazonium salt.

The method is based on the equation describing the modification of absorbance under pseudo-first order conditions. Therefore under the large excess of one reactant:

$$\frac{A_\infty - A}{A_\infty - A_0} = \frac{[A]_0}{[A]_0 + [B]_0} \cdot e^{-k_1 t} + \frac{[B]_0}{[A]_0 + [B]_0} \cdot e^{-k_2 t} \quad (1)$$

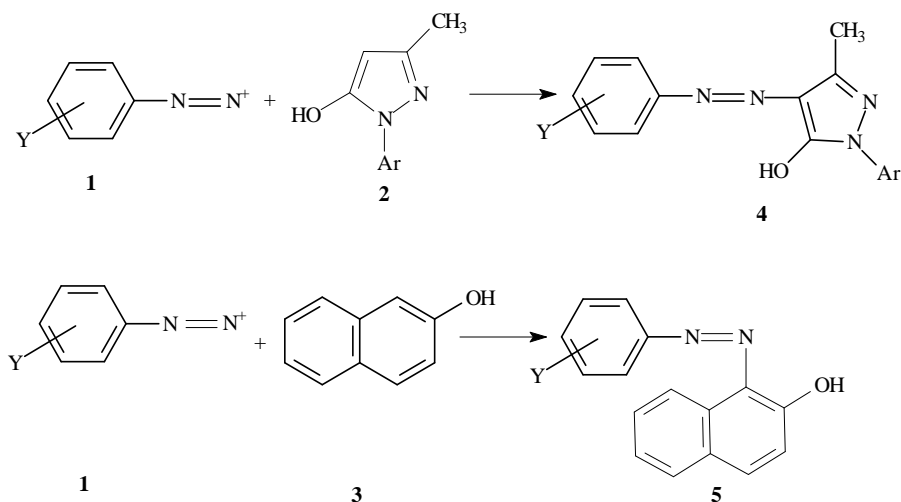


Figure 1. Indicator reaction ($Y = H$ or CH_3)

Providing that $k_1 > 5k_2$, towards the end of the process, the reaction of 1-phenyl-3-methylpyrazolin-5-one (**2**) with anilinediazonium salt has been accomplished and the first exponential term gets vanished. It means that, within this period of time, only the reaction of 1-phenyl-3-methylpyrazolin-5-one (**2**) and *para*-toluidinediazonium ion (k_2) take place. The rapid process (k_1) has been already accomplished. Thus:

$$\ln \frac{A_\infty - A}{A_\infty - A_0} = \ln \frac{[B]_0}{[A]_0 + [B]_0} - k_2 \cdot t \quad (2)$$

By plotting $\ln \frac{A_\infty - A}{A_\infty - A_0}$ versus t a straight line should be obtained. The

rate constant k_2 is the slope of the line and $\ln \frac{[B]_0}{[A]_0 + [B]_0}$ (the fraction of *para*-toluidine in the initial mixture) as the intercept can be obtained. Figure 2 presents this kind of plot.

By using these values and transforming equation (1) into a form containing known amounts in the left side, the following is obtained:

$$\ln \left(\frac{A_\infty - A}{A_\infty - A_0} - \frac{[B]_0}{[A]_0 + [B]_0} \cdot e^{-k_2 \cdot t} \right) = \ln \left[\frac{[A]_0}{[A]_0 + [B]_0} \right] - k_1 \cdot t \quad (3)$$

By plotting left side of equation (3) as a function of time (figure 2), using experimental date obtained at the beginning of the kinetic measurement, the ratio of aniline can be determined from the intercept of the line.

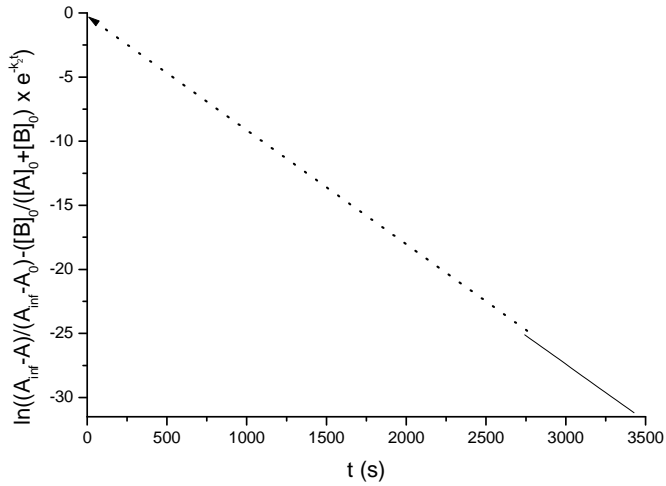


Figure 2. Determination the ratio of *para*-toluidine

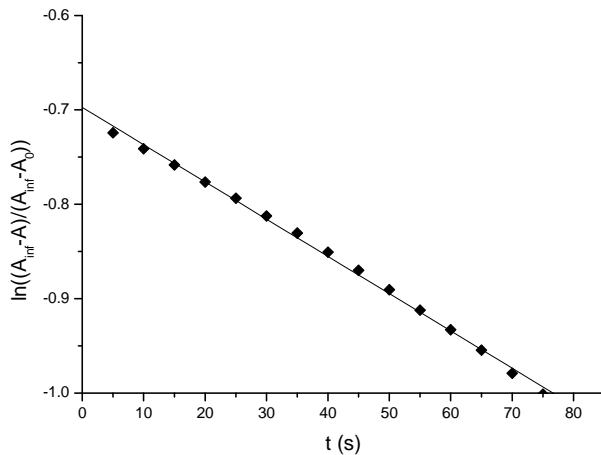


Figure 3. Determination the ratio of 1-phenyl-3-methylpyrazolin-5-one

Table 1.

The prediction for some mixtures of *para*-toluidine and aniline

Analyte Ratio	Analyte fraction				Relative errors %	
	addend	found				
	<i>p</i> -toluidine	aniline	<i>p</i> -toluidine	aniline	<i>p</i> -toluidine	aniline
1:1	50.0	50.0	50.1	49.8	0.2	-0.4
1:2	33.3	66.6	31.4	66.9	-5.7	0.5
2:1	66.6	33.3	65.8	32.3	-1.2	-3.0
1:4	25.0	75.0	23.8	74.8	-4.8	-0.3
4:1	75.0	25.0	73.0	24.1	-2.7	-3.6
1:5	20.0	80.0	19.8	81.7	-1.0	2.1
5:1	80.0	20.0	83.6	18.8	4.5	-6.0

Table 2.The prediction for some mixtures of β -naphthol and 1-phenyl-3-methylpyrazolin-5-one

Analyte Ratio	Analyte fraction (%)				Relative errors (%)	
	addend	found				
	β -naphthol	Phenil-pyrazolone	β -naphthol	Phenil-pyrazolone	β -naphthol	Phenil-pyrazolone
1:1	50.0	50.0	50.2	49.7	+0.40	-0.60
1:2	33.3	66.6	31.6	66.5	-5.11	-0.15
2:1	66.6	33.3	65.7	32.8	-1.35	-1.50
1:4	25.0	75.0	24.0	75.4	-4.00	+0.53
4:1	75.0	25.0	72.0	25.3	-4.00	+1.20
1:5	20.0	80.0	19.5	82.1	-2.50	+2.63
5:1	80.0	20.0	81.7	18.5	2.13	-5.50

A similar method¹⁴ was used for the determination of 1-phenyl-3-methylpyrazolin-5-one and β -naphthol in mixture. The indicator reaction was the coupling reaction between benzenediazonium salts and 1-phenyl-3-methylpyrazolin-5-one or β -naphthol. In this case the prediction for some mixtures is presented in Table 2. Total concentration of analyte is determined from total concentration of products or via initial rate¹⁵.

Several measurements were performed in the presence of various concentrations of metal ions usually present in rivers or wastewaters such as Cu^{2+} , Fe^{3+} , Zn^{2+} , Mn^{2+} , and Pb^{2+} . The concentration up to 8.5×10^{-4} M were used that exceeded common concentration of these ions in waters. No effect on the initial rate has been noticed.

CONCLUSIONS

The method permit to determine mixture of para-toluidine with aniline and mixture of 1-phenyl-3-methylpyrazolin-5-one with β -naphthol.

Relative errors are quite good ranging between the limit 0.5 - 6.0 %.

The usual metal ions frequently present in water do not interfere with the measurement.

ACKNOWLEDGEMENTS

The research was supported by CNCSIS (grant type A No. 164), for which the authors gratefully acknowledge.

REFERENCES

1. Quintero M. C., Silva M., Perez-Bendito D., *Talanta*, **1989**, 36, 717-722
2. Gonzales V., Rubio S., Gomez-Hens A., Perez-Bendito D., *Anal. Lett.*, **1988**, 21, 993-1008

3. Forster E., Silva M., Otto M., Perez - Bendito D., *Talanta*, **1993**, 40, 1505-1510
4. Ballesteros L., Perez - Bendito D., *Anal. Chim. Acta*, **1986**, 182, 213-218
5. Ballesteros L., Perez - Bendito D., *Analyst*, **1983**, 108, 443-451
6. Ballesteros L., Perez - Bendito D., *Mikrochim. Acta*, **1986**, 1, 123-126
7. Perez - Bendito D., *Differential Rate Determinations*, in "Encyclopedia of Analytical Chemistry", (Meyers R. A. Eds.) John Wiley&Sons, Ltd., Vol. 12, **2000**, 11098
8. Bye A, Fox AF., *Clin. Chem.* **1974**, 20, 288-296
9. Bratton AC, Marshall EK., *J. Biol. Chem.*, **1939**, 128, 537-549
10. Michaelis L, Schubert MP, Granick S, *J. Am. Chem. Soc.*, **1939**, 61, 1981-1994
11. Tawa R, Hirose S., *Chem. Pharm. Bull.*, **1980**, 28(7), 2136-2143
12. Baldea I, Ghirişan A, Panea I, *J. Chem. Soc. Perkin Trans 2*, **1992**, 1715-1719
13. Cristea I, Farcaşan V, Panea I, *Roum.*, **1984**, P. 84355
14. Copolovici L., Baldea I., "Kinetic determination of aromatic amines in mixture using a logarithmic extrapolation method", "Proceedings of 3rd International Conference of the Chemical Societies of the South-Eastern European Countries on "Chemistry in the New Millennium - an Endless Frontier ", Bucureşti, 22.09-25.09 **2002**
15. Copolovici L., Baldea I., *Anal. & Bioanal. Chem.*, **2002**, 374, 13-15

1-AZA-5-HYDROXYMETHYL-3,7-DIOXABICYCLO[3.3.0]OCTANES: CHELATING PROPERTIES RELATED TO THEIR CONFORMATIONAL CHIRALITY

CARMEN MAIEREANU^a, ERIC CONDAMINE^b,
IOAN SILAGHI-DUMITRESCU and MIRCEA DARABANTU^{a*}

^aDepartment of Organic Chemistry, "Babes-Bolyai" University,
11 Arany János Str., 400028 Cluj-Napoca, Romania

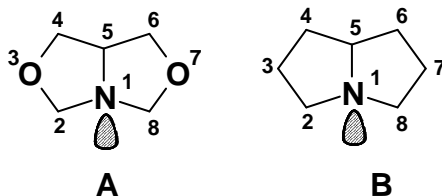
^bInstitut de Recherche en Chimie Organique Fine (I.R.C.O.F.),
Université de Rouen, BP 08, F-76131 Mont Saint-Aignan, France

^cDepartment of Inorganic Chemistry, "Babes-Bolyai" University,
11 Arany János Str., 400028 Cluj-Napoca, Romania

ABSTRACT. A structural approach is considered for some representative title compounds in order to explain their behaviour in gas phase (*ab initio* theoretical calculation) and in solution (dynamic NMR and IR methods). The results in terms of conformational analysis and chelate hydrogen bonds are discussed.

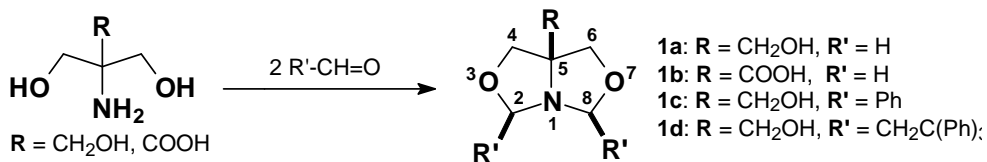
1. INTRODUCTION

The 1-aza-3,7-dioxabicyclo[3.3.0]octane heterocyclic saturated system **A** (**Scheme 1**), as a synthetic easily available analogue of the core alkaloid pyrrolizidine, 1-azabicyclo[3.3.0]octane **B** is very well known along more than a half century¹ by the large use of its (poly)substituted derivatives.



Scheme 1

Of particular interest, the C-5 (and optionally C-2, -8) substituted structures of type **A** are mentioned to be fertilisers, plasticisers, biocides, pesticides etc. mainly due to the simplicity of their synthesis: direct cyclocondensation between 2-substituted-2-amino-1,3-propanediols and a large variety of carbonyl compounds (**Scheme 2**).²⁻⁹



Nevertheless, the stereochemistry of this class of compounds remained obscure for more than 20 years after the synthesis of the parent compound of the series (Senkus, 1945)¹, *r*-1-aza-*c*-5-hydroxymethyl-3,7-dioxabicyclo[3.3.0]octane¹ **1a** (**Scheme 2**); thus, the structural knowledge in the field followed step by step the evolution of the NMR spectroscopy.¹⁰⁻¹³

Indeed, the basic stereochemical approach focused in considering, first, the magnitude of the geminal coupling patterns J_{gem} in the motif X-CH₂-Y- (X, Y = -N<, -NH-, -O-, -S-) including the 1,3-oxazolidine >N-CH₂-O- fragment in the title compounds (seen as *cis*-fused double 1,3-oxazolidine system, Crabb *et al.*¹⁰⁻¹²).

The first attempt to provide evidence for the general mobility of the 5-substituted-1-aza-3,7-dioxabicyclo[3.3.0]octane skeleton (suggested by inspection of Dreiding models and ¹H NMR spectra at variable temperature) was reported by Crabb in 1973.¹¹

Later developments in the field by our group revealed more essential features:¹⁴⁻¹⁶

i) the absence of pyramidal inversion of the bridged nitrogen in both 4- or 5-substituted-1-aza-3,7-dioxabicyclo[3.3.0]octanes.

ii) the flipping of the basic molecular skeleton for some 5-hydroxymethyl derivatives in non polar solvents.

iii) the conformational and configurational chirality of these systems.

The structure in solid state of the 1-aza-3,7-dioxabicyclo[3.3.0]octane skeleton was scarcely analysed. To our knowledge, only two X-rays determined structures are known so far: by O'Connor¹⁷ in 1973 {*r*-1-aza-3,7-dioxabicyclo[3.3.0]octane-*c*-5-carboxylic acid **1b** copper salt, **Scheme 2**} and more recently (2000) by Pavia¹⁸ {*r*-1-aza-*c*-5-hydroxymethyl-*c*-2-*c*-8-diphenyl-3,7-dioxabicyclo[3.3.0]octane **1c** (**Scheme 2**)}.

In the present work, we attempt to a more comprehensive approach starting from one of the basic term of the series, *r*-1-aza-*c*-5-hydroxymethyl-(dynamic NMR and IR) and two related analogues.

2. RESULTS AND DISCUSSION

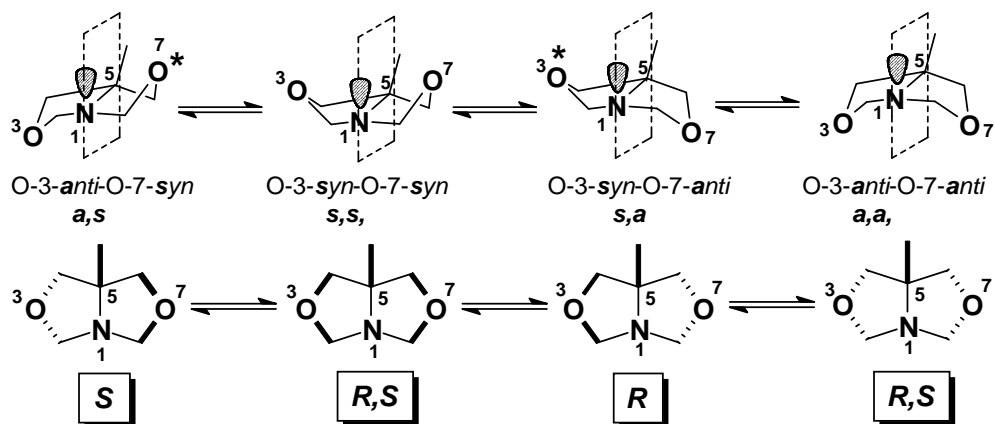
2.1. Conformational chirality

The *r*-1-aza-3,7-dioxabicyclo[3.3.0]-*c*-5-octane heterocyclic saturated system is intrinsic heterofacial. The crucial importance of this detail originates from our previous considerations about the conformational chirality exhibited by the skeleton itself (**Scheme 3**).¹⁵

Thus, one has to observe the four distinct conformers discriminated by the disposal of the oxygen atoms O-3, -7 with respect to the plane delimited by the lone-pair of the bridged nitrogen atom, N-1, C-5 and the ligand attached at C-5 (optionally H, not depicted). This plane is either an element of chirality or symmetry, depending on the sense of the puckering in the two oxazolidine rings, seen as O-envelope conformers: in enantiomeric conformers O-3-*anti*-O-7-*syn* and O-3-*syn*-O-7-*anti* (the *cis* ligands: the lone pair at N-1 and/or the ligand at C-5 are chosen as reference for the descriptors *syn* and *anti*), the sequence rule as N-1>C-5>H (or the ligand at C-5) indicates different configurations. If the *syn* successively labelled oxygen (*) is arbitrarily

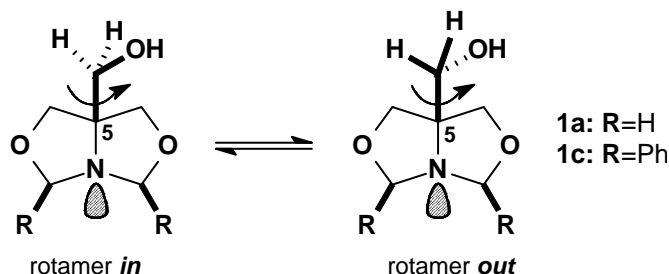
¹ The basic stereochemistry of the skeleton as *cis*-fused system is already very well documented;10-15, 17,18 according to I.U.P.A.C. nomenclature, the lone pair at N-1 is designed "P" as fiducial substituent.

given higher precedence than the *anti* one (that is, O-*syn* is always placed closer to the *cis* substituents), configuration *R* or *S* are easily to recognise. If so, the conformers O-3-*syn*-O-7-*syn* and O-3-*anti*-O-7-*anti*, are *mutatis-mutandis* diastereomeric *meso*-forms. If the substituent linked at C-5 is hydroxymethyl, besides the conformers described above, one has to also consider the corresponding possible rotamers generated by the (free?) rotation around the bond C-5-CH₂OH (**Scheme 4**).



Scheme 3

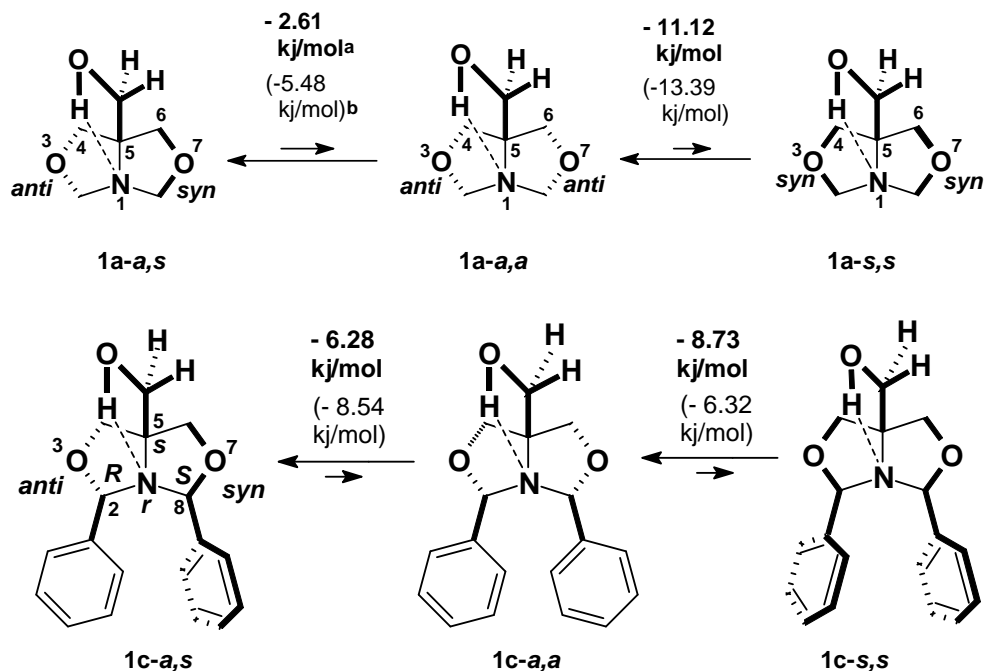
Depending on the orientation of the C-5-hydroxymethyl group, for the present discussion, only two rotamers were seen relevant to discriminate: rotamer *in* (in which intramolecular interactions are expected) and rotamer *out* (in which intermolecular interactions are expected).



Scheme 4

2.2. Evidence provided by *ab initio* RHF/6-31 G* molecular orbital calculation

The above anticipations were preliminarily checked by theoretical calculation (level RHF/6-31G* with optimisation of total energy). Thus, as shown in **Scheme 5**, the parent compound **1a** was involved in a double conformational equilibrium between three skeleton conformers as rotamers *in*. The oxazolidine ring inversion took place about the C-O-C bonds since only O-3(7) envelope conformers were revealed. The same was valid if two phenyl groups were linked at positions C-2, -8 in an *all cis* spatial disposal with respect to ligands attached at N-1, C-2, -5, -8 (compound **1c**).



^a total difference between the total energies ($\Delta\Delta E$ values) taking into account the orientation of the hydroxymethyl group

^b total difference between the total energies ($\Delta\Delta E$ values) by neglecting the orientation of the hydroxymethyl group

Scheme 5

The most stable conformer was the rotamer **1a-a,s** in which the oxygen in C-5-hydroxymethyl group was oriented as attempting to develop an intramolecular hydrogen bond with the *pseudo*-axial lone pair at N-1. Supplementary inspection of Dreiding model of **1a-a,s** indicated this interaction to be plausible: the calculated distances between the hydroxyl proton and the lone pair at N-1 $N\dots H-O$ were found to range between 2.400-2.600 Å.

The incidence of an intramolecular hydrogen bond seemed to reduce the differences between the total energy of the most stable skeleton conformers (**1a**, **1c⁻-s,s** > **1a**, **1c-a,a** > **1a**, **1c-a,s**). Indeed, in **Scheme 5**, in round brackets, there are mentioned the same differences between the corresponding total energies ($\Delta\Delta E$ values) by neglecting the orientation of the C-5-hydroxymethyl group (previously described by us).¹⁵ From the three possible skeleton diastereomeric conformers discriminated as **a,a** – **a,s** – **s,s** the later was disfavoured (and presumably even ruled out).

* it must however be observed the *configurational chirality* exhibited by **1c** at C-2, -8, possessing opposite configuration. Thus, **1c** is a *meso* form, N-1 and C-5 being *pseudo* chiral centers.

To conclude, the flexibility of the compounds **1a** and **1c** consisted globally in an enantiomeric inversion **1a**, **1c-a,s** → **1a**, **1c-a,a** → **1a**, **1c-s,a** (one oxazolidine ring inversion, **Scheme 3, 5**). The differences between the total energies of the chiral and the *meso* form conformation were too small (about 0.6 kcal/mol for **1a**) in order to anticipate the frozen arrangement **a,s** or **a,a**.

In the end, we note that the X-rays previously determined structure for the compound **1b** by O'Connor (**Scheme 2**) was in agreement with our calculation, as **1b-a,a** frozen conformer.¹⁷ Moreover, the calculated conformer **1c-a,s** was perfectly consistent with the X-rays determined structure by Pavia.¹⁸

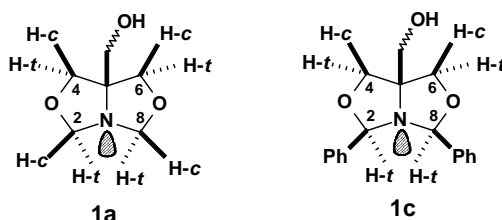
2.3. Conformational analysis based on dynamic NMR spectroscopy

In our recent paper,¹⁵ we reported a satisfactory agreement between theoretical calculations and dynamic ¹H NMR data concerning the behaviour at low temperature (in non polar solvent, toluene-*d*₈) of the compounds **1a** and **1c**: the anticipated mobility of the bicyclic skeleton was evidenced by the general coalescence found for all the peaks assigned to the heterocyclic part of the molecule at about –40 °C for **1a** and –60 °C for **1c**. Unfortunately, they crystallised from the solvent below coalescence, preventing us to continue this investigation.

For the present discussion we assumed that the coalescence earlier found for the compounds **1a** and **1c** in toluene-*d*₈ depicted, in fact, the slow skeletal motion of their rotamers *in*, or at least shifted conformational equilibria in which they were the dominant species (**Scheme 3-5**). Therefore, we extended our NMR analysis by using solvents possessing different chelating ability. The results are summarised in **Table 1**.

Table 1

¹H NMR data (δ, ppm) for the compounds **1a**, **c**



Nr.	Solvent	T_i (K)	H-2(8)-c ^a	H-2(8)-t ^a	H-4(6)-c	H-4(6)-t
		T_f (K)				
1a	Toluene- <i>d</i> ₈	298	3.94	4.14	3.28	3.45
		233	3.93	4.35	3.21	3.53
	CDCl ₃	298	4.40	4.45	3.73	3.77
	DMSO- <i>d</i> ₆	298	4.26	4.39	3.66	3.71
	MeOD- <i>d</i> ₄	328	4.408	4.431	3.764	3.805
		180	4.397	4.431	3.788	3.788
1c	Toluene- <i>d</i> ₈	298	-	5.32	3.77	3.52
		213	-	5.24	3.93	3.58
	DMSO- <i>d</i> ₆	298	-	5.58	3.93	3.82
	MeOD- <i>d</i> ₄	328	-	5.565	4.071	3.895
		180	-	5.510	3.954	3.877

^a the location of heterocyclic protons as *c* (*cis*) or *t* (*trans*) with respect to the lone pair of N-1 and the C-5-hydroxymethyl group as by means of NOE-diff Experiments¹⁵ was previously reported by us.

The ^1H NMR spectra at variable temperature are presented in **Figures 1-3**. For comparison, the spectra previously recorded in toluene- d_8 are also shown.¹⁵ They support the below discussion.

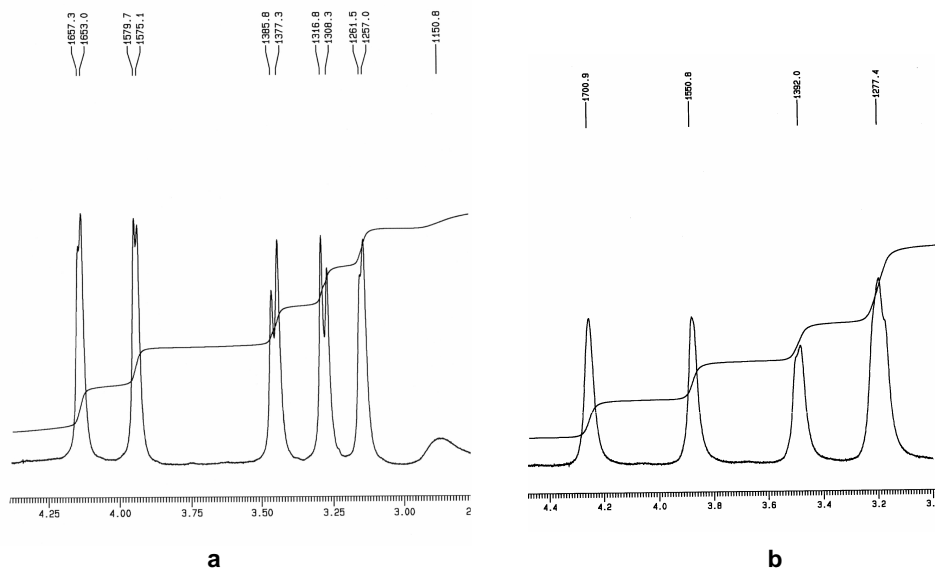


Figure 1. ^1H NMR spectra of the compound **1a** in toluene- d_8 (400 MHz); **a**) 273 K (from downfield to upfield, see assignments in **Table 1**): H-2(8)-t, H-2(8)-c, H-4(6)-t, H-4(6)-c, 5- CH_2O , OH; detail **b**) coalescence at 233 K

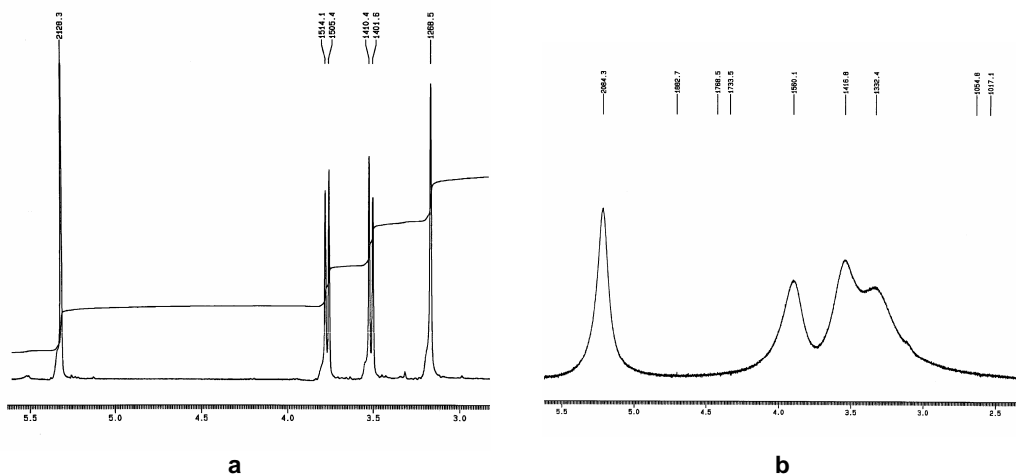
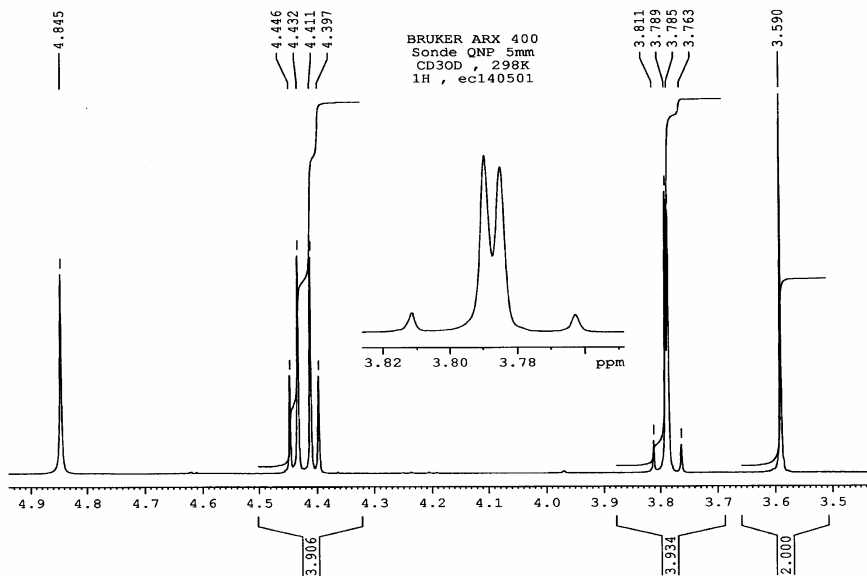
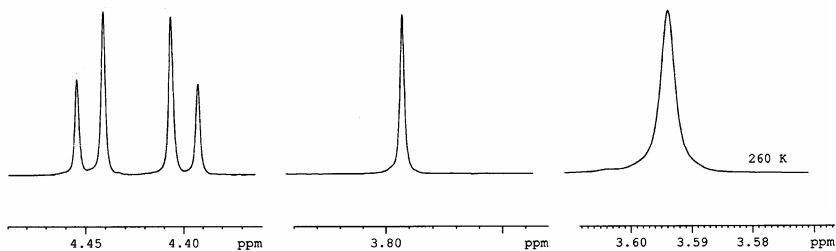


Figure 2. ^1H NMR spectra of the compound **1c** in toluene- d_8 (400 MHz); detail **a**) 273 K (from downfield to upfield, see assignments in **Table 1**): H-2(8)-t, H-4(6)-c, H-4(6)-t, 5- CH_2O ; detail **b**) coalescence at 213 K.

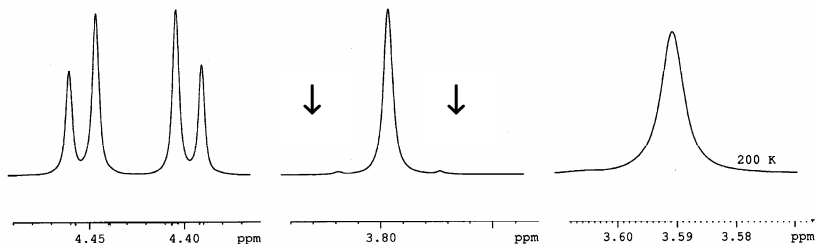
1-AZA-5-HYDROXYMETHYL-3,7-DIOXABICYCLO[3.3.0]OCTANES...



a



b



c

Figure 3. ^1H NMR spectra of the compound **1a** in MeOD-d_4 (400 MHz); detail **a**) 328 K (from downfield to upfield, see **Table 1**): H-2(8)-t, H-2(8)-c, H-4(6)-t, H-4(6)-c, 5- CH_2O ; detail **b**) coalescence at 260 K; detail **c**) new splitting at 200 K.

A priori, single DMSO- d_6 allowed us to assign **1a** and **1c** as rather flipping rotamers **out** because the hydroxyl proton was clearly displayed as a partially overlapped doublet of doublets (a triplet) with a typical 3J value as 5.0-5.5 Hz in a domain not larger than 0.25 ppm (4.89 – 5.16 ppm).

Obviously, DMSO- d_6 had to be ruled out for experiments at low temperatures. Hence, compound **1a** was tested by variable temperature NMR experiments in MeOD- d_4 ; it was expected that in this solvent, **1a** be also strongly chelated, involving this time, besides all heteroatoms, the rotamer **out**. Indeed, careful inspection of spectra revealed the coalescence of the aliphatic methylenes C-4(6) (AB system $\Delta\delta / ^2J=1.16$, doublet of doublets $^2J=9.0$ Hz, **Figure 3a**) into a singlet at 260 K (A_2 system, **Figure 3b**) and kept as such up to 220 K. Indeed, in the end of our analysis, the methylenes C-4(6) exhibited a partially overlapped doublet of doublets (another AB system $\Delta\delta / ^2J=1.02$, $^2J=9.0$ Hz, **Figure 3c**). No modification was detected in the aminalic part (O-3-C-2-N-1-C-8-O-7) of the molecule.

Completely different than in toluene- d_6 , the similarity between **1a** and **1c** disappeared if MeOD- d_4 was used (**Table 1**): no coalescence was observed for **1c**, but an important decrease of geminal anisochrony in the aliphatic zone C-4-C-5-C-6 (from about 0.18 ppm to 0.08 ppm) due, presumably, to a slight shielding of protons H-4(6)-*c* promoted, by the slower rotation of the two *cis*-phenyl ring. Although this evolution was similar to **1a**, it might be assigned that the diphenyl derivative **1c** was a much more flipping structure in MeOD- d_4 than in toluene- d_6 and more flipping than **1a** in both solvents.¹⁹

In turn, the 5-hydroxymethyl derivative **1a** revealed higher flexibility in non-polar solvents ($T_c=233$ K as rotamers **in**) than in chelating ones (MeOD- d_4 , $T_c=260$ K as rotamers **out**). On the other hand, the coalescence found for **1a** in MeOD- d_4 in the aliphatic zone (**Figure 3a-c**) was normal since in any alternative conformation the protons H-4(6)-*c* and H-4(6)-*t* were diastereotopic (**Scheme 3, 5**). So, the last splitting of the unique signal at coalescence could be assigned: avoiding extrapolation of our results, we believe that the conformational evolution of **1a** was towards a symmetrical frozen structure of type **1a-a,a** (*meso* form, **Scheme 5**).

2.4. Evidence provided by the IR spectroscopy

The behaviour of the 5-hydroxymethyl group was also examined by IR spectroscopy. Thus, the selected 5-hydroxymethyl derivatives **1a**, **1c** and **1d** were analysed in chloroform, which best allowed the variations of concentration. The choice for the above structures was evidently motivated by the absence at C-2(8) of any other chelating fragment, in order to avoid unpredictable intermolecular interactions, other than already investigated. The results are collected in **Table 2**.

As expected, the two typical bands in the region of interest (up to 3400 cm^{-1}) were displayed: a strong absorption (large band) assigned to ν_{assoc} and a very weak band at higher frequency for $\nu_{\text{non-assoc}}$. Dilution step by step was carried out until (reasonably) equal absorbencies were displayed.

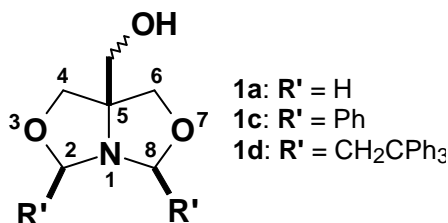
Our conclusions are resumed as follows:

The *cis*-diphenyl derivative **1c** was the less sensitive to the variations of concentration and the comparison with **1a** and **1d** regarding $\Delta\nu=f(\Delta C)$ values inferred us about its preferred association: it is very likely that the intermolecular hydrogen bonds were mainly realised between C-5- $\text{CH}_2\text{O}-\text{H}\dots\text{N}$ groups belonging each to a different unit (as rotamers **out**). That is, at higher concentration, **1c** was less associated than **1a** and **1d** since its bridged nitrogen was more "protected" by the

two-phenyl groups from both steric and electronic points of view. In the case of compound **1d**, the intercalation of a methylene group between C-2, -8 and the bulky triphenylmethane environments avoided this steric hindrance.

Table 2

Relevant absorptions (as ν , cm^{-1}) in IR spectra of the compounds **1a**, **1c** and **1d**



No.	C (mol l^{-1})	ν OH assoc. (cm^{-1})	ν OH non assoc. (cm^{-1})	$\Delta\nu$ non assoc. vs. assoc. (cm^{-1})	$\Delta\nu_{\text{assoc.}} = f(\Delta C)$ (cm^{-1})
1a	0.5000	3457	3628	171	81
	0.1000	3462	3627	165	
	0.0500	3469	3628	159	
	0.0250	3483	3628	145	
	0.0125	3521	3628	107	
	0.0062	3538	3628	90	
1c	0.5020	3523	3627	104	24
	0.2510	3533	3627	94	
	0.1250	3540	3627	87	
	0.0625	3542	3627	85	
	0.0064	3547	3627	80	
	0.0012	3547	3627	80	
1d	0.2500	3465	3637	172	89
	0.1250	3485	3635	150	
	0.0625	3495	3635	140	
	0.0312	3516	3637	121	
	0.0031	3553	3636	83	

Following dilution, there was an obvious convergence towards the absorption around 3545 cm^{-1} which could be assigned as the intramolecular hydrogen bond developed, in all three cases, by the rotamers *in* (a five membered chelate). The small differences observed should be the consequence of the expected variable basicity of the bridged nitrogen in a particular environment. The influence of the substituents linked at C-2, -8 consisted, this time, in their specific electronic effect.

In the end, considering as characteristic for the present cases the magnitude of the medium final value $\Delta\nu_{\text{non-assoc. vs. assoc.}}$ (**Table 2**) about 85 cm^{-1} , it should be mentioned its similarity with 1,3-alkanediols of type $\text{RR}'\text{C}(\text{CH}_2\text{OH})_2$ ($78\text{-}89 \text{ cm}^{-1}$);²⁰ it was greater than in cycloalkane-1,2- or 1,3-diols ($33\text{-}61 \text{ cm}^{-1}$).^{21,22}

3. CONCLUSION

The structural investigation for some 1-aza-5-hydroxymethyl-3,7-dioxabicyclo[3.3.0]octanes consisted in three points of view whose coherence was ensured by considering: the conformational chirality of the basic skeleton and its flexibility

around the C-O-C bonds. The last one depends on the chelating aptitude of the solvent and orientation (rotamers *in - out*) of a hydroxymethyl group linked at C-5. The energetic barrier of the ring inversion was influenced by the polarity of the solvent. Two fused 1,3-oxazolidine O-envelope conformers was a useful stereochemical approach for the azadioxabicyclooctane system since good to excellent agreements were found between theoretical calculation and experimental data.

4. EXPERIMENTAL

Current NMR spectra were recorded on Bruker® AM300 instrument operating at 300 and 75 MHz for ¹H and ¹³C nuclei respectively.

Dynamic NMR spectra were performed on Bruker® ARX400 instrument operating at 400 and 100 MHz for ¹H and ¹³C nuclei respectively with each step 10 K decreasing temperature. No SiMe₄ was added; chemical shifts were measured against the solvent peak. All NMR spectra were measured in anhydrous commercially available deuterated solvents. All chemical shifts (δ values) were given throughout in ppm; all coupling patterns (*J* values) were given throughout in Hz. Locking, shimming and acquisition were made without spinning.

IR spectra were performed on a Perkin-Elmer® 16 PC FT-IR spectrometer. Only relevant absorptions were listed [throughout in cm⁻¹: weak (w), medium (m) or (s) strong].

Molecular orbital calculation: the conformational space of the systems have been investigated by using the "Conformer Distribution" facility (MMFF force field) from Spartan'o2® [Spartan'o2, Wavefunction, Inc. Irvine, CA]. The set of conformers thus generated has been subjected, within the same package, to full geometry optimization at the RHF/6-31G* *ab initio* level. The default convergence criteria (Energy = 0.000001 hartrees, rms gradient = 0.000450 hartrees/bohr) have been imposed throughout all the *ab initio* computations.

The synthesis of the compounds **1a**, **1c** and **1d** was previously reported by us¹⁵ according to Senkus^{1,8} and Crabb.¹¹

REFERENCES

1. Senkus, A. C. *J. Am. Chem. Soc.* **1945**, *67*, 1515-1519
2. Nougier, R.; Crozet, M.; Vanelle, P.; Maldonado, J. *Tetrahedron Lett.* **1985**, *26*, 5523-5524
3. Zayed, S. E.; Pak. *J. Sci. Ind. Res.* **1987**, *30*, 432 – 438; *Chem. Abstr.* **1988**, *108*, 94446y
4. Buur, A.; Bundgaard, H. *Arch. Pharm. Chem. Sci. Ed.* **1987**, *15*, 76-86
5. Vanelle, P.; De Meo, M. P.; Maldonado, J.; Nougier, R.; Crozet, M. P.; Laget, M.; Dumenil, G. *Eur. J. Med. Chem.* **1990**, *25*, 241-250
6. Mattson, A.; Norin, T. *Synth. Commun.* **1994**, *24*, 1489-1491
7. Eastman Kodak Fr. Pat. 1,504,886; *Chem. Abstr.* **1969**, *70*, P67863z
8. Senkus, M. U. S. Pat. 2,401,196; *Chem. Abstr.* **1946**, *40*, P5446² and related Patents
9. Barbulescu, N.; Moga, S. Gh.; Sintamarian, A.; Cuza, O.; Vasilescu, V.; Rom. Pat. 83,939; *Chem. Abstr.* **1985**, *102*, P149252r and related Patents connected to the subject.
10. Cookson R. C.; Crabb, T. A. *Tetrahedron* **1968**, *24*, 2385-2397
11. Crabb, T. A.; Hall, M. J.; Williams, R. O. *Tetrahedron* **1973**, *29*, 3389-3398
12. Barkworth, M. R.; Crabb, A. T. *Org. Mang. Res.* **1981**, *17*(4), 260-264
13. Anteonis, M. *Bull. Soc. Chim. Belges* **1966**, *75*, 413-425

14. Darabantu, M.; Plé, G.; Mager, S.; Gaina, L.; Cotoră, E.; Mates, A.; Costas, L. *Tetrahedron* **1997**, *53*, 1891-1908
15. Darabantu, M.; Plé, G.; Maierăanu, C.; Silăghi-Dumitrescu, I.; Ramondenc, Y.; Mager, S. *Tetrahedron* **2000**, *56*, 3799-3816
16. Maierăanu, C.; Darabantu, M.; Plé, G.; Berghian, C.; Condamine, E.; Ramondenc, Y.; Silăghi-Dumitrescu, I.; Mager, S. *Tetrahedron* **2002**, *58*, 2681-2693
17. Brush, J. R.; Magee, R. J.; O'Connor, M. J.; Teo, S. B.; Geue, R. J.; Snow, M. R. *J. Am. Chem. Soc.* **1973**, 2034-2035
18. Monge, S.; Sélambaron, J.; Carré, F.; Verducci, J.; Roque, J. P.; Pavia, A. A. *Carbohydr. Res.* **2000**, *328*, 127-133
19. Friebolin, H. *Basic One- and Two Dimensional NMR Spectroscopy*, VCH Verlagsgesellschaft/VCH: Weinheim/New York, **1991**; p 271-290
20. Von Schleyer, P. R. *J. Am. Chem. Soc.* **1961**, *83*, 1368-1373
21. Kuhn, L. P. *J. Am. Chem. Soc.* **1954**, *76*, 4323-4326
22. Cole, A. R. H.; Jefferies, P. R. *J. Chem. Soc.* **1956**, 4391-4397

STEREOCONTROLLED SYNTHESIS BY ANOMERIC EFFECTS OF SUBSTITUTED 1-AZA-3,7-DIOXABICYCLO[3.3.0]OCTANES

CARMEN MAIEREANU,^a IOAN SILAGHI-DUMITRESCU,^b CAMELIA BERGHIAN,^b
MONICA PINTEA,^a MARIJANA FAZEKAS^a and MIRCEA DARABANTU^{a*}

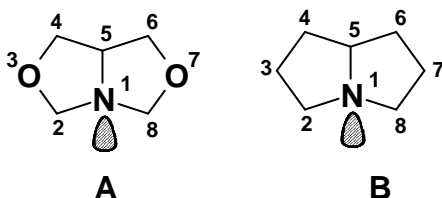
^aDepartment of Organic Chemistry, "Babes-Bolyai" University,
11 Arany János Str., 400028 Cluj-Napoca, Romania

^bDepartment of Inorganic Chemistry, "Babes-Bolyai" University,
11 Arany János Str., 400028 Cluj-Napoca, Romania

ABSTRACT. First coherent examples of stereocontrolled ring closure in 1-aza-3,7-dioxabicyclo[3.3.0]octane series were found to originate in the anomeric effects of the aminalic part of this heterobicyclic saturated system; experimental data were in agreement with the theoretical calculation; the roll of the bulky substituents is also pointed out.

1. INTRODUCTION

The heterocyclic saturated system 1-aza-3,7-dioxabicyclo[3.3.0] octane (**A**) was discovered in 1945 by Senkus;^{1,2} the elucidation of the structure soon after by chemical methods by Pierce^{3,4} revealed the analogy between **A** (as 3,7-dioxa analogue and fused 1,3-oxazolidine system) and the core alkaloid, namely pyrrolizidine (**B**, **Scheme 1**).



Scheme 1

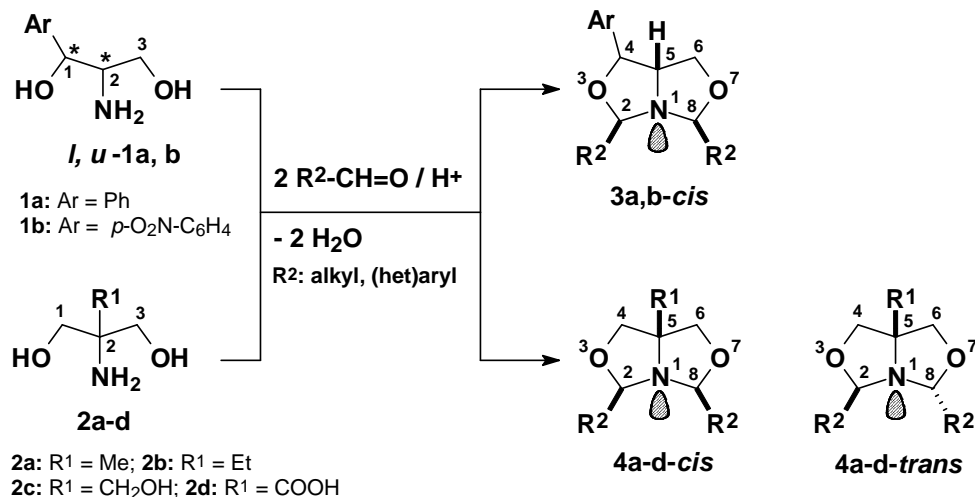
Presumably, because of this resemblance, very large series of substituted derivatives of **A** were prepared along more than a half of century since they revealed significant useful applications.⁵⁻¹⁴ On the other hand, their most convenient synthesis (nucleophilic cyclocondensation between C-substituted 2-amino-1,3-propanediols, the so called "serinols" and carbonyl compounds) is simple, direct and efficient with high yields (**Scheme 2**).

Furthermore, the multiple applications of the title compounds largely prevailed the structural investigations (conformational analysis, chirality, diastereoisomerism, etc).¹⁵⁻¹⁸

The first hypothesis regarding their diastereomerism at the aminalic stereocenters C-2, -8 belongs to Edgerton as early as 1959 (**Scheme 2**, compound **3b**, R² = Ph).^{19,20} In the period of '70's, Crabb postulated the global stereochemistry of the bicycle as *cis*-fused oxazolidine flipping system¹⁵⁻¹⁷ (the lone pair at N-1 and the ligand at C-5

* darab@chem.ubbcluj.ro; darabantu@cluj.astral.ro

as references). Soon later this basic geometry was independently confirmed by the X-rays determined structure by O'Connor (**Scheme 2**, compound **4d**, $R^1 = \text{COOH}$, $R^2 = \text{H}$, cooper salt).²¹ In 2000, another X-rays determined structure by Pavia (**Scheme 2**, compound **4c-cis**, $R^2 = \text{Ph}$) made known the importance of the anomeric effects in each oxazolidine ring supported by the contraction of the bonds N-C-2(8) with respect to N-C-5.²²⁻²⁶



Scheme 2

All these structural assignments confirmed the heterofacial type of the molecular skeleton.

However, in our days, minor attention was paid to enlargement of the diastereomerism in this class.^{9,11} Thus, in the series **3a, b**, considering the configuration at C-4 kept identical with C-1 (as in the starting materials **1a, b**), the cyclocondensation would yield four diastereomers about the new chiral centers C-2 and C-8: *2R,8S*; *2S,8R*; *2S,8S*; *2R,8R*. Indeed, under kinetic control, our preceding findings revealed the existence of all these four diastereomers (**Scheme 2**, compound **3b**, $R^2 = \text{Ph}$). In contrast, under thermodynamic control, in a large sequence of syntheses performed with (het)aryl aldehydes, the serinol **1b** (as *like* enantiomerically pure diastereomer, *1S,2S*) yielded diastereoselectively the structures **3b** possessing all ligands (C-2, -4, -8) *cis*-oriented with respect to the *cis*-junction of the bicycle (hence, an absolute configuration *1R,2R,4S,5S,8S*).²⁷⁻³⁰ We called this spatial arrangement “*all cis*”: the lone pair at N-1 and all the ligands attached at C-2, -4, -8.

Later investigations by us in the series **2a-d** evidenced the same stereochemical behaviour: indeed, compounds possessing the “*all cis*” arrangement (the lone pair at N-1 and the ligands attached at C-2, -5 and -8, **4-cis**, **Scheme 2**) were basically dominant with respect to **4-trans**¹ (diastereomeric ratios from 80:20 to 100:0 *cis* vs.

¹ A previous detailed by us discussion of this diastereomerism indicated series **4 cis** as *meso* forms meanwhile **4 trans** are intrinsic chiral about C-2 and C-8; for the present discussion, entering into all these details is not necessary.³¹ The same is valid for conformational chirality exhibited by this heterocyclic system.^{32,33}

trans).³¹ Therefore, hereafter we kept this more simple nomenclature as *cis* or *trans* restricted to orientation of the ligands linked at C-2(8) (**Scheme 2**).

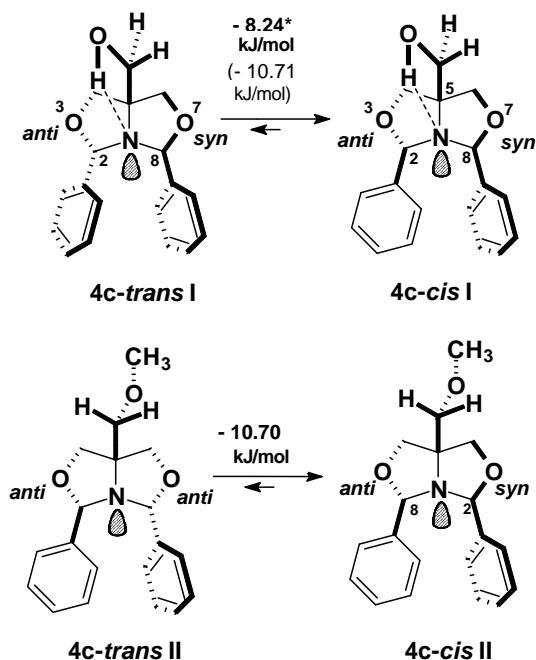
To our knowledge, no explanation was provided so far for this diastereoselectivity. In addition, recently reported more sophisticated structures of type **4** were surprisingly not defined from this point of view.¹³

2. RESULTS AND DISCUSSION

2.1. Theoretical approach by means of RHF 6/31-G* molecular orbital calculation

We start the present discussion by examining the compound **4c I** and its O-methyl derivative **4c II** (**Scheme 3**).

The compound **4c I** was readily available by cyclocondensation between TRIS® **2c** and benzaldehyde (**Scheme 2**). According to the NMR spectra of the crude reaction mixture, the diastereoselectivity under thermodynamic control (24 hrs, 110°C) was 5:1 **4c-cis I** : **4c-trans I**, consequently a ΔG value about 5 kJ/mol. The calculated difference between the total energy of these diastereomers ($\Delta\Delta E$ values), as shown in **Scheme 3**, was not quite consistent with the experiment; indeed, it was found 10.7 kJ/mol. It is of note that in **Scheme 3** the fully optimised geometry is given for the most stable conformer belonging each to the series **4c-cis I** or **4c-trans I**.



*in boldface: $\Delta\Delta E$ values by considering the orientation of the hydroxymethyl group; in brackets, the $\Delta\Delta E$ value by neglecting the orientation of the hydroxymethyl group.

Scheme 3

Unpredictably, in each series, the $\Delta\Delta E$ values between considerable *conformational* diastereomers (e.g. issued from the rotation about C-O-C bonds, including also the possible phenyl rotamers (not depicted) were found slightly greater than the difference between *configurational* diastereomers *cis-trans*. The diverse orientations of the C-5 hydroxymethyl group in **4c-cis I** or **4c-trans I** (not depicted) as well as the same difference between the O-methyl forms **4c-cis II** and **4c-trans II** indicated no importance in comparison with the basic **4c-I**.

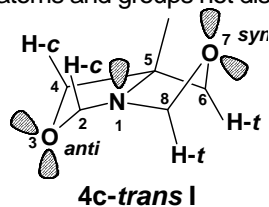
2.2. Theoretical approach by means of anomeric effects

In this approach, we considered the 1-aza-3,7-dioxabicyclo[3.3.0]octane system as two "independent" 1,3-oxazolidines, possessing the phenyl ligand at C-2 (oxazolidine numbering) but differently oriented, e.g., in *trans*. Next, for the compound **4c-trans I** we estimated the anomeric effects as main delocalising interactions in the aminalic zone of the heterocycle O-C-N (kJ/mol). The results are collected in **Table 1** and detailed in **Scheme 4**.

Thus, the two-oxazolidine rings are oriented in opposite sense (O-3-*anti* and O-7-*syn*) as two frozen O-envelope conformers. Since the problem under examination, refer to the *pseudo*-equatorial orientation of the two phenyl rings, we strictly focused on the hyperconjugation involving the two *pseudo*-axial σ_{C-H} bonds in the aminalic part of the molecule (O-C-N-C-O), as quantitative manifestation of the anomeric effects. One must observe that in the O-7-*syn* oxazolidine ring, the position C-8 was a significant anomeric center and the corresponding delocalising interactions are $lp_{O-7-ax} \rightarrow \sigma^*_{C-8-H-8-t}$ and $lp_{N-1} \rightarrow \sigma^*_{C-8-H-8-t}$. Indeed, only the depicted orbitals were antiperiplanar and from energetic point of view, their total interaction was about 67 kJ/mol. On the contrary, in the O-3-*anti* oxazolidine ring but one similar interaction was found: $lp_{O-3-ax} \rightarrow \sigma^*_{C-2-H-2-c}$ supported by about 41 kJ/mol. That is, the O-7-*syn* oriented oxazolidine ring was much more hyperconjugated with respect to the O-C(H)-N bond. Its structure can also be described by *two* non-bonding formulae (**Scheme 4**) meanwhile for the O-3-*anti* oxazolidine ring but *one* non-bonding structure can be imagined.

Table 1

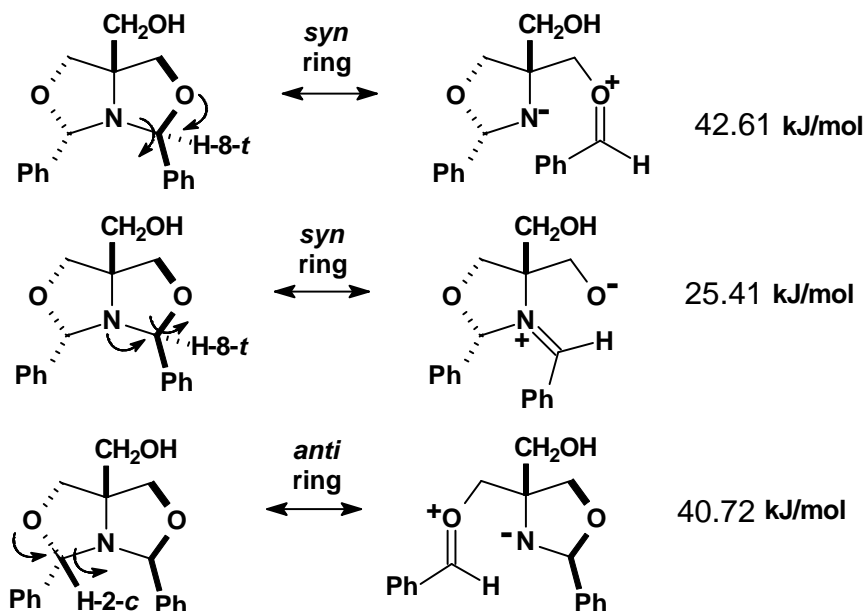
Calculated main delocalising interactions (selected as $E > 25$ kJ/mol) for the compound **4c-trans I** (for reason of simplicity, atoms and groups not discussed are omitted in formulae).



NMO Donors (lp) ^a	Acceptors MO (σ^* , kJ/mol)						
	C2-O3	N1-C2	N1-C8	C2-H2-c	C8-H8-t	C4-H4-c	C6-H6-t
N-1	46.38	-	-	-	25.41	-	-
O-3-ax ^b	-	-	-	40.72	-	39.64	-
O-3-eq	-	31.93	-	-	-	-	-
O-7-ax	-	-	-	-	42.61	-	38.51
O-7-eq	-	-	31.73	-	-	-	-

^a depicted lone pairs as Non bonding Molecular Orbital

^b orientation of the involved NMO as axial (or equatorial)



Scheme 4

To conclude, our diagnostic is that the **4c-trans I** should be less stable than **4c-cis I** in which both benzyl carbons C-2, -8 should be comparably hyperconjugated.³²

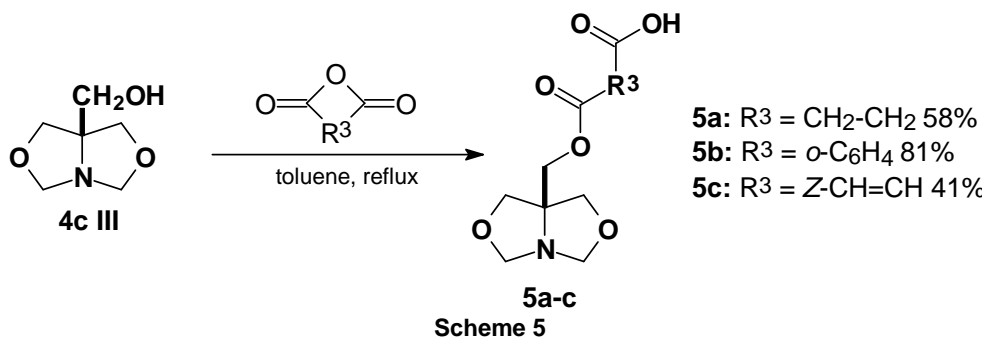
There are two experimental evidence to prove the importance of the delocalisations of type $lp_{O(N)} \rightarrow \sigma^*_{C-H}$ in 1,3-oxazolidine ring. Thus, if the aryl aldehyde involved in the ring closure have a strong withdrawing substituent at the *para* position vs. the benzyl carbon (*p*-nitrobenzaldehyde and 4-pyridyl aldehyde), the diastereoselectivity is reversed: 100:0 **4c trans** vs. **cis** and 75:25 respectively.^{9,11,31} That is, diastereoselectivity is sensitive to the polarity of the C-2(8)-H bond and its corresponding E_{LUMO} .

2.3. Experimental evidence for the anomeric effect from the bridged nitrogen

The calculation resumed in **Table 1** also indicated a strong hyperconjugation involving the bridged nitrogen: $lp_N \rightarrow \sigma^*_{C-2-O-3}$: 46.38 kJ/mol. As recently emphasised in the literature,²² this interaction is specific for the geometry of the compound **4c-cis I**. In the absence of the two phenyl groups linked at C-2, -8 (compound **4c III**, $R^2 = H$, **Scheme 2**), the same anomeric effect calculated by us was smaller: 40.46 kcal/mol.

We attempted at checking the meaning of this effect: we converted the compound **4c III** in carboxylic derivatives by *O*-acylation (**Scheme 5**).

In the ¹H NMR spectra of the compounds **5a-c** the carboxylic proton was unambiguously located in the region 10 – 11 ppm (typical broad singlet), as in authentic COOH groups. Hence, no amfionic form we could assign for any of the compounds **5a-c** since the lone pair of the bridged nitrogen was too involved in hyperconjugation and presumably insensitive to proton donors possessing K_a values in the domain 10^{-4} - 10^{-5} .



2.4. The *trans* stereocontrol by bulky substituents

In the present research, we were also interested in orienting the (complete ?) diastereoselectivity of the double ring closure in 1-aza-3,7-dioxabicyclo[3.3.0]ctanes towards *trans* diastereomers. Since ring closure with aryl aldehydes appeared to be governed by the anomeric effects, we considered the long-established influence of a bulky substituent attached to the carbonyl functionality.

Before discussing the results, some conclusions arising from earlier research of our group³¹ should be reminded (**Scheme 2**): the “all *cis*” arrangement **4c cis** operated in each of the below cases:

i) if but one of the ligands was Ar (e.g. ring closure with two different aldehydes from which one is formaldehyde).

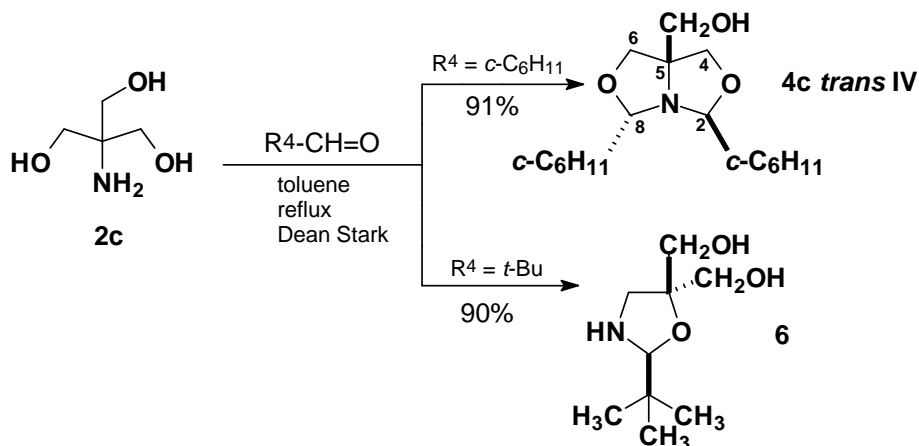
ii) if one of the ligand is Ar and the other oxazolidine was a spiranic structure (e.g. ring closure with two different carbonyl compounds: an aryl aldehyde and a C-5-7-cyclanone)

iii) for bulky aldehydes [e.g. $R^4 = (\text{Ph})_3\text{CCH}_2$] if the bulkiness was remote by at least one carbon from the reaction site.

Keeping in mind these examples, we treated TRIS[®] **2c** with two bulky aldehydes in 1:2 molar ratio (thermodynamic control: 24 hrs in refluxing toluene with continuous removal of water). The syntheses are described in **Scheme 6**.

The cyclocondensation with cyclohexancarboxaldehyde gave directly **4c trans IV** with complete *trans* diastereoselectivity; surprisingly, the reaction carried out with 1:1 molar ratio **2c** : aldehyde afforded the same compound (together with the corresponding amount of unreacted TRIS[®]) to prove that the intermediate mono oxazolidine was more reactive than **2c** itself (hence, non isolable). Careful inspection of Drieding models supported the *trans* stereochemistry for **4c IV** together with its NMR spectra (see **EXPERIMENTAL**).

In contrast, if trimethylacetaldehyde was used, constantly only one ring closure took place (mono oxazolidine **6**) to demonstrate the anticipated steric hindrance promoted by the bulky substituent, *t*-Butyl. It seemed to us the behaviour of trimethylacetaldehyde in the above conditions as similar with the C-5-7-cyclanones: but one ring closure took place (to yield the corresponding spiro mono oxazolidines, previously reported by us).



3. CONCLUSION

The *cis* or *trans* diastereoselectivity in the ring closure of C-2-, -8 substituted 1-aza-3,7-dioxabicyclo[3.3.0]octanes in reaction with carbonyl compounds can be explained taking into account:

- i) the anomeric effects in the final structure (reaction with aryl aldehydes); they favour an "all *cis*" stereochemistry.
- ii) the bulky substituents linked directly to carbonyl group promoted either the *trans* diastereoselectivity or but a single ring closure, to yield simple C-2-substituted-1,3-oxazolidines.

4. EXPERIMENTAL

General

Melting points are uncorrected; they were carried out on ELECTROTHERMAL[®] 9100 instrument.

NMR spectra were recorded on Bruker[®] AM300 instrument operating at 300 and 75 MHz for ¹H and ¹³C nuclei respectively. No SiMe₄ was added; chemical shifts were measured against the solvent peak. All NMR spectra were measured in anhydrous commercially available deuterated solvents. All chemical shifts (δ values) were given throughout in ppm; all coupling patterns (*J* values) were given throughout in Hz. Locking, shimming and acquisition were made without spinning.

IR spectra were performed on a Perkin-Elmer[®] 16 PC FT-IR spectrometer. Only relevant absorptions were listed [throughout in cm⁻¹: weak (w), medium (m) or (s) strong].

Molecular orbital calculation: the conformational space of the systems have been investigated by using the "Conformer Distribution" facility (MMFF force field) from Spartan'o2[®] [Spartan'o2, Wavefunction, Inc. Irvine, CA]. The set of conformers thus generated has been subjected, within the same package, to full geometry optimization at the RHF/6-31G* *ab initio* level. The default convergence criteria (Energy = 0.000001 hartrees, rms gradient = 0.000450 hartrees/bohr) have been imposed throughout all the *ab initio* computations.

Natural bond orbital analysis³⁴ has been carried out with the Gaussian 98 system [Gaussian 98, Revision A.11.3, M. J. Frisch, G. W. Trucks, H. B. Schlegel, G. E. Scuseria, M. A. Robb, J. R. Cheeseman, V. G. Zakrzewski, J. A. Montgomery, Jr., R. E. Stratmann, J. C. Burant, S. Dapprich, J. M. Millam, A. D. Daniels, K. N. Kudin, M. C. Strain, O. Farkas, J. Tomasi, V. Barone, M. Cossi, R. Cammi, B. Mennucci, C. Pomelli, C. Adamo, S. Clifford, J. Ochterski, G. A. Petersson, P. Y. Ayala, Q. Cui, K. Morokuma, N. Rega, P. Salvador, J. J. Dannenberg, D. K. Malick, A. D. Rabuck, K. Raghavachari, J. B. Foresman, J. Cioslowski, J. V. Ortiz, A. G. Baboul, B. B. Stefanov, G. Liu, A. Liashenko, P. Piskorz, I. Komaromi, R. Gomperts, R. L. Martin, D. J. Fox, T. Keith, M. A. Al-Laham, C. Y. Peng, A. Nanayakkara, M. Challacombe, P. M. W. Gill, B. Johnson, W. Chen, M. W. Wong, J. L. Andres, C. Gonzalez, M. Head-Gordon, E. S. Replogle, and J. A. Pople, Gaussian, Inc., Pittsburgh PA, 2002.] run under Linux.

The syntheses of the discussed compounds: **4c-cis I**, **4c-trans I**, **4c-cis II**, and **4c III** were made according to literature¹⁻⁴ or previous published data by us.^{31,32}

Typical procedure for the synthesis of the compounds 5a-c

r-1-Aza-*c*-5-hydroxymethyl-3,7-dioxabicyclo[3.3.0]octane (1.45 g, 10 mmol) **4c III** (**Scheme 5**) and the corresponding anhydride (10 mmol) in dry toluene (25 mL) were refluxed with vigorous stirring. The reaction was monitored by TLC (eluent benzene : methanol 3:1 v/v; double visualisation whenever possible: I₂ bath and UV 254 nm) and stopped when the starting materials were detected in small traces only (8 – 16 hrs). The reaction mixture was filtered hot and the toluene solution was evaporated under vacuum to dryness. The crude product was isolated by crystallisation from ether to yield the title compounds **5a-c**.

***r*-1-Aza-*c*-5-succinyloxymethyl-3,7-dioxabicyclo[3.3.0]octane (5a)** (58%) white crystalline powder mp 71-73 °C (Et₂O); [Found: C, 49.09; H, 6.01; N, 5.88. C₁₀H₁₅NO₆ requires C, 48.97; H, 6.16; N, 5.71%]; *R*_f (75% benzene/methanol) 0.60; *v*_{max} (CH₃Cl film) 3430 (w), 2950 (s), 2503 (m), 1772 (s), 1479 (m), 1408 (m), 1371 (s), 1344 (s), 1272 (s), 1220 (9s), 1172 (9s), 1172 (9s), 1119 (9s), 1060 (s), 1022 (9s), 995 (s), 973 (s), 932 (s), 844 (s), 760 (s), 681 (s), 661 (s) cm⁻¹; δ_H (300 MHz CDCl₃) 10.40 (1H, bs, COOH), 4.47 (2H, d, *J*=5.5 Hz, H-2 -8), 4.41 (2H, d, *J*=5.5 Hz, H-2, -8), 4.15 (2H, s, CH₂O), 3.76 (4H, s, H-4, -6); δ_C (75 MHz CDCl₃) 171.9 (1C, COOH), 167.6 (1C, COO), 87.9 (2C, C-2, -8), 73.7 (2C, C-4, -6), 71.3 (1C, C-5), 66.3 (1C, 5-CH₂O), 28.8 (2C, CH₂).). MS (Cl, CH₄); *m/z* (rel. int.): 244.8 (<2), 145.1 (25), 127.2 (100), 100.1 (19).

***r*-1-Aza-*c*-5-phthaloyloxymethyl-3,7-dioxabicyclo[3.3.0]octane (5b)** (81%) white crystalline powder mp 121-123 °C (Et₂O); [Found: C, 56.98; H, 5.01; N, 4.88. C₁₄H₁₅NO₆ requires C, 57.33; H, 5.15; N, 4.77%]; *R*_f (75% benzene/methanol) 0.75; *v*_{max} (CH₃Cl film) 3441 (w), 2875 (9s), 2854 (s), 2475 (m), 1731 (s), 1692 (s), 1600 (m), 1579 (s), 1291 (s), 1262 (s), 1126 (s), 1096 (s), 1038 (s), 950 (s), 804 (s), 773 (s), 744 (9s), 710 (s), 699 (s), 584 (m) cm⁻¹; δ_H (300 MHz CDCl₃) 11.0 (1H, bs, COOH), 7.82 (1H, m), 7.62 (1H, m), 7.54 (2H, m), 4.55 (2H, d, *J*=5.2 Hz, H-2 -8), 4.40 (2H, d, *J*=5.2 Hz, H-2, -8), 4.40 (2H, s, CH₂O), 3.88 (2H, d, *J*=9.2 Hz, H-4, -6), 3.83 (2H, d, *J*=9.2 Hz, H-4, -6); δ_C (75 MHz CDCl₃) 171.1 (1C, COOH), 168.2 (1C, COO), 132.7 (1C, Cq arom.), 132.2 (1C, CH arom.), 131.5 (1C, CH arom.), 131.2 (1C, Cq arom.), 130.0 (1C, CH arom.), 129.0 (1C, CH arom.), 87.9 (2C, C-2, -8), 74.0 (2C, C-4, -6), 71.4 (1C, C-5), 67.7 (1C, 5-CH₂O); MS (Cl, CH₄); *m/z* (rel. int.): 244.8 (<2), 145.1 (25), 127.2 (100), 100.1 (19); MS (Cl, CH₄); *m/z* (rel. int.): 293 (<1), 148.1 (50), 127.2 (100), 99.3 (5).

***r*-1-Aza-*c*-5-maleloxymethyl-3,7-dioxabicyclo[3.3.0]octane (5c)** (41%) white crystalline powder mp 83-86 °C (Et₂O); [Found: C, 48.99; H, 5.01; N, 5.88. C₁₀H₁₃NO₆ requires C, 49.38; H, 5.38; N, 5.75%]; *R_f* (75% benzene/methanol) 0.65; *v*_{max} (CH₃Cl film) 3400 (s), 2884 (m), 1742 (s), 1648 (m), 1583 (m), 1370 (m), 1252 (s), 1218 (s), 1172 (s), 1069 (s), 1057 (s), 928 (s), 828 (m), 815 (m), 761 (s), 664 (m), 572 (m) cm⁻¹; δ_H (300 MHz CDCl₃) 10.20 (1H, bs, COOH), 6.31 (1H, d, *J*=12.0 Hz), 6.22 (1H, d, *J*=12.0 Hz), 4.51 (2H, d, *J*=5.2 Hz, H-2 -8), 4.41 (2H, d, *J*=5.2 Hz, H-2, -8), 4.25 (2H, s, CH₂O), 3.78 (4H, s, H-4, -6); δ_C (75 MHz CDCl₃) 167.6 (1C, COOH), 166.0 (1C, COO), 133.0 (1C, CH=), 128.8 (1C, CH=), 87.1 (2C, C-2, -8), 74.0 (2C, C-4, -6), 71.6 (1C, C-5), 67.5 (1C, 5-CH₂O). MS (CI, CH₄); *m/z* (rel. int.): 243.1 (<2), 145.3 (30), 126.8 (100), 97.8 (40).

Typical procedure for the synthesis of the compounds **4c trans IV** and **6**

TRIS® (3.69 g, 30 mmol) **2c** (Scheme 2, **6**) and cyclohexanecarboxaldehyde (7.07g, 63 mmol) in dry toluene (100 mL) were refluxed with vigorous stirring for 24 hrs in a Dean Stark trap with continuous removal of water. The reaction was monitored by TLC (eluent benzene : methanol 3:1 v/v; visualisation in I₂ bath) and stopped when the starting materials were detected in small traces only. The reaction mixture was filtered hot and the toluene solution was evaporated under vacuum to dryness. The crude product was isolated by crystallisation from ether to yield the title compound **4c trans IV**.

In identical conditions compound **6** was prepared, starting from TRIS® **2c** (1.545 g, 12.8 mmol), and trimethylacetaldehyde (2.30 g, 3 mL, 26.7 mmol).

***r*-1-Aza-*c*-2-*t*-8-dicyclohexyl-*c*-5-hydroxymethyl-3,7-dioxabicyclo[3.3.0]octane (4c trans IV)** (91%) white crystalline powder mp 118-119 °C (Et₂O); [Found: C, 70.07; H, 9.90; N, 4.88. C₁₈H₃₁NO₃ requires C, 69.87; H, 10.08; N, 4.52%]; *R_f* (75% benzene/methanol) 0.50; δ_H (300 MHz CDCl₃) 4.46 (1H, d, *J*=6.0 Hz, H-8-*c*), 4.17 (1H, d, *J*=6.0 Hz, H-2-*t*), 3.73 (1H, d, *J*=10.9 Hz, H-6-*t*), 3.63 (1H, d, *J*=8.5 Hz, H-4-*t*), 3.57 (2H, d, *J*=10.9 Hz, CH_aH_bOH, H-6-*c*), 3.46 (1H, d, *J*=11.9 Hz, CH_aH_bOH), 3.37 (1H, d, *J*=8.5 Hz, H-4-*c*), 1.9 – 1.4 (11H, m), 1.3 – 0.9 (11H, m); δ_C (75 MHz CDCl₃) 104.7 (1C, CH), 95.7 (1C, CH), 70.1 (1C, CH₂), 66.7 (1C, Cq), 65.6 (1C, CH₂), 64.7 (1C, CH₂), 42.5 (1C, CH), 42.2 (1C, CH), 29.1 (1C, CH₂), 28.7 (1C, CH₂), 27.4 (1C, CH₂), 26.8 (1C, CH₂), 26.6 (1C, CH₂), 26.2 (1C, CH₂), 26.1 (1C, CH₂), 26.0 (1C, CH₂). MS (CI, CH₄); *m/z* (rel. int.) 308.8 (<3), 214.8 (11), 182.9 (18), 148.5 (<3), 131.1 (21), 103.2 (100).

2-*t*-Butyl-4,4-dihydroxymethyl-1,3-oxazolidine (6) (90%) yellowish crystalline powder mp 47-49 °C (Et₂O); [Found: C, 56.80; H, 9.90; N, 7.77. C₉H₁₉NO₃ requires C, 57.12; H, 10.11; N, 7.41%]; *R_f* (75% benzene/methanol) 0.60; δ_H (300 MHz CDCl₃) 4.13 (1H, s, H-2), 3.66 (2H, d, *J*=10.9 Hz, CH₂OH), 3.61 (1H, bs, NH), 3.57 (1H, d, *J*=8.6 Hz, H-4), 3.55 (1H, d, *J*=10.9 Hz, CH₂OH), 3.53 (1H, d, *J*=8.3, H-4), 3.50 (1H, d, *J*=10.9 Hz, CH₂OH), 3.43 (1H, d, *J*=9.0 Hz, OH), 3.40 (1H, d, *J*=7.9 Hz, OH); δ_C (75 MHz CDCl₃) 98.5 (1C, C-2), 70.3 (1C, C-4), 66.6 (1C, C-5), 64.4 (1C, CH₂OH), 64.0 (1C, CH₂OH), 33.9 [1C, C(CH₃)₃], 25.4 [1C, C(CH₃)₃]. MS (CI, CH₄); *m/z* (rel. int.) 132.0 [100, M-(*t*-Bu)], 84 (14), 57 (60).

REFERENCES

1. Senkus, A. C. *J. Am. Chem. Soc.* **1945**, *67*, 1515-1519
2. Senkus, M. U. S. Pat. 2,401,196; *Chem. Abstr.* **1946**, *40*, P5446⁴ and related Patents
3. Pierce, S.; Lunsford, D. C.; Raiford Jr., R. W.; Rush, J. L.; Riley, D. W. *J. Am. Chem. Soc.* **1951**, *73*, 2595-2596
4. Pierce, S.; Lunsford, D. C. *J. Am. Chem. Soc.* **1951**, *73*, 2596-2598
5. Tilford, C. H.; Van Campen Jr., M. G.; Shelton, R. S. *J. Am. Chem. Soc.* **1947**, *69*, 2902-2906
6. Eastman Kodak Fr. Pat. 1,504,886; *Chem. Abstr.* **1969**, *70*, P67863z
7. Broadbent, H. S.; Burnham, W. S.; Sheely, R. M.; Olsen, R. K. *J. Heterocyclic Chem.* **1976**, *13*, 337-348
8. Barbulescu, N.; Moga, S. G.; Sintamarian, A.; Cuza, O.; Vasilescu, V.; *Rom. Patent*, 83, 939; *Chem. Abstr.* **1985**, *102*, P149252r and related patents.
9. Nougier, R.; Crozet, M.; Vanelle, P.; Maldonado, J. *Tetrahedron Lett.* **1985**, *26*, 5523-5524
10. Zayed, S. E.; Pak. J. Sci. Ind. Res. **1987**, *30*, 432 – 438; *Chem. Abstr.* **1988**, *108*, 94446y
11. Vanelle, P.; M. De Meo, M. P.; Maldonado, J.; Nougier, R.; Crozet, M. P.; Laget, M.; Dumenil, G. *Eur. J. Med. Chem.* **1990**, *25*, 241-250
12. Mattson, A.; Norin, T. *Synth. Commun.* **1994**, *24*, 1489-1491
13. Bonnet, D.; Pascal, J.; Grass-Masse, H.; Melnyk, O. *Tetrahedron Lett.* **2001**, *42*, 1875-1877
14. Buur, A.; Bundgaard, H. *Arch. Pharm. Chem. Sci. Ed.* **1987**, *15*, 76-86
15. Cookson R. C.; Crabb, T. A. *Tetrahedron* **1968**, *24*, 2385-2397
16. Crabb, T. A.; Hall, M. J.; Williams, R. O. *Tetrahedron* **1973**, *29*, 3389-3398
17. Barkworth, M. R.; Crabb, A. T. *Org. Mang. Res.* **1981**, *17*(4), 260-264
18. Anteunis, M. *Bull. Soc. Chim. Belges* **1966**, *75*, 413-425
19. W. H. Edgerton, J. R. Fisher and G. W. Moersch, *J. Org. Chem.*, **1954**, *19*, 593-596
20. W. H. Edgerton, J. R. Fisher and G. W. Moersch, *J. Am. Chem. Soc.* **1957**, *79*, 6487-7490
21. Brush, J. R.; Magee, R. J.; O'Connor, M. J.; Teo, S. B.; Geue, R. J.; Snow, M. R. *J. Am. Chem. Soc.* **1973**, 2034-2035
22. Monge, S.; Sélambaron, J.; Carré, F.; Verducci, J.; Roque, J. P.; Pavia, A. A. *Carbohydr. Res.* **2000**, *328*, 127-133
23. Sélambarom, J.; Monge, S.; Carré, F.; Roque, P. J.; Pavia, A. A. *Tetrahedron* **2002**, *58*, 9559-9566
24. Sélambarom, J.; Carré, F.; Fruchier, A.; Roque, P. J.; Pavia, A. A. *Tetrahedron* **2002**, *58*, 4439-4444
25. Lemieux, R. U.; Kulling, H. J. *J. Am. Chem. Soc.* **1958**, *80*, 6098-6105
26. Lemieux, R. U. *Pure Appl. Chem.* **1971**, *27*, 527-547
27. M. Darabantu, S. Mager, G. Ple and Camelia Puscas, *Heterocycles*, **1995**, *10*, 2327-2356
28. M. Darabantu, S. Mager, C. Puscas, G. Ple, M. Bogdan, E. Cotoră and I. Bratu, *Rev. Rom. Chim.*, **1994**, *39*(8), 955-966
29. M. Darabantu, S. Mager, C. Puscas, M. Bogdan, G. Ple, E. Cotoră and D. Kovacs, *Rev. Rom. Chim.*, **1995**, *40*(5), 453-461
30. M. Darabantu, G. Ple, S. Mager, L. Gaina, E. Cotoră, A. Mates and L. Costas, *Tetrahedron*, **1997**, *53*, 1891-1908
31. M. Darabantu, G. Plé, C. Maiereanu, I. Silaghi-Dumitrescu, Y. Ramondenc and S. Mager *Tetrahedron*, **2000**, *56*, 3799 – 3816
32. Maiereanu, C.; Darabantu, M.; Plé, G.; Berghian, C.; Condamine, E.; Ramondenc, Y.; Silaghi-Dumitrescu, I.; Mager, S. *Tetrahedron* **2002**, *58*, 2681-2693
33. Manuscript in preparation
34. Reed, A. E.; Curtiss, L. A.; Weinhold, F. *Chem. Rev.* **1988**, *88*, 899-926

FIRST EXAMPLE OF SELECTIVE NUCLEOPHILICITY OF 1-AZA-5-HYDROXYMETHYL-3,7-DIOXABICYCLO[3.3.0]OCTANES IN ALKOXIDE FORM

CAMELIA BERGHIAN,^{a,c} CARMEN MAIEREANU,^{b,c} NELLY PLÉ,^c
GÉRARD PLÉ^c and MIRCEA DARABANTU^{b,c*}

^aDepartment of Inorganic Chemistry, "Babes-Bolyai" University,
11 Arany János Str., 400028 Cluj-Napoca, Romania

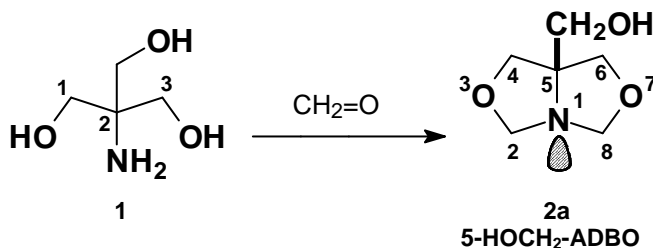
^bDepartment of Organic Chemistry, "Babes-Bolyai" University,
11 Arany János Str., 400028 Cluj-Napoca, Romania

^cInstitut de Recherche en Chimie Organique Fine (I.R.C.O.F.),
Université de Rouen, BP 08, F-76131 Mont Saint-Aignan, France

ABSTRACT. A rapid and efficient synthesis consisting in the exploit of the nucleophilicity of 1-aza-3,7-dioxabicyclo[3.3.0]octane-5-yl-methoxy group in alkoxide form against reactive halo compounds and masked imidoyl chlorides (as chlorinated π deficient systems) is described. First reaction conditions depending on the halogen and other leaving groups, together with (regio) selectivity of the substitution are discussed.

1. INTRODUCTION

The 1-aza-3,7-dioxabicyclo[3.3.0]octane heterocyclic saturated system is known since 1945 when, starting from TRIS[®] (α,α,α -trimethylolaminomethane) **1** and formaldehyde, the first synthesis of the parent term, having a hydroxymethyl group linked at position C-5 of the skeleton, was reported by Senkus (**Scheme 1**).¹



Scheme 1

After the elucidation of this type of structure by chemical methods (Senkus and Pierce),²⁻⁴ a large series of substituted C-2(8), -4(6), -5 derivatives with claimed biological activity were prepared.

The reason for this dedicated attention appears stimulated by the ease of the synthesis: direct cyclocondensation between C-substituted 2-amino-1,3-propanediols (better known by their trivial name issued from the pharmaceutical chemistry as *serinol*s) and a great variety of carbonyl compounds.⁵⁻²⁰ Though determined mainly on applied research, only minor importance was paid to different functionalisation of 1-aza-3,7-dioxabicyclo[3.3.0]octanes, seen as:

* darab@chem.ubbcluj.ro; darabantu@cluj.astral.ro

- i) *cis* fused double 1,3-oxazolidine systems.
- ii) 3,7-dioxa-analogues of the core alkaloid, namely pyrrolizidine.²¹

Direct substitution at the carbon ring is still unknown.

Since the period of '50's, only azadioxabicyclooctanes bearing at C-5 a hydroxymethyl group (optionally C-2, -8 substituted derivatives of **2a**, **Scheme 1**) seemed to be suitable to additional functionalisation by predictable methods (e.g. CH₂O-acylation,^{3-5,7,8,12,22} thionation²³ and more recently, by Dess-Martin oxidation¹³). The prepared structures are all reported to be of pharmaceutical interest.^{7,8,12,13,24}

Succeeding to our recent findings in the field of stereochemistry of substituted 1-Aza-3,7-Dioxabicyclo[3.3.0]Octanes^{8,15,16,25} (hereafter throughout abbreviated simply as **ADBO**) we were paying attention to its C-5 advanced functionalisation. Thus, we considered the parent compound of the 5-hydroxymethyl derivatives, *r*-1-aza-*c*-5-hydroxymethyl-3,7-dioxabicyclo[3.3.0]octane **5-HOCH₂-ADBO**, **2a** (**Scheme 1**) as well as its *c*-2, *c*-8-diphenyl analogue **2b** to be convertible to 5-alkoxymethyl derivatives *via* the corresponding alkoxides. To our knowledge, this reaction was but once reported by Broadbent in 1976 (deprotonation with sodium metal in refluxing THF).⁷ In order to test their nucleophilicity, we needed a larger coherent series of compounds.

Based on our earlier results relating to selective (or exhaustive) nucleophilic replacement of chlorine in certain π -deficient systems,^{27,28} we focused on chlorodiazines (e.g. chloropyrimidines): indeed, they were seen in the above circumstance as masked imidoyl chlorides including their well known use as building blocks for structures possessing biological properties.

In this paper, the introductory synthetic and structural results are discussed.

2. RESULTS AND DISCUSSION

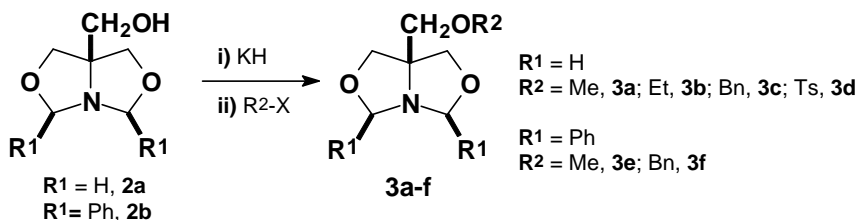
2.1. Synthesis of 5-Alkoxymethyl derivatives of 1-aza-3,7-dioxabicyclo[3.3.0]octane

In order to obtain the title compounds, we first converted **2a** and its *cis*-C-2, -8 diphenyl analogue **2b** into their potassium alkoxides upon treatment with potassium hydride in a nearly stoichiometric ratio. This reagent was able to provide, in a much milder conditions than previously reported by Broadbent,⁷ an efficient nucleophile against reactive halo-compounds (**Scheme 2**).

Only the potassium alkoxides of **2a**, **2b** exhibited the desired reactivity. The less basic sodium hydride (also tested) appeared to us not useful since deprotonation only partially occurred. We mention the strong by unexpected nucleophilicity of potassium alkoxide of **2a** proved by the synthesis of the 5-tosyloxymethyl derivative **3d**. Thus, although our initial attempt was to obtain dimeric etheral forms of **2a** [e.g. possessing a linkage as O-(CH₂)_n-O n=1, 2], its reaction as O-potassium form with 1,2-ethylene glycol ditosylate (2:1 molar ratio respectively) afforded the O-tosyl derivative **3d** in good yield (hence, the β -tosylethoxide was the leaving group). In a "traditional" route, by using tosylchloride as electrophile, **3d** was isolated with a comparable yield (**Scheme 2**).

* Stereochemical descriptors *r* (reference) and *c* (*cis*) are used according to I.U.P.A.C. in order to simplify discussion arising from the basic stereochemistry of this molecule as *cis* fused double oxazolidine system (the lone pair at N-1 is the fiducial substituent).²⁶ This spatial arrangement, together with the absence of any pyramidal inversion at N-1 are already very well documented.^{7,11,14-17,25}

FIRST EXAMPLE OF SELECTIVE NUCLEOPHILICITY...



- i) 1.00:1.05 molar ratio **2a (2b)** : KH; 1.5 - 2.0 hrs. at 40°C in anh. THF
 ii) 1.10:1.00 molar ratio R²-X : **2a (2b)** in anh. THF.

Compound	R ² -X	Yield (%)
3a	MeI	45
3b	EtI	66
3c	BnBr	50
3d	TsO-CH ₂ -CH ₂ -OTs	75
	TsCl	67
3e	MeI	50
3f	BnBr	50

Scheme 2

No reaction occurred with diiodomethane. No elimination product was detected during the synthesis of **3b**.

All new ethers **3a-f** revealed convincing NMR spectra for the envisaged structures. We note however that the ¹H NMR experiments performed at low temperature (toluene-*d*₈) evidenced no modification of the signals (not discussed in this paper); that is, all compounds **3a-f** were more flipping structures than their starting materials (**2a, 2b**).

2.2. Synthesis of 5-pyrimidinylloxymethyl derivatives of 1-aza-3,7-dioxabicyclo[3.3.0]octane

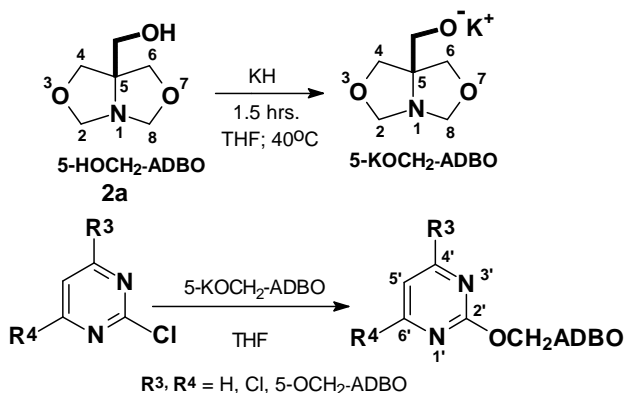
Encouraged by these results in the aliphatic series, the same tactic was straightforward in chloropyrimidines series. The preliminary data are presented below regarding (poly)chloropyrimidines. They exhibited useful and comparable reactivity (**Scheme 3, Table 1**). Both complete and selective substitutions were examined.

As accepted, reasonably poor reactivity of the chlorine linked at position C-2' (numbering according to pyrimidine) was observed (preparation of the compound **4a**); additional chlorine atoms in the molecule facilitated exhaustive substitution, leading to the compounds **4b, 4d** and **4g** (in **Table 1** overall yields as isolated material by simple crystallisation are given).

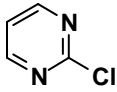
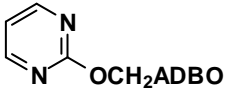
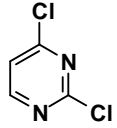
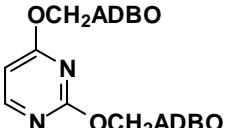
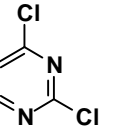
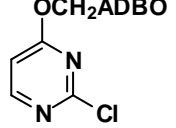
Some problems arose when selective substitutions were attempted.

Thus, 2',4'-dichloropyrimidine showed weaker aptitude against selective monosubstitution than its 4',6'-regioisomer (compounds **4c** and **4e** respectively) although yields appeared identical: thus, for **4c**, the regioselectivity was initially about 2:1 (substitution at C-4' vs. C-2', 6 hrs. at 65°C). Repeated failures we encountered in order to separate the regioisomers since they exhibited more or

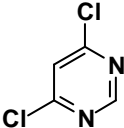
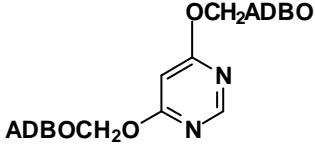
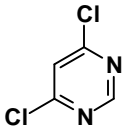
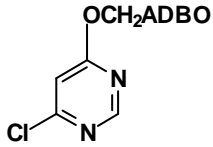
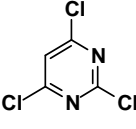
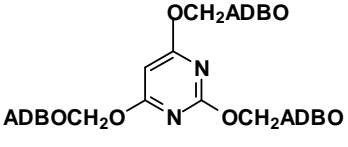
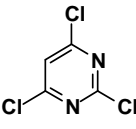
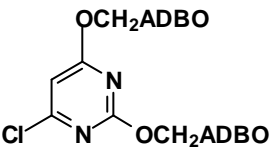
less the same R_f values on a large scale of mixtures of eluents. That is, we had to find conditions in order to more favour C-4' vs. C-2' substitution in 2',4'-dichloropyrimidine. They were found by cooling the potassium alkoxide of the starting **2a** as THF suspension at -78°C before adding the 2',4'-dichloropyrimidine. Then, the reaction mixture was very gently let to reach the room temperature. The content of the major regioisomer **4c** was this time about 75% (revealed by the ^1H NMR spectrum of the crude reaction mixture). This allowed the separation of pure major **4c** by simple crystallisation.

**Table 1**

Results of the synthesis in the chloropyrimidine series;
preparation of the compounds **4a-g**

Starting material	Molar Ratio Diazine: KH:2a	Time (hrs.)	Temp. ($^\circ\text{C}$)	Main Products and Yields (%)
	1.00:1.10:1.05	4	70	 4a - 60
	1.00:2.00:2.00	6	40	 4b - 80
	1.00:1.00:1.00	24	$-78 \rightarrow \text{r.t.}$	 4c - 63

FIRST EXAMPLE OF SELECTIVE NUCLEOPHILICITY...

Starting material	Molar Ratio Diazine: KH:2a	Time (hrs.)	Temp. (°C)	Main Products and Yields (%)
	1.00:2.15:2.05	24	45	 4d - 81
	1.00: 1.05:1.00	19	-78→r.t.	 4e - 63
	1.00:3.15:3.00	21	65	 4f - 58
	1.00:2.00:2.00	22	-78→r.t.	 4g - 76

The same strategy performed on 4',6'-dichloropyrimidine provided the chemoselectivity (mono- vs. disubstitution) as 82:18 **4e** : **4d**.

The above protocol was then repeated in the case of the synthesis of disubstituted compound **4g** and excellent regioselectivity and yield were again obtained. It must be observed the unexpected orientation of the second substitution in 2',4',6'-trichloropyrimidine (at C-2' in lieu of C-6'), fully confirmed by the NMR spectra of **4g**: two different 5-OCH₂-ADBO environments with equal intensity of all typical ¹H and ¹³C NMR signals respectively were displayed.

In the end, we note a general valid remark regarding the separation of this class of compounds: flash chromatography on silica gel could be successfully used only if the difference between the number of ADBO units linked to the pyrimidine skeleton was at least 1 for the components of the mixture: decreasing *R_f* values as starting chloropyrimidine > ADBO-monosubstituting- > ADBO-disubstituting- ≈ 5-HOCH₂-ADBO > ADBO-trisubstituting pyrimidine were constantly observed in each case.

All compounds **4a-g** provided NMR spectra consistent with the depicted structures. We note their common stereochemistry connected to the heterofacial character of the ADBO skeleton: they were rotamers in which the π-deficient diatropic ring was oriented as to deshield the *cis* protons with respect to the *trans* ones in the

ADBO motif. Consequently, the geminal anisochrony in the aliphatic part of the bicycle [H-4(6)-*c* vs. H-4(6)-*t*, $\Delta\delta$, ppm.] was revealed only by A.S.I.S. (**Aromatic Solvent Induced Shifts**) phenomena (see **Figures 1, 2** and **EXPERIMENTAL** for the compound **4f**).^{29,30}

3. CONCLUSION

1-Aza-5-hydroxymethyl-3,7-dioxabicyclo[3.3.0]octanes can be easily functionalised at position C-5 *via* potassium alkoxides upon treatment with various reactive halo compounds and selected π -deficient systems, such as (poly)chloropyrimidines. The reaction can be carried out with good to excellent yields, chemo- and regioselectivities respectively. The synthetic protocol is simple, in mild conditions and very efficient.

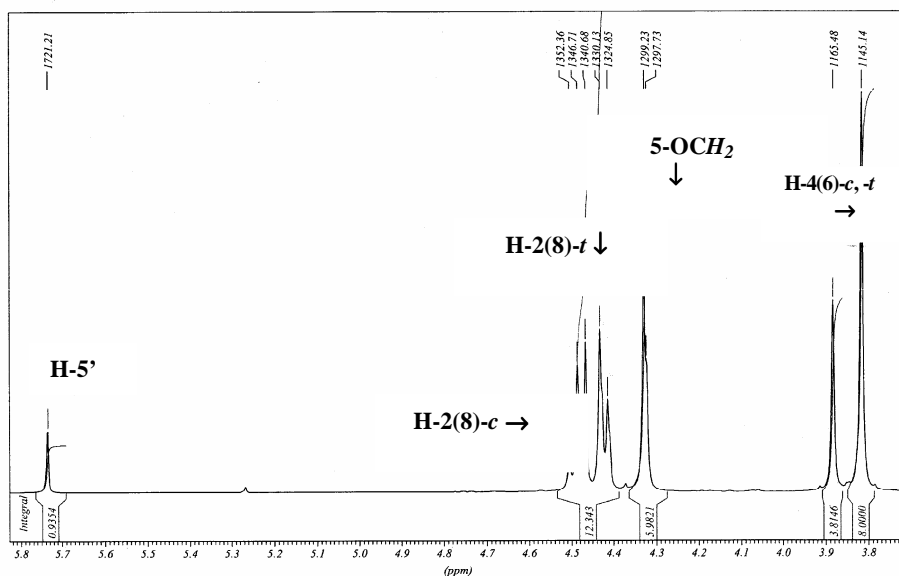
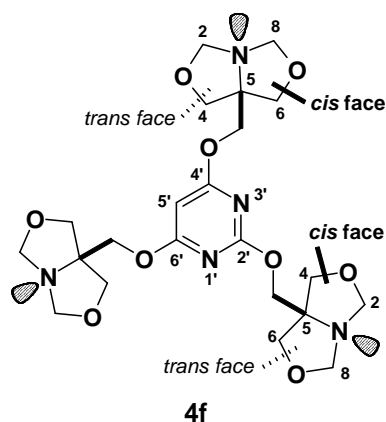


Figure 1. ¹H NMR spectrum of the compound **4f** (300 MHz, CDCl₃)

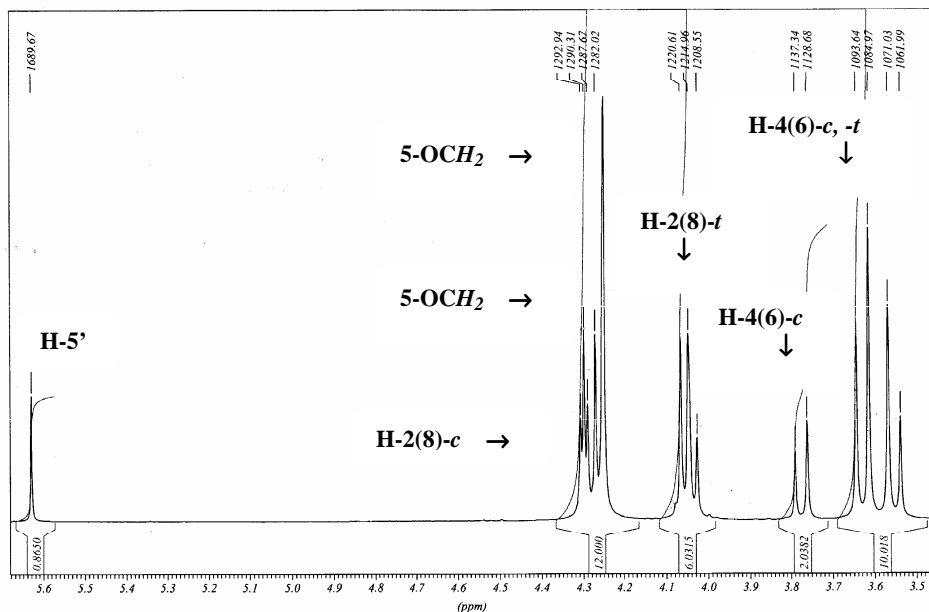


Figure 2. ^1H NMR spectrum of the compound **4f** (300 MHz, C_6D_6)

4. EXPERIMENTAL

General

Melting points are uncorrected; they were carried out on ELECTROTHERMAL[®] 9100 instrument.

Current NMR spectra were recorded on Bruker[®] AM300 instrument operating at 300 and 75 MHz for ^1H and ^{13}C nuclei respectively. For the compound **4b**, Bruker[®] DMX 500 instrument was used operating at 500 and 125 MHz for ^1H and ^{13}C nuclei respectively. No SiMe_4 was added; chemical shifts were measured against the solvent peak, throughout re-calibrated for CDCl_3 or C_6D_6 . All NMR spectra were measured in anhydrous commercially available deuterated solvents. All chemical shifts (δ) values are given throughout in ppm; all coupling patterns (J) values are given throughout in Hz.

TLC was performed by using aluminium sheets with silica gel 60 F_{254} (Merck[®]); flash column chromatography was conducted on Silica gel Si 60 (40–63 μm , Merck[®]).

IR spectra were performed on a Perkin-Elmer[®] 16 PC FT-IR spectrometer. Only relevant absorptions are listed [throughout in cm^{-1} : weak (w), medium (m) or (s) strong]. Mass spectra (MS) were recorded on an ATI-Unicam Automass[®] apparatus, fitted (or not) with a GC-mass coupling (high-resolution J&W column, 30 m, 0.25 mm ID, flow rate: 1.2 mL min^{-1}).

All syntheses were performed under dry nitrogen atmosphere. THF was freshly distilled from Na/benzophenone prior to use. All solvents and starting materials were of commercial quality. The starting materials **2a** and **2b** were prepared according to literature¹ and our improved protocol.¹⁶

General procedure for the preparation of the compounds **3a-f**

In freshly distilled THF (50 mL) and under nitrogen atmosphere, potassium hydride (for the synthesis of compounds **3a-c**: 1.400 g as 30% oily suspension, 0.421 g 100%, 10.50 mmol; for the synthesis of compounds **3e** and **3f**: 0.683 g as 30% oily suspension, 0.205 g 100%, 5.12 mmol) was suspended with stirring. Fine powdered *r*-1-aza-*c*-5-hydroxymethyl-3,7-dioxabicyclo[3.3.0]octane **2a** (1.450 g, 10.00 mmol) [or *r*-1-aza-*c*-5-hydroxymethyl-3,7-dioxo-*c*-2-*c*-8-diphenyl-bicyclo[3.3.0]octane **2b** (1.450 g, 4.88 mmol)] was one pot added at room temperature. The resulted suspension was warmed at 40°C for 1.5-2.0 hrs. (until no more hydrogen was formed) then cooled at room temperature to afford a fine white clear suspension. The corresponding electrophile (for the synthesis of compounds **3a-c** 11.00 mmol; for the synthesis of compounds **3e** and **3f** 5.37 mmol) was one pot added as freshly distilled THF solution (10 mL) at room temperature. The reaction mixture was warmed at 55-60°C for 10-15 min., then let to gently cool and kept with stirring at room temperature over night (12-24 hrs.). The TLC monitoring indicated the starting materials (**2a** and **2b**) absent or in small traces only (double visualisation: first UV 254 nm for the compounds **3c**, **3e** and **3f** then I₂ bath; single visualisation in I₂ bath for the compounds **3a** and **3b**). During condensation, the reaction mixture turned brown and potassium halide was formed abundantly. The reaction was quenched at room temperature with water (100 mL) and dichloromethane (100 mL) with vigorous stirring. After separation, the organic layer was washed with water (about 3 x 50 mL) to pH = 7.5-8.0 then dried over MgSO₄. After filtering, the organic solution was evaporated under vacuum to dryness to yield the crude product, which was purified by flash column chromatography or directly crystallised from an appropriate solvent to yield the title compounds **3a-f**.

***r*-1-Aza-*c*-5-methoxymethyl-3,7-dioxabicyclo[3.3.0]octane (3a)** (45%) yellowish oil (flash column chromatography, eluent pentane : acetone 1:1 v/v); [Found: C, 52.55; H, 8.50; N, 9.11. C₇H₁₃NO₃ requires C, 52.81; H, 8.23; N, 8.80%]; *R*_f (50% pentane/acetone) 0.70; *v*_{max} (CH₃Cl film) 2921 (s), 2857 (m), 1737 (w), 1470 (w), 1387 (w), 1263 (w), 1120 (w), 1074.3 (w), 1019 (w), 798 (w) cm⁻¹. δ_{H} (300 MHz CDCl₃) 4.42 (2H, d, *J*=5.5 Hz, H-2, -8-*t*), 4.38 (2H, d, *J*=5.5 Hz, H-2, -8-*c*), 3.75 (4H, s, H-4, -6, -*c*, -*t*), 3.40 (2H, s, 5-OCH₂), 3.34 (3H, s, OCH₃); δ_{C} (75 MHz CDCl₃) 88.5 (2C, C-2, -8), 76.4 (1C, 5-CH₂O), 74.7 (2C, C-4, -6), 72.2 (1C, C-5), 59.9 (1C, OCH₃). MS (CI, CH₄); *m/z* (rel. int.): 149 (55), 129 (8), 97 (18), 79 (18), 57 (100).

***r*-1-Aza-*c*-5-ethoxymethyl-3,7-dioxabicyclo[3.3.0]octane (3b)** (66%) yellowish oil (flash column chromatography, eluent pentane : Et₂O 2:1 v/v); [Found: C, 55.2; H, 9.1; N, 8.3. C₈H₁₅NO₃ requires C, 55.47; H, 8.73; N, 8.09%]; *R*_f (66% pentane/Et₂O) 0.80; *v*_{max} (CH₃Cl film) 2975 (m), 2932 (s), 2863 (s), 1653 (w), 1636 (w), 1465 (m), 1445 (w), 1374 (m), 1363 (m), 1352 (m), 1274 (m), 1176 (s), 1157 (s), 1110 (s), 1045 (s), 1022 (s), 929 (s), 877 (m) cm⁻¹. δ_{H} (300 MHz CDCl₃) 4.33 (2H, d, *J*=5.3 Hz, H-2, -

8-*t*), 4.29 (2H, d, $J=5.3$ Hz, H-2, -8-*c*), 3.67 (4H, s, H-4, -6, -*c*, -*t*), 3.40 (2H, q, $J=7.0$ Hz, OCH_2CH_3), 3.37 (2H, s, 5- OCH_2), 1.06 (3H, t, $J=7.0$ Hz, $-\text{CH}_2\text{CH}_3$); δ_{C} (75 MHz CDCl_3) 88.4 (2C, C-2, -8), 74.8 (2C, C-4, -6), 74.2 (1C, 5- OCH_2), 72.2 (1C, C-5), 67.4 (1C, CH_2CH_3), 15.3 (1C, CH_2CH_3). MS (CI, CH_4); m/z (rel. int.): 174(70) [M^++1], 128 (25), 114 (100), 99 (7), 86 (15), 58 (25).

***r*-1-Aza-*c*-5-benzyloxymethyl-3,7-dioxabicyclo[3.3.0]octane (3c)** (50%) yellowish oil (flash column chromatography; Et_2O : heptane 3.5:1.0 v/v); [Found: C, 66.59; H, 7.15; N, 6.22. $\text{C}_{13}\text{H}_{17}\text{NO}_3$ requires C, 66.36; H, 7.28; N, 5.95%]; R_f (78% Et_2O /heptane) 0.65; ν_{max} (CH_3Cl film) 2939 (s), 2866 (s), 1502 (w), 1461 (m), 1364 (m), 1286 (w), 1217 (m), 1189 (m), 1102 (s), 1051 (s), 1036 (s), 936 (s), 798 (w), 756 (s), 706 (s) cm^{-1} . δ_{H} (300 MHz CDCl_3) 7.34 – 7.28 (5H, m, Ph), 4.53 (2H, s, OCH_2Ph), 4.44 (2H, d, $J=5.5$ Hz, H-2, -8-*t*), 4.40 (2H, d, $J = 5.5$ Hz, H-2, -8-*c*), 3.80 (4H, s, H-4, -6, -*c*, -*t*), 3.50 (2H, s, 5- OCH_2); δ_{C} (75 MHz CDCl_3) 138.2 (1C, Cq, arom.), 128.9 (1C, CH arom.), 128.2 (2C, CH arom.), 128.1 (2C, CH arom.), 88.5 (2C, C-2, -8), 75.0 (2C, C-4, -6), 74.1 (1C, OCH_2Ph), 73.9 (1C, 5- OCH_2), 72.3 (1C, C-5). MS (CI, CH_4); m/z (rel. int.): 236 (100) [M^++1], 158 (10), 129 (29), 114 (96), 91 (90), 58 (36).

***r*-1-Aza-3,7-dioxa-*c*-5-tosyloxymethylbicyclo[3.3.0]octane (3d)** (70%) yellowish crystalline powder, mp 124–125 °C (direct crystallisation from Et_2O); [Found: C, 51.81; H, 6.05; N, 4.98. $\text{C}_{13}\text{H}_{17}\text{NSO}_5$ requires C, 52.16; H, 5.72; N, 4.68%]; R_f (78% Et_2O /heptane) 0.65; ν_{max} (CH_3Cl film) 2856 (w), 1636 (s), 1357 (m), 1186 (m), 1166 (s), 1135 (w), 1045 (m), 971 (m), 927 (w), 840 (m) cm^{-1} . δ_{H} (300 MHz CDCl_3) 7.77 (2H, d, $J=8.1$ Hz, Ts), 7.35 (2H, d, $J=8.1$ Hz, Ts), 4.38 (2H, d, $J=5.5$ Hz, H-2, -8-*t*), 4.33 (2H, d, $J = 5.5$ Hz, H-2, -8-*c*), 3.99 (2H, s, 5- OCH_2), 3.73 (2H, d, $J=9.2$ Hz, H-4, -6-*t*), 3.70 (2H, d, $J=9.2$ Hz, H-4, -6-*c*), 2.44 (3H, s, CH_3); δ_{C} (75 MHz CDCl_3) 145.7 (1C, Cq, Ts), 132.7 (1C, Cq, Ts), 130.4 (2C, CH, Ts), 128.4 (2C, CH, Ts), 88.2 (2C, C-2, -8), 74.0 (2C, C-4, -6), 72.5 (1C, 5- OCH_2), 71.3 (1C, C-5), 22.1 (1C, CH_3). MS (CI, CH_4); m/z (rel. int.): 300 (3) [M^++1], 146 (40), 128 (100), 93 (22), 65 (17).

***r*-1-Aza-*c*-5-methoxymethyl-*c*-2-*c*-8-diphenyl-3,7-dioxabicyclo[3.3.0]octane (3e)** (50%) yellowish crystalline powder, mp 73–74 °C (flash column chromatography, eluent pentane : Et_2O 1:1 v/v) [Found: C, 73.55; H, 7.11; N, 4.41. $\text{C}_{19}\text{H}_{21}\text{NO}_3$ requires C, 73.29; H, 6.80; N, 4.52%]; R_f (50% pentane/ Et_2O) 0.75; ν_{max} (CH_3Cl film) 2995 (m), 2884 (s), 1466 (m), 1392 (m), 1314 (w), 1199 (m), 1111 (s), 927 (m), 701 (s) cm^{-1} . δ_{H} (300 MHz CDCl_3) 7.44 – 7.42 (4H, m, Ph), 7.30 – 7.22 (6H, m, Ph), 5.47 (2H, s, H-2, -8-*t*), 3.96 (2H, d, $J = 9.0$ Hz, H-4, -6-*c*), 3.80 (2H, s, H-4, -6-*t*), 3.27 (2H, s, 5- OCH_2), 3.17 (3H, s, OCH_3); δ_{C} (75 MHz CDCl_3) 140.1 (2C, Cq., Ph); 128.9 (2C, CH arom.), 128.7 (4C, CH. Arom.), 128.6 (4C, CH arom.), 97.5 (2C, C-2, -8), 78.0 (1C, 5- CH_2O), 74.0 (2C, C-4, -6), 73.5 (1C, C-5), 59.8 (1C, OCH_3). MS (CI, CH_4); m/z (rel. int.): 312 (7) [M^++1], 266 (95), 234 (42), 206 (100), 160 (20), 105 (50), 77 (46), 51 (34).

***r*-1-Aza-*c*-5-benzyloxymethyl-*c*-2-*c*-8-diphenyl-3,7-dioxabicyclo[3.3.0]octane(3f)** (50%) yellowish crystalline powder, mp 84–85 °C (flash column chromatography; eluent Et_2O : heptane 1.5:1.0 v/v); [Found: C, 77.81; H, 6.88; N, 3.44. $\text{C}_{25}\text{H}_{25}\text{NO}_3$ requires C, 77.49; H, 6.50; N, 3.61%]; R_f (60% Et_2O /heptane) 0.70; ν_{max} (CH_3Cl film) 3041 (w),

2866 (m), 1457 (m), 1203 (m), 1097 (s), 1033 (m), 742.8 (s), 701 (s) cm^{-1} . δ_{H} (300 MHz CDCl_3) 7.41 – 7.39 (4H, m, Ph), 7.26 – 7.11 (11H, m, Ph), 5.46 (2H, s, H-2, -8-*f*), 4.32 (2H, s, OCH_2Ph), 3.98 (2H, d, $J = 9.0$ Hz, H-4, -6-*c*), 3.82 (2H, d, $J = 9.0$ Hz, H-4, -6-*f*), 3.67 (2H, s, 5- OCH_2); δ_{C} (75 MHz CDCl_3) 140.1 (2C, Cq., Ph); 138.4 (1C, Cq., Ph), 128.9 (2C, CH arom.), 128.8 (2C, CH arom.), 128.7 (4C, CH arom.), 128.1 (1C, CH arom.), 127.9 (2C, CH arom.), 127.6 (4C, CH arom.), 97.6 (2C, C-2, -8), 75.5 (1C, OCH_2Ph), 74.1 (2C, C-4, -6), 73.9 (1C, 5- OCH_2), 73.6 (1C, C-5). MS (Cl, CH_4); m/z (rel. int.): 388 (99) [$\text{M}^+ + 1$], 266 (15), 91 (50).

Typical procedure for the preparation of the compounds 4a-g

At room temperature, in a perfectly dried 100 mL three necked round bottom flask and under nitrogen atmosphere, potassium hydride (1.000 g as 30% oily suspension, 0.300 g 100%, 7.48 mmol) was rapidly introduced and washed three times with dry ligroine (optionally pentane, hexane) (30 mL): each time about 5 min. stirring and 5 min. complete decanting. Dry and freshly distilled THF (50 mL) was then introduced with stirring to yield a fine grey suspension. Fine powdered 1-aza-5-hydroxymethyl-3,7-dioxabicyclo[3.3.0]octane 5- HOCH_2 -ADBO **2a** (1.085 g-0.987 g, 7.48-6.80 mmol, see **Table 1**) was added and the reaction mixture was heated at 40-45°C for 1.0-1.5 hrs. until no more hydrogen was formed and a white fine suspension was obtained. For the synthesis of the compounds **4a**, **4b**, **4d** and **4f** the corresponding (poly)chloropyrimidine was rapidly injected as dry and freshly distilled THF (10 mL) solution, at room temperature (see **Table 1** for specific molar ratios, temperatures and time reaction). For selective substitution, in the case of compounds **4c**, **4e** and **4g** the reaction mixture was cooled at -78°C prior the addition by injection of the corresponding chloropyrimidine as dry and freshly distilled THF (10 mL) solution. Then, it was let to reach very gently the room temperature. The TLC monitoring was performed systematically until the starting materials were absent or in small traces only. Double visualisation is required: first UV 254 nm for detection of the (di)azines then I_2 bath, for 5- HOCH_2 -ADBO **2a** detection. During condensation, the reaction mixture turned coloured and potassium chloride was formed abundantly. The reaction was carefully quenched at room temperature with water (100 mL) and dichloromethane (100 mL) with vigorous stirring. After separation, the organic layer was colourless or very pale yellow. It was washed with water (about 3x50 mL) to pH=7.5-8.0 then dried over MgSO_4 . After filtering, the organic solution was evaporated under vacuum to dryness to yield the crude product as a solid (usually already crystalline mass). The crude NMR spectra were performed by using this material. The title pure compounds **4a-g** were isolated by direct crystallisation or flash column chromatography as indicated below.

Scale up of the synthesis: 0.800-1.500 g **5-HOCH₂-ADBO, 2a**.

2-{*r*-1-Aza-3,7-dioxabicyclo[3.3.0]octane-*c*-5-yl}-methoxypyrimidine (4a) (60%) yellow crystalline powder, mp 107-109 °C (crystallisation from pentane); [Found: C, 53.59; H, 5.61; N, 19.22. $\text{C}_{10}\text{H}_{13}\text{N}_3\text{O}_3$ requires: C, 53.81; H, 5.87; N, 18.92%]; R_f (75% ligroine/acetone) 0.40; ν_{max} (film NaCl) 2858 (w), 1569 (s), 1431 (s), 1332 (s), 1300 (m), 1137 (w), 1021 (s), 925 (m), 814 (w), 682 (w) cm^{-1} . δ_{H} (300 MHz CDCl_3) *heteroaromatic*: 8.44 (2H, d, $J = 4.9$ Hz, H-4, -6), 6.90 (1H, dd as t, $J = 4.9, 4.9$ Hz, H-5); *alicyclic*: 4.45 (2H,

d, $J=5.5$ Hz, H-2, -8-c), 4.38 (2H, d, $J=5.5$ Hz, H-2, -8- \dot{t}), 4.35 (2H, s, 5-OCH₂), 3.87 (2H, d, $J=9.4$ Hz, H-4, -6-c), 3.84 (2H, d, $J=9.4$ Hz, H-4, -6- \dot{t}); δ_C (75 MHz CDCl₃) *heteroaromatic*: 165.2 (1C, C-2), 159.7 (2C, C-4, -6), 115.8 (1C, C-5); *alicyclic*: 88.5 (2C, C-2, -8), 74.7 (2C, C-4, -6), 71.7 (1C, C-5), 70.6 (1C, 5-OCH₂). MS (EI, 70 eV); m/z (rel. int. %): 222 (10) [M⁺-1], 206 (12), 176 (14), 148 (8), 128 (100), 109 (16), 98 (11).

2,4-Bis{*r*-1-aza-3,7-dioxabicyclo[3.3.0]octane-*c*-5-yl}-methoxypyrimidine (4b) (80%) white crystalline powder, mp 136-137 °C (crystallisation from pentane); [Found: C, 52.61; H, 6.01; N, 15.58. C₁₆H₂₂N₄O₆ requires: C, 52.45; H, 6.05; N, 15.29%]; R_f (75% ligroine/acetone) 0.20; ν_{\max} (film NaCl) 2590 (w), 2863 (w), 1585 (s), 1449 (m), 1416 (s), 1336 (m), 1274 (m), 1181 (w), 1098 (s), 1021 (m), 928 (m), 749 (w) cm⁻¹. δ_H (300 MHz CDCl₃) *heteroaromatic*: 8.15 (1H, d, $J=5.7$ Hz, H-6), 6.35 (1H, d, $J=5.7$ Hz, H-5); *alicyclic linkage at C-2*: 4.46 (2H, d, $J=5.5$ Hz, H-2, -8-c), 4.40 (2H, d, $J=5.5$ Hz, H-2, -8- \dot{t}), 4.35 (2H, s, 5-OCH₂), 3.86 (4H, s, H-4, -6, -c, - \dot{t}); *alicyclic linkage at C-4*: 4.45 (2H, d, $J=5.5$ Hz, H-2, -8-c), 4.39 (2H, d, $J=5.5$ Hz, H-2, -8- \dot{t}), 4.33 (2H, s, 5-OCH₂), 3.80 (4H, s, H-4, -6, -c, - \dot{t}); δ_C (75 MHz CDCl₃) *heteroaromatic*: 171.1 (1C, C-4), 165.0 (1C, C-2), 159.4 (1C, C-6), 102.6 (1C, C-5); *alicyclic*: 88.6 and 88.4 (4C, C-2, -8), 74.7 and 74.3 (4C, C-4, -6), 71.7 and 70.7 (2C, 5-OCH₂), 69.3 and 68.3 (2C, C-5); δ_H (500 MHz C₆D₆) *heteroaromatic*: 8.05 (1H, d, $J=6.0$ Hz, H-6), 6.15 (1H, d, $J=6.0$ Hz, H-5); *alicyclic linkage at C-2*: 4.40 (2H, s, 5-OCH₂), 4.30 (2H, d, $J=5.3$ Hz, H-2, -8-c), 4.05 (2H, d, $J=5.3$ Hz, H-2, -8- \dot{t}), 3.77 (2H, d, $J=8.7$ Hz, H-4, -6-c), 3.64 (2H, d, $J=8.7$ Hz, H-4, -6- \dot{t}); *alicyclic linkage at C-4*: 4.23 (2H, d, $J=5.3$ Hz, H-2, -8-c), 4.21 (2H, s, 5-OCH₂), 4.04 (2H, d, $J=5.3$ Hz, H-2, -8- \dot{t}), 3.56 (2H, d, $J=8.9$ Hz, H-4, -6-c), 3.51 (2H, d, $J=8.9$ Hz, H-4, -6- \dot{t}); δ_C (125 MHz C₆D₆) *heteroaromatic*: 171.1 (1C, C-4), 165.5 (1C, C-2), 158.9 (1C, C-6), 102.3 (1C, C-5); *alicyclic linkage at C-2*: 88.1 (2C, C-2, -8), 74.3 (2C, C-4, -6), 72.7 (1C, C-5), 70.7 (1C, 5-OCH₂); *alicyclic linkage at C-4*: 88.2 (2C, C-2, -8), 73.9 (2C, C-4, -6), 71.5 (1C, C-5), 69.2. (1C, 5-OCH₂) MS (EI, 70 eV); m/z (rel. int. %): 366 (<1) [M⁺], 238 (6), 208 (6), 128 (68), 114 (100), 98 (14), 68 (27), 42 (32), 41 (60).

4-{*r*-1-Aza-3,7-dioxabicyclo[3.3.0]octane-*c*-5-yl}-methoxy-2-chloropyrimidine (4c) (63%) white crystalline powder, mp 139-140 °C (direct crystallisation from dichloromethane : pentane 1:2 v/v); [Found: C, 47.08; H, 4.81; N, 16.65. C₁₀H₁₂N₃O₃Cl requires: C, 46.61; H, 4.69; N, 16.44%]; R_f (75% ligroine/acetone) 0.50; ν_{\max} (film NaCl) 2857 (w), 1636 (s), 1582 (s), 1545 (m), 1446 (m), 1327 (s), 1230 (m), 1102 (w), 1017 (m) cm⁻¹. δ_H (300 MHz CDCl₃) *heteroaromatic*: 8.30 (1H, d, $J=5.7$ Hz, H-6), 6.67 (1H, d, $J=5.7$ Hz, H-5); *alicyclic*: 4.47 (2H, d, $J=5.3$ Hz, H-2, -8-c), 4.42 (2H, d, $J=5.3$ Hz, H-2, -8- \dot{t}), 4.40 (2H, s, 5-OCH₂), 3.81 (4H, s, H-4, -6, -c, - \dot{t}); δ_C (75 MHz CDCl₃) *heteroaromatic*: 170.4 (1C, C-4), 160.6 (1C, C-2), 159.5 (1C, C-6), 107.4 (1C, C-5); *alicyclic*: 88.6 (2C, C-2, -8), 74.2 (2C, C-4, -6), 71.7 (1C, C-5), 69.9 (1C, 5-OCH₂). MS (EI, 70 eV); m/z (rel. int. %): 257.5 (<1) [M⁺], 212 (9), 197 (12), 169 (11), 114 (100), 86 (10), 68 (14), 58 (11), 42 (16), 41 (50).

4,6-Bis{*r*-1-aza-3,7-dioxabicyclo[3.3.0]octane-*c*-5-yl}-methoxypyrimidine (4d) (81%) yellowish crystalline powder, mp 146-148 °C (direct crystallisation from pentane); [Found: C, 52.70; H, 5.88; N, 14.98. C₁₆H₂₂N₄O₆ requires: C, 52.45; H, 6.05; N, 15.29%]; R_f (75% ligroine/acetone) 0.35; ν_{\max} (film NaCl) 2950 (w), 2858 (m), 1593 (s), 1563 (s), 1457 (m), 1421 (m), 1341 (m), 1195 (m), 1137 (m), 1095 (m), 1039 (s), 933 (m), 674 (m)

cm^{-1} . δ_{H} (300 MHz CDCl_3) *heteroaromatic*: 8.38 (1H, s, H-2), 6.08 (1H, s, H-5); *alicyclic*: 4.49 (4H, d, $J=5.7$ Hz, H-2, -8-c), 4.44 (4H, d, $J=5.7$ Hz, H-2, -8-t), 4.38 (4H, s, 5-OCH₂), 3.84 (8H, s, H-4, -6, -c, -t); δ_{C} (75 MHz CDCl_3) *heteroaromatic*: 171.0 (2C, C-4, -6), 157.8 (1C, C-2), 91.4 (1C, C-5); *alicyclic*: 88.6 (4C, C-2, -8), 74.4 (4C, C-4, -6), 71.9 (2C, C-5), 69.4 (2C, 5-OCH₂); MS (EI, 70 eV); m/z (rel. int. %): 367 (<1) [$\text{M}^+ + 1$], 274 (3), 252 (2), 168 (8), 128 (100), 98 (4).

6-{*r*-1-Aza-3,7-dioxabicyclo[3.3.0]octane-*c*-5-yl}-methoxy-4-chloropyrimidine (4e) (63%) white crystalline powder, mp 118-119 °C (flash column chromatography, eluent ligroine : acetone 3:1 v/v); [Found: C, 46.33; H, 5.02; N, 16.59. $\text{C}_{10}\text{H}_{12}\text{N}_3\text{O}_3\text{Cl}$ requires: C, 46.61; H, 4.69; N, 16.31%]; R_f (75% ligroine/acetone) 0.60; ν_{max} (film NaCl) 2956 (w), 2884 (s), 1574 (s), 1546 (s), 1454 (s), 1387 (w), 1343 (s), 1314 (m), 1264 (w), 1213 (w), 1140 (m), 1094 (s), 1040 (s), 1007 (s), 981 (m), 868 (w), 749 (s), 678 (w) cm^{-1} . δ_{H} (300 MHz CDCl_3) *heteroaromatic*: 8.50 (1H, s, H-2), 6.74 (1H, d, $J=0.8$ Hz, H-5); *alicyclic*: 4.44 (2H, d, $J=5.7$ Hz, H-2, -8-c), 4.38 (2H, d, $J=5.7$ Hz, H-2, -8-t), 4.38 (2H, s, 5-OCH₂), 3.78 (4H, s, H-4, -6, -c, -t); δ_{C} (75 MHz CDCl_3) *heteroaromatic*: 170.2 (1C, C-6), 161.3 (1C, C-4), 158.5 (1C, C-2), 108.2 (1C, C-5); *alicyclic*: 88.5 (2C, C-2, -8), 74.2 (2C, C-4, -6), 71.7 (1C, C-5), 69.8 (1C, 5OCH₂). MS (EI, 70 eV); m/z (rel. int. %): 256.5 (2) [$\text{M}^+ - 1$], 240 (8), 210 (7), 128 (100), 98 (7).

2,4,6-Tris{*r*-1-aza-3,7-dioxabicyclo[3.3.0]octane-*c*-5-yl}-methoxypyrimidine (4f) (58%) yellowish crystalline powder, mp 188-189 °C (pentane : dichloromethane, 2:1 v/v); [Found: C, 51.53; H, 6.45; N, 14.11. $\text{C}_{22}\text{H}_{31}\text{N}_5\text{O}_9$ requires: C, 51.86; H, 6.13; N, 13.75%]; R_f (50% ligroine/acetone) 0.50; ν_{max} (film NaCl) 2857 (s), 1600 (s), 1405 (m), 1382 (s), 1325 (m), 1192 (w), 1095 (w), 923 (m) cm^{-1} . δ_{H} (300 MHz CDCl_3) *heteroaromatic*: 5.74 (1H, s, H-5); *alicyclic linkage at C-2*: 4.50 (2H, d, $J=5.5$ Hz, H-2, -8-c), 4.42 (2H, d, $J=5.5$ Hz, H-2, -8-t), 4.325 (2H, s, 5-OCH₂), 3.88 (4H, s, H-4, -6, -c, -t); *alicyclic linkage at C-4, -6*: 4.48 (4H, d, $J=5.5$ Hz, H-2, -8-c), 4.42 (4H, d, $J=5.3$ Hz, H-2, -8-t), 4.331 (4H, s, 5-OCH₂), 3.82 (8H, s, H-4, -6, -c, -t); δ_{C} (75 MHz CDCl_3) *heteroaromatic*: 172.4 (2C, C-4, -6), 164.3 (1C, C-2), 84.9 (1C, C-5); *alicyclic linkage at C-2*: 88.3 (2C, C-2, -8), 74.7 (2C, C-4, -6), 71.6 (1C, 5-OCH₂), 70.8 (1C, C-5); *alicyclic linkage at C-4, -6*: 88.6 (4C, C-2, -8), 74.4 (4C, C-4, -6), 71.8 (2C, 5-OCH₂), 69.4 (2C, C-5); MS (EI, 70 eV); m/z (rel. int. %): 510 (8) [M^+], 297 (<1), 256 (<1), 197 (4), 158 (4), 128 (100), 98 (4).

2,6-Bis{*r*-1-aza-3,7-dioxabicyclo[3.3.0]octane-*c*-5-yl}-methoxy-4-chloro pyrimidine (4g) (76%) white crystalline powder, mp 142-144 °C (flash column chromatography, eluent ligroine : acetone 2:1 v/v, then recrystallisation from dichloromethane : pentane 1:2 v/v); [Found: C, 48.31; H, 4.99; N, 14.19. $\text{C}_{16}\text{H}_{21}\text{N}_4\text{O}_6\text{Cl}$ requires: C, 47.95; H, 5.28; N, 13.98%]; R_f (66% ligroine/acetone) 0.45; ν_{max} (film NaCl) 2852 (s), 1635 (w), 1577 (s), 1416 (m), 1325 (m), 1137 (m), 1093 (m), 1023 (m) 917 (w) cm^{-1} . δ_{H} (300 MHz CDCl_3) *heteroaromatic*: 6.43 (1H, s, H-5); *alicyclic linkage at C-2*: 4.49 (2H, d, $J=5.5$ Hz, H-2, -8-c), 4.42 (2H, d, $J=5.5$ Hz, H-2, -8-t), 4.38 (2H, s, 5-OCH₂), 3.87 (4H, s, H-4, -6, -c, -t); *alicyclic linkage at C-6*: 4.48 (2H, d, $J=5.5$ Hz, H-2, -8-c), 4.41 (2H, d, $J=5.5$ Hz, H-2, -8-t), 4.35 (2H, s, 5-OCH₂), 3.81 (4H, s, H-4, -6, -c, -t); δ_{C} (75 MHz CDCl_3) *heteroaromatic*: 171.9 (1C, C-6), 164.4 (1C, C-2), 162.4 (1C, C-4), 101.6 (1C, C-5); *alicyclic*: 88.5 and 88.4 (4C, C-2, -8), 74.5 and 74.2 (4C, C-4, -6), 71.7 and 71.6 (2C, C-5), 71.2 and 70.1 (2C, 5-OCH₂); MS (EI, 70 eV); m/z (rel. int. %): 400.5 (5) [$\text{M}^+ - 1$], 365 (5), 128 (100), 98 (7).

REFERENCES

1. Senkus, A. C. *J. Am. Chem. Soc.* **1945**, *67*, 1515-1519
2. Senkus, M. U. S. Pat. 2,401,196; *Chem. Abstr.* **1946**, *40*, P5446⁴ and related Patents
3. Pierce, S.; Lunsford, D. C.; Raiford Jr., R. W.; Rush, J. L.; Riley, D. W. *J. Am. Chem. Soc.* **1951**, *73*, 2595-2596
4. Pierce, S.; Lunsford, D. C. *J. Am. Chem. Soc.* **1951**, *73*, 2596-2598
5. Tilford, C. H.; Van Campen Jr., M. G.; Shelton, R. S. *J. Am. Chem. Soc.* **1947**, *69*, 2902-2906
6. Darabantu, M.; Mager, S.; Plé, G.; Puscas, C. *Heterocycles* **1995**, *41*, 2327-2356 and the literature cited therein.
7. Broadbent, H. S.; Burnham, W. S.; Sheely, R. M.; Olsen, R. K. *J. Heterocyclic Chem.* **1976**, *13*, 337-348
8. Barbulescu, N.; Moga, S. G.; Sintamarian, A.; Cuza, O.; Vasilescu, V.; *Rom. Patent*, 83, 939; *Chem. Abstr.* **1985**, *102*, P149252r and related patents.
9. Nougier, R.; Crozet, M.; Vanelle, P.; Maldonado, J. *Tetrahedron Lett.* **1985**, *26*, 5523-5524
10. Zayed, S. E.; Pak. *J. Sci. Ind. Res.* **1987**, *30*, 432 – 438; *Chem. Abstr.* **1988**, *108*, 94446y
11. Vanelle, P.; M. De Meo, M. P.; Maldonado, J.; Nougier, R.; Crozet, M. P.; Laget, M.; Dumenil, G. *Eur. J. Med. Chem.* **1990**, *25*, 241-250
12. Mattson, A.; Norin, T. *Synth. Commun.* **1994**, *24*, 1489-1491
13. Bonnet, D.; Pascal, J.; Grass-Masse, H.; Melnyk, O. *Tetrahedron Lett.* **2001**, *42*, 1875-1877
14. Cookson R. C.; Crabb, T. A. *Tetrahedron* **1968**, *24*, 2385-2397
15. Darabantu, M.; Plé, G.; Mager, S.; Gaina, L.; Cotoră, E.; Mates, A.; Costas, L. *Tetrahedron* **1997**, *53*, 1891-1908
16. Darabantu, M.; Plé, G.; Maierănu, C.; Silaghi-Dumitrescu, I.; Ramondenc, Y.; Mager, S. *Tetrahedron* **2000**, *56*, 3799-3816.
17. Monge, S.; Sélambaron, J.; Carré, F.; Verducci, J.; Roque, J. P.; Pavia, A. A. *Carbohydr. Res.* **2000**, *328*, 127-133
18. Sélambaron, J.; Monge, S.; Carré, F.; Roque, P. J.; Pavia, A. A. *Tetrahedron* **2002**, *58*, 9559-9566
19. Sélambaron, J.; Carré, F.; Fruchier, A.; Roque, P. J.; Pavia, A. A. *Tetrahedron* **2002**, *58*, 4439-4444
20. Brush, J. R.; Magee, R. J.; O'Connor, M. J.; Teo, S. B.; Geue, R. J.; Snow, M. R. *J. Am. Chem. Soc.* **1973**, 2034-2035
21. Crabb, T. A.; Hall, M. J.; Williams, R. O. *Tetrahedron* **1973**, *29*, 3389-3398
22. Laurent, P. A.; Riehl, M.; Frazao, C. S. *Bull. Soc. Chim. Fr.* **1967**, *10*, 3868-3872
23. Cobb, R. L. U. S. Pat. 3,843,726; *Chem. Abstr.* **1975**, *82*, P861193t
24. Cardona, C.; Gawley, R. E. *J. Org. Chem.* **2002**, *67*, 1411-1413
25. Maierănu, C.; Darabantu, M.; Plé, G.; Berghian, C.; Condamine, E.; Ramondenc, Y.; Silaghi-Dumitrescu, I.; Mager, S. *Tetrahedron* **2002**, *58*, 2681-2693
26. Eliel, E. L.; Wilen, H. S. *Stereochemistry of the Organic Compounds*; John Wiley & Sons, Inc. 1994; pp 488 – 492, 1199
27. Darabantu, M.; Lequeux, T.; Pommelet, J. C.; Plé, N.; Turck, A.; Toupet, L. *Tetrahedron Lett.* **2000**, *41*, 6763-6767
28. Darabantu, M.; Lequeux, T.; Pommelet, J. C.; Plé, N.; Turck, A. *Tetrahedron* **2001**, *57*, 739-750
29. Laszlo, P. *Bull. Soc. Chim. Fr.* **1964**, *10*, 2658-2561
30. Nikki, K. *Magn. Res. Chem.* **1990**, *28*, 385-388

FIRST EXAMPLE OF 1-AZA-3,7-DIOXABICYCLO[3.3.0]OCTANE-5-YL-METHOXY SYSTEM AS DIRECTED *ORTHO*-METALLATION GROUP

CAMELIA BERGHIAN,^{a,c} CARMEN MAIEREANU,^{b,c} NELLY PLÉ,^c ALAIN TURCK,^c
ERIC CONDAMINE^c and MIRCEA DARABANTU^{b,c*}

^aDepartment of Inorganic Chemistry, "Babes-Bolyai" University, 11 Aranyi János Str., 400028 Cluj-Napoca, Romania

^bDepartment of Organic Chemistry, "Babes-Bolyai" University, 11 Aranyi János Str., 400028 Cluj-Napoca, Romania

^cInstitut de Recherche en Chimie Organique Fine (I.R.C.O.F.), Université de Rouen, BP 08, F-76131 Mont Saint-Aignan, France

ABSTRACT. The first synthetic and stereochemical approach (supported by NMR data) is described for two title compounds by complete regioselective metallation of some π -deficient systems of type pyrazine bearing a 1-aza-3,7-dioxabicyclo[3.3.0]octane-5-yl-methoxy fragment as directed *ortho*-metallating group.

1. INTRODUCTION

Advances in the field of directed *ortho*-metallation with organo lithium reagents of azines and diazines have been recently and comprehensively reviewed.^{1,2} The exploit of this methodology (the so called **DoM** reaction) is now widely documented as of fundamental synthetic importance in order to access functionalised π -deficient systems in clean, rapid, selective and high yields transformation.

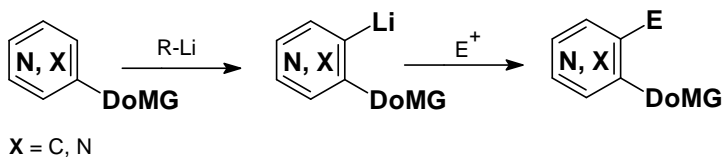
In this context, of a crucial relevance are the Directed *ortho*-Metallation Groups (**DoMGs**) whose increasing diversity makes in our days the method overall attractive. Thus, halo-, trifluoromethyl-, oxygen- (OH, OR, OCONR₂, OSONR₂), sulphur- (SO₂NR₂, SO_nR, n=1, 2), nitrogen- (NHCOR, NHCOOR), carbon- (COOH, CONHR, CONR₂, COR, >C=N-OH etc) based DoMGs revealed their synthetic utility (**Scheme 1**).

Few examples are known in which the DoMG was a heterocyclic saturated system: 1,3-dioxane-2-yl (in pyrazine and pyridine series);^{4,5} 1,3-dioxolane-2-yl,⁶ pyrrolidine-1-yl⁷ and piperidine-1-yl⁸ (in pyridine series). However, their use was described primarily to mask (as protecting groups) carbonyl and amino functionality linked *ortho* to the reaction site rather than connected to a peculiar stereochemistry of the DoMGs of this type.

Following our findings in the field of synthesis and stereochemistry of substituted 1-Aza-3,7-DioxaBicyclo[3.3.0]Octanes⁹⁻¹² (hereafter abbreviated simply as **ADBO**), we established that *r*-1-aza-*c*-5-hydroxymethyl-3,7-dioxabicyclo[3.3.0]octane **5-HOCH₂-ADBO** as well as certain C-2, -8 substituted analogues can be easily and selectively converted to 5-hetaryloxymethyl derivatives of ADBO *via* their corresponding potassium alkoxides upon treatment with (poly)chloro π -deficient systems.¹⁴ Next, we decided to test their aptitude in the metallation methodology applied to some new synthesised 5-hetaryloxymethyl compounds, e.g. in pyrazine series.

* darab@chem.ubbcluj.ro; darabantu@cluj.astral.ro

Stereochemical descriptors *r* (referenece) and *c* (*cis*) are used according to I.U.P.A.C. in order to simplify discussion arising from the basic stereochemistry of this molecule as *cis* fused double oxazolidine system (lone pair at N-1 is the fiducial substituent).¹³

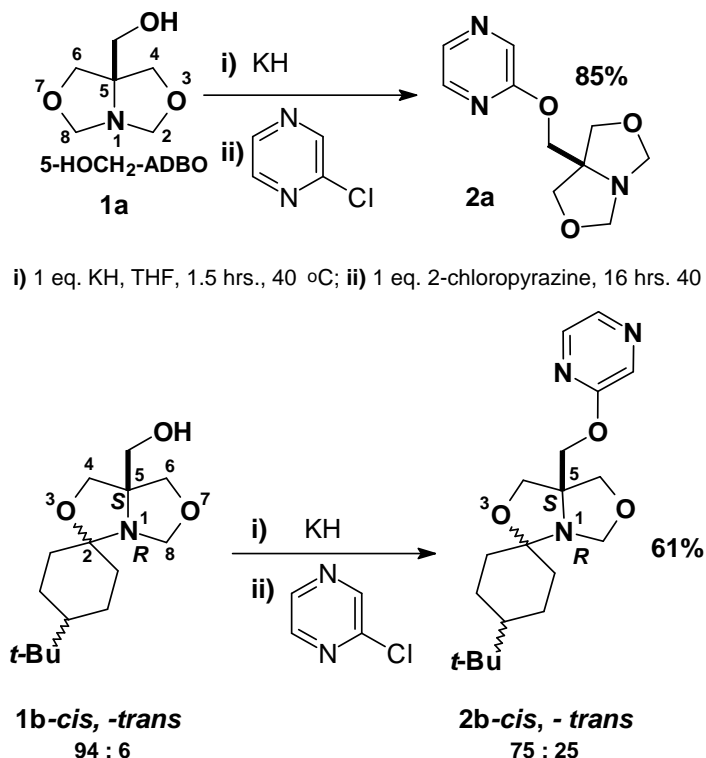


Scheme 1

2. RESULTS AND DISCUSSION

2.1. Synthesis of *r*-1-aza-3,7-dioxa-*c*-5-pyrazinyloxymethyl-bicyclo[3.3.0]octanes

Starting from the ADBO derivatives **1a** and **1b**, the ADBO substituting pyrazines **2a** and **2b** were prepared succeeding our synthetic protocol (**Scheme 2**).¹⁴ As yields demonstrated, it worked well also with 2-chloropyrazine. One must observe the stereochemistry of the starting material, the spiranic ADBO **1b**, which was used as racemate (in **Scheme 2** and hereafter throughout just one enantiomer $1R^*,5S^*$ is depicted) and as non separable mixture of diastereomers 94:6 **1b-cis** and **1b-trans** (O-3 and *t*-Bu group as references).



i) 1.05 eq. KH, THF, 1.5 hrs., 45 °C; ii) 1.1 eq. 2-chloropyrazine, 2 hrs., reflux;
iii) 12 hrs., r.t.

Scheme 2

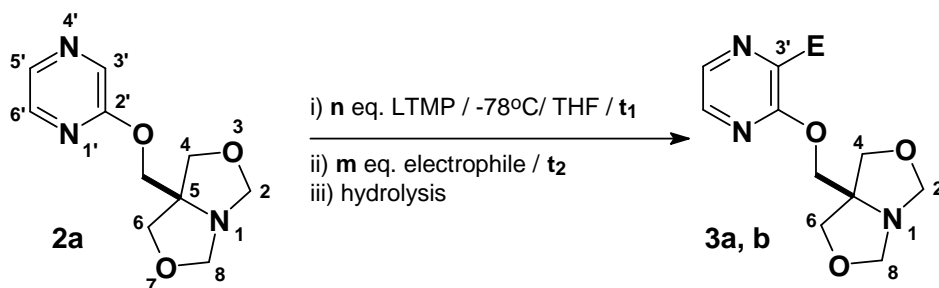
Following the chemistry depicted in **Scheme 2**, **1b** afforded **2b** as a diastereomeric mixture, 75:25 **2b-cis** : **2b-trans**. The ratio was calculated from the ^1H NMR spectrum of the isolated product by means of the well-separated peaks in the heteroaromatic zone; that is, all other relevant signals belonging to the two *cis* (*trans*) spiro-ADBO environment were completely overlapped. We explained simply this new diastereomeric ratio by the fact that crude **2b** (isolated in 96% yield) was directly crystallised from ligroine in which the *cis* diastereomer seemed to be more soluble. We opted for this alternative since the separation by column chromatography of C-2, -8 substituted ADBO derivatives often fails; indeed, too small were the differences between their R_f values together with decomposition on silica gel (see EXPERIMENTAL).¹¹

2.2. Functionalisation by metallation

The metallation of the compounds **2a**, **2b** was straightforward.

The first attempt was carried on compound **2a** (**Scheme 3**).

In this purpose, we considered the comparative data focusing on the metallation of 2-methoxypyrazine.^{15,16} Treatment of **2a** with 1.1 eq. of LTMP (4,4,6,6-lithiotetramethylpiperidide, as for 2-methoxypyrazine) at -78°C for 60 min. followed by quench with 20% DCl/D₂O (at -78°C) afforded the starting material in 99% yield. Deuteration was 84% at C-3' if 2.1 eq. of LTMP were used, as revealed by the ^1H NMR spectrum of the crude reaction mixture. The best result (98% deuterium incorporation in the crude product) was obtained with 4 eq. of LTMP (compound **3a**).



Compound	E	n	t ₁	m	t ₂	Temp. (°C)	Yield ^a (%)
3a	D ^b	1.1	60	8.0	-	-78	0
	D	2.1	60	8.0	-	-78 to r.t.	84
	D	4.0	60	8.0	-	-78	98
3b	Ph-CHOH	4.0	60	4.0	Overnight	-78 to r.t.	79

^a as isolated pure compounds, after flash column chromatography and subsequent recrystallisation (**3b**); for **3a**, as deuterium incorporation in the quantitatively isolated crude product (^1H NMR monitoring)

^b 8 eq. DCl as 20% g/g D₂O solution was used

Scheme 3

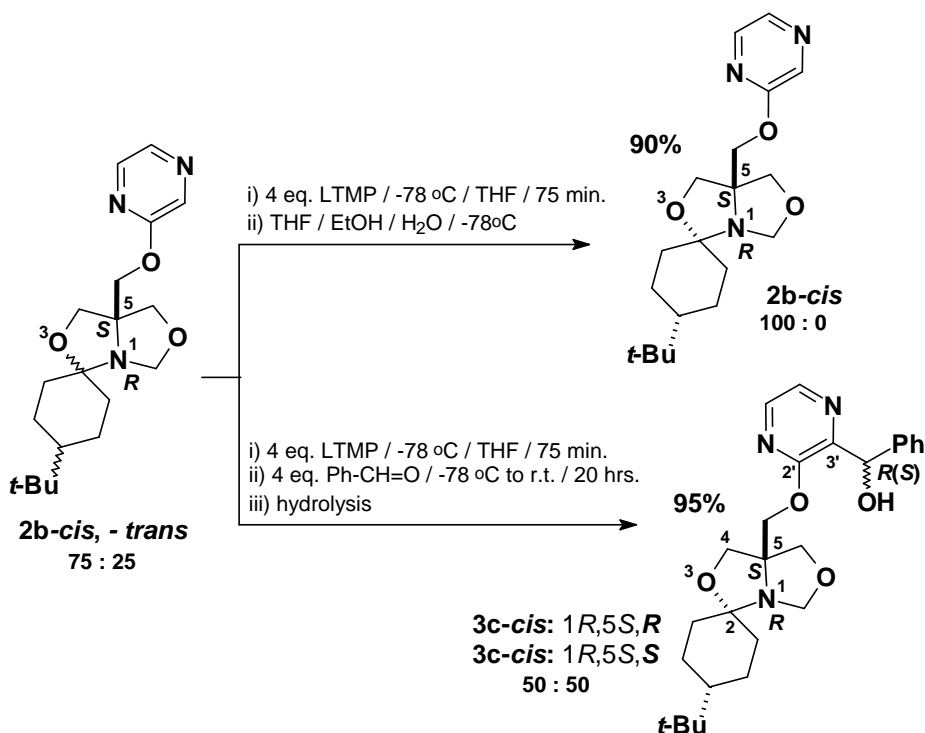
In identical conditions, the lithio-derivative of **2a**, upon treatment with benzaldehyde as electrophile, yielded the chiral diarylmethanol **3b** with good yield and complete *ortho*-regioselectivity.

The NMR spectra of **3b** nicely displayed the expected diastereotopic positions (as $\Delta\delta$ values) in the ADBO moiety: C-2 vs. C-8 and C-4 vs. C-6. We have seen of interest our study by selecting benzaldehyde as typical electrophile since the synthesis of the chiral diaryl methanols of type **3b** appeared to us closer to 5-OCH₂-ADBO intimate structure, including its above exhibited ability as **DoMG**.¹¹

Our option was then supported by the results obtained when metallation of the mixture **2b-cis** and **2b-trans** was carried out. We figured that more details about the behaviour of azadioxabicyclooctane system as **DoMG** could be obtained if a diastereomeric compound built on this skeleton was involved. That is, the chiral spiro-ADBO compound **2b** was chosen as apt for this tentative (**Scheme 4**).

Metallation of **2b** quantitatively yielded, after work up, the crude equimolar mixture of two compounds **3c** (*de* 0%, 100% *ortho*-regioselectivity). However, by flash column chromatography, they were eluted together, although it was twice performed.

Hence, we focused on identification of the compounds **3c**.



Scheme 4

Initial inspection of their ¹H NMR spectrum evidenced two stereoisomers with excellent partition of all peaks in the aliphatic region but complete overlapping in the heteroaromatic zone.

Two hypothesis were selected to be more plausible:

i) 3c should be a 1:1 mixture of *cis* and *trans* diastereomers each having the same configuration of the α -hydroxybenzyl chiral center (e.g. 1:1 *R-cis* and *R-trans* or 1:1 *S-cis* and *S-trans*); this would involve not only a complete asymmetric induction but also an isomerisation *cis* \rightarrow *trans* of the spiranic skeleton (from 75:25 in **2b** to 50:50 in **3c**).

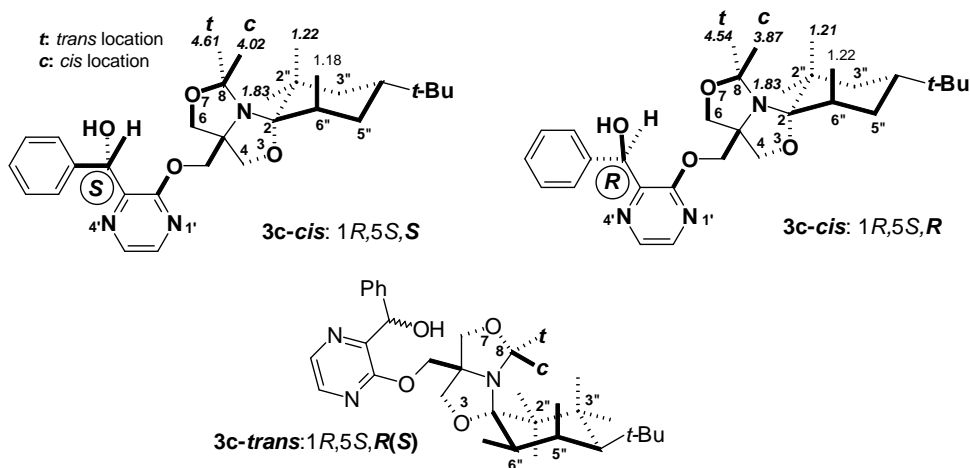
ii) 3c should be a 1:1 mixture of either *cis* or *trans* diastereomers having an opposite configuration (*R* or *S*) of the α -hydroxybenzyl chiral center (e.g. 1:1 *R-cis* and *S-cis* or 1:1 *R-trans* and *S-trans*); this would involve no steric predilection towards a certain diastereoselectivity but a complete isomerisation either *cis* \rightarrow *trans* or *trans* \rightarrow *cis* from **2b** to **3c**.

Complete systematic NMR investigations solved this very difficult problem.

In a first step, the ^1H and ^{13}C assignments for each of the compounds **3c** were realised by means of 2D homo- and heteronuclear NMR experiments: ^1H - ^{15}N , ^1H - ^{13}C (HSQC^{17,18} and HMBC^{19,20}), ^1H - ^1H (COSY and TOWNY).^{21,22} Next, the stereochemistry as *cis* or *trans* of **3c** was revealed by the correlation of the dipolar interactions observed in 2D ^1H - ^1H (NOESY^{23,24} and ROESY)^{25,26} experiments with the protons estimated distances (\AA) in all the possible modellised diastereomers, as described **i)** and **ii)** above.²⁷

Obviously, this minute analysis was dedicated mainly to the spiranic oxazolidine motif in **3c**.

A good concordance we found between the estimated interatomic distances (\AA) in the **3c-cis-1R,5S,S(R)** diastereomer and the detectable dipolar interactions in 2D ^1H - ^1H NMR experiments (**Scheme 5**).



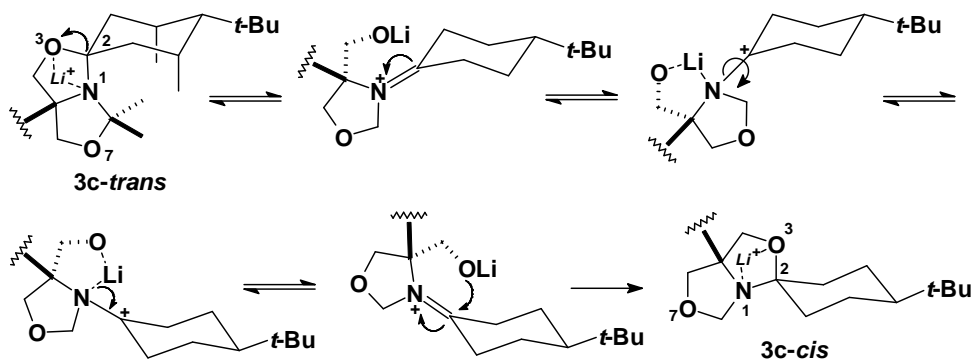
italicised: positions (as δ , ppm) involved in relevant dipolar interaction as predicted by modellised structures and confirmed by NOESY and ROESY experiments.

Scheme 5

We finished that the stereoisomers of type **3c** have both the same *cis* geometry, the single difference between them originating from the opposite configuration of the α -hydroxybenzyl chiral center.

Though our effort to use a chiral ADBO in an asymmetric synthesis failed (*de* 0%), we re-checked the validity of this conclusion by an alternative attempt (**Scheme 4**). In fact, it was not clear for us the change in stereochemistry of the spiranic ADBO from 75:25 *cis* : *trans* (in the starting **2b**) to 100:0 *cis* : *trans* (in **3c**). For this reason, we lithiated **2b** in the same and accurate conditions but we quenched the reaction with water. We isolated in 90% yield the crude product **2b** as unique *cis* diastereomer (^1H - and ^{13}C -NMR spectra monitoring).

This result supports our hypothesis concerning the interaction between ADBO and the Li-metallating reagent (e.g. chelation of Li by the most basic oxygen O-3 and N-1, followed by ring opening - ring closure) but observable only for configured azadioxabicyclooctane fragments (e.g. of type **2b** as proposed in **Scheme 6**).



Scheme 6

In the end, we note our verdict to be in agreement with the pioneering results of Pierce in 1951 (ring opening of the ADBO with Grignard reagents)^{28,29} and our very recent assignments^{11,30} (confirmed soon later by Pavia³¹): spontaneous-, Lewis acids- or even intramolecular hydrogen bonds-assisting stereoelectronic ring opening - ring closure in 2-substituted-1,3-oxazolidines.

3. CONCLUSION

The 1-aza-3,7-dioxabicyclo[3.3.0]octane-5-yl-methoxy group attached to pyrazine revealed clear and convincing aptitudes as Directed *ortho*-Metallating Group in the lithiation of these substrates. Although the quantitative and qualitative results seem similar with those previously reported for the methoxy analogous, the specific reaction conditions were enough different. Hence, azadioxabicyclooctane system itself can be considered as having a typical and versatile chelating behaviour against organo-lithium reagents, regardless its 5-yl-methoxy functionality. Organo-lithium reagents can assist ring opening-ring closure of the 1-aza-3,7-dioxabicyclo[3.3.0]octane system.

4. EXPERIMENTAL

General

Melting points are uncorrected; they were carried out on ELECTROTHERMAL[®] 9100 instrument.

Current NMR spectra were recorded on Bruker[®] AM300 instrument operating at 300 and 75 MHz for ¹H and ¹³C nuclei respectively. NMR analysis for the compound **3c** was performed on Bruker[®] DMX500 instrument operating at 500 and 125 MHz for ¹H and ¹³C nuclei respectively. No SiMe₄ was added; chemical shifts were measured against the solvent peak, throughout re-calibrated for CDCl₃ or C₆D₆. All NMR spectra were measured in anhydrous commercially available deuterated solvents. All chemical shifts (δ) values are given throughout in ppm; all coupling patterns (*J*) values are given throughout in Hz.

Labelling of the positions in the ADBO motif as c (cis) or t (trans) was made with respect to the fiducial substituent, the lone pair at N-1. Numbering of the position was made 1 → 8 for the ADBO fragment, 1' → 6' for the pyrazine ring and 1'' → 6'' for the spiranic cyclohexane.

TLC was performed by using aluminium sheets with silica gel 60 F₂₅₄ (Merck[®]); flash column chromatography was conducted on Silica gel Si 60 (40-63 μ m, Merck[®]).

IR spectra were performed on a Perkin-Elmer[®] 16 PC FT-IR spectrometer. Only relevant absorptions are listed [throughout in cm⁻¹: weak (w), medium (m) or (s) strong]. Mass spectra (MS) were recorded on an ATI-Unicam Automass[®] apparatus, fitted (or not) with a GC-mass coupling (high-resolution J&W column, 30 m, 0.25 mm ID, flow rate: 1.2 mL min⁻¹).

All syntheses were performed under dry nitrogen atmosphere. THF was freshly distilled from Na/benzophenone prior to use. All solvents and starting materials were of commercial quality.

The modeling of the compounds **3c** was made by using Cerius-2 program: Cerius-2 Simulation Tool User's Reference, version 4.0. Molecular Simulation software for material science. Molecular Simulation Incorporated, San Diego, CA, USA 1999.²⁷

The synthesis and the conformational analysis of the compound **1b** we described in detail elsewhere.¹¹

Typical procedure for the synthesis of the compounds 3a-c by Directed *ortho*-Metallation methodology

In 50 mL freshly distilled THF and under nitrogen atmosphere and with vigorous stirring, dry 2,2,6,6-tetramethylpiperidine (HTMP) from freshly opened bottle (0.688 mL, 0.565 g 100%, 0.576 g 98%, 4 mmol) was injected; the solution was cooled at (-10)-(-15 °C) in an ice bath then *n*-BuLi (2.50 mL as 1.6 M solution in hexane, 4.00 mmol, optionally 1.54 mL as 2.6 M in hexane) was injected. The clear yellowish solution was stirred at (-10)-(-15 °C) for additional 15 min., then cooled at -78 °C. The starting ADBO-substituting pyrazine **2a, b** (1.00 mmol) as freshly distilled THF solution (2-10 mL) was introduced. Specific conditions to perform the reaction are presented in **Schemes 3** and **4**. TLC monitoring was made as follows: 0.2-0.3 mL from the reaction mixture were rapidly quenched with 2 mL 1:1 v/v mixture ethyl acetate (optionally ether): water. The sample was collected from the organic layer after vigorous stirring and separation. The reaction was quenched according to one of the following variant:

A. In the case of deuterated compound **3a** the reaction was quenched at $-78\text{ }^{\circ}\text{C}$ with 8 eq. of DCI as 20% g/g solution in D_2O . Then it was let to reach the room temperature. The next work up was made according to variant **C** (see below).

B. In the case of compounds **2b** the reaction was quenched at $-78\text{ }^{\circ}\text{C}$ with 10 mL 1:1 v/v THF : EtOH. Then it was let to reach the room temperature. The next work up was made according to variant **C** (see below).

C. In the case of compounds **3b, c**, the reaction was quenched at room temperature with 100 mL 1:1 v/v dichloromethane : water. After separation, the aqueous layer was extracted with dichloromethane (2x15 mL) then the combined organic solution was washed with water (x25 mL) to neutrality. After drying on MgSO_4 and filtering, the dichloromethane solution was evaporated under vacuum to dryness. The obtained oily residue was analysed by NMR as crude reaction mixture; for deuterated compound **3a** (**Note 1**). For the rest of the compounds **3b, c**, the mixtures were purified by column chromatography to yield the title compounds **3b, c** (**Note 2**).

Note 1: for mono deuterated compound **3a** the magnitude of the corresponding integral is given as percentages with respect to the most intense signal.

Note 2: CARE! TLC monitoring of all reactions and separations by column chromatography evidenced very weak absorption in UV (254 nm); concentrated samples should be used.

Preparation of the compound 2b

The compound **2b** was prepared following the same protocol as for **2a**: from compound **1b** (as mixture of 96:4 *cis* : *trans* diastereomers, 0.650 g, 2.4 mmol) and potassium hydride (0.330 g as 30% KH, 0.100 g 100%, 2.5 mmol) in anhydrous THF (40 mL), upon treatment with chloropyrazine (0.236 mL, 0.297 g, 2.6 mmol, 2 hrs. at reflux then 12 hrs. at room temperature) and work up, 0.802 g the crude product **2b** was obtained. Subsequent recrystallisation from ligroine afforded 0.517 g of the title compound **2b** as a mixture of 75:25 *cis* : *trans* diastereomers.

2-{*r*-1-Aza-3,7-dioxabicyclo[3.3.0]octane-*c*-5-yl}-methoxypyrazine (2a) (85%) yellowish crystalline powder, mp $128\text{--}129\text{ }^{\circ}\text{C}$ (pentane); [Found: C, 53.50; H, 6.09; N, 18.55. $\text{C}_{10}\text{H}_{13}\text{N}_3\text{O}_3$ requires: C, 53.81; H, 5.87; N, 18.82%]; R_f (75% ligroine/ acetone) 0.40; ν_{max} (film NaCl) 2868 (m), 1524 (s), 1465 (m), 1413 (s), 1361 (m), 1289 (s), 1134 (m), 1032 (s), 1002 (s), 915 (s), 832 (m), 692 (m) cm^{-1} . δ_{H} (300 MHz CDCl_3) *heteroaromatic*: 8.19 (1H, d, $J=1.5$ Hz, H-3), 8.09 (1H, d, $J=3.0$ Hz, H-5), 8.01 (1H, dd, $J=1.5, 1.5$ Hz, H-6); *alicyclic*: 4.47 (2H, d, $J=5.7$ Hz, H-2, -8-c), 4.41 (2H, d, $J=5.7$ Hz, H-2, -8-f), 4.33 (2H, s, 5- OCH_2), 3.83 (4H, s, H-4, -6, -c, -f); δ_{C} (75 MHz CDCl_3) *heteroaromatic*: 160.1 (1C, C-2), 140.9 (1C, C-6), 137.5 (1C, C-3), 136.1 (1C, C-5); *alicyclic*: 88.6 (2C, C-2, -8), 74.4 (2C, C-4, -6), 71.9 (1C, C-5), 69.0 (1C, 5- O-CH_2). MS (EI, 70 eV); m/z (rel. int. %): 223 (6) [M^+], 178 (14), 163 (13), 114 (100), 98 (17), 86 (9), 68 (26), 58 (11), 42 (18), 41 (59).

(1*R,5*S**)-2-{*r*-1-aza-*r*-3-oxa-7-oxa-2-(*c*-4-tertbutylspirocyclohexyl)-bicyclo [3.3.0]octane-*c*-5-yl}-methoxypyrazine (2b-*cis*)** and **(1*R**,5*S**)-2-{*r*-1-aza-*r*-3-oxa-7-oxa-2-(*t*-4-tertbutylspirocyclohexyl)-bicyclo[3.3.0]octane-*c*-5-yl}-methoxypyrazine (2b-*trans*)** (61%) yellow crystalline powder, mp $103\text{--}105\text{ }^{\circ}\text{C}$ (as mixture of diastereomers *cis* : *trans* 75:25); [Found: C, 65.79; H, 8.19; N, 11.85. $\text{C}_{19}\text{H}_{29}\text{N}_3\text{O}_3$ requires: C, 65.68; H, 8.41; N, 12.09%]; R_f (75% ligroine/acetone) 0.60; ν_{max} (film NaCl) 2940 (s), 2857 (m), 1529

(s), 1465 (m), 1408 (s), 1284 (s), 1080 (w), 1005 (m), 909 (w) cm^{-1} . **Diastereomer 2b-cis**: δ_{H} (300 MHz CDCl_3) *heteroaromatic*: 8.21 (1H, s, H-3), 8.11 (1H, d, $J=3.0$ Hz, H-5), 8.03 (1H, d, $J=2.6$ Hz, H-6); *alicyclic*: 4.79 (1H, d, $J=7.5$ Hz, H-8-c), 4.42 (1H, d, $J=10.6$ Hz, 5- OCH_aH_b), 4.29 (1H, d, $J=10.6$ Hz, 5- OCH_aH_b), 4.15 (1H, d, $J=7.5$ Hz, H-8-t), 4.04 (1H, d, $J=9.2$ Hz, H-4-c), 3.86 (1H, d, $J=9.2$ Hz, H-4-t), 3.77 (1H, d, $J=8.7$ Hz, H-6-c), 3.65 (1H, d, $J=8.7$ Hz, H-6-t), 1.97-1.79 (2H, m, cyclohexyl), 1.77-1.67 (1H, m, cyclohexyl), 1.60-1.45 (2H, m, cyclohexyl), 1.44-1.15 (3H, m, cyclohexyl), 1.03-0.89 (1H, m, cyclohexyl), 0.81 [9H, s, $\text{C}(\text{CH}_3)_3$]; δ_{C} (75 MHz CDCl_3) *heteroaromatic*: 160.3 (1C, C-2), 140.8 (1C, C-6), 137.4 (1C, C-3), 136.2 (1C, C-5); *alicyclic*: 98.1 (1C, C-2), 82.0 (1C, C-8), 73.8 (1C, C-6), 72.0 (1C, C-5), 71.6 (1C, C-4), 69.7 (1C, 5-O- CH_2), 47.5 (1C, CH, cyclohexyl), 38.5, 32.7, 32.2, 24.7 (4x1C, CH_2 cyclohexyl), 28.0 [3C, $\text{C}(\text{CH}_3)_3$], 24.5 [1C, $\text{C}(\text{CH}_3)_3$]. **Diastereomer 2b-trans**: δ_{H} (300 MHz CDCl_3 only distinct peaks are listed) *heteroaromatic*: 8.09 (1H, s, H-5), 8.01 (1H, s, H-6); δ_{C} (75 MHz CDCl_3) *heteroaromatic*: 136.3 (1C, C-5); *alicyclic*: 96.2 (1C, C-2), 68.4 (1C, 5- OCH_2), 47.3 (1C, CH cyclohexyl), 37.8 (1C, CH_2 cyclohexyl). MS (EI, 70 eV); m/z (rel. int. %): 348 [M^+] (50), 334 (11), 318 (27), 292 (13), 252 (100), 234 (15), 222 (35), 194 (50), 165 (7), 152 (9), 98 (70).

2-{*r*-1-Aza-3,7-dioxabicyclo[3.3.0]octane-*c*-5-yl}-methoxy-[3-²H]-pyrazine (3a) (98%); δ_{H} (300 MHz CDCl_3) *heteroaromatic*: 8.23 (1H, d, $J=1.1$ Hz, H-3, 1.7%), 8.13 (1H, d, $J=3.0$ Hz, H-5, 93%), 8.06 (1H, d, $J=2.8$ Hz, H-6, 100%); *alicyclic*: see compound 2a. MS (EI, 70 eV); m/z (rel. int. %): 225 (5) [$\text{M}^+ + 1$], 207 (5), 177 (4), 128 (100%), 98 (9).

Rac-2-{*r*-1-aza-3,7-dioxabicyclo[3.3.0]octane-*c*-5-yl}-methoxy-3- α -hydroxybenzylpyrazine (3b) (79% after column chromatography, 51% after recrystallisation) yellowish crystalline powder, mp 84-85 °C (column chromatography, eluent AcOEt : ligroine 20:1 v/v then recrystallisation from pentane); [Found: C, 61.79; H, 6.10; N, 12.45. $\text{C}_{17}\text{H}_{19}\text{N}_3\text{O}_4$ requires: C, 61.99; H, 5.81; N, 12.76%]; R_f (95% AcOEt/ligroine) 0.40; v_{max} (film NaCl) 3600 (s), 2863 (w), 2356 (w), 1540 (w), 1419 (s), 1320 (w), 1176 (m), 1093 (w), 1042 (s), 925 (m), 700 (s) cm^{-1} . δ_{H} (300 MHz CDCl_3) (*hetero*)*aromatic*: 8.07 (1H, d, $J=2.8$ Hz, H-5), 7.96 (1H, d, $J=2.8$ Hz, H-6), 7.30-7.10 (5H, m); 5.71 (1H, d, $J=4.7$ Hz, CHOH), 5.05 (1H, d, $J=4.7$ Hz, OH); *alicyclic*: 4.36 (1H, d, $J=5.7$ Hz, H-8-c), 4.31 (1H, d, $J=5.7$ Hz, H-8-t), 4.29 (1H, d, $J=6.4$ Hz, H-2-c), 4.26 (1H, d, $J=10.9$ Hz, 5- OCH_aH_b), 4.25 (1H, d, $J=6.4$ Hz, H-2-t), 4.14 (1H, d, $J=10.9$ Hz, 5- OCH_aH_b), 3.64 (2H, s, H-6-c, -t), 3.38 (1H, d, $J=9.0$ Hz, H-4-t), 3.28 (1H, d, $J=9.0$ Hz, H-4-c); δ_{C} (75 MHz CDCl_3) (*hetero*)*aromatic*: 156.8 (1C, C-2), 146.2 (1C, C-3), 141.9 (1C, C-q arom.), 140.3 (1C, C-5), 135.5 (1C, C-6), 128.9 (2C, CH arom.), 128.5 (1C, CH arom.), 127.6 (2C, CH arom.); *alicyclic*: 88.4 [1C, C-2(8)], 88.3 [1C, C-(2)8], 74.32 [1C, C-4(6)], 74.28 [1C, C-(4)6], 71.9 (1C, CHOH), 71.6 (1C, C-5), 69.3 (1C, 5- OCH_2). MS (EI, 70 eV); m/z (rel. int. %): 328 (3) [$\text{M}^+ - 1$], 312 (100), 281.9 (13), 254.8 (10), 211.7 (11), 186.8 (8), 128 (75), 98 (32).

Rac-(*R,1*R**,5*S**)-2-{*r*-1-aza-*r*-3-oxa-7-oxa-2-(*c*-4-*tert*butylspirocyclohexyl)-bicyclo[3.3.0]octane-*c*-5-yl}-methoxy-3- α -hydroxybenzylpyrazine (3c-*cis*-1*R*,5*S*,*R*)** and **Rac-(*S**,1*R**,5*S**)-2-{*r*-1-aza-*r*-3-oxa-7-oxa-2-(*t*-4-*tert*butylspirocyclohexyl)-bicyclo[3.3.0]octane-*c*-5-yl}-methoxy-3- α -hydroxybenzylpyrazine (3c-*cis*-1*R*,5*S*,*S*)** (95%) white crystalline powder, mp 96-98 °C (column chromatography, eluent ligroine :

acetone 4:1 v/v then, crystallisation from pentane as non separable 1:1 mixture of diastereomers labelled as **3c-cis-1R*,5S,R** and **3c-cis-1R*,5S,S** respectively, see **Scheme 4** and **5**; [Found: C, 69.11; H, 8.19; N, 8.97. C₂₆H₃₅N₃O₄ requires: C, 68.85; H, 7.78; N, 9.26%]; *R_f* (80%ligroine/acetone) 0.60 and 0.40; ν_{\max} (film NaCl) 3431 (s), 2945 (m), 2857 (m), 1638 (m), 1416 (s), 1080 (m), 1023 (m), 700 (s) cm⁻¹. *The hereafter reported NMR data refer to labelling of the molecular positions as described in Scheme 5. Diastereomer 3c-cis-1R*,5S*,S**: δ_{H} (500 MHz C₆D₆) (*hetero*)aromatic: 7.66 (1H, d *J*=3.0 Hz, H-5'), 7.53 (1H, d, *J*=2.5 Hz, H-6'), 7.26 (2H, m, *ortho* phenyl), 7.05 (2H, m, *meta* phenyl), 6.98 (1H, m, *para* phenyl); *alicyclic*: 4.61 (1H, d, *J*=7.5 Hz, H-8-*t*), 4.28 (1H, d, *J*=10.5 Hz, 5-OCH_aH_b), 4.02 (1H, d, *J*=8.0 Hz, H-8-*c*), 4.00 (1H, d, *J*=12.0 Hz, 5-OCH_aH_b), 3.55 (1H, d, *J*=8.5 Hz, H-6-*t*), 3.44 (1H, d, *J*=9.0 Hz, H-4-*t*), 3.41 (1H, d, *J*=8.5 Hz, H-6-*c*), 3.37 (1H, d, *J*=9.0 Hz, H-4-*c*), 1.83 (1H, ddd, *J*=3.2, 6.4, 12.6 Hz, H-2"-eq.), 1.77 (1H, ddd, *J*=3.0, 6.5, 12.6 Hz, H-6"-eq.), 1.22 (1H, m, H- H-2"-ax.), 1.18 (1H, m, H-6"-ax.), 1.50 (4H, m, H-3", -5", -ax., -eq.), 0.83 [9H, s, C(CH₃)₃], 0.81 (1H, m, H-4"-ax.); δ_{C} (125 MHz C₆D₆) (*hetero*)aromatic: 157.56 (1C, C-2'), 143.3 (1C, C-3'), 143.2 (1C, C-*q* phenyl), 140.5 (1C, C-5'), 135.49 (1C, C-6'), 129.2 (2C, *meta* CH phenyl), 128.7 (1C, *para* CH phenyl); 128.3 (2C, *ortho* CH phenyl); *alicyclic*: 98.4 (1C, C-2), 82.2 (1C, C-8), 73.9 (1C, C-6), 72.8 (1C, C-4), 71.18 (1C, 5-O-CH₂), 70.91 (1C, C-5), 48.03 (1C, C-4"), 39.6 (1C, C-6"), 32.91 [1C, C(CH₃)₃], 32.32(1C, C-2"), 28.36 [3C, C(CH₃)₃], 25.33 (1C, C-5"), 25.04 (1C, C-3"); δ_{N} (500 MHz C₆D₆): 96.9 (1N, N-1), 281.3 (1N, N-1'), 319.4 (1N, N-4"). **Diastereomer 3c-cis-1R*,5S*,R***: δ_{H} (500 MHz C₆D₆) (*hetero*)aromatic: 7.66 (1H, d *J*=3.0 Hz, H-5'), 7.53 (1H, d, *J*=2.5 Hz, H-6'), 7.27 (2H, m, *ortho* phenyl), 7.05 (2H, m, *meta* phenyl), 6.98 (1H, m, *para* phenyl); *alicyclic*: 4.54 (1H, d, *J*=7.5 Hz, H-8-*t*), 4.18 (1H, d, *J*=10.5 Hz, 5-OCH_aH_b), 4.14 (1H, d, *J*=10.5 Hz, 5-OCH_aH_b), 3.87 (1H, d, *J*=8.0 Hz, H-8-*c*), 3.80 (1H, d, *J*=9.0 Hz, H-4-*t*), 3.56 (1H, d, *J*=9.0 Hz, H-4-*c*), 3.34 (1H, d, *J*=8.5 Hz, H-6-*t*), 3.06 (1H, d, *J*=8.5 Hz, H-6-*c*), 1.89 (1H, ddd, *J*=3.2, 6.5, 13.8 Hz, H-6"-eq.), 1.83 (1H, ddd, *J*=3.2, 6.4, 12.6 Hz, H-2"-eq.), 1.22 (1H, m, H- H-6"-ax.), 1.21 (1H, m, H-2"-ax.), 1.50 (4H, m, H-3", -5", -ax., -eq.), 0.83 [9H, s, C(CH₃)₃], 0.84 (1H, m, H-4"-ax.); δ_{C} (125 MHz C₆D₆) *aromatic*: 157.61 (1C, C-2'), 147.1 (1C, C-3'), 143.0 (1C, C-*q* phenyl), 140.5 (1C, C-5'), 135.46 (1C, C-6'), 129.2 (2C, *meta* CH phenyl), 128.7 (1C, *para* CH phenyl); 128.3 (2C, *ortho* CH phenyl); *alicyclic*: 98.4 (1C, C-2), 82.0 (1C, C-8), 73.9 (1C, C-6), 72.8 (1C, C-4), 71.18 (1C, C-5), 70.91 (1C, 5-OCH₂), 48.06 (1C, C-4"), 32.95 [1C, C(CH₃)₃], 32.6 (1C, C-6"), 32.3 (1C, C-2"), 28.38 [3C, C(CH₃)₃], 25.36 (1C, C-5"), 25.07 (1C, C-3"); δ_{N} (500 MHz C₆D₆): 96.7 (1N, N-1), 281.3 (1N, N-1'), 319.4 (1N, N-4"). MS (EI, 70 eV); *m/z* (rel. int. %): 454 [M⁺+1] (65), 436 (20), 423 (18), 300 (40), 282 (75), 252 (100), 222 (18), 185 (13), 128 (95), 98 (77).

Isomerisation of (1R*,5S*)-2-{*r*-1-aza-*r*-3-oxa-7-oxa-2-(*t*-4-tertbutylspirocyclohexyl)-bicyclo[3.3.0]octane-*c*-5-yl}-methoxypyrazine (2b-*trans*) into (1R*,5S*)-2-{*r*-1-aza-*r*-3-oxa-7-oxa-2-(*c*-4-tertbutylspirocyclohexyl)-bicyclo[3.3.0]octane-*c*-5-yl}-methoxypyrazine (2b-*cis*)

According to the typical procedure for metallation and the same reaction conditions (**Scheme 4**), the mixture was quenched with water as 1:1:1 v/v/v mixture with EtOH/THF at -78 °C. After typical preliminary work up, the isolated compound (in 90% yield as *crude product*) exhibited identical NMR spectra with only the major

component **2b-cis** from the already described mixture **2b-cis, -trans**. After identification, the compound was simply crystallised from pentane; mp 77-78 °C. Scale up of the synthesis: 0.5 mmol mixture **2b-cis, -trans**.

REFERENCES

1. Mongin, F.; Quéguiner, G. *Tetrahedron* **2001**, *57*, 4059-4090
2. Turck, A.; Plé, N.; Mongin, F.; Quéguiner, G. *Tetrahedron* **2001**, *57*, 4489-4505
3. Pollet, P.; Turck, A.; Plé, N.; Quéguiner, G. *J. Org. Chem.* **1999**, *64*, 4512-4515
4. Zhang, C. Y.; Tour, J. M. *J. Am. Chem. Soc.* **1999**, *121*, 8783-8790
5. Lavergne, O.; Lesueur-Ginot, L.; Pla Rodas, F.; Kasprzyk, P. G.; Pommier, J.; Demarquay, D.; Prévost, G.; Ulibarri, G.; Rolland, A.; Schiano-Liberatore, A.-M.; Harnett, J.; Pons, D.; Camara, J.; Bigg, D. C. H. *J. Med. Chem.* **1998**, *41*, 5410-5419
6. Henegar, K. E.; Ashford, S. W.; Baughman, T. A.; Sih, J. C.; Gu, R.-L. *J. Org. Chem.* **1997**, *62*, 6588-6597
7. Sammakia, T.; Hurley, T. B. *J. Org. Chem.* **1999**, *64*, 4652-4664
8. Remuzon, P.; Bouzard, D.; Jacquet, J. -P. *Heterocycles* **1993**, *36*, 431-434
9. Darabantu, M.; Mager, S.; Plé, G.; Puscas, C. *Heterocycles* **1995**, *41*, 2327-2356 and the literature cited therein.
10. Darabantu, M.; Plé, G.; Mager, S.; Gaina, L.; Cotoră, E.; Mates, A.; Costas, L. *Tetrahedron* **1997**, *53*, 1891-1908
11. Darabantu, M.; Plé, G.; Maierănu, C.; Silaghi-Dumitrescu, I.; Ramondenc, Y.; Mager, S. *Tetrahedron* **2000**, *56*, 3799-3816; see patents cited therein and related to the subject.
12. Maierănu, C.; Darabantu, M.; Plé, G.; Berghian, C.; Condamine, E.; Ramondenc, Y.; Silaghi-Dumitrescu, I.; Mager, S. *Tetrahedron* **2002**, *58*, 2681-2693
13. Eliel, E. L.; Wilen, H. S. *Stereochemistry of the Organic Compounds*; John Wiley & Sons, Inc. 1994; pp 488 – 492, 1199
14. Manuscript in preparation
15. Ward, J. S.; Merritt, L. *J. Heterocycl. Chem.* **1991**, *28*, 765-768
16. Turck, A.; Trohay, D.; Mojovic, L.; Plé, N.; Quéguiner, G. *J. Organomet. Chem.* **1991**, *412*, 301-310
17. Bax, A.; Griffey, R. H.; Hawkins, B. L. *J. Magn. Reson.* **1983**, *55*, 301-315
18. Bax, A.; Subramanian, S. *J. Magn. Reson.* **1986**, *67*, 565-569
19. Bax, A.; Summers, M. F. *J. Am. Chem. Soc.* **1986**, *108*, 2093-2094
20. Willker, W.; Leibfritz, D.; Kerssebaum, R.; Bermel, W. *Magn. Reson. Chem.* **1993**, *31*, 287-292
21. Aue, W. P.; Bartholdi, E.; Ernst, R. R. *J. Chem. Phys.* **1976**, *64*, 2229-2246
22. Hurd, R. E. *J. Magn. Reson.* **1990**, *87*, 422-425
23. Jeener, J.; Meier, B. H.; Bachman, P.; Ernst, R. R. *J. Chem. Phys.* **1979**, *71*, 4546-4553
24. Parella, T.; Sanchez-Ferrando, F.; Virgili, A. *J. Magn. Reson.* **1997**, *125*, 145-148
25. Bothner-By, A. A.; Stephens, R. L.; Lee, J. M.; Warren, C. D.; Jeanloz, R. W. *J. Am. Chem. Soc.* **1984**, *106*, 811-813
26. Bax, A. A.; Davis, D. G. *J. Magn. Reson.* **1985**, *63*, 207-213
27. Duber, O.; Arnaud, G.; Condamine, E.; Piettre, S. *Org. Lett.* **2002**, *4*(3), 359-362

28. Pierce, S.; Lunsford, D. C.; Raiford Jr., R. W.; Rush, J. L.; Riley, D. W. *J. Am. Chem. Soc.* **1951**, *73*, 2595-2596
29. Pierce, S.; Lunsford, D. C. *J. Am. Chem. Soc.* **1951**, *73*, 2596-2598
30. Maiereanu, C.; Darabantu, M.; Plé, G.; Berghian, C.; Condamine, E.; Ramondenc, Y.; Silaghi-Dumitrescu, I.; Mager, S. *Tetrahedron* **2002**, *58*, 2681-2693
31. Sélambarom, J.; Monge, S.; Carré, F.; Roque, P. J.; Pavia, A. A. *Tetrahedron* **2002**, *58*, 9559-9566

EI-MS UNIDIRECTIONAL TRIPLE HYDROGEN REARRANGEMENT I. THE CASE OF LONG CHAIN PHENYLAZOBENZOATES

IOAN OPREAN ^{a)}, BIANCA MOLDOVAN ^{a)}, RADU OPREAN ^{b)}

^{a)}Faculty of Chemistry and Chemical Engineering, Organic Chemistry Department, "Babeş-Bolyai" University, 400028 Cluj-Napoca, Romania

^{b)}Faculty of Pharmacy, "Iuliu Hațieganu" University of Medicine and Pharmacy, Cluj-Napoca, Romania

ABSTRACT. The aim of our study was to determine the various hydrogen rearrangements in the mass spectra of some long chain esters. We demonstrated that in the EI-MS spectra of long chain phenylazobenzoates appears a triple hydrogen rearrangement ion because of the migration of the hydrogen from the hydrocarbonated part to the phenyl rest of the molecule if the chain has more than 8 carbon atoms. The abundance of this ion proceeds to the extent of 0,5% to 70% of the basis peak of the mass spectrum and it exhibits an increase with the increase of the chain length.

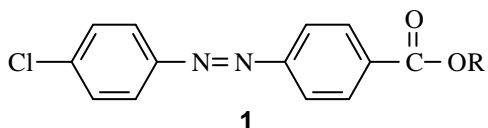
Keywords: mass spectrometry, hydrogen rearrangement, phenylazobenzoates

INTRODUCTION

Unidirectional double hydrogen rearrangement reactions are characteristic features in the mass spectra of many esters [1], whereas unidirectional triple hydrogen migrations are extremely rare [2]. This phenomenon was observed only in the particular case of alkyl esters of trimellitic anhydride.[3]

We have found that unidirectional hydrogen rearrangement reactions take place in the long chain esters of *p*-(4'-chlorophenylazo)benzoic acid **1** (CABE) with a greater probability that in the cases previously mentioned.

p-Phenylazobenzoates have been synthesized as useful derivatives of normal alcohols [4].



The main aim of the present work is to report the EI mass spectra of more than 20 *n*-alkyl esters of *p*-(4'-chlorophenylazo) benzoic acid (CABE), devoting our attention to the factors that influence the appearance and the abundance of the triple hydrogen rearrangement ions.

EXPERIMENTAL

The saturated alcohols used were commercially available and obtained from Analabs (Germany) as a fatty alcohol kit, and odd carbon alcohols were purchased from Sigma Chemical Co. and used without further purification.

Mass spectra were recorded on a GC-MS system, at 70 eV, model Hewlett-Packard 5890 II/5972.

For the synthesis of *p*-(4'-chlorophenylazo)benzoates **1** we had to adapt the method of Hecker [5] to microscale. A mixture of 2,8 mg *p*-(4'-chlorophenylazo) benzoyl chloride (0,01 mM), the appropriate alcohol (0,015 mM), 10 μ L pyridine and 1 mL benzene was left standing for 24 h by room temperature. The benzene solution was successively extracted twice with 0,1 N H₂SO₄, saturated NaHCO₃ solution and water, dried over sodium sulfate and filtered. The benzene solution was chromatographically separated on silicagel using benzene as eluent and the solvent was removed.

RESULTS AND DISCUSSION

Figures 1 and 2 show the EI mass spectra (70 eV) of *n*-butyl (C₄-CABE) and *n*-tetradecyl *p*-(4'-chlorophenylazo)benzoate (C₁₄-CABE), respectively.

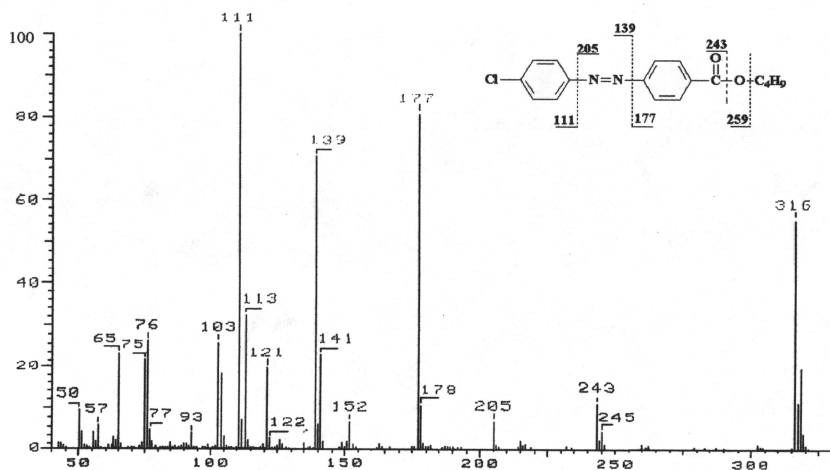


Fig. 1. Mass spectrum of *n*-butyl-*p*-(4'-chlorophenylazo)benzoate **1d** (C₄-CABE)

From Fig.1 it is apparent that, in the case of the *n*-butyl *p*-(4'-chlorophenylazo) benzoate (C₄-CABE), the most abundant ions are generated by alternative C-N cleavage of phenylazo group [6] (m/z: 111, 139, 177, 205). Cleavage of the acyl-oxygen bond generates the m/z ion 243 (10%), while an oxygen-alkyl cleavage with concurrent transfer of one or two hydrogen atoms (m/z 260, respectively m/z 261) characteristic for *n*-butyl benzoate [1] has a minimal importance. (<1%).

On the contrary, it was found from Fig.2 that, in the case of *n*-tetradecyl *p*-(4'-chlorophenylazo) benzoate (C₁₄-CABE) the peak of m/z ion 261 (28%) corresponding to the oxygen-alkyl cleavage with transfer of two hydrogens is accompanied by a more abundant peak at m/z 262 (53%) corresponding to a triple hydrogen transfer. Interesting was to remark that no C-C cleavage in the long chain of the ester was observed in contrast to the other esters [7]. Partial spectra of C₁-C₁₈ alkyl *p*-(4'-chlorophenylazo)benzoates are shown in the Table 1.

From the Table 1 is to be observed that, compounds **1a-1d** (C₁-C₄ CABE) show very similar spectra with the *n*-butyl-*p*-(4'-chlorophenylazo)benzoate (C₄-CABE) from Fig.1. In the spectra of **1e-1g** (C₅-C₇ CABE) the peak m/z 260 (1H transfer)

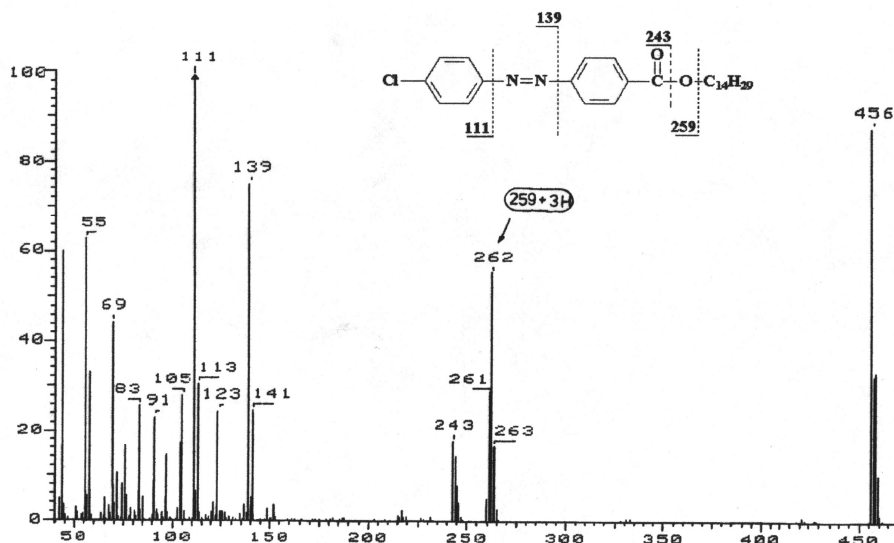


Fig. 2. Mass spectrum of *n*-tetradecyl-*p*-(4'-chlorophenylazo)benzoate **1n** (C₁₄-CABE)

Table 1
Partial EI-MS spectra of *n*-alkyl *p*-(4'-chlorophenylazo)benzoates **1** (R=alkyl) (C₁-C₁₈ CABE)

Crt. No.	R	Relative intensity of ions (%) (base peak=100)	
		261* (2H)	262* (3H)
1a	CH ₃	-	-
1b	C ₂ H ₅	-	-
1c	C ₃ H ₇	-	-
1d	C ₄ H ₉	-	-
1e	C ₅ H ₁₁	0,6	-
1f	C ₆ H ₁₃	1,0	-
1g	C ₇ H ₁₅	1,7	-
1h	C ₈ H ₁₇	3,4	0,5
1i	C ₉ H ₁₉	6,0	8,0
1j	C ₁₀ H ₂₁	7,2	7,0
1k	C ₁₁ H ₂₃	14,0	35,0
1l	C ₁₂ H ₂₅	19,2	30,0
1m	C ₁₃ H ₂₇	27,0	60,0
1n	C ₁₄ H ₂₉	27,0	53,0
1o	C ₁₅ H ₃₁	41,0	92,0
1p	C ₁₆ H ₃₃	35,0	70,0
1q	C ₁₇ H ₃₅	31,0	62,0
1r	C ₁₈ H ₃₇	42,0	87,0

* corrected for naturally occurring heavy isotopic contributions

becomes more intensive and appears a new peak at m/z 261 (2H transfer). The peak m/z 262 corresponding to a triple hydrogen transfer (3H) proceeds in the compounds **1h-1r** to the extent of 0,5-70% of the base peak of spectrum. The abundance of this ion exhibits an increase with the increase of chain's length. The same chain length dependence shows the abundance of the ions m/z 261 (2H transfer) and m/z 244 (m/z 262- H_2O).

From the Fig. 3 we can observe that this dependence is more accentuated in the case of triple hydrogen transfer ions (m/z 262).

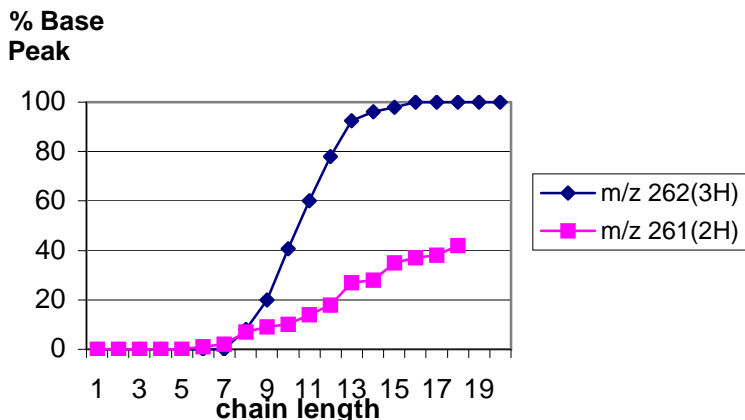
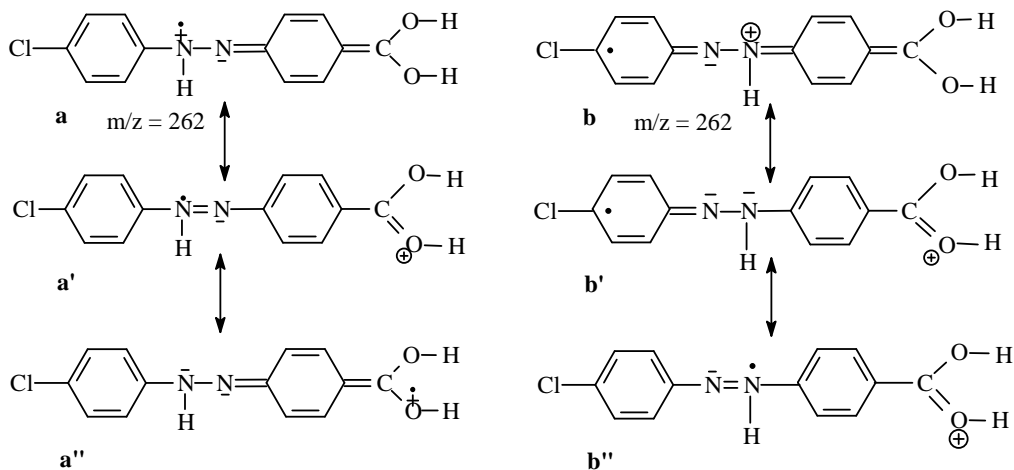


Fig. 3. Effect of chain length on relative intensities of rearranged ions in C_1 - C_{18} CABE

The genesis of the ion m/z 262 (3H) is possible to explain through a long-range intramolecular interaction between alkyl chain and nitrogen atoms of the azo group accompanied by the expected transfer of two hydrogens typical for carboxylic acid esters, in a similar manner with hydrogen migration in long chain esters of trimellitic anhydride [3]. The multiple resonance formula of this ions (a, a', a'' or b, b', b'') explain, probably, its great abundance.



CONCLUSIONS

In the EI-MS spectra of long chain phenylazobenzoates appears a triple hydrogen rearrangement ion because of the migration of the hydrogen from the hydrocarbonated part to the phenyl rest of the molecule if the chain has more than 8 carbon atoms.

REFERENCES

1. C. Djerassi and C. Fenselau, *J. Am. Chem. Soc.*, **1965**, *87*, 5756
2. S. Meyerson, I. Puskas and E.K. Fields, *J. Am. Chem. Soc.*, **1973**, *95*, 6056
3. J. Cable, C. Djerassi, *J. Am. Chem. Soc.*, **1971**, *93*, 3905
4. E. O. Woolfolk, F.E. Beach and S.P. McPherson *J. Org. Chem.*, **1955**, *20*, 391
5. E. Hecker, *Chem. Ber.*, **1955**, *88*, 1666
6. J.A. Vollmin, P. Pachlatko and W. Simon, *Helv. Chem. Acta*, **1969**, *52*, 737
7. S. Meyerson, E.S. Kuhn, I. Puskas, E. Fields, L. Leitch and T.A. Sullivan, *Org. Mass. Spectrom.*, **1983**, *18*, 110

EI-MS UNIDIRECTIONAL TRIPLE HYDROGEN REARRANGEMENT. II. THE CASE OF LONG CHAIN BENZOATES

BIANCA MOLDOVAN ^{a)}, IOAN OPREAN ^{a)}, RADU OPREAN ^{b)}

^a Faculty of Chemistry and Chemical Engineering,
Organic Chemistry Department "Babeş-Bolyai"
University, 400028 Cluj-Napoca, Romania

^b Faculty of Pharmacy, "Iuliu Hațieganu" University
of Medicine and Pharmacy, Cluj-Napoca, Romania

ABSTRACT. Similarly with our previously reported EI-MS spectra of long chain phenylazobenzoates, unidirectional triple hydrogen rearrangement was also observed in the series of some diazobenzoates and analog long chain esters as well as in the series of some benzoate long chain esters containing electron withdrawing substituents in the aromatic moiety. The intensity of the triple hydrogen rearrangement ion is in good agreement with σ - Hammett values.

Keywords: EI-MS spectrometry, triple hydrogen rearrangement, σ - Hammett, benzoates

INTRODUCTION

In a previous work [1] we reported an unidirectional triple hydrogen rearrangement in the mass spectra of some long chain chlorophenylazobenzoates.

Unidirectional double hydrogen rearrangement reactions are characteristic features in the mass spectra of many esters [2], whereas unidirectional triple hydrogen migrations are extremely rare [3]. This phenomena was observed only in the particularly case of the *n*-alkyl esters of the trimellitic anhydride.[4].

The aim of the present work was to determine if the chlorine atom, the azo-group or the aromatic ring have an influence on the occurrence and the abundance of the triple hydrogen rearrangement ion. Therefore, we intended to synthesize a series of *n*-alkyl esters of phenyldiazobenzoates without the chlorine atom in the *p*'-position as well as series with modified diazo-group.

EXPERIMENTAL

The saturated alcohols used were commercially available and obtained from Analabs (Germany) as a fatty alcohol kit, and odd carbon alcohols were purchased from Sigma Chemical Co. and used without further purification.

Mass spectra were recorded on a GC-MS system, at 70 eV, model Hewlett-Packard 5890 II/5972.

The tetradecyl ester of N-(4-carboxybenzylidene) aniline **2** was prepared by the condensation of aniline with the tetradecyl ester of terephthalaldehydic acid by refluxing 4 hours in benzene and in the presence of catalytic amounts of toluene-*p*-sulfonic acid, in analogy with the alkyl N-benzylideneanthranylates [5].

The tetradecyl ester of 4-carboxyl-N-(benzylidene)aniline **3** was prepared by the condensation of benzaldehyde with the tetradecyl *p*-aminobenzoate in benzene 4 hours under reflux in the presence of catalytic amounts of toluene-*p*-sulfonic acid, in analogy with the alkyl N-benzylideneanthranylates [5].

The tetradecyl ester of 4-carboxystilbene **4** was prepared by the condensation of cinnamic acid with the diazonium salt of tetradecyl *p*-aminobenzoate in analogy with other alkyl esters of 4-carboxystilbene [6].

The tetradecyl *p*-aminobenzoate **5** was prepared by treatment of the sodium *p*-aminobenzoate with myristyl bromide (Sigma) in dimethylformamide at 130°C, in analogy with other long chain benzoates [7].

Substituted alkyl benzoates **6-11** were prepared from different benzoyl chlorides, tetradecyl alcohol, pyridine and benzene. The initial mixture was refluxed for one hour [8]. The corresponding nitro- and cyanobenzoyl chlorides are commercially available products (Sigma). The terephthalaldehydic acid chloride was prepared by boiling the terephthalaldehydic acid with thionyl chloride [9].

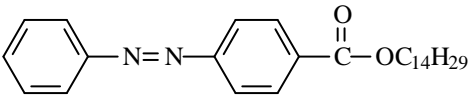
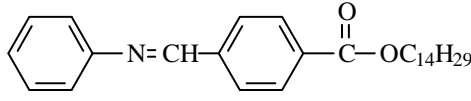
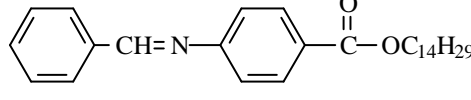
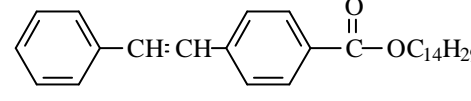
The tetradecyl *p*-nitrobenzenesulfonate **12** was prepared from commercial *p*-nitrobenzenesulfonyl chloride and myristyl alcohol in analogy with other long chain benzenesulfonates[10].

RESULTS AND DISCUSSION

The triple hydrogen rearrangement is not limited to the mass spectra of long chain esters of *p*-(4'-chlorophenylazo)benzoates previously described [1]. In Table 1 are presented some selected data from the mass spectra of different aromatic long chain esters. From the examples it is to conclude that the presence of the chlorine atom in the phenylazobenzoates is not necessary, but it is useful for fragments identification.

Table 1

The occurrence of hydrogen transfer ions in some diazobenzoates and analog long chain esters

Comp. No.	Structure	Rel. Int* %		
		[1H]	[2H]	[3H]
1		4	24	33
2		8	100	2
3		27	42	13
4		1	0,5	-

* corrected for naturally heavy occurring isotopic contributions

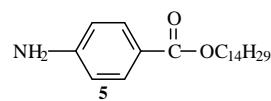
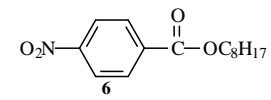
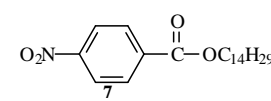
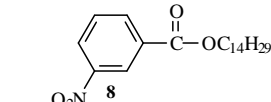
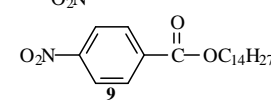
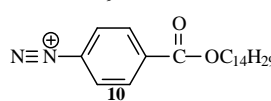
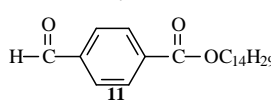
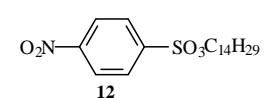
By alternative replacement of one nitrogen atom from the N=N group with CH group in the compound **1**, the abundance of the ion m/z 227 corresponding to the triple hydrogen migration decreases (compounds **2** and **3**). By replacement of both nitrogen atoms with CH=CH group the triple hydrogen migration disappears altogether (compound **4**).

This fact suggests that the substituent from the *para*-position of the benzoate ester may influence the appearance of the triple rearranged ion. To elucidate this supposition we studied the mass spectra of some benzoate long chain esters with different substituents on the aromatic ring. (Table 2)

The mass spectra of unsubstituted [1] *p*- and *m*-methoxy- as well as *p*-amino long chain long chain benzoates show no triple hydrogen rearrangement.

Table 2

The occurrence of hydrogen transfer ions in some substituted aromatic long chain esters

Structure	Rel. Int* %		
	[1H]	[2H]	[3H]
	100	8	-
	1	34	17
	1	37	81
	4	8	23
	1	29	76
	2	93	22
	2	100	57
	-	5	3

*corrected for naturally occurring heavy isotopic contributions

The presence of a NO₂, CN, or CHO group in the *p*- or *m*- position in the long chain benzoates appears to be essential for the triple hydrogen transfer. This substituent effect on the triple hydrogen transfer is in good agreement with Hammett's σ_p values (Table 3).

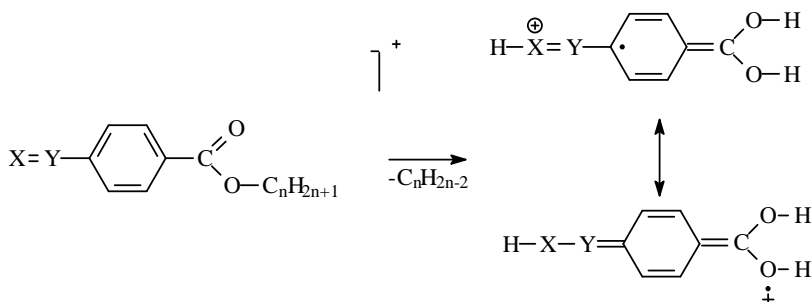
Table 3

The abundance *p*-X-C₆H₄COOH₃/*p*-X-C₆H₄COOH₂ ratio and the σ_p values for several alkylbenzoates

X	[3H]/[2H]	σ_p
NH ₂	0	-0,66
OCH ₃	0	-0,27
H	0	0
CN	0,24	0,66
CHO	0,57	0,22
N=N-C ₆ H ₅	1,37	0,64
NO ₂	2,19	0,778

CONCLUSIONS

It may be concluded that electron withdrawing substituents in long chain benzoates favorise the building of triple hydrogen transfer ions. This phenomenon is present in the corresponding substituted long chain sulphonates too.



In view of their intrinsic interest as well as their significant mechanistic implications, we are continuing in our laboratory the examination of unidirectional triple hydrogen rearrangements in long chain compounds.

REFERENCES

1. I.Oprean, B. Moldovan, R. Oprean, *Studia Chem.* **2003**
2. C. Djerassi and C. Fenselau, *J. Am. Chem. Soc.*, **1965**, *87*, 5756
3. S. Meyerson, I. Puskas and E.K. Fields, *J. Am. Chem. Soc.*, **1973**, *95*, 6056
4. J. Cable, C. Djerassi, *J. Am. Chem. Soc.*, **1971**, *93*, 3905
5. D. Johnston, G.W. Smart and D. Smith, *Org. Mass Spectrom.*, **1984**, *11*, 609
6. H. Meerwein, E. Büchner and K. vanEmster, *J. Prakt.Chem*, **1939**, *152*, 237
7. M. Winnik and P.T. Kwong, *Org. Mass Spectrom.*, **1976**, *10*, 346
8. L. McMaster and F. F. Ahman, *J. Am. Chem. Soc.*, **1928**, *50*, 145
9. H. Simonis, *Chem. Ber.*, **1912**, *45*, 1584
10. D.A. Shirley, G.A. Smith, M.Brown and W. Reedy, *J. Org. Chem.*, **1952**, *17*, 199

SYNTHESIS AND REACTIVITY OF DIFLUOROMETHYLENE BRIDGED DIPHOSPHA-DERIVATIVES

R. TÖTÖS, I. SILAGHI-DUMITRESCU*

*"Babeș-Bolyai" University, Faculty of Chemistry and Chemical Engineering,
Arany János Street, Nr. 11; 400028 Cluj-Napoca, Romania*

INTRODUCTION

The chemistry of organophosphorus compounds has been developing very rapidly in the last four decades. This is primarily due to the considerable theoretical and especially practical importance of these compounds. The application of organophosphorus compounds as insecticides in agriculture, medicine, extractants, flotation agents in mining, plasticisers and stabilizers for polymers, antioxidants for lubricating oils, and the manufacture of non-combustible fabrics and materials are well known.^{1,2,3}

Some α -fluorinated alkanephosphonic acids such as difluoromethane-diphosphonic acid^{4,5,6} have already been the subjects of interest as analogues of biological phosphoryl species. There is generally a conspicuous lack of methods for the preparation of other difluoromethanephosphonates. Such compounds have been postulated to possess biologically superior properties to those of analogous nonhalogenated phosphonates. However, there are generally few synthetic methods available, which lead to other difluoromethane-phosphonates.⁷

Difluoromethylene bridged diphospha-derivatives were obtained for the first time by D. J. Burton and R.M. Flynn,⁸ using the Michaelis-Arbuzov rearrangement. The same authors have obtained also the difluoromethane diphosphonic acid, which is a stable and strong acid.⁵ This analogous of the pyrophosphoric acid ($H_2P_4O_7$) has a much bigger stability of the P–C–P motif toward hydrolysis in comparison with the P–O–P motif. From this reason difluoromethane diphosphonic acid can be used as chelating agent (bidentate ligand) for the modification of the properties of biological systems.

Unlike other substituents, fluorine does not introduce large steric perturbations and imparts increased hydrolytic stability as well as oxygen solubility. These properties make them useful compounds in other applications, e.g., as substitutes for additives to H_3PO_4 in fuel cell electrolytes.⁹

Inhibition of acetylcholinesterase by organophosphorus compounds is generally responsible for their acute toxicity.^{10,11,12} Difluoromethylenediphosphonic acid was not found to be toxic, diphosphonates of the type P–C–P are valuable agents in the regulation of calcium metabolism in experimental laboratory animals and are potentially useful therapeutic agents for diseases involving abnormal calcification and excessive bone resorption.⁴

1. Building up the P–CF₂–P Skeleton

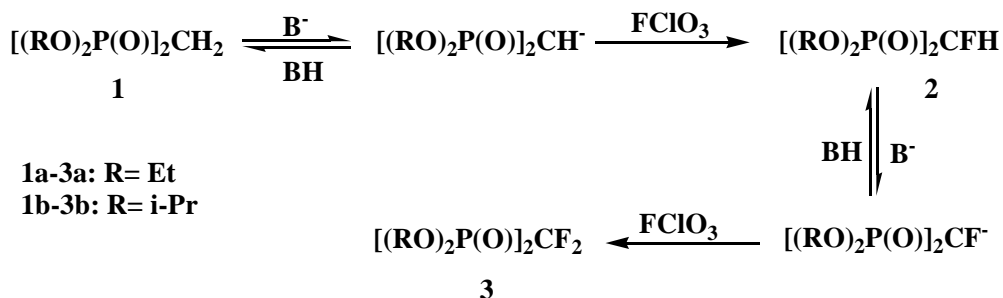
1.1. Fluorination of a methylenediphosphonate with $FCIO_3$

There are just a few methods for building up the P–CF₂–P skeleton using mono- and diphosphonous compounds as starting materials. One of these methods uses the acidity of the methylene group of the tetraethyl methylenediphosphonate.

Methylenediphosphonates can be metalated with sodium, potassium, sodium hydride and *n*-butyllithium. The metalated methylenediphosphonates can be alkylated with active organic halides. They also can be halogenated with bromine, sodium hypochlorite¹³ or perchlorofluoride^{6,14}, obtaining the corresponding mono- and dihaloderivatives.

Perchloryl fluoride must have been used as an electrophilic fluorinating agent, because fluorine gas, perfluoropiperidine or perfluoro-2,6-dimethyl-piperidine each led to partial fluorine substitution of hydrogens at all possible sites in tetraethyl methylenediphosphonate.

Treatment of the sodium salt of tetraethyl methylenediphosphonate with an excess of FCIO_3 in THF or toluene, results in the formation in good yields of tetraethyl-monofluoromethylenediphosphonate mixed with difluoromethylenediphosphonate (Scheme 1).^{6,14}



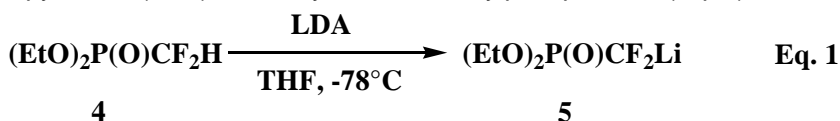
Scheme 1. Fluorination of methanediphosphonate esters with FCIO_3

The fluorination reaction proceeds as a titration of base with perchloryl fluoride and shows a readily recognizable endpoint marked by a characteristic color change from dark pale to yellow. The ratio of the mono- and difluorinated products depends on the choice of conditions, and is about $\mathbf{2b:3b} = 4:1$ using NaH as base and THF as solvent. By suitable adjustment of the proportion of starting materials, either product can be made to predominate. Using 1 equiv. of potassium *tert*-Butoxide as base, tetraisopropyl monofluoromethane-diphosphonate (**2b**) was obtained in 48% yield, with 2 equiv. of the base, the difluoro (**3b**) derivative could be prepared directly in 43% yield, with an increase to 73% being possible on further reaction of the monofluoroproduct.

Compounds **2** and **3** cannot be separated easily by fractional distillation due to their similar boiling points. They can be readily separated by conventional or flash chromatography on silica gel using ethylacetate/ethanol (9:1) as eluent.⁶

1.2. Reaction of dialcoxyphosphoryldifluoromethane with LDA

Another method for building a $\text{P-CF}_2\text{-P}$ skeleton uses the action of lithium diisopropylamide (LDA) on diethyl difluoromethylphosphonate (Eq. 1).^{15,16}

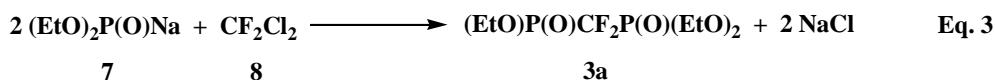


Addition of diethylchlorophosphate as electrophile to the organolithium compound gave tetraethyl difluoromethylenediphosphonate in good yield (74%) (Eq. 2).¹⁶



1.3. Direct method: Synthesis from Dialkylsodiophosphite and CF_2X_2 ($\text{X}=\text{Cl}, \text{Br}$)

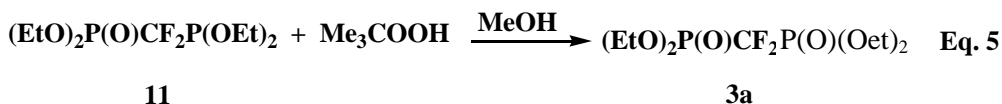
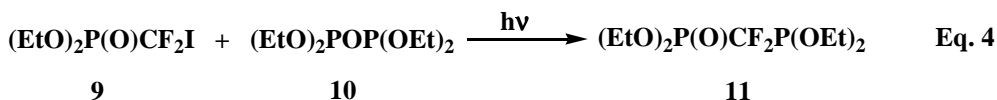
Using the Michaelis-Becker reaction between diethyl sodiophosphite in toluene and CF_2Cl_2 , tetraethyl difluoromethylenediphosphonate can be obtained with 40% yield (Eq. 3).¹⁷



Using CF_2Br_2 instead of CF_2Cl_2 **3a** could be also obtained but presents difficulties by isolation due to the increased side product formation and gives low yields.^{8,18,19} The advantage of using CF_2Br_2 over the CF_2Cl_2 is, the easier handling of CF_2Br_2 , being a liquid.

1.4. The photochemical method

Bisphosphonates can be obtained also by a photochemical procedure.²⁰ The reaction of $(\text{EtO})_2\text{P}(\text{O})\text{CF}_2\text{I}$ and $(\text{EtO})_2\text{POP}(\text{OEt})_2$ under UV light (254 nm) resulted in the corresponding mixed P^{III} and P^{V} intermediate $(\text{EtO})_2\text{P}(\text{O})\text{CF}_2\text{P}(\text{OEt})_2$, which affords the bisphosphonate **3a** $[(\text{EtO})_2\text{P}(\text{O})]_2\text{CF}_2$ upon oxidation (Eq. 4 and Eq. 5).²¹

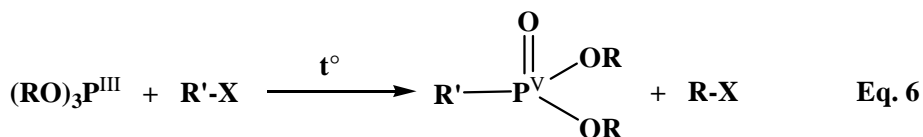


A disadvantage of this method is the use of the precursor **9**, which requires a multistep synthesis.^{18,22}

1.5. The Michaelis-Arbuzov Reaction

The Michaelis-Arbuzov rearrangement is one of the most versatile pathways for the formation of carbon-phosphorus bonds, and involves the reaction of an ester of trivalent phosphorus with alkyl halides. This can be used as the first step for the synthesis of the CF_2 bridged diphosphorus esters and its derivatives. The reaction was discovered by Michaelis²³ in 1898 and studied in detail by Arbuzov²⁴ and other researchers.

The Arbuzov rearrangement is the reaction of an alkyl halide with a trialkyl phosphite, yielding a dialkyl alkylphosphonate (Eq. 6).



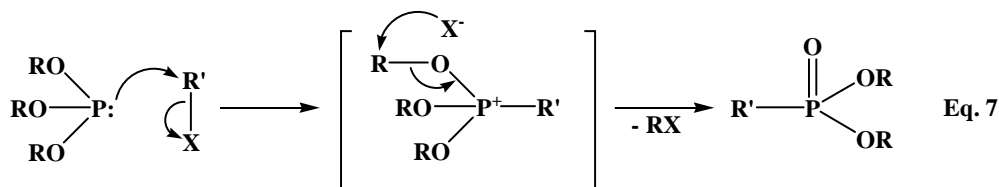
R = alkyl (aryl, etc.)

R' = alkyl (aryl, etc.)

X = Cl, Br, I

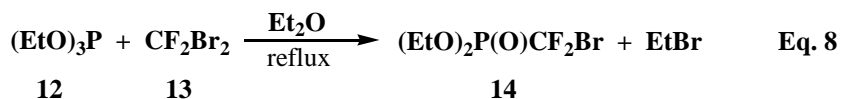
Thus, during the transformation, a trivalent phosphorus (P^{III}) is converted into a pentavalent phosphorus (P^{V}). In general, the alkyl group of the halide gets attached to the phosphorus, and one alkyl group from the phosphite combines with halogen to form the new alkyl halide.²⁵⁻²⁷

The mechanism of a normal Michaelis-Arbuzov reaction involves two $\text{S}_{\text{N}}2$ processes (Eq. 7).

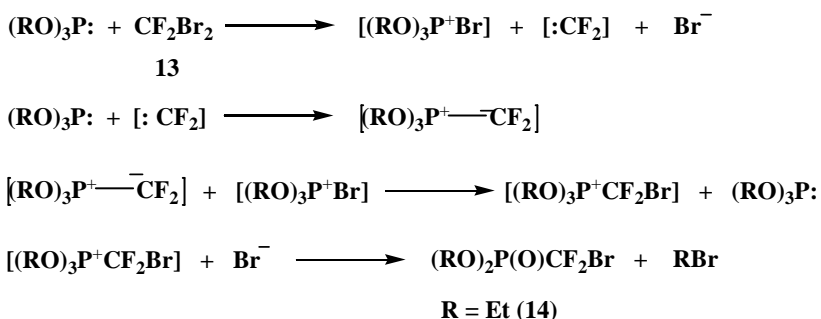


The lone pair of electrons of the phosphite attacks the alkyl group of the alkyl halide to form the addition compound in which the alkyl groups R' gets attached to the phosphorus, *i.e.* phosphorus-carbon bond forming step. At higher temperatures the quasiphosphonium cation undergoes nucleophilic attack on the alkyl rest of a P-O-R motive, through its own cation X' , resulting in the formation of the P=O bond and the elimination of the alkyl group as the new alkyl halide. When the alkyl groups of the phosphite and the alkyl halides are identical ($\text{R}=\text{R}'$), the process resumes to the isomerisation of the phosphite.

In this manner reacts triethylphosphite with dibromodifluoromethane to give bromodifluoromethylphosphonate **14** (Eq. 8).^{5,8,28-30}



In contrast to the normal Michaelis-Arbuzov reaction ($\text{S}_{\text{N}}2$ mechanism), the bromo-F-methylphosphonate esters are formed *via* a carbene trapping mechanism (Scheme 2).³¹

**Scheme 2.** The carbene trapping mechanism

Using triethylphosphite as reactant and diethyl ether as solvent, compound **14** could be obtained with excellent yield (Y95%).²⁸

Table 1.

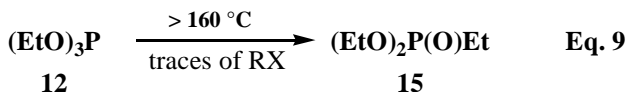
Yields of **14** as function of **R** and the solvent used

R	Solvent	(RO) ₂ P(=O)CF ₂ Br % 14
Me	TG	55
Et	Et ₂ O	95
Et	TG	55
<i>n</i> -Bu	Et ₂ O	65
<i>i</i> -Pr	TG	42

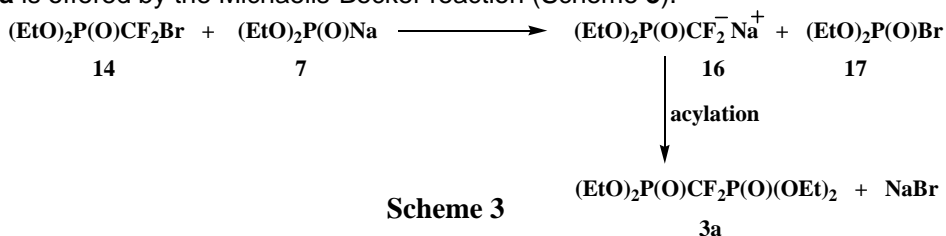
TG - tetraglyme; Et₂O – diethyl ether

Tetraethyl difluoromethylenediphosphonate **3a** cannot be obtained through another Michaelis-Arbusov reaction between **12** and **14**.

Heating the reaction mixture at higher temperatures (>160 °C) the triethylphosphite **12** undergoes an internal Michaelis-Arbusov rearrangement, due to the presence of the alkyl halide rests from the former reaction, which acts as a catalyst for the internal rearrangement (Eq. **9**).^{26,27}

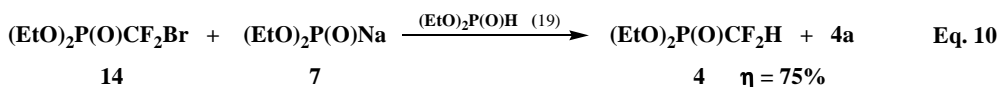


An alternative route in order to obtain the desired difluoromethylenediphosphonate **3a** is offered by the Michaelis-Becker reaction (Scheme **3**).^{5,31}

**Scheme 3**

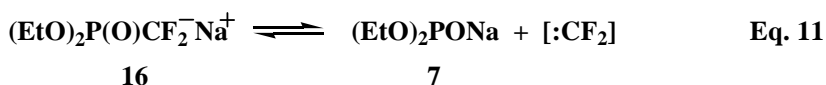
The mechanism of this Michaelis-Becker type reaction (**Scheme 3**) involves not an S_N2 displacement of bromide by phosphite, but rather a positive halogen extraction of bromine followed by *in situ* acylation of the phosphate ylide **16**, to give the desired diphosphonate **3a**.

Evidence for the bromonium ion extraction in the initial step is the formation of the reduced phosphonate **4**, when the reaction is carried out in the presence of dialkyl phosphite, i.e. incomplete reaction of diethyl phosphite with Na in order to obtain **7** observed by Burton et. al.⁸ (Eq. 10).



The same authors observed also a scrambling of the difluorocarbene by using bromo-difluoromethyl dibutylphosphonate and sodium diethylphosphite in order to obtain the mixed bisphosphonate, which was always accompanied by one or two symmetrical diphosphonates.⁸

There is equilibrium between compounds **7** and **16** (Eq. 11).



Despite the moderate yield,³¹ the Michaelis-Becker reaction remains the best route to symmetrical bis-phosphonates.

2. Reactivity of difluoromethylene bridged diphospha-derivatives

2.1. Transesterification of difluoromethylenediphosphonates

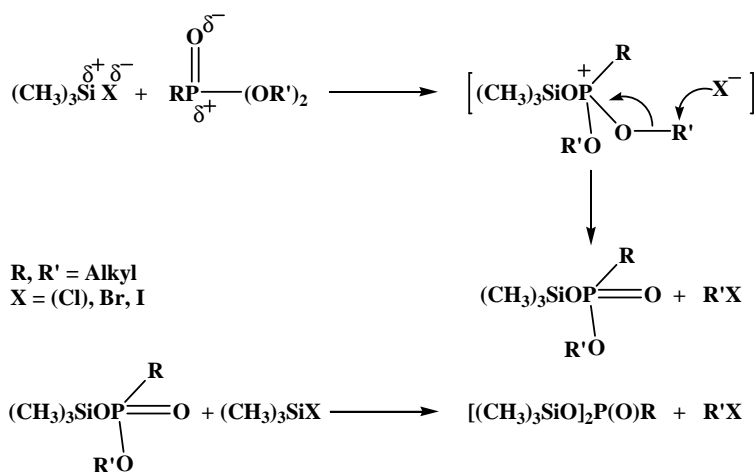
Reaction of phosphonates with PCl_5 in order to obtain halogenated phosphonates is a well-known method, but unfortunately cannot be used for the synthesis of halogenated alkylene-bisphosphonates.^{1,32} The corresponding phosphonic acid cannot be chlorinated with PCl_5 because its insolubility in inert solvents suitable for chlorination, and obtaining such a phosphonic acid directly from alkylphosphonates requires an vigorous hydrolytic route resulting in the cleavage of one or more P–C bonds.⁵

A cleavage of the P–C bonds can be avoided using bis-(trimethylsilyl) phosphonates, which reacts with PCl_5 under mild and neutral conditions.³³

Bis-(trimethylsilyl)phosphonates can be obtained through dealkylation of phosphonic acid dialkyl esters by bromotrimethylsilane.^{5-7,34,35}

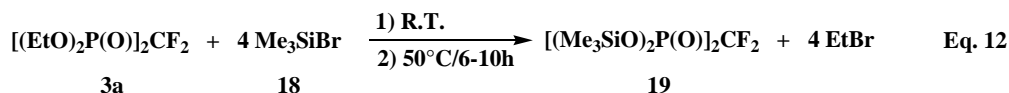
The mechanism of the silylation proposed by Rabinowitz³⁶ is shown in **Scheme 4**.

The attack of the silicon over the phosphoryl oxygen atom (P=O) is followed by the attack of the halogene X^- on the esters alkyl group, with the formation of the alkyl-trimethylsilyl mixed ester. A second series of the above mentioned reactions lead to the formation of the bis(trimethylsilyl)phosphonate. According to this mechanism where the halogen ion is involved as nucleophile and leaving group at the same time, it's evident that the process is accelerated in function of the X as follows: $V_{\text{Cl}} < V_{\text{Br}} < V_{\text{I}}$, and the reaction conditions become more and more milder.³⁴

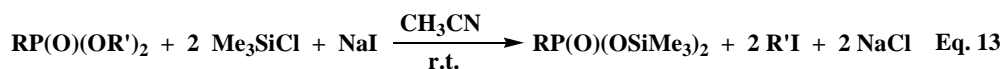


Scheme 4. Mechanism of the silylation of a phosphonate

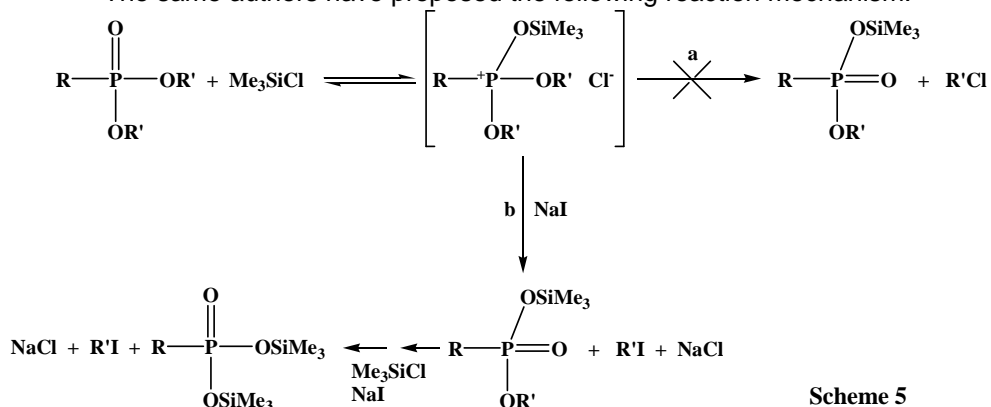
Using $(\text{CH}_3)_3\text{SiBr}$ as silylating agent, **19** can be obtained with high yield (Y 98%)^{5,37} corresponding to Eq. 12:



Another alternative method uses iodotrimethylsilane for dealkylation^{38,39}, which reacts easily with dialkylphosphonates at 10-40°C and with a high selectivity, carboxyl and other functional groups remaining unchanged.³⁸ Chlorotrimethylsilane mixed with alkaline bromides or iodides,^{33,40,41} is also a suitable dealkylating mixture, giving good results especially for the synthesis of phosphonic acids.



The same authors have proposed the following reaction mechanism:^{40,41}

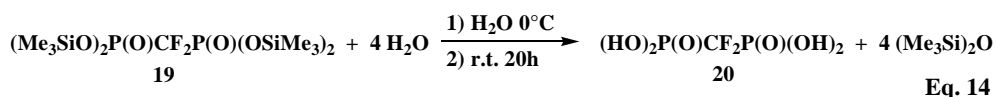


Scheme 5

The attack of the silicon on the sp^3 oxygen atom with the formation of the phosphonium intermediate is a fast and reversible step. The second step, the attack of the X^- ion on the phosphonium intermediate is slow and irreversible. Cl^- and I^- coexists in the reaction mixture and a competition between the attack of the Cl^- and the I^- , occurs; the latter being more nucleophile way **b** will be preferred, which leads to the formation of the monosilylated compound. With the repetition of this step the bistrimethylsilylphosphonate is obtained.⁴⁰

The trimethylsilyl esters are easily hydrolyzed under mild conditions to the corresponding phosphonic acids, which was the scope of the research in almost all cases.^{34,35,38}

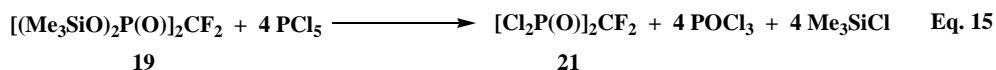
Hydrolysis of the bistrimethylsilylester **19** leads to the formation of difluoromethane-diphosphonic acid with almost 100% yield.⁵



Compound **24** was found to be a tetrabasic acid with three points of equivalence, corresponding to the neutralization of 2, 1, 1 acid protons. The acid constants were determined by titration with NaOH.^{5,6}

2.2. Synthesis of halogenated diphosphonates and diphosphonites

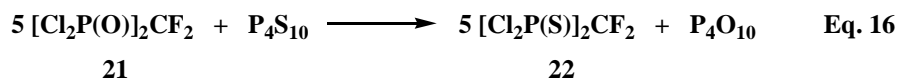
The chlorination of **20** can be carried out easily with PCl_5 at r.t. with an yield over 90% (Eq. **15**).^{1,7,33}



Because direct reduction of a $\text{P}=\text{O}$ bond to P^{III} proceeds quite difficult, the next step in order to obtain difluoromethylenebis-(dichlorophosphane) is the synthesis of difluoromethylenebis-(thiophosphonic dichloride).

Halogenated diphosphonates can be sulfurated with P_4S_{10} or PSCl_3 to bis-thiophosphonates with moderate yield.³²

In analogous way to the synthesis of methylenebis-(thiophosphonic dichloride) by Maier³² sulfuration of difluoromethylenebis-(phosphonic dichloride) was carried out with P_4S_{10} (Eq. **16**).



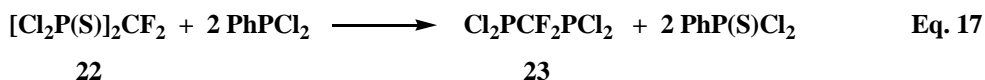
For this process temperatures over 190°C are needed, because in the case of incomplete reaction the mixture contains **21**, **22** and the asymmetric product $\text{Cl}_2\text{P}(\text{O})\text{CF}_2\text{P}(\text{S})\text{Cl}_2$ which cannot be separated by distillation at reduced pressure.

Adding catalytic amounts of AlCl_3 to the reaction mixture the yield of the process could be raised over 60%.⁴²

Through the high temperatures, cleavage of **21** and **22** occurs under the building of volatile compounds like POCl_3 , PSCl_3 , PCl_3 , which could be identified by ^{31}P -NMR spectroscopy.

The distillation residue contains P_4S_{10} , P_4O_{10} , $P_4S_xO_{10-x}$ ($x = 1-9$) and a difluoromethylene bridged compound $P_4S_4O_4(CF_2)_2$.⁴³

The P=S bond in thiophosphonates (**22**) can be easily reduced to P^{III} using Ph_2PCl ^{44,45} or $PhPCl_2$ ⁴⁶ as reducing agent. (Eq. 17).



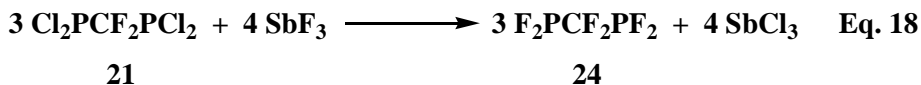
Compounds **21**, **22**, and **23** can serve as starting materials for the synthesis of non-cyclic derivatives, and using primary amines or hydrazines aza-diphosphetidines respectively diazadiphospholidines can be obtained through ring closure reaction.

Despite the high reactivity of the three above-mentioned compounds, they are much less studied than their methylene bridged analogues.

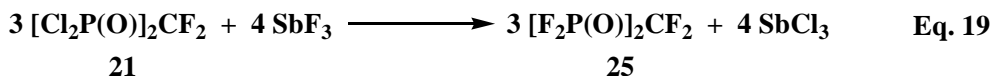
3. Synthesis of functional derivatives of the halogenated diphosphonates and diphosphonites

3.3.1. Fluorination of bis(dichlorides) **21**, **22**, and **23**

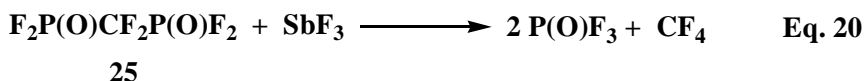
Organophosphorus fluorides can be obtained through halogen exchange of the corresponding chlorides (**21**, **22**, and **23**) with SbF_3 , AsF_3 or alkali halides.^{44,46}



Pentavalent compounds can be also fluorinated, but their receptivity towards fluorination is lower than that of trivalent derivatives. Fluorination of difluoromethanebis (phosphonic dichloride) can be achieved using AsF_3 or SbF_3 .

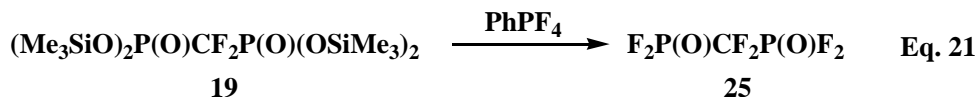


In this case the tetrafluoride **25** formed must be removed from the reaction mixture to avoid secondary reactions with the SbF_3 , which lead to the decomposition of the product:



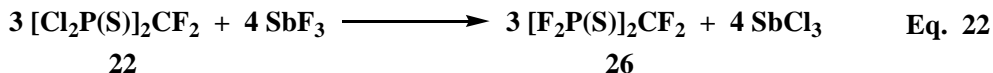
The decomposition proceeds rapidly and after short time the tetrafluorodiphosphonate is no more spectroscopically detectable.⁴²

Another route to obtain the tetrafluoride **25** is the treatment of the tetrasilyl ester **19** with $PhPF_4$ (phenyltetrafluorophosphorane):^{53,54}



In this case the decomposition of the tetrafluorobisphosphonate **25** is inevitable, its formation was proved spectroscopically, pure **25** couldn't be isolated through distillation.

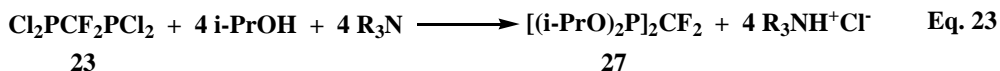
By the fluorination of difluoromethylenebis(thiophosphonic dichloride) cleavage of **22** and **26** was observed with the formation of volatile compounds. Among them F_3P and F_3PS were identified by gas IR spectroscopy.



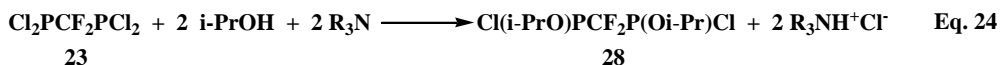
Fluoride **26** has been purified by distillation and analyzed by ^{31}P and ^{19}F -NMR spectroscopy.⁴³

3.3.2. Alcoholysis of bis(dichlorides) **21**, **22**, and **23**

Difluoromethylene bridged bis(phosphonic/phosphinic dichlorides) can be easily esterified with alcohols, in the presence of a base such as a tertiary amine or pyridine^{46,49,51} or with alkaline alcoholates (alkoxides).⁵¹ This way can be obtained esters, which gives low yields using the direct way (Arbuzov reaction) ($R = Me, Pr, i\text{-}Pr$).⁴⁶



Using 1:2 molar ratios of difluoromethylenebis(dichlorophosphane): alcohol+amine, difluoromethylenebis(phosphonochloridites) can be obtained with good yields,⁵⁰

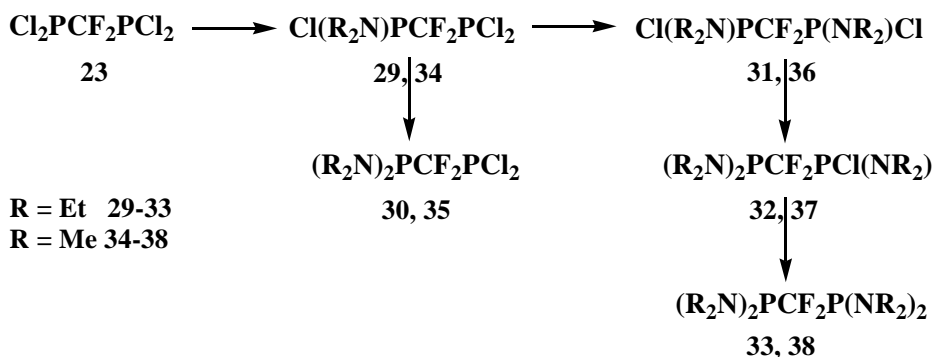


which can be further reacted with alcohols, amines, organometallic compounds forming different mixed substituted derivatives in form of stereoisomers.⁵²

3.3.3. Aminolysis of bis(dichlorides) **21**, **22**, and **23**

The synthesis of $-NR_2$ substituted diphosphorus derivatives can be achieved through the substitution of one or more halogens using dialkylamines or dialkylaminotrimethylsilanes.⁴⁸

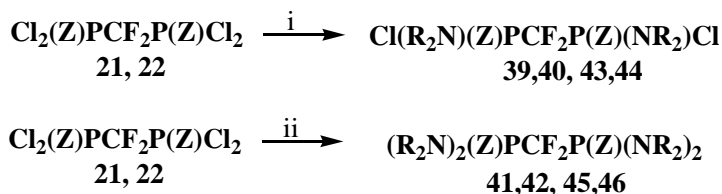
In the case of aminolysis of difluoromethylenebis-(dichlorophosphane) with dialkylamino-trimethylsilanes the reaction proceeds as in Scheme 6.



Scheme 6

Using 1:2 molar ratios of **23** and aminosilanes formation of pure **31**, and **36** was observed. No formation of the geminally disubstituted derivatives **30** and **35** was observed. Using 1:4 (or more) molar ratio of **23** and aminosilanes, pure **37** and **38** were obtained. At molar ratios under 1:2 and up to 1:4, the formation of mixtures is observed containing mono-, di-, and trisubstituted intermediates.⁴³

In the case of **21** and **22** reactions with dimethyl- and diethylamino-trimethylsilane are as follows (Scheme 7):



i: 2 R_2NSiMe_3

ii: 4 R_2NSiMe_3

$\text{R} = \text{Me}$, **39**, **41**, **43**, **45**

$\text{R} = \text{Et}$, **40**, **42**, **44**, **46**

$\text{Z} = \text{O}$, **39**, **40**, **41**, **42**

$\text{Z} = \text{S}$, **43**, **44**, **45**, **46**

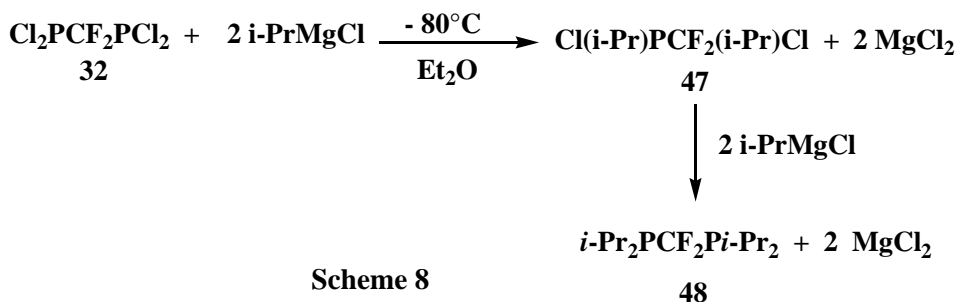
Scheme 7

Diamine **40** is formed also by a 1:0.67 ratios of **21**:aminosilane. The tetrasubstituted derivative **42** cannot be obtained using this method only by oxidation of **33** with DMSO at reduced temperatures. The substitution process stops at the stage of **40** even by the use of a 1:4 molar ratio of **21**:aminosilane. Using a molar ratio of 1:2 **21**:dimethylaminotrimethylsilane **39** can be isolated as single product. At 1:4 molar ratio **41** could be obtained in pure form in contrast to **42**. By molar ratios of **21**:aminosilanes under 1:2 and up to 1:4, formation of different mixtures is observed containing mono-, di-, and trisubstituted intermediates.⁴³ No formation of geminally disubstituted compounds was observed.

The aminolysis of difluoromethylenebis(thiophosphonic dichloride) (**22**) undergoes different as by **21**, only formation of mixtures are observed. The tetrasubstituted derivatives (**45**, **46**) can be obtained only by sulfuration of the corresponding trivalent compounds **33** and **38**.

3.3.4. Reactions with organometallic compounds

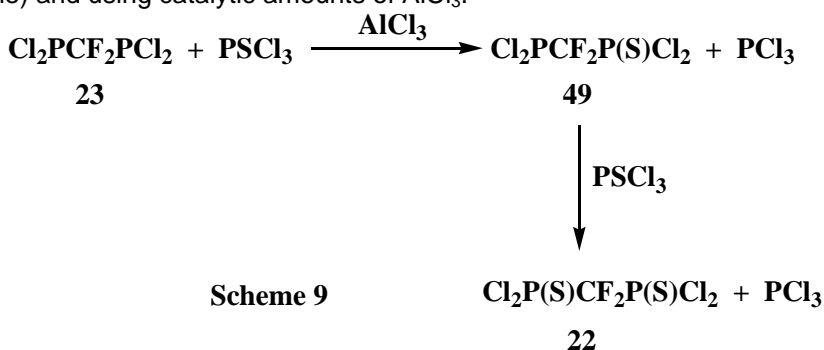
All difluoromethylene-bridged diphosphachlorides react easily with organometallic compounds. Reaction with *i*-PrMgCl proceeds in two steps, first the 1,3-disubstituted derivative is formed. Due to the sterical hindrance of the *i*-Pr group no geminally disubstituted derivative **47** is formed. In the second step (slow) the tetrasubstituted derivative **48** is formed, this is possible because the *i*-Pr group does not deactivate the phosphorus atoms.



The synthesis of tetrasubstituted compounds of the type $\text{R}_2\text{P}(\text{Y})\text{CF}_2\text{P}(\text{Y})\text{R}_2$ is limited to some cases ($\text{Y} = \text{e}^-$ pairs, $\text{R} = \text{i-Pr}$, Me) the yields are low, so an indirect method is preferred which uses the reaction of esters (PhO) with RMgl .⁵¹

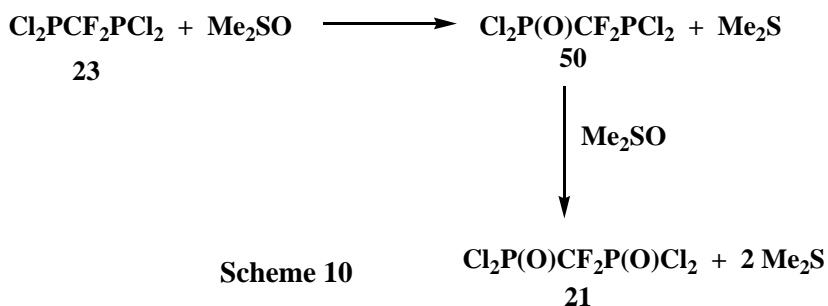
3.3.5. Oxidation and sulfuration of trivalent derivatives

Sulfuration of the trivalent derivatives can be achieved using elementary sulfur or thiophosphoryl trichloride (PSCl_3), in most cases in a high boiling solvent (toluene) and using catalytic amounts of AlCl_3 .⁴⁷



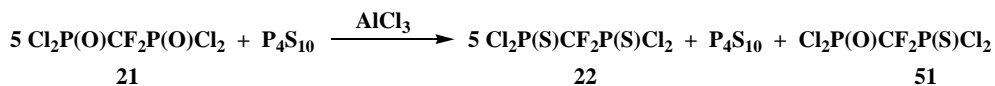
By the use of 1 equivalent of PSCl_3 the monosulfurated **49** is obtained, by the use of 2 equivalents or more of PSCl_3 only the disulfurated derivative **22** was obtained.

Oxidation of trivalent derivatives can be achieved using DMSO at low temperature (-80°C), the reaction is easily manageable, mono- and dioxides are obtained depending on the molar ratio $\text{P(III)}:\text{DMSO}$ used.⁴⁹



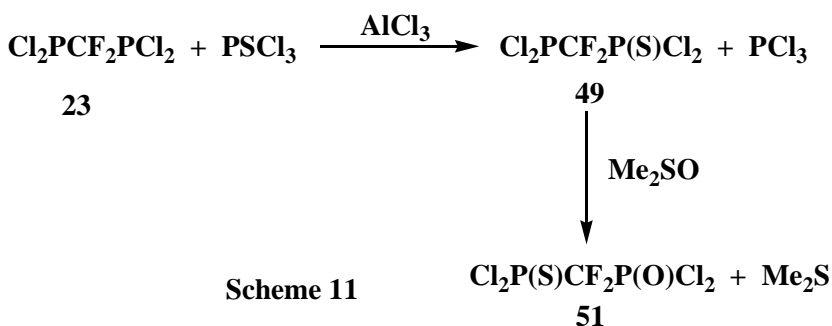
Through oxidation/sulfuration can be obtained some derivatives, which are formed as intermediates and cannot be separated from complex mixtures.

$\text{Cl}_2\text{P}(\text{O})\text{CF}_2\text{P}(\text{S})\text{Cl}_2$ (**51**), is obtained as an intermediate in the following reaction (Eq. 25):

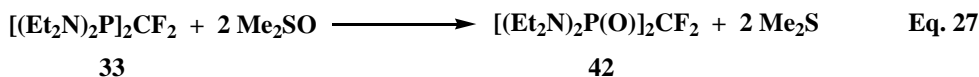
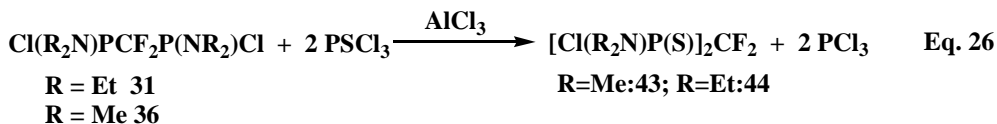


Eq. 25

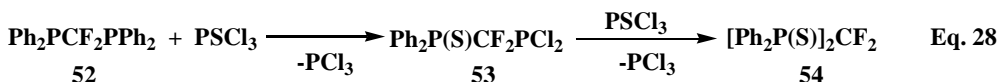
Pure (**51**) can be obtained by the following procedure, using two consecutive sulfuration/oxidation reactions:



Also some amines containing P(V), which cannot be obtained through direct aminolysis of the corresponding pentavalent compounds, are successfully synthesized through oxidation or sulfuration of the corresponding P(III) derivatives, e.g. Eq. 26 and Eq. 27:



Must be mentioned that not only halogenides but also phosphanes can be oxidized/sulfurated, for e.g. difluoromethylenebis(diphenylphosphane):



This sulfuration reaction proceeds slowly, after 7h/110 °C (toluene as solvent) ca. 10% of the asymmetric product **53** can be observed, for total sulfuration reflux for another 7h under the same conditions are required.

It can be concluded that the first oxidation (sulfuration) of a difluoromethylene bridged diphosphorus compound undergoes more rapidly, than the oxidation of the second phosphorus atom of the same molecule.⁵⁵

CONCLUSIONS

Difluoromethylene bridged diphospha-derivatives are easily obtained through the Michaelis-Arbuzov reactions from a trialkyl phosphite using CF₂Br₂. The halogenated compounds **21**, **22** and **23** can be used for the synthesis of a wide variety of functional derivatives by halogen exchange, alcoholysis, aminolysis, alkylation, arylation and oxidation.

Through reaction of the above mentioned dichlorides (**21**, **22** and **23**) with primary amines and hydrazines lead to the formation of four-, and five-membered ring-systems are expected.

REFERENCES

1. J. J. Richard, K.E. Burke, J.W. O'Laughlin, C.V. Banks, *J. Am. Chem. Soc.*, **1961**, *83*, 1722.
2. M. Duc, B. Boutevin, B. Ameduri, *J. Fluorine Chem.*, **2001**, *112*, 3.
3. A.N. Pudovik, G.E. Yastrebova, *Russian Chem. Rev.*, **1970**, *39*(7), 562.
4. T. Fonong, D. J. Burton, D. J. Pietrzyk, *Anal. Chem.*, **1983**, *55*, 1089.
5. D. J. Burton, D. J. Pietrzyk, T. Ishihara, T. Fonong, R. M. Flynn, *J. Fluorine Chem.*, **1982**, *20*, 617.
6. C. E. McKenna, Pei-de Shen, *J. Org. Chem.*, **1981**, *46*, 4573.
7. D.J. Burton, L. G. Sprague, *J. Org. Chem.*, **1988**, *53*, 1523.
8. D. J. Burton, R. M. Flynn, *J. Fluorine Chem.*, **1980**, *15*, 263.
9. T. Mahmood, J. M. Shreeve, *Inorg. Chem.*, **1986**, *25*, 3128.
10. Y. Margalit, G. Amitai, Y. Ashani, *Phosphorus and Sulfur*, **1977**, *3*, 315.
11. C. Monard, J. Quinchon, *Bull. Soc. Chim. Fr.*, **1961**, 1084, 1086.
12. M. F. Sartori, *Chem. Rev.*, **1951**, *48*, 246.
13. O. T. Quimby, J. D. Curry, D. A. Nicholson, J. B. Prentice, C. H. Roy, *J. Organomet. Chem.*, **1968**, *13*, 199.
14. G. M. Blackburn, D. A. England, F. Kolkman, *J.C.S. Chem. Comm.*, **1981**, 930.
15. L. Z. Soborovskii, N. F. Baina, *J. Gen. Chem. USSR.*, **1959**, *29*, 1115.
16. M. Obayashi, E. Ito, K. Matsui, K. Kondo, *Tetrahedron Lett.*, **1982**, *23*, 2323.
17. G. M. Blackburn, G. E. Taylor, *J. Organomet. Chem.*, **1988**, *348*, 55.
18. H. K. Nair, R. D. Guneratne, A. S. Modak, D. J. Burton, *J. Org. Chem.*, **1994**, *59*, 2393.
19. D. W. Hutchinson, D. M. Thornton, *J. Organomet. Chem.*, **1988**, *340*, 93.
20. H. K. Nair, D. J. Burton, *J. Am. Chem. Soc.*, **1994**, *116*, 6041.
21. H. K. Nair, D. J. Burton, *J. Am. Chem. Soc.*, **1997**, *119*, 9137.
22. D. J. Burton, T. Ishihara, M. Maruta, *Chem. Lett.*, **1982**, 755.
23. Michaelis, A., Kaehne, R., *Chem. Ber.*, **1898**, *31*, 1048
24. Arbuzov, A.E., *J. Russ. Phys. Chem. Soc.*, **1906**, *38*, 687
25. T. B. Brill, S. J. Landon, *Chem. Rev.* **1984**, *84*, 577.

26. A. K. Bhattacharya, G. Thyagarajan, *Chem. Rev.*, **1981**, 81, 415.
27. H.-G. Henning, G. Hilgetag, *Z. Chem.*, **1967**, 7, 169.
28. D. J. Burton, R. M. Flynn, *J. Fluorine Chem.*, **1977**, 10, 329.
29. D. J. Burton, R. M. Flynn, *Synthesis*, **1979**, 8, 615.
30. L. G. Sprague, D. J. Burton, R. D. Guneratne, W. E. Bennett, *J. Fluorine Chem.*, **1990**, 49, 75.
31. D. J. Burton, T. Ishihara, R. M. Flynn, *J. Fluorine Chem.*, **1982**, 20, 121.
32. L. Maier, *Helvetica Chimica Acta*, **1965**, 48, 133.
33. T. Morita, Y. Okamoto, H. Sakurai, *Chem. Lett.*, **1980**, 435.
34. C. E. McKenna, M. T. Higa, N. H. Cheung, M.-C. McKenna, *Tetrahedron Lett.*, **1977**, 155.
35. C. E. McKenna, J. Schmidhauser, *J.C.S. Chem. Comm.*, **1979**, 739.
36. R. Rabinowitz, *J. Org. Chem.*, **1963**, 28, 2975.
37. Gross, H., Böck, Ch., Costisella, B., Gloede, J., *Journal f. prakt. Chemie*, **1978**, 320, 344
38. Balckburn, G.M., Ingleson, D., *J.C.S. Chem. Comm.*, **1978**, 870.
39. A. H. Schmidt, *Chem. Ztg.*, **1980**, 104, 253.
40. T. Morita, Y. Okamoto, H. Sakurai, *Tetrahedron Lett.*, **1978**, 28, 2523.
41. T. Morita, Y. Okamoto, H. Sakurai, *Bull. Chem. Soc. Jpn.*, **1981**, 54, 267.
42. K.-H. Reichert, *Diplomarbeit*, Braunschweig 1986.
43. A. Groddeck, *Dissertation*, Braunschweig 1990.
44. Fild, M., Schmutzler, R., in Kosolapoff: *Organic Phosphorous Compounds*, **1972**, 4, 75-153
45. M. Fild, J. Heinze, W. Krüger, *Chem. Ztg.*, **1977**, 101, 259.
46. M. Fild, K.-H. Reichert, *Chem.-Ztg.*, **1987**, 111, 176.
47. Z. S. Novikova, A. A. Prishchenko, I. F. Lutsenko, *J. Gen. Chem. USSR*, **1977**, 47, 707
48. Houben-Weyl **E1**, pp. 106-183 Elsevier 1982
49. Z. S. Novikova, A. A. Prishchenko, I. F. Lutsenko, *J. Gen. Chem. USSR*, **1979**, 49, 707
50. Z. S. Novikova, A. A. Prishchenko, I. F. Lutsenko, *J. Gen. Chem. USSR*, **1979**, 49, 616
51. H. Schmidbaur, S. Schnatterer, *Chem. Ber.*, **1986**, 119, 2832
52. S. Hietkamp, H. Sommer, O. Stelzer, *Chem. Ber.*, **1984**, 117, 3400
53. R. Schmutzler, *J. Chem. Soc.*, **1964**, 4551
54. R. Schmutzler, *Angew. Chem.*, **1965**, 77, 530
55. K. Ruhnau, *Dissertation*, Braunschweig **1992**

HORSERADISH PEROXIDASE - CATALYZED OXIDATION OF WATER - INSOLUBLE PHENOTHIAZINES

R. SILAGHI-DUMITRESCU, S. AMTHOR, C. PAIZS, C. MAJDIK, M. TOSA,
P. MOLDOVAN, A. SAS, L. TAMAS, F.D. IRIMIE*

*Department of Chemistry and Chemical Engineering,
"Babes-Bolyai University",
400028 Cluj-Napoca, Romania*

ABSTRACT. Horseradish peroxidase catalyzes the oxidation of N-alkyl phenothiazine derivatives to the corresponding sulfoxides and sulfones in the presence of a co-solvent. The reaction conditions may also be controlled so as to yield the sulfoxide in quantitative yields.

INTRODUCTION

Horseradish peroxidase (HRP) is a hemoprotein known to catalyze the oxidation of a wide range of compounds. Its normal catalytic cycle involves the oxidation by hydrogen peroxide of the native state of the enzyme (ferric), forming an intermediate, "Compound I", which is two oxidation equivalents above the resting state and contains a porphyrin radical cation and a ferryl group. Compound I then interacts with the substrate, yielding Compound II (one oxidation equivalent above the resting state) and substrate radical cation. Compound II similarly reacts with another substrate molecule to yield the ferric state of the enzyme and a substrate radical cation [1,2].

Peroxidases have been associated with several physiological events [1,2]. From this point of view phenothiazine derivatives have already been studied as substrates for enzymatic oxidation with HRP. This is due to the fact that phenothiazines demonstrate antihistamine, cholinolytic, sedative or neuroleptic activity [3,4]. While the influence of all components of the reaction mixture has been examined in previous studies, little attention was paid to the possibility of using non water-soluble phenothiazines. Performing the reaction in organic media would greatly enhance the range of prospective substrates for HRP.

Our interest in the chemistry of heterocycles has recently led to the synthesis of some N-alkyl-phenothiazines as well as of the respective sulfoxides and sulfones [5]. Here, we report the HRP-catalyzed oxidation of these water-insoluble N-alkyl-phenothiazines in the presence of co-solvents (cf. Figure 1).

RESULTS AND DISCUSSION

As reported elsewhere [3,4], the oxidation of phenothiazines may be conveniently monitored as a decrease in absorbance at 300 nm as well as an increase in absorbance at 340 nm. The 340-nm peak is taken to indicate formation of the phenothiazine sulfoxide, which is one of the determined reaction products (cf. Figure 1). We therefore monitored our reaction mixtures at 340 nm. In addition,

a pink phenothiazine radical cation has been reported to transiently form upon oxidation of water-soluble phenothiazine derivatives [3,4]. We did indeed observe such pink intermediates in our own experiments, but no further data is reported on them here.

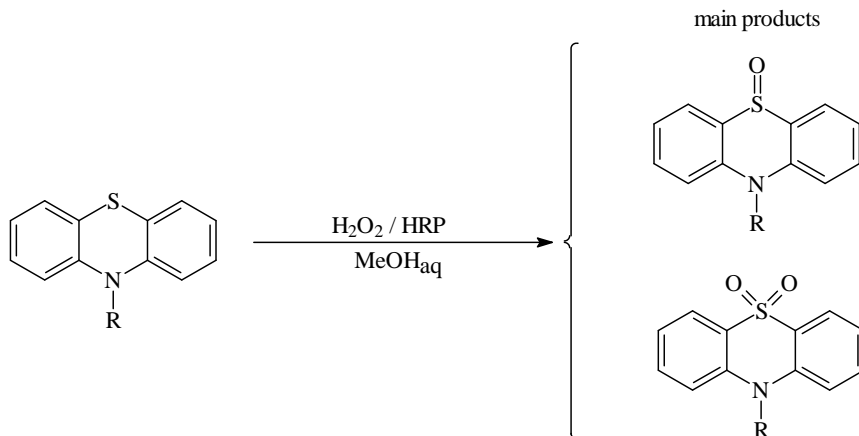


Figure 1. HRP catalyzed oxidation of *N*-substituted phenothiazine derivatives (*R* = propyl, iso-propyl, amyl, methyl, ethyl)

Figure 1 shows the change of absorbance during the HRP-catalyzed oxidation of *N*-propyl phenothiazine (PrFT) with 1.6 mM H₂O₂. Initial rates are shown in Table 1. This data allows the apparent *K_m* for PrFT to be estimated at 60 μM (a similar value was obtained by employing 160 mM H₂O₂).

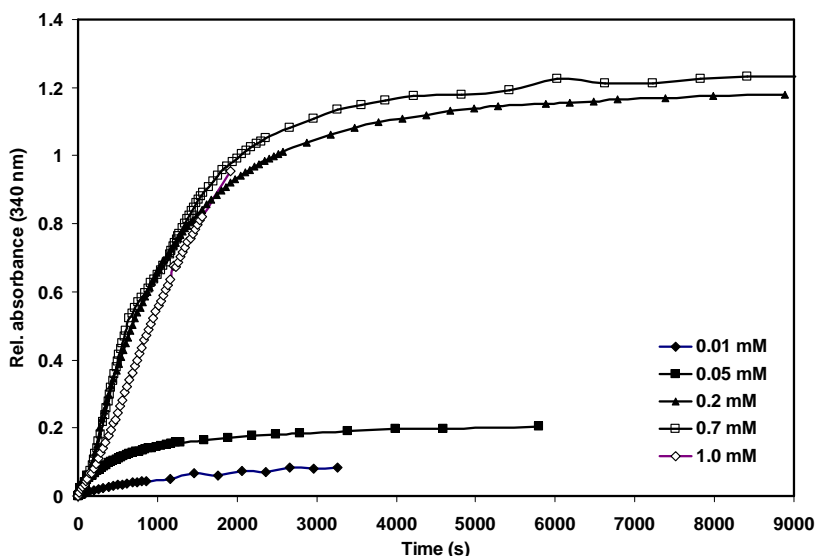


Figure 2. The influence of phenothiazine concentration on the HRP catalyzed oxidation of PrFT (monitored as absorbance increase at 340 nm).

Table 1.

Initial rate vs. PrFT concentrations.

c(PrFT)/mM	v/min ⁻¹
0.01	0.0038
0.05	0.0102
0.2	0.041
0.7	0.0372
1.0	0.0312

The presence of phenothiazine sulfoxide as well as sulfone in the reaction mixtures used for kinetic studies was verified using thin layer chromatography against chemically synthesized authentic samples. Besides these two products, which were expected based on previous studies [3,4], we also found other three to four products, of unknown identity. This disagrees with previously published reports, that only sulfoxide and sulfone were products of the HRP-mediated oxidation of N-substituted phenothiazines. Possible explanations for this difference may include the presence of a co-solvent in our experiments, or differences in HRP preparations used. Perhaps relevant to this issue, we found that the sulfoxide and the sulfone of PrFT, under the same conditions as used for HRP-catalyzed oxidation of PrFT, did induce slight increases in the extinction at 340 nm, and unidentified products of sulfone and sulfoxide metabolism by HRP were found by thin layer chromatography.

Figure 3 and Table 2 indicate that the optimum pH for the HRP-catalyzed oxidation of PrFT is between 6 and 6.5.

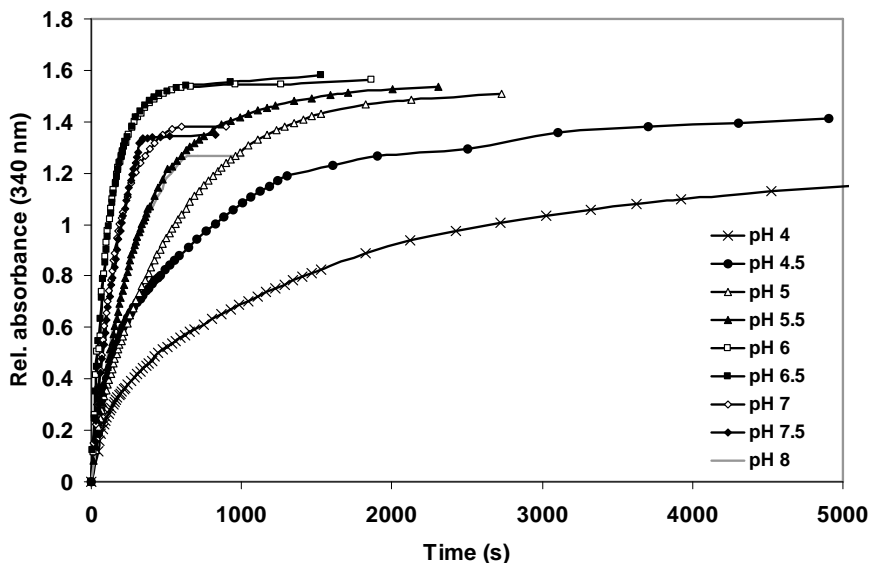


Figure 3. pH dependency of PrFT oxidation catalyzed by HRP, monitored as absorbance increase at 340 nm.

Table 2

Initial rate of the oxidation in dependence of the pH.

pH	v/min ⁻¹
4	0.204
4.5	0.276
5	0.267
5.5	0.324
6	0.894
6.5	0.681
7	0.441
7.5	0.426
8	0.291

Figure 4 and Table 3 illustrate oxidation of various N-alkyl phenothiazines by HRP (methyl – Me, ethyl - Et, propyl- Pr, iso-propyl – iPr, amyl – Am). Notably, oxidation of PrFT was more than three times faster than that of iPrFT, although these two phenothiazine derivatives are structurally very similar.

Table 3

Initial rate of the oxidation depending for various N-alkyl-phenothiazines.

substrate	v/min ⁻¹
MeFT	0.354514
EtFT	0.498
PrFT	0.531429
iPrFT	0.153943
AmFT	0.310971

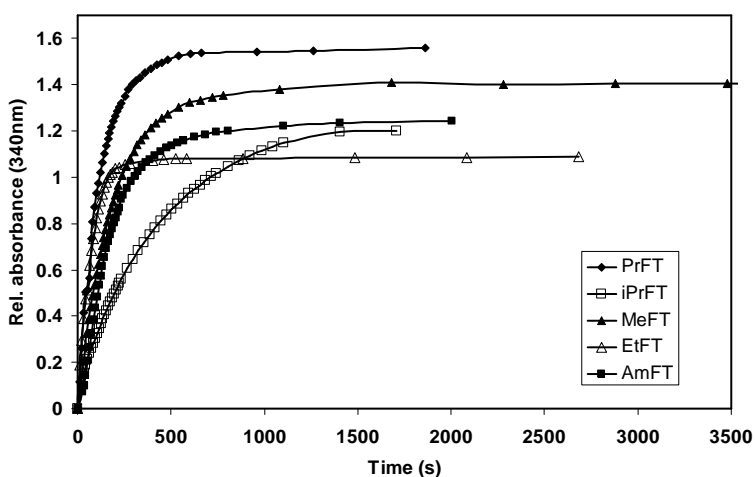


Figure 4. HRP-catalyzed oxidation of different phenothiazines, monitored as absorbance increase at 340 nm.

Since TLC analyses of the reaction mixtures used for kinetic studies revealed the presence of both the sulfoxide and sulfone as reaction products, we sought to optimize reaction conditions so as to obtain phenothiazine sulfoxide as the sole reaction product. Indeed, we found that simply adding the hydrogen peroxide in small increments over the course of 1 to 2 hours, allowed formation of PrFT as the sole reaction product and in quantitative yields. The product was extracted with ethyl acetate from the reaction mixture and analyzed independently to confirm identity with a chemically synthesized sample.

In conclusion, we have shown that water-insoluble N-alkyl phenothiazines are selectively oxidized by HRP in the presence of a co-solvent, and that the reaction may be applied for preparation in very good yields of N-alkyl phenothiazine sulfoxides.

EXPERIMENTAL

Horseradish peroxidase was an aqueous preparation, prepared and analyzed as described elsewhere [6]. Phenothiazine derivatives were chemically prepared as previously described [5]. All other reagents were of analytical grade.

The HRP, extracted from horseradish was used as an aqueous solution to catalyze the oxidation of 2-propyl- (PrFT), 2-i-propyl- (iPrFT) 2-methyl- (MeFT), 2-ethyl- (EtFT) and 2-amylphenothiazine (AmFT) by H_2O_2 . The oxidation of PrFT (0.01; 0.05; 0.2; 0.7; 1.0mM) by H_2O_2 (0.16; 1.6 mM) was done in a medium containing acetate buffer (pH 5.5), methanol (25-60% vol.), and HRP solution (0.1ml).

Alternatively, the reaction of PrFT (0.2mM) with H_2O_2 was carried out in different media containing acetate buffer (pH 4;4.5; 5; 5.5; 6) or phosphate buffer (pH 6.5; 7; 7.5; 8), methanol (52%vol.), and HRP solution (1 μ M).

This led to the optimization of the reaction, so that different derivatives of phenothiazine could be oxidized under the same conditions: Phenothiazine (0.2 mM), H_2O_2 (0.45mM), HRP (1 μ M), methanol (52% vol.) in acetate buffer (pH 6).

All reaction mixtures were extracted with ethyl acetate in order to analyze the reaction products by TLC. In selected cases, melting points and the spectral data of reaction products were obtained, and shown to be identical with those previously described independently synthesized samples [5], confirming the reaction products.

ACKNOWLEDGEMENT: We are grateful to Mr. R. Dumitru for his help on the enzyme preparations.

REFERENCES

1. J. Everse, K. Everse, B.M. Grisham, "Peroxidases in Chemistry and Biology", CRC Press, Boca Raton, 1991.
2. B.C. Saunders, in G.L. Eichhorn, "Inorganic Biochemistry", Elsevier, Amsterdam, 1973, pp 955-1024.

3. V. V. Rogozhin, V. V. Verkhoturov, *Biochemistry (Moscow)* 1998, **63(5)**, 661-666
4. L. Galzigna, V. Rizolli, M. P. Schiappelli, M. P. Rigobello, M. Scarpa, A. Rigo, *Free Radic. Biol. Med.* 1996, **20(6)**, 807.
5. Tosa, M. Paizs, C. Majdik, C. Poppe, L. Kolonits, P. Silberg, I.A. Novak, L., Irimie, F.D., *Heterocycl. Commun.*, 2001, **7**, 277-283
6. R. Silaghi-Dumitrescu, F.D. Irimie, C. Paizs, C. Majdik, M. Tosa, P. Moldovan, A. Sas, L. Tamas, *Studia Universitatis Babes-Bolyai, Chemia*, 2003, **XLVIII**, 177-182.

STUDY OF ARSENIC DETERMINATION IN SOIL BY SPECTROMETRIC METHODS WITH AND WITHOUT HYDRIDE GENERATION

TIBERIU FRENTIU¹, MICHAELA PONTA¹, NADIA ALEXA¹, GEORGIANA MECULESCU¹, MARIN SENILA², BELA ABRAHAM², EMIL CORDOS¹

¹ Babes-Bolyai University, Department of Analytical Chemistry, Str. Arany Janos 11, 400028 Cluj-Napoca, Romania

² Research Institute for Analytical Instrumentation, Str. Donath 67, 400293 Cluj-Napoca, Romania

ABSTRACT. Arsenic determination in soil from residential and industrial area by inductively coupled plasma atomic emission spectrometry (ICP-AES) with and without hydride generation (HG) and hydride generation quartz furnace atomic absorption spectrometry (HG-QF-AAS) was investigated. The used HG device was manufactured at the Research Institute for Analytical Instrumentation, Cluj-Napoca, Romania. ICP-AES with direct liquid sample nebulization (limit of quantitation, LOQ 25 mg Kg⁻¹) was suitable for As determination in contaminated soil, while HG-ICP-AES, five times more sensitive, allowed As determination in soil from both contaminated and non-contaminated area. According to the t-Test, ICP-AES and HG-ICP-AES gave similar As contents only in contaminated soils, while HG-ICP-AES and HG-QF-AAS gave similar As contents for all the analyzed samples. HG-ICP-AES and HG-QF-AAS furnished the same LOQ for As (5 mg Kg⁻¹). The determination of As in a reference soil sample (5 replicates) proved both in HG-ICP-AES and HG-QF-AAS good precision (RSD 11.6%; 11.0%) and recovery degree (102.5±11.9 %; 101.2±11.2 %).

INTRODUCTION

Arsenic is an ubiquitous natural element in environment and is known to be carcinogenic for humans [1]. Natural causes such as land erosion, volcanism, or anthropogenic activities as mining, smelting, glass manufacturing, pharmaceutical industry, electronics, pesticides favor high inputs of As in each of the environmental compartments [2]. Arsenic is present in almost all soils but when its concentration exceeds 5 mg Kg⁻¹ it represents a human health risk [2,3]. As the arsenic species have different properties that influence bioavailability, the speciation of As in soil samples is necessary for toxicological and environmental assessment. The determination of the total As is always necessary and offers useful primary information about the As level in soil.

The most common methods for the determination of As in soil are atomic absorption spectroscopy (AAS) [4], atomic fluorescence spectroscopy (AFS) [5, 6], inductively coupled plasma atomic emission spectroscopy (ICP-AES) [7] or inductively coupled plasma mass spectrometry (ICP- MS) [3]. Coupling these techniques with a hydride generation system (HG) to generate volatile arsine is the common step to improve sensitivity of As determination [8] at very low concentration.

The aim of this paper was to study the possibility to determine As in soil in industrial and residential area by ICP-AES, HG-ICP-AES and HG-QF-AAS and to investigate the suitability to use the hydride generator manufactured at the *Research*

Institute for Analytical Instrumentation, Cluj- Napoca, Romania, in the derivatisation step. Data for As obtained by HG-ICP-AES were compared with those resulted in ICP-AES and hydride generation quartz furnace atomic absorption spectrometry (HG-QF-AAS), respectively.

The accuracy of the total arsenic determination was tested by analyzing a House Reference Material of soil (HRM2, Imperial College, UK).

Samples were collected in the town of Baia-Mare, North Romania, known as having a significant pollution with heavy metals such as Cu, Pb and Zn as well as traces of Cd and As [9, 10]. The town of Baia-Mare is the site of two major companies (Romplumb Co. and Phoenix Co.) to process ores containing Fe, Cu, Pb and Zn supplied by mining companies in the area. Ores contain also sulfoarsenides, which are converted by roasting into As_2O_3 . Although the resulted sulphurous gases are purified during the chemical process using electrical filters and washing with H_2SO_4 , the residual gases still contain both traces of heavy metals and arsenic species soluble or insoluble in water. Thus airborne particulate matter deposits and consequently contaminates the soil with heavy metals and arsenic compounds.

EXPERIMENTAL

Apparatus

A SPECTROFLAME (SPECTRO, Germany) atomic emission spectrometer coupled or not with a hydride generator manufactured at the *Research Institute for Analytical Instrumentation (ICIA), Cluj-Napoca, Romania*, and a Perkin-Elmer model 5000 atomic absorption spectrometer coupled with the same hydride generator were employed.

The SPECTROFLAME (SPECTRO, Germany) atomic emission spectrometer consists of a free-running plasma generator (27.12 MHz, 1200 W), a plasma torch viewed in radial direction and a double scanning monochromator for UV (160 – 336 nm) and Vis (335 – 800 nm) ranges, respectively. The monochromator used in the UV range is filled with high purity nitrogen quality. The sample is aspirated into the plasma by a two-channel peristaltic pump and nebulized using a Meinhardt nebulizer type and double pass Scott type chamber mounted in thermostated room. The emission signal is detected by a Thorn EMI 9781 R photomultiplier. Experimental data are processed using the *Smart Analyzer* soft. Details about characteristics and operating conditions for the SPECTROFLAME scanning spectrometer are given in Table 1.

The atomic absorption spectrometer (Perkin-Elmer-5000) was equipped with a quartz atomizer cell (170 mm length, 12 mm i.d.) built at the *Research Institute for Analytical Instrumentation, Cluj-Napoca, Romania*. The atomizer was heated at controlled temperature ($900 \pm 10^\circ C$) by a 700 W power supply using a Nichrome resistance heater. An arsenic hollow cathode lamp (S.&J. Juniper, Harlow, UK) operated at 12 mA was used as radiation source in AAS. The operating conditions for the Perkin-Elmer 5000 Spectrometer are shown in Table 2.

The AsH_3 generated in the HG device is separated in a gas-liquid separator and carried out by an Ar flow into the plasma or quartz atomizer cell where the atomization takes place. The absorbance of As is measured 60 s after the sample introduction in the hydride generator.

Table 1

Instrumentation and operating conditions for the SPECTROFLAME ICP-AES.

Equipment	Characteristics
Generator	Free – running 27.12 MHz, manually controlled power between 750 – 1400 W, operating power 1200 W.
Plasma torch	Water-cooled copper induction coil inductively coupled plasma. The torch is viewed in radial direction. Argon flow rates: <ul style="list-style-type: none"> - Outer gas 12 L min⁻¹. - Intermediate gas 1 L min⁻¹. - Nebulizer gas 1 L min⁻¹.
Torch cooler system	Recirculation of cooling water without automated control of the temperature.
Sample introduction system	2 channel peristaltic pump, 2 mL min ⁻¹ solution intake, concentric nebulizer Meinhardt type K (TR-30-K3), double pass Scott type spray chamber mounted in a thermo stated room controlled by the computer.
Optics	Scanning spectrometer with a double monochromator. UV range 160 – 336 nm filled with high purity nitrogen quality, grating with 3600 lines mm ⁻¹ , focal length 750 mm, thermostated at 15 ± 0.5 °C, entrance slit width 15 µm. Vis range 335 – 800 nm, grating with 2400 lines mm ⁻¹ , focal length 750 mm, thermostated at 15 ± 0.5 °C, 8 entrance slits, one for each optic fiber with a width of 10 µm. Plasma viewing through an optical fiber for the UV range and 8 optical fibers for the Vis range, respectively. Optical detector: 9781 R photomultiplier powered at 1000 V (Thorn EMI, Ruislip, Middlesex, Great Britain). Wavelength: As 193.7 nm
Data processing	Soft: Smart Analyzer, Pentium III CPU 450 MHz (SPECTRO, Kleve, Germany).

Table 2

Operating conditions for Perkin-Elmer 5000 atomic absorption spectrometer

Parameter	Conditions
Hollow cathode lamp current	12 mA
Calibration type	peak height
Measurement time	10 s
Wavelength	As 193.7 nm
Spectral band width	0.5 nm
Background correction	No

The hydride generator is equipped with a three-channel peristaltic pump, tygon tubing and a reaction coil connected to a gas-liquid separator.

The operating conditions for the HG both in HG-ICP- AES and HG-QF-AAS are summarized in the Table 3.

Table 3.

Operating conditions for the hydride generator	
Parameter	Conditions
Sample flow rate/ mL min ⁻¹	8
HCl carrier flow rate/ mL min ⁻¹	1
NaBH ₄ carrier flow rate/ mL min ⁻¹	1
Ar carrier flow rate/ mL min ⁻¹	100

The flow-rates of the reagents and sample can be adjusted either by changing the inner diameter of the tygon tubes or the rotation speed of the peristaltic pump. Thus, to achieve flow-rates of 8 mL min⁻¹ for the sample and 1 mL min⁻¹ for the reagents tygon tubes with inner diameters of 2.29 mm and 0.76 mm respectively, were used. The working principle of the gas-liquid separator for QF-AAS and ICP-AES are presented in fig. 1. In the QF-AAS technique, after separation of the residual liquid, the Ar stream containing arsine was introduced in the quartz furnace at a flow-rate of 100 mL min⁻¹. In ICP-AES technique, the gas flow leaving the gas-liquid separator was mixed with an additional Ar stream of 1 mL min⁻¹ and introduced into the plasma.

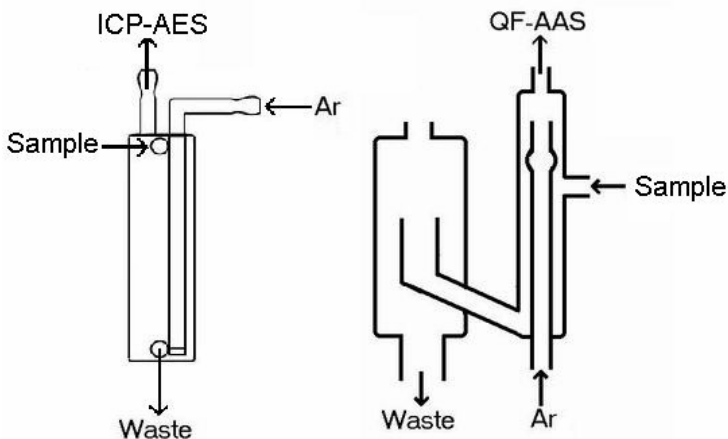


Fig.1 The gas-liquid separators

The experimental set-up of the HG-ICP-AES and HG-QF-AAS is shown in fig. 2.

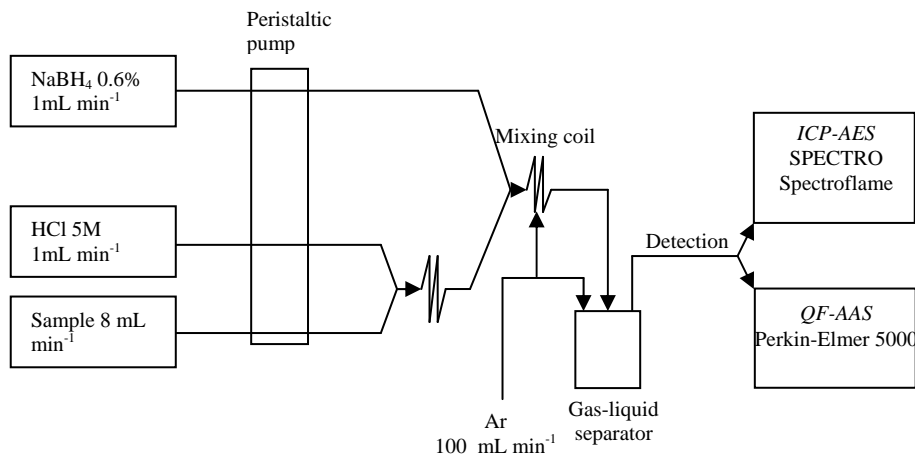


Fig. 2. Experimental set-up of HG-ICP-AES and HG-QF-AAS for As determination

Reagents and standard solutions

All solutions were prepared using analytical-reagent grade chemicals (Fluka-Germany) and distilled water.

A 1000 mg L⁻¹ stock solution of As³⁺ was prepared by dissolving 0.1320 g of As₂O₃ in 2.5 mL 20% NaOH, followed by neutralization with 32% HCl using phenolphthalein as indicator. The final volume of 100 mL was adjusted with 1M HCl. This stock solution was used to prepare stock solution of 100 mg L⁻¹ As³⁺ and of 1 mg L⁻¹ As³⁺.

A 5M stock solution of HCl was prepared by dilution of 32% HCl at appropriate volume with distilled water. This solution was used as carrier fluid to the hydride generator.

A 0.6% stock solution of NaBH₄ was prepared by dissolving 0.6 g of NaBH₄ and 0.5 g of NaOH in 100 mL of water. This solution was used for hydride generation as reducing agent.

A 10% stock solution of KI was prepared by dissolving 10 g of KI in 100 mL of distilled water and was used to pre-reduce As⁵⁺ to As³⁺ in 1M HCl medium.

A saturated solution of Mg(NO₃)₂ was prepared to extract As from soil samples.

Calibration curves for As determination were plotted in the ranges of 0-10 mg L⁻¹ (ICP-AES), 0-50 µg L⁻¹ (HG-ICP-AES) and 0-10 µg L⁻¹ (HG-QF-AAS). The pre-reduction of As⁵⁺ to As³⁺ was carried out using 10 % KI and 10 M HCl, then the reduction to arsine occurred in the operating conditions shown in Table 3.

Methodology for the determination of arsenic in soil

Soil samples from both industrial and residential zones in the Baia-Mare town were collected from 5 cm depth. The samples were dried slowly at room temperature, then in an oven at 60°C for 12 hours. The soil was milled and sieved and the fraction less than 200 μm was kept in brown bottles with stoppers till analysis.

Amounts of 0.25 g of soil were weighed in beakers and volumes of 1 mL of saturated $\text{Mg}(\text{NO}_3)_2$ solution were added. Beakers were gently shaken and heated for 12 hours in a furnace at maximum 400°C. After 12 hours the beakers were cooled at room temperature and volumes of 5 mL of 10M HCl were added. The beakers were shaken overnight, then the contents were diluted to 100 mL with distilled water and filtered. The solutions were kept in plastic bottles before analysis.

By ICP-AES, As was determined after direct nebulization of the sample solutions into the plasma. To determine As by HG-ICP-AES or HG-QF-AAS, a pre-reduction step of As^{5+} to As^{3+} was necessary prior to hydride generation. Thus, an appropriate aliquot volume of the previous solution was transferred in a volumetric flask and followed the pre-reduction treatment with 10 mL of 10M HCl and 10 mL of 10% KI, then was put in a boiling water bath (80 °C) for 1 hour. The solution was cooled down to room temperature and diluted with distilled water to 50 mL. The aliquot volume of the sample to be pre-reduced and diluted was chosen so that the final As content to fall within the calibration range of the HG method. The reduction to arsine occurred in the operating conditions presented in Table 3.

RESULTS AND DISCUSSIONS

Calibration characteristics. The characteristics of the calibration curves for As in ICP-AES with direct nebulization, HG- ICP-AES and HG-QF-AAS are presented in Table 4.

Table 4

Characteristics of calibration curves for As determination by
ICP-AES, HG-ICP-AES and HG-QF-AAS

Technique	Calibration range	Slope (m)	RSD of slope (%)	Correlation coefficient (R)
ICP-AES	0 – 10 mg L^{-1}	4406 a.u. [*] / mg L^{-1}	11.50	1
HG-ICP-AES	0 – 50 $\mu\text{g L}^{-1}$	45164 a.u. [*] / mg L^{-1}	3.30	1
HG-QF-AAS	0 – 10 $\mu\text{g L}^{-1}$	0.026 A ^{**} / mg L^{-1}	5.20	0.9999

^{*} arbitrary units ^{**} absorbance units

According to data in Table 4, the slope of the calibration curve in HG-ICP-AES is one order of magnitude higher than that in ICP-AES, which means a better sensitivity when a reducing stage is present. No comparison is possible between calibration characteristics of AES and AAS because the calculated parameters have different relative values. As the standard deviations of slopes show, the techniques based on hydride derivatisation are more precise (lower RSDs) compared to ICP-AES with direct introduction of the liquid sample into the plasma and offer a better stability of the signal in As determination. On the other hand, RSDs of the calibration slopes

in HG-ICP-AES and HG-QF-AAS (3.3 % ; 5.2 %) are close and provide good precision. The values of 1 or almost 1 for the correlation coefficients of all three calibration curves proved good linear dynamic range and good precision in all three techniques.

Limit of detection (LOD) and limit of quantitation (LOQ) for As in soil samples

LOD and LOQ for As determination by ICP-AES, HG-ICP-AES and HG-QF-AAS are presented in Table 5. The LODs for HG-ICP-AES and HG-QF-AAS expressed as mg Kg^{-1} soil were calculated taking into account the dilution factor and the weight of soil sample. The LOQ was considered to be five times the LOD.

Table 5

Limit of detection and quantitation for As in soil			
Technique	LOD/ $\mu\text{g L}^{-1}$	LOD/ mg Kg^{-1}	LOQ/ mg Kg^{-1}
ICP-AES	12*	5	25
HG-ICP-AES	0.2*	1	5
HG-QF-AAS	0.2**	1	5

* calculated as $3 \sigma_b$ (standard deviation of background)/m (slope of calibration) [11]
 ** mass characteristic calculated as 0.004343/m

According to data in Table 5, the detection limit of As in ICP-AES with direct liquid sample nebulization (5 mg Kg^{-1}) is five times higher than that when a hydride generation device is coupled with either ICP-AES or AAS (1 mg Kg^{-1}). The improvement of LOD by applying the derivatization to arsine is the result of both excellent sample introduction efficiency and matrix removal. Thus, considering the 100% sample introduction efficiency and the sample flow rate of 8 mL min^{-1} in the HG technique compared to cca. 5 % and 2 mL min^{-1} respectively, in the direct nebulisation, the amount of analyte reaching the plasma in the derivatisation procedure is higher at least two orders of magnitude. On the other hand, the matrix separation when HG is used eliminates interference in plasma.

Corroborating the LOQs with the recommended maximum As contents in different types of soil (Table 6), one can say that ICP-AES ($\text{LOQ } 25 \text{ mg Kg}^{-1}$) is not appropriate to determine As in non-contaminated soil ($\leq 5 \text{ mg Kg}^{-1}$), but only in contaminated soil containing more than 25 mg Kg^{-1} . For this kind of samples ICP-AES seems to be sensitive enough to quantitate As with at least 10 % precision.

The determination of As in soil in the range 5 mg Kg^{-1} (normal value) – 25 mg Kg^{-1} (alert value, insensitive soil; action trigger value, sensitive soil) can be carried out only if As is reduced to arsine prior the detection by ICP-AES or AAS ($\text{LOQ } 5 \text{ mg Kg}^{-1}$).

Arsenic determination in soil

Six soil samples collected in the town of Baia-Mare from industrial (S1, S2) and residential area (S3-S6) were prepared according to the methodology described above and As was determined by ICP-AES with direct nebulisation, HG-ICP-AES and HG-QF-AAS, respectively. The mean results (3 successive measurements) are shown in Table 7. In order to compare the results the *t* Test was used and a confidence level of 95% was considered [11].

Table 6

Recommended maximum As level in different type of soils according to Romanian Guideline [12]

mg Kg ⁻¹	Normal value	Alert values		Action trigger values	
		Sensitive soil	Insensitive soil ^{**}	Sensitive soil	Insensitive soil ^{**}
	5	15	25	25	50

* residential and agricultural zones

** industrial and commercial zones

Table 7

Comparative results for As determination in soil with and without hydride generation (n=3)

Sample	ICP-AES	HG-ICP-AES	HG-QF-AAS	t _{calc}	t _{calc}	t _{tab} (P=0.05 v=4)
	mg Kg ⁻¹ (mean±s [*])			ICP-AES/ HG-ICP- AES	HG-ICP- AES/ HG- AAS	
S1	1578±28	1653±39	1740±72	2.70	1.84	
S2	1631±10	1578±53	1723±69	1.70	2.72	
S3	--	10.0±0.9	11.8±0.8	-	2.59	
S4	8.0±7.0	35.0±2.7	33.0±2.0	6.23	0.98	2.78
S5	93±11	109±7	110±7	2.12	0.17	
S6	44.0±3.0	110±6	98.0±5.0	17.04	2.66	

* standard deviation

Comparison of results for As determination in soil by ICP-AES and HG-ICP-AES

Adopting the null hypothesis there is no significant difference between the As mean content determined by the two methods for a confidence level of 95% when $t_{\text{calc}}(\text{ICP-AES}/\text{HG-ICP-AES})$ is lower than t_{tab} for the corresponding number of degrees of freedom. As seen in Table 7, the null hypothesis is retained in three cases out of six (S1, S2, S5) and is rejected in two cases (S4, S6), as there is a significant difference between As contents found by ICP-AES and by HG-ICP-AES. In addition, in the case of two samples (S3, S4) with As levels below or slightly above the LOQ in ICP-AES (25 mg Kg⁻¹), As could not be determined (S3) or the error was almost 100% (S4). Results obtained by HG-ICP-AES were always higher compared to those obtained by direct nebulisation (systematic negative error) due probably to the depressive effect of the high Mg content in the sample on As emission. Thus, in accordance with the previous findings, As can be determined by ICP-AES with good precision only in contaminated soils.

Comparison of results for As determination in soil by HG-QF-AAS and HG-ICP-AES

The *t*-Test shows that there is no significant difference for a 95% confidence level between HG-ICP-AES and HG-AAS in the As determination in six soil samples encompassing a wide concentration range, as $t_{\text{calc}} < t_{\text{tab}}$ (Table 7). LOD of As in soil is 5 mg Kg^{-1} in both techniques and, consequently, the alert value for sensitive zones (15 mg Kg^{-1}) can be detected by HG-ICP-AES/HG-AAS using the hydride generator.

Accuracy of HG-ICP-AES and HG-QF-AAS

The accuracy of arsenic determination by HG-ICP-AES and HG-QF-AAS was tested by determining the total arsenic content in a soil House Reference Material (HRM2, Imperial College, UK). The average values found for the total arsenic content and their 1s uncertainties (5 replicates) compared to the certified value are shown in Table 8.

The good recovery of As in the reference material proves that the used methodology in sampling preparation and the analysis techniques are proper to determine As in soil with good performance.

Table 8

Analysis of soil reference material

Reference material	Certified		Found			
	Mean \pm s $\mu\text{g g}^{-1}$	n*	HG-QF-AAS		HG-ICP-AES	
	Mean \pm s $\mu\text{g g}^{-1}$	n*	Mean \pm s $\mu\text{g g}^{-1}$	n*	Mean \pm s $\mu\text{g g}^{-1}$	n*
HRM2	153.3 \pm 14.9	151	155.2 \pm 17.1	5	157.1 \pm 18.3	5

* number of measurements

RSD/ %	11.0	11.6
Recovery/ %	101.2 \pm 11.2	102.5 \pm 11.9

CONCLUSIONS

The comparison of ICP-AES, HG-ICP-AES and HQ-QF-AAS performance for As determination in soil has shown that ICP-AES allows an accurate As determination only in contaminated soils according to Romanian Guideline. For the analysis of polluted soils no hydride generation is necessary. When a derivatization stage using HG is introduced prior to detection by either AES or AAS, As could be determined in both non-contaminated and contaminated soils as the limit of quantitation improves five times compared to the non-derivatised ICP-AES. The tested hydride generator has good analytical performance that allows the determination of As in soil with good precision and accuracy.

REFERENCES

1. V. Cappuyns, S. Van Herreweghe, R. Swennen, R. Ottenburgs, J. Deckers; *The Science of the total Environment*, 2002, **295**, 217-240
2. D.Lievremont, M.-A. N'negue, Ph. Behra, M.,-C. Lett, *Chemosphere*, 2003, **51**, 419-428
3. R. Pongratz, *The Science of the Total Environment*, 1998, **224**, 133-141
4. A. Marin, A. Lopez-Gonzalvez, C. Barbas, *Analytica Chimica Acta*, 2001, **442**, 305-318
5. S. Garcia-Manyes, G. Jimenez, A. Padro, R. Rubio, G. Rauret, *Talanta*, 2002, **58**, 97-109
6. M. Vergara Gallardo, Y. Bohari, A. Astruc, M. Potin-Gautier, M. Astruc, *Analytica Chimica Acta*, 2001, **441**, 257-268
7. C.F. Balasoiu, G. J. Zagury, L. Deschenes, *The Science of the Total Environment*, 2001, **280**, 239-255
8. L. Cifuentes, G. Crisostomo, J. P. Ibanez, J. M. Casas, F. Alvarez, G. Cifuentes, *Journal of Membrane Science*, 2002, **207**, 1-16
9. E.A. Cordos, T. Frentiu, A.M. Rusu, G. Vatca, *Analyst*, 1995, **120**, 725.
10. T. Frentiu, M. Ponta, A. Rusu, S.D. Anghel, A. Simon, E.A. Cordos, *Analytical. Letters*, 2000, **33**, 323.
11. J.C. Miller, J.N. Miller, *Statistics for Analytical Chemistry*. Ellis Horwood Limited, Chichester, 2nd edn., 1988, p. 53-62 and 120-124.
12. Monitorul Oficial, 303/bis/06.11.1997

THE INFLUENCE OF LIPOIC ACID ON BRIGGS-RAUSCHER OSCILLATING REACTION

GABRIELLA SZABÓ, CS. BOLLA, LAURA JÁNOS and CS. RÁCZ

Babeș-Bolyai University, Faculty of Chemistry and Chemical Engineering, Department of Physical Chemistry

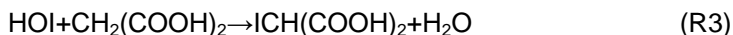
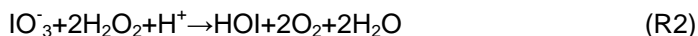
ABSTRACT. Active Briggs-Rauscher mixture is developing through two competing paths: a radical and a non-radical one. Antioxidant added to the mixture reacts with free radicals involved in the radical path and inhibits the oscillations. Addition of lipoic acid (the antioxidant we used) to Briggs-Rauscher mixture causes the immediate cessation of oscillations. After some time the oscillations reappears. The inhibition time depends on the concentration of the lipoic acid.

INTRODUCTION

Briggs-Rauscher (BR) oscillatory reaction represents the oxidation of malonic acid by hydrogen peroxide and iodate with manganese (II) ions as a catalyst, in acidic medium.

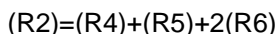
Cook [1] started the investigations regarding to the mechanism of BR and was followed by Noyes and Furrow. They studied BR mixture in batch conditions and proposed a skeleton mechanism [2, 3, 4]. A similar mechanism was proposed by De Kepper and Epstein [5] but they were taking into account several phenomena that appear in open conditions (continuous-flow stirred tank reactor, CSTR). Fujieda and Ogata [6], Happel and Sellers [7] reported a mechanistic study of this oscillatory reaction, too.

According to their proposal the global reaction (R1), consisted in the oxidation and iodination of malonic acid or its derivative, represents the sum of two steps (R2), (R3).

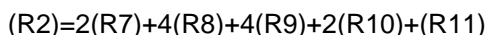
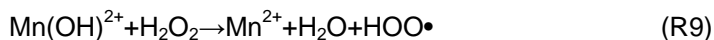


Reaction (R2) takes place in two different ways.

At high iodide-ion concentration the mechanism will obey a non-radical path:



If the iodide-ion concentration is smaller than a critical value, the reaction (R2) will follow the radical path:



When iodide-ion concentration increases above the critical value, the radical way changes into the non-radical one. The skeleton of the mechanism was presented above in order to explain the oscillations in the concentration of the main intermediates: iodine, iodide-ion, oxyiodine species like HOI, HIO₂, IO₂ and hydroperoxyl radical HOO•.

The existence of the radical path makes BR suitable to react with antioxidants. Franz [8] reported for the first time such an experience, followed by Cervellati and Furrow [9, 10, 11]. Antioxidants that were added to an active BR mixture caused the immediate cessation of oscillations. After some time the oscillatory behavior is regenerated. The inhibition time depends linearly on the concentration of the antioxidant. Cervellati and Furrow assumed that the antioxidant added to BR mixture subtracts HOO• radicals and stops the oscillatory regime.

This inhibitory effect on the active BR of the free-radical scavengers indicates a possibility to develop an analytical procedure for monitoring their antioxidant activity.

The aim of the present paper is to report the antioxidant activity of lipoic acid (1,2-dithiolane-pentanoic acid) via inhibition effect on active BR mixture.

RESULTS AND DISCUSSION

In biological systems the antioxidant capacity of lipoic acid occurs through different mechanisms such as metal chelation, activated oxygen species scavenging, recycling of other antioxidants or repair of damaged molecules induced by oxidative stress [12].

The addition of lipoic acid solution to the active BR mixture causes the immediate cessation of the oscillations. After some time the oscillatory behavior was regenerated.

This behavior is presented in Figure 1. It is to be mentioned that frequency and amplitude of oscillations was the same before and after the break.

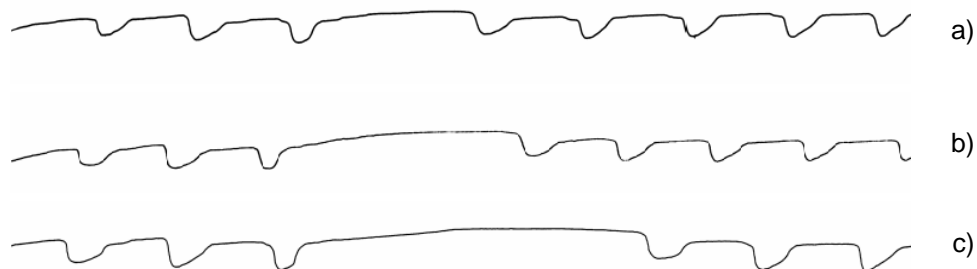


Figure 1. Inhibitory effect of the lipoic acid solutions:
a) $0.31 \cdot 10^{-3} \text{ M}$, b) $0.63 \cdot 10^{-3} \text{ M}$, c) $1.25 \cdot 10^{-3} \text{ M}$

The inhibition time (the time elapsed between the cessation and the regeneration of the oscillatory regime) depends linearly on the concentration of the lipoic acid. The dependence of the inhibition time vs. concentration of lipoic acid is presented in Figure 2.

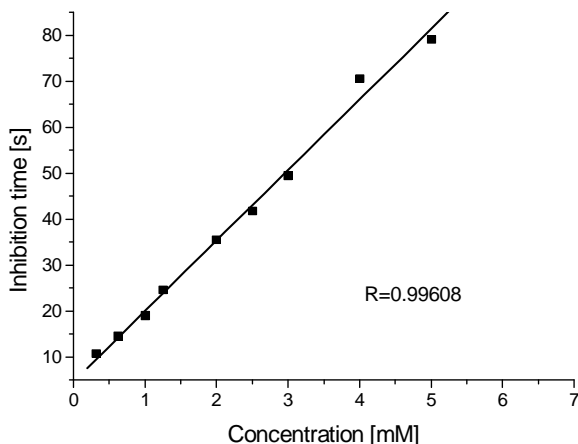


Figure 2. Graph of the inhibition time vs. concentration of lipoic acid

This linear relationship between the inhibition time and the concentration of the lipoic acid indicates the possibility to develop an analytical method for monitoring the activity of antioxidant. This method is simple, rapid and reproducible. At low lipoic acid concentrations (below 0.3 mM) the inhibition time is comparable with the oscillation period, for this reason the linear correlation between the inhibition time and the concentration is not observable.

EXPERIMENTAL

Briggs-Rauscher mixture was prepared in a double-walled glass reactor. Experiments were carried out in thermostated conditions, VEB-MLW type thermostat was used. The temperature of the mixture was controlled by a circulating water bath. A magnetic stirrer ensured uniform mixing. In order to follow the time course of redox potential a platinum electrode and a double-junction saturated calomel electrode were used. Time course of redox potential was monitored with a "Metrohm E 478" recorder. Inhibition time was determined with a stopper-watch.

The reactants sodium iodate (Chemapol, c.p.), manganese (II) sulfate (Reactivul, c.p.), hydrogen peroxide (Merck p.a.), sulfuric acid (Riedel De Haen, p.a.), malonic acid (Reachim, p.a.), potassium iodide (Reactivul, p.a.), potassium nitrate (Reactivul, p.a.) and lipoic acid (Merck p.a.) were used without further purification. Stock solutions were made. The first solution was obtained by mixing the sulfuric acid and the sodium iodate. The acid's concentration was kept 0.2 M and the iodate's concentration was 0.16 M. 0.1 M malonic acid and 0.026 M manganese (II) sulfate composed the second solution. The third solution was the hydrogen peroxide, its concentration was 2.64 M. These solutions were mixed in such a way that $[H^+]=0.05$ M; $[\text{malonic acid}]=0.025$ M; $[\text{Mn(II)}]=0.0065$ M $[\text{H}_2\text{O}_2]=1.32$ M and $[\text{IO}_3^-]=0.04$ M concentrations were ensured.

Lipoic acid was dissolved in water-ethanol mixture (4:1) and a stock solution was made. Its concentration was $5 \cdot 10^{-3}$ M.

REFERENCES

1. D. O. Cooke, *J. Chem. Soc., Chem. Commun.*, **1984**.
2. S. D. Furrow, R. M. Noyes, *J. Am. Chem. Soc.* **1982**, *104*, 38.
3. S. D. Furrow, R. M. Noyes, *J. Am. Chem. Soc.* **1982**, *104*, 42.
4. S. D. Furrow, *J. Phys. Chem.*, **1989**, *93*, 2817.
5. P. De Kepper, I. R. Epstein, *J. Am. Chem. Soc.*, **1982**, *104*, 49.
6. S. Fujieda, H. Ogata, *Talanta*, **1996**, 1989.
7. J. Happel, P. H. Sellers, *J. Phys. Chem.*, **1991**, *95*, 7740.
8. D. A. Franz, *J. Chem. Educ.* **1991**, *68*, 57.
9. R. Cervellati, K. Honer, S. Furrow, C. Neddens, S. Costa, *Helv. Chim. Acta*, **2001**, *84*, 3533.
10. R. Cervellati, N. Crespi-Perellino, S. Furrow, A. Minghetti, *Helv. Chim. Acta*, **2000**, *83*, 3179.
11. K. Honer, R. Cervellati, C. Neddens, *Eur. Food Res. Technol.*, **2002**, *214*, 356.
12. F. Navari-Izzo, M.F. Quartacci, C. Sgherri, *Plant Phys. And Biochem.*, **2002**, *40*, 463.

PREPARATION AND POROUS STRUCTURE DETERMINATION OF RESORCINOL-FORMALDEHYDE AND CARBON AEROGELS

VIRGINIA DANCIU^a, L.C. COTET^a, VERONICA COȘOVEANU^a, P. MARGINEAN^b

^a "Babeș-Bolyai" University, Faculty of Chemistry and Chemical Engineering, Electrochemical Research Laboratory, Arany Janos St., 11, Cluj-Napoca

^b National Institute for Research and Development of Isotopic and Molecular Technologies, Donath St., 71-103, Cluj-Napoca

ABSTRACT. Carbon aerogels are special porous materials consisting of interconnected nanometer-sized particles with small interstitial pores, this structure determining a very high surface area and a high electrical conductivity. These aerogels have found use as electrode materials in several electrochemical devices, most notably, aerocapacitors and electrosorption processes. In order to obtain a matrix for sensor development we studied the preparation and morphology of the C-aerogels. Carbon aerogels were prepared by the sol-gel polycondensation of resorcinol (R) with formaldehyde (F) in a slightly basic aqueous solution (Na₂CO₃) followed by supercritical drying with CO₂ and pyrolysis of obtained resorcinol-formaldehyde (RF) aerogels in an inert atmosphere. The porous structures of the resorcinol-formaldehyde (RF) and carbon (C) aerogels were estimated by krypton adsorption. It was found that the mesopore structure (pore and distribution) strongly depends on the sol-gel reaction, drying and pyrolysis conditions.

KEYWORDS: Resorcinol-formaldehyde aerogel, Carbon aerogel, sol-gel poly-condensation, supercritical drying, porosity

1. INTRODUCTION

The preparation of aerogels starts with the controlled conversion of sol into gel, such as the growth of clusters or polymer chains from a chemical solution, the cross-linking of the primary entities, and the formation of a network. A supercritical drying allows the liquid to drain from the delicate gel structure without any collapse or shrinkage caused by surface tension of the liquid at evaporation [1-3].

Pekala *et al.* prepared the first organic aerogels from the polycondensation of resorcinol (1,3-dihydroxybenzene) with formaldehyde, followed by supercritical drying. The authors have experimentally elucidated the influence of the resorcinol / catalyst mole ratio on the porous structure of RF aerogels. Subsequent pyrolysis of these materials at an elevated temperature (1050°C) in an inert atmosphere produces carbon aerogels [4-7].

Carbon aerogels are unique porous materials consisting of interconnected nanometer – sized particles (3 – 30nm) with small interstitial pores (< 50nm). The aerogel chemical composition, microstructure and physical properties can be controlled at the nanometer scale, giving rise to unique optical, thermal, acoustic, mechanical and electrical properties. Among their many applications, carbon aerogels are used as electrode materials in several electrochemical devices, most notably, aerocapacitors and electrosorption processes [7-10]. Carbon aerogels provide an almost ideal

electrode material because of their high electrical conductivity (10 - 100 S/cm), high surface areas (400 - 1000 m²/g), interconnected and open pore structure with controllable pore size (30 - 500Å).

In order to obtain a matrix for sensor development, RF and carbon aerogels are prepared by sol-gel method using a SAMDRI-PVT-3D supercritical dryer. The influence of the amount of reactants, diluent and basic catalyst used in the polycondensation and the porous structures are experimentally studied in view to obtain a mesoporous structure of the aerogels.

2. EXPERIMENTAL SECTION

2.1. Synthesis of RF aquagels

RF aquagels were synthesized by polycondensation of resorcinol with formaldehyde according to Pekala *et al.* [4-8], for α to ϵ type of gels, and Tamon *et al.* [11-16], for D_I to D_{VII} gels. Na₂CO₃ p.a. (Reactivul, Bucuresti) was used as basic catalyst. RF solutions were prepared from resorcinol (MERCK – Schuchardt, for synthesis, >99%), formaldehyde (S.C. REMED PRODIMPEX S.R.L., research grade, 37 wt% formaldehyde stabilized with 8 wt% methanol). The water used as diluent was distilled after ion exchange; its electric resistivity was $\geq 50 \times 10^4 \Omega\text{m}$ and its pH was 5.8. The synthesis conditions are listed in table 1. The (α - ϵ) RF aquagels were obtained by transferring the resorcinol-formaldehyde mixtures into glass ampoules (10 cm³ capacity), sealed with an methane torch and placed in an oven at 85 ± 3 °C for 7 days. The solutions progressively changed color from clear to yellow, to orange, to deep red as a function of the reaction time. Gel time was a function of the percent solids in the mixture and the catalyst level. Upon completion of the cure cycle, the glass ampoules were removed from the oven and cooled to room temperature. After removal from the ampoules, the RF gels were placed in an agitated bath of 0.125% trifluoroacetic acid at 45 °C for 3 days in order to assist the further condensation of hydroxymethyl groups remained in the gels and the increasing in the compressive modulus of the gels.

The (D_I – D_{VIII}) RF aquagels were obtained by curing the solutions, put in sealed ampoules, for 1 day at room temperature, 1 day at 50°C and 3 days at 90°C.

Table 1

RF aquagels preparation conditions

RF type	R/F [mol/mol]	Solid weight [%]	R/Na ₂ CO ₃ [mol/mol]	R/ H ₂ O [g/cm ³]	F/Na ₂ CO ₃ [mol/mol]	pH
α	0.500	5	50	0.033	100	7.37
β	0.500	5	76.31	0.033	152.6	7.15
γ	0.500	5	96.66	0.033	193	7.05
δ	0.510	4	102.12	0.033	200	7.23
ϵ	0.512	3.5	107.69	0.033	210	7.35
D_I	0.500	14.49	200	0.122	400	6.67
D_{II}	0.500	16.19	75	0.141	150	6.98
D_{III}	0.500	16.18	100	0.141	200	7.15
D_{IV}	0.500	16.14	200	0.141	400	7.05
D_V	0.500	27.73	200	0.325	400	6.50
D_{VI}	0.500	43.28	200	0.930	400	6.38
D_{VII}	0.500	43.35	200	0.926	400	6.64

2.2. Preparation of RF aerogels

RF hydrogels were dried under following supercritical conditions. The prepared hydrogels have the structure filled with water. Because water is poorly soluble in CO₂, there is danger that water remains in the gel structure after supercritical drying with CO₂. For this reason, the gels were immersed in excess of pure acetone or absolute ethanol for >1 week after washing (3 – 4 times) with acetone or ethanol. The hydrogel was placed in the Samdri chamber (20 cm³) with acetone or absolute ethanol. The chamber was then sealed. In order to prevent vaporization of the liquid CO₂ the chamber of the SAMDRI-PVT-3D dryer (Tousimis Research Corp., USA) is cooled (with liquid CO₂) to near 0°C. Then, the liquid carbon dioxide slowly flows (fill rate: 0.43 – 1.3 ml/min) from the siphon – type bomb to the dryer until the pressure reaches about 54.3 atm.

The liquid CO₂ flowed through the chamber at 3 – 5 cm³/min and 0 – 10°C for 4 hours and acetone or ethanol was washed out by CO₂. The critical temperature and pressure of CO₂ are 31°C and 73.5 atm. Hence, the temperature of the chamber was increased above the critical temperature of CO₂ and acetone (ethanol) inside the gel was supercritically extracted at 42°C for 10 - 60 min. After the supercritical extraction, the inside of chamber was slowly depressurized to atmospheric pressure at 42°C for 60 min. and the RF aerogel was obtained. After aging the aerogels at 60 °C for 2 hours, the porous structure of the aerogels was determined using Kr adsorption at liquid N₂ temperature.

2.3. Preparation of C aerogels

We prepared carbon aerogels by pyrolysis of RF aerogels in a conventional furnace. N₂ flowed through a quartz reactor containing the RF aerogels set in the furnace at 8 cm³/min during the pyrolysis. The furnace was heated to 250°C at 4°C/min, maintained at this temperature for 2 hours, then was heated, with the same rate, to 850° and maintained 4 hours. After pyrolysis, the furnace was cooled at the room temperature under its own thermal mass.

2.4. Characterization of the RF and C aerogels

The porous structure of RF and C aerogels was determined by Kr adsorption. The adsorption isotherms were obtained using an all glass installation (INCDTIM Cluj-Napoca), at a partial pressure of 0.05-0.35. The samples were preheated for 2h at 60°C before measurement, after their degasification in vacuum. The adsorption and desorption isotherms of Kr were measured at temperature of liquid nitrogen.

The BET surface area (S_{BET}), mesopore size distribution and microporosity were determined. The pore size distribution was estimated by applying the Dollimore-Heal method [17] to the measured desorption isotherms and the microporosity (slit width: 0.35-1.0) was evaluated by the t-plot method [18].

3. RESULTS AND DISCUSSIONS

3.1. Appearance of RF aerogels

RF-aerogels were prepared by changing the mole ratios of resorcinol to basic catalyst (R/C), the ratios of resorcinol to pure water (R/H₂O, g/cm³) or the mole ratios of resorcinol to formaldehyde (R/F). Color, transparency and hardness of RF-aerogels depended on R/Na₂CO₃, R/H₂O or R/F ratios used in the sol-gel polycondensation. Although the gels were reddish yellow in color and transparent for 50<R/C<200, they become dark with decreasing R/Na₂CO₃.

As for influence of R/H₂O on the aquagel characters, the dark reddish yellow and soft gels were obtained for low R/H₂O, and light reddish yellow and hard ones were prepared for high R/H₂O.

The gels prepared under the conditions of low R/F had a light color and those prepared for high R/F had a dark color.

3.2. Porous structure of RF-aerogels

RF aerogels prepared by supercritical drying with CO₂ had the same color as the RF aquagels.

3.2.1. Effect of R/Na₂CO₃ on porous structure of RF-aerogels

We prepared RF aerogels by changing R/Na₂CO₃ ratio under the conditions of R/H₂O = 0.033 (α - ε RF aerogels) and respectively 0.141 (D_{II}-D_{IV} RF aerogels) and R/F = 0.5 and we determined their porous structure by Kr adsorption. Figures 1 and 2 show that for high Na₂CO₃ concentration (*i.e.* R/Na₂CO₃ = 50), the aerogels have high BET surface areas of *ca* 800 m²/g and large mesopore volumes of *ca* 3.5 cm³/g. For low Na₂CO₃ concentration, S_{BET} and V_{meso} decrease with increasing R/Na₂CO₃. S_{micro} and V_{micro} are much smaller and have similar R/Na₂CO₃ dependencies.

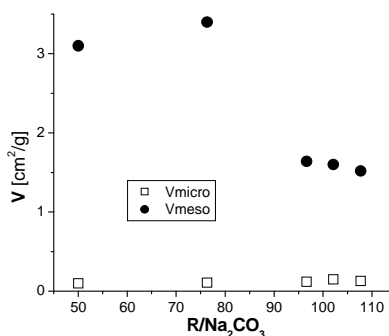
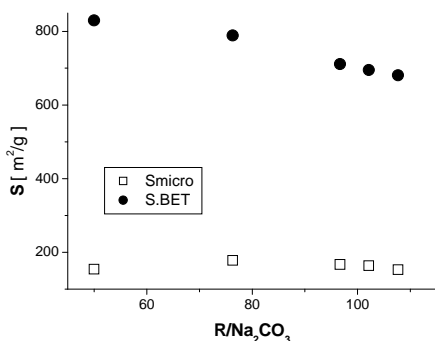


Figure 1. Influence of R/Na₂CO₃ on the BET surface area and surface area of micropores of $\alpha, \beta, \gamma, \delta, \varepsilon$ RF aerogels

Figure 2. Influence of R/Na₂CO₃ on the volume of mesopores (V_{meso}) and micropores (V_{micro}) of $\alpha, \beta, \gamma, \delta, \varepsilon$ RF aerogels

Figure 3 shows some examples of pore size distribution of RF aerogels. For R/Na₂CO₃= 75, the aerogels have monodisperse distribution (a single peak), while for R/Na₂CO₃ = 200 a polydisperse distribution (some peaks) was obtained.

3.2.2. Effect of R/H₂O on porous structure of RF aerogels

S_{BET} and S_{micro} seem to be independent of R/H₂O as shown figure 4; the results suggest that the particle size constituting the network structure of aerogels is independent of R/H₂O.

PREPARATION AND POROUS STRUCTURE OF RF AND C AEROGELS

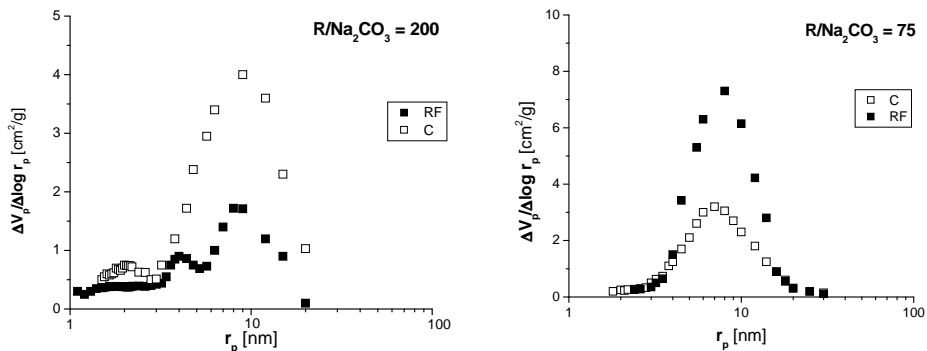


Figure 3. Pore size distribution of RF and C aerogels; $R/H_2O = 0.141$ and $R/F = 0.5$

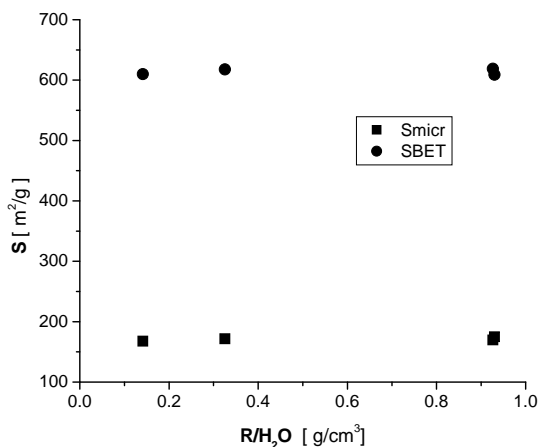


Figure 4. Influence of R/H_2O on the BET surface area and surface area of micropores of RF aerogels

Figure 5 shows that V_{meso} increases with increasing R/H_2O ; the aerogels have monodisperse distribution only at $R/H_2O = 0.325$; in all other studied cases having a polydisperse distribution.

3.2.3. Effect of R/F ratio on porous structure of RF aerogels

For the RF-aerogels prepared under the conditions of $R/Na_2CO_3=100$, $R/H_2O = 0.033$ and $R/F = 0,34 - 0,58$ it was observed that S_{BET} was independent of R/F and V_{meso} was larger for $R/F > 0.40$. S_{micro} and V_{micro} were independent of R/F ratio and smaller than S_{BET} and V_{meso} .

3.3. Porous structure of C-aerogels

C aerogels were prepared by pyrolysing RF aerogels at 850°C. The aerogels turned from dark reddish yellow and transparent to black and opaque. The porous structure of the carbon aerogels was analyzed by the Kr adsorption method.

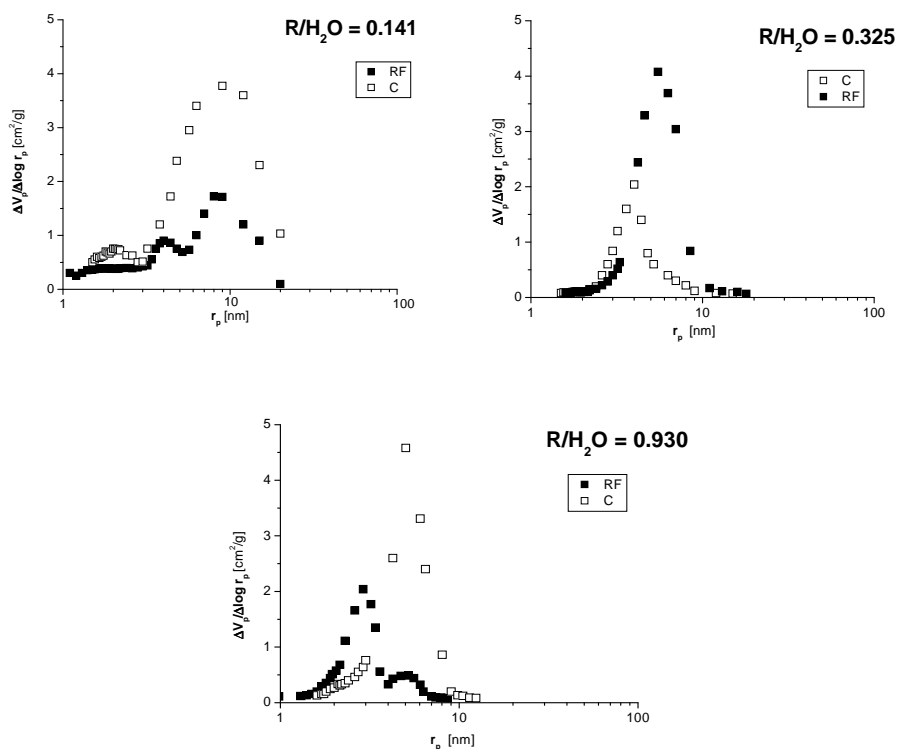


Figure 5. Pore size distribution of RF and C aerogels ($R/Na_2CO_3 = 200$ and $R/F = 0.5$)

Table 2 shows that S_{BET} increases for all prepared samples suggesting the formation of micropores. V_{meso} increases or decreases by pyrolysis of RF aerogels. Carbon aerogel prepared from RF aerogel having a monodisperse distribution gives a smaller mesopore volume than the RF aerogel (see fig. 3 - 5).

Table 2.

Morphological characteristics of RF and C aerogels

Conditions of sol-gel polycondensation	Aerogel type	$S_{BET} \times 10^{-2}$ [m ² /g]	V_{meso} [cm ³ /g]	r_{peak} [nm]	$S_{micro} \times 10^{-2}$ [m ² /g]	$V_{micro} \times 10^2$ [cm ³ /g]
R/C= 50; R/F=0.5; R/H ₂ O=0,033	RF-α	7.89	3.81	4.5	-	-
	C-α	8.45	3.51	3.7	1.67	3.00

PREPARATION AND POROUS STRUCTURE OF RF AND C AEROGELS

Conditions of sol-gel polycondensation	Aerogel type	$S_{\text{BET}} \times 10^{-2}$ [m ² /g]	V_{meso} [cm ³ /g]	r_{peak} [nm]	$S_{\text{micro}} \times 10^{-2}$ [m ² /g]	$V_{\text{micro}} \times 10^{-2}$ [cm ³ /g]
R/C= 76; R/F=0.5; R/H ₂ O=0,033	RF-β C- β	7.62 8.04	3.92 3.57	5.3 4.9	- 1.84	- 4.00
R/C= 97; R/F=0.5; R/H ₂ O=0,033	RF-γ C- γ	6.56 6.84	3.01 2.48	5.6 3.8	- 1.91	- 5.00
R/C= 102; R/F=0.51; R/H ₂ O=0,033	RF-δ C-δ	6.27 6.47	2.87 2.35	5.7 3.7	- 1.95	- 5.40
R/C= 108; R/F=0.51; R/H ₂ O=0,033	RF-ε C- ε	6.05 6.38	2.77 2.26	5.8 3.5	- 2.05	- 5.50
R/C= 75; R/F=0.5; R/H ₂ O=0,141	RF-DII C-DII	7.35 8.39	3.34 2.78	6.9 6.1	0.88 3.07	5.00 12.00
R/C= 100; R/F=0.5; R/H ₂ O=0,141	RF-DIII C-DIII	6.98 7.09	2.29 1.68	9.2 5.1	1.02 2.48	4.89 6.00
R/C= 200; R/F=0.5; R/H ₂ O=0,141	RF-DIV C-DIV	6.39 10.21	2.98 2.38	9.7 5.4	1.48 12.5	3.76 4.80

4. CONCLUSIONS

The RF aerogels are mesoporous materials with high surface (600 – 800 m²/g) areas and have few micropores. The mesoporous structure of RF aerogels depends on the R/Na₂CO₃ and R/H₂O ratios used in the sol-gel polycondensation. The RF aerogels have monodisperse porous structures for low mole ratio of resorcinol to basic catalyst or for the high ratio of resorcinol to water. The surface area of RF aerogel can be controlled by the rapport R/Na₂CO₃. The mesopore volume changes greatly with R/Na₂CO₃ or R/H₂O ratios.

Carbon aerogels have larger surface areas than the corresponding RF aerogels and during pyrolysis of RF aerogels the micropores are formed. Carbon aerogel prepared from RF aerogel having a monodisperse distribution gives a smaller mesopore volume than the RF aerogel.

To control the porous structures of carbon aerogels it is very important to control the structures of RF aerogels.

ACKNOWLEDGMENT

This research was supported by the Ministry of Education, Research and Youth of Romania, in the frame of MATNANTECH Program, under contract no. C 101(204)/2002.

REFERENCES

1. S.S. Kistler, *Nature*, 1931, **127**, 741
2. J. Fricke, *Aerogels*, ed. J. Fricke, Springer-Verlag, New York, 1986; pp. 2-19
3. G.M. Pajonk, S.J. Teichner, *Aerogels*, ed. J. Fricke, Springer-Verlag, New York, 1986; pp. 193-199
4. R.W. Pekala, *J. Mater. Sci.*, 1989, **24**, 3221
5. R.W. Pekala, *Mater. Res. Soc. Proc.*, 1990, **171**, 285
6. R.W. Pekala, C.T. Alviso, M. Kong, S.S. Husley, *J. Non-Cryst. Solids*, 1992, **145**, 90
7. R.W. Pekala, D.W. Schaefer, *Macromolecules*, 1993, **26**, 5487
8. R.W. Pekala, *Ultrastructure Processing of Advanced Materials*, D.R. Uhlmanjn, D.R. Ulrich, Eds., John Wiley and Sons, Inc., New York, NY, 1992, 711
9. T.D. Tran, C.T. Alviso, S.S. Hulsey, J.K. Nielsen, R.W. Pekala, *Mat. Res. Soc. Symp. Proc.*, 1996, **431**, 461
10. R.W. Pekala, C.T. Alviso, J.K. Nielsen, T.D. Tran, G.M. Reynolds, M.S. Dresselhaus, *Mat. Res. Soc. Symp. Proc.*, 1995, **393**, 413
11. H. Tamon, H. Ishizaka, *Carbon*, 1998, **36**, 1397
12. H. Tamon, T. Sone, M. Okazaki, *J. Colloid Interface Sci.*, 1997, **188**, 162
13. H. Tamon, H. Ishizaka, T. Araki, M. Okazaki, *Carbon*, 1998, **36**, 1257
14. H. Tamon, H. Ishizaka, *J. Colloid Interface Sci.*, 1998, **206**, 577
15. T. Yamamoto, T. Nishimura, T. Suzuki, H.Tamon, *Drying Technology*, 2001, **19 (7)**, 1319
16. T. Yamamoto, T. Yoshida, T. Suzuki, S.R. Mukai, H.Tamon, *J. Colloid Interface Sci.*, 2002, **245**, 391
17. D. Dollimore, G.R. Heal, *J. Appl. Chem.*, 1964, **14**, 109
18. B.C. Lippens, J.H. Boer, *J. Catal.*, 1965, **4**, 319